U.S. DEPARTMENT OF COMMERCE
National Technical Information Service

PB-263 348

Mathematical Modeling of Simulated Photochemical Smog

Systems Applications, Inc, San Rafael, Calif

Prepared for

Environmental Sciences Research Lab, Research Triangle Park, N C

Jan 77

PB 263 348

EPA-600/3-77-011
January 1977

Ecological Research Series

UNITED STATES ENVIRONMENTAL PROTECTION AGENCY

REPRODUCED BY
NATIONAL TECHNICAL
INFORMATION SERVICE
U.S. DEPARTMENT OF COMMERCE
SPRINGFIELD, VA. 22161

RESEARCH REPORTING SERIES

Research reports of the Office of Research and Development, U.S. Environmental Protection Agency, have been grouped into five series. These five broad categories were established to facilitate further development and application of environmental technology. Elimination of traditional grouping was consciously planned to foster technology transfer and a maximum interface in related fields. The five series are:

1. Environmental Health Effects Research
2. Environmental Protection Technology
3. Ecological Research
4. Environmental Monitoring
5. Socioeconomic Environmental Studies

This report has been assigned to the ECOLOGICAL RESEARCH series. This series describes research on the effects of pollution on humans, plant and animal species, and materials. Problems are assessed for their long- and short-term influences. Investigations include formation, transport, and pathway studies to determine the fate of pollutants and their effects. This work provides the technical basis for setting standards to minimize undesirable changes in living organisms in the aquatic, terrestrial, and atmospheric environments.

This document is available to the public through the National Technical Information Service, Springfield, Virginia 22161.

TECHNICAL REPORT DATA

(Please read Instructions on the reverse before completing)

1. REPORT NO. EPA-600/3-77-011	2.	3. RECIPIENT'S ACCESSION NO.
4. TITLE AND SUBTITLE MATHEMATICAL MODELING OF SIMULATED PHOTOCHEMICAL SMOG		5. REPORT DATE January 1977 6. PERFORMING ORGANIZATION CODE
7. AUTHOR(S) G. Z. Whitten and H. H. Hugo		8. PERFORMING ORGANIZATION REPORT NO.
9. PERFORMING ORGANIZATION NAME AND ADDRESS Systems Applications, Inc. 950 Northgate Drive San Rafael, California 94903		10. PROGRAM ELEMENT NO. 1AA603 (1AA008) 11. CONTRACT/GRANT NO. Contract No. 68-02-0580
12. SPONSORING AGENCY NAME AND ADDRESS Environmental Sciences Research Laboratory Office of Research and Development U.S. Environmental Protection Agency Research Triangle Park, NC 27711		13. TYPE OF REPORT AND PERIOD COVERED Final 6/75 - 6/76 14. SPONSORING AGENCY CODE EPA-ORD
15. SUPPLEMENTARY NOTES		

16. ABSTRACT

This report deals with the continuing effort to develop a chemical kinetic mechanism to describe the formation of photochemical smog. Using the technique of computer modeling to simulate smog chamber data, several explicit kinetic mechanisms for specific hydrocarbons were analyzed and a generalized kinetic mechanism was proposed for use in dynamic urban airshed models. Computer simulations of propylene/NO_x, butane/NO_x, 1-butene/NO_x, and propylene/butane/NO_x systems were performed to simulate the smog chamber data collected by the University of California, Riverside. The general kinetic mechanism, which is based on the carbon bonding found in the hydrocarbon system, is described. Simulations using this new carbon-bond mechanism were also compared with the smog chamber data on the propylene/NO_x, butane/NO_x, propylene/butane/NO_x, and toluene/NO_x systems. The usefulness and validity of the computer modeling is also discussed relative to the current understanding of the smog formation process.

17. KEY WORDS AND DOCUMENT ANALYSIS

a. DESCRIPTORS	b. IDENTIFIERS/OPEN ENDED TERMS	c. COSATI Field/Group
* Air pollution		13B
* Reaction kinetics		07D
* Photochemical reactions		07E
Test chambers		14B
* Mathematical models		12A
* Computerized simulation		09B

18. DISTRIBUTION STATEMENT RELEASE TO PUBLIC	19. SECURITY CLASS *(This Report)* UNCLASSIFIED	21. NO. OF PAGES 307
	20. SECURITY CLASS *(This page)* UNCLASSIFIED	22. PRICE 9.75 - 3.00

EPA Form 2220-1 (9-73)

ATTENTION

AS NOTED IN THE NTIS ANNOUNCEMENT, PORTIONS OF THIS REPORT ARE NOT LEGIBLE. HOWEVER, IT IS THE BEST REPRODUCTION AVAILABLE FROM THE COPY SENT TO NTIS.

EPA-600/3-77-011
January 1977

MATHEMATICAL MODELING OF SIMULATED PHOTOCHEMICAL SMOG

by

G. Z. Whitten, H. Hogo

Systems Applications, Incorporated
950 Northgate Drive
San Rafael, California 94903

Contract No. 68-02-0580

Project Officer

Marcia C. Dodge

Chemistry and Physics Division
Environmental Sciences Research Laboratory
Research Triangle Park, North Carolina 27711

U.S. ENVIRONMENTAL PROTECTION AGENCY
OFFICE OF RESEARCH AND DEVELOPMENT
ENVIRONMENTAL SCIENCES RESEARCH LABORATORY
RESEARCH TRIANGLE PARK, NORTH CAROLINA 27711

DISCLAIMER

This report has been reviewed by the Environmental Sciences Research Laboratory, U.S. Environmental Protection Agency, and approved for publication. Approval does not signify that the contents necessarily reflect the views and policies of the U.S. Environmental Protection Agency, nor does mention of trade names or commercial products constitute endorsement or recommendation for use.

ABSTRACT

This report deals with the continuing effort to develop a chemical kinetic mechanism to describe the formation of photochemical smog. Using the technique of computer modeling to simulate smog chamber data, several explicit kinetic mechanisms for specific hydrocarbons were analyzed and a generalized kinetic mechanism was proposed for use in urban airshed models. Refinements and improvements were made on the initial work reported by Durbin et al. (1975). Computer simulations of propylene/NO_x, butane/NO_x, 1-butene/NO_x, and propylene/butane/NO_x systems were performed to simulate smog chamber data collected by the University of California, Riverside. The general kinetic mechanism, which is based on the carbon bonding found in the hydrocarbon system, is described. Simulations using this new carbon-bond mechanism were also compared with the smog chamber data on propylene/NO_x, butane/NO_x, propylene/butane/NO_x, toluene/NO_x, and 1-butene/NO_x systems. The usefulness and validity of the computer modeling is discussed relative to the current understanding of the smog formation process.

Preceding page blank

CONTENTS

ABSTRACT iii

FIGURES vii

TABLES ix

I INTRODUCTION 1

II INORGANIC CHEMISTRY 8

- A. NO-OH· Reaction 8
- B. HNO_2 Photolysis 8
- C. NO_2-OH·-M Reaction 9
- D. $HO_2\cdot$-NO_2 Reaction 9
- E. $HO_2\cdot$-NO Reaction 10
- F. HNO_2 Formation 11
- G. HNO_3 Formation 12

III ORGANIC CHEMISTRY 13

- A. Propylene/NO_x Chemistry 13
  - 1. Propylene-OH· Reaction 14
  - 2. Peroxy Radical Chemistry 16
  - 3. Reactions of Olefins with Nitrate Radicals ($NO_3\cdot$) . . . 25
  - 4. Formyl Radical Chemistry 27
  - 5. Aldehyde Chemistry 28
  - 6. Olefin-O_3 Reactions 29
  - 7. PAN Chemistry 30
  - 8. Propylene-O Atom Reaction 33
  - 9. Simulation Results 34
  - 10. Discussion of the Propylene/NO_x Systems 77
- B. Butane/NO_x Chemistry 83
  - 1. Hydrogen Abstraction from Butane by Hydroxyl Radicals . 85
  - 2. Alkoxyl Radical Chemistry 85
  - 3. Formation and Destruction of Methylethylketone (MEK). . 94
  - 4. Simulation Results 97
  - 5. Discussion of the Butane/NO_x Systems 106

III ORGANIC CHEMISTRY (Continued)

C. Propylene/Butane/NO_x Chemistry 128
  1. Simulation Results 129
  2. Discussion of the Propylene/Butane/NO_x Systems 172
D. Toluene/NO_x Chemistry 174
E. 1-Butene/NO_x Chemistry 180
  1. Oxidation of 1-Butene 181
  2. Simulation Results 182
  3. Discussion of the 1-Butene/NO_x Systems 197

IV A NEW GENERALIZED LUMPED MECHANISM 199
A. Revision of the HSD Mechanism 201
B. The New Generalized Mechanism 201
  1. Rate Constants for Hydrocarbon Classes 207
  2. Sources of Radicals in the Carbon-Bond Mechanism . . . 213
C. Simulation Results 216
  1. Butane/NO_x Systems 216
  2. Propylene/NO_x Systems 227
  3. Propylene/Butane/NO_x Systems 228
  4. 1-Butene/NO_x Systems 241
  5. Toluene/NO_x Systems 241
D. Discussion of the Carbon-Bond Mechanism 277

V GENERAL DISCUSSION 280

REFERENCES 290

FIGURES

III-1 Simulation of PAN Chemistry 32

III-2 Factorial Block for Propylene/NO_x Systems 40

III-3 to III-64 Computer Simulations of UCR Data on Propylene/NO_x Systems 41

III-65 Relative Intensity for Different UCR Runs 80

III-66 Acetaldehyde Cross Sections for Two Different Simulations 81

III-67 Unrecovered Carbon as a Function of Time for Various Runs (Not Corrected for Dilution) 95

III-68 Measured MEK Concentration as a Function of Time for Various Runs 96

III-69 Effect of Including Biacetyl Photolysis 98

III-70 Factorial Block for Butane/NO_x Systems 107

III-71 to III-103 Computer Simulations of UCR Data on Butane/NO_x Systems 108

III-104 Factorial Block for Propylene/Butane/NO_x Systems . . . 131

III-105 to III-167 Computer Simulations of UCR Data on Propylene/Butane/NO_x Systems 140

III-168 Factorial Block for 1-Butene/NO_x Systems 183

III-169 to III-180 Computer Simulations of UCR Data on 1-Butene/NO_x Systems 191

IV-1 to IV-17 Computer Simulations of UCR Data on Butane/NO_x Systems with the Carbon-Bond Mechanism 217

IV-18 to IV-39 Computer Simulations of UCR Data on Propylene/NO_x Systems with the Carbon-Bond Mechanism 229

IV-40 to IV-60 Computer Simulations of UCR Data on Propylene/Butane/NO_x Systems with the Carbon-Bond Mechanism 242

IV-61 to IV-69 Computer Simulations of UCR Data on 1-Butene/NO_x Systems with the Carbon-Bond Mechanism 256

IV-70 to IV-92 Computer Simulations of UCR Data on Toluene/NO_x Systems with the Carbon-Bond Mechanism 262

V-1a Percentage Differences Between Predictions of Explicit Mechanisms and Measurements of Maximum One-Hour-Average Ozone Concentrations 285

V-1b Differences Between Predictions of Explicit Mechanisms and Measurements of Maximum One-Hour-Average Ozone Concentrations 285

V-2a Percentage Differences Between Predictions of Carbon-Bond Mechanism and Measurements of Maximum One-Hour-Average Ozone Concentrations 286

V-2b Differences Between Predictions of Carbon-Bond Mechanism and Measurements of Maximum One-Hour-Average Ozone Concentrations 286

V-3a Percent Differences Between the Maximum One-Hour-Average Ozone Concentrations Predicted by the Carbon-Bond Mechanism and by the Explicit Mechanisms . . 287

V-3b Differences Between the Maximum One-Hour-Average Ozone Concentrations Predicted by the Carbon-Bond Mechanism and by the Explicit Mechanisms 287

TABLES

III-1 Rate Constants for the Olefin-OH· Reaction 16

III-2 Thermochemistry of Alkoxyl Radicals 18

III-3 Comparison of the Reactivities of $O(^3P)$ Atoms, Ozone, and NO_3 Toward Olefins 26

III-4 Mechanism for PAN Decomposition 31

III-5 The Propylene/NO_x Mechanism 35

III-6a Initial Conditions for Simulations of Propylene/NO_x Systems 39

III-6b Photolysis Rate Constants for Simulations of Propylene/NO_x Systems 40

III-7 Percent Carbon Recovery for Propylene/NO_x Systems . . . 77

III-8 Predicted and Measured Maximum One-Hour-Average Ozone Concentrations for the Propylene/NO_x Systems 84

III-9 Percent Carbon Mass Recovery for Butane/NO_x Systems . . 93

III-10 Percent Carbon Mass Recovery for Run EC-44 93

III-11 The Butane/NO_x Mechanism 99

III-12a Initial Conditions for Simulations of Butane/NO_x Systems 105

III-12b Photolysis Rate Constants for Simulations of Butane/NO_x Systems 105

III-13 Predicted and Measured Maximum One-Hour-Average Ozone Concentrations for the Butane/NO_x Systems 125

III-14 Percent Carbon Mass Recovery for Propylene/ Butane/NO_x Systems 130

III-15a Initial Conditions for Simulations of Propylene/ Butane/NO_x Systems 130

III-15b Photolysis Rate Constants for Simulations of Propylene/Butane/NO_x Systems 131

III-16 The Propylene/Butane/NO_x Mechanism 132

III-17 Predicted and Measured Maximum One-Hour-Average Ozone Concentrations for the Propylene/Butane/NO_x Systems . . 173

III-18 Percent Carbon Mass Recovery for Toluene/ NO_x Systems 175

III-19 Rate Constants for Reactions Involving Hydroxyl Radicals and Aromatic Hydrocarbons 176

III-20 The 1-Butene/NO_x Mechanism 184

III-21a Initial Conditions for Simulations of 1-Butene/NO_x Systems 189

III-21b Photolysis Rate Constants for Simulations of 1-Butene/NO_x Systems 189

III-22 Percent Carbon Mass Recovery for 1-Butene/ NO_x Systems 190

III-23 Predicted and Measured Maximum One-Hour-Average Ozone Concentrations for the 1-Butene/NO_x Systems 198

IV-1 The Original Hecht, Seinfeld, Dodge Mechanism 202

IV-2 The Carbon-Bond Mechanism 205

IV-3 Reactivities per Carbon Atom for Several Alkanes 209

IV-4 Rate Constants per Double Bond for the Reactions of Some Olefins with OH· at 300°K 210

IV-5 Initial Conditions for Simulations of the Toluene/NO_x Systems 276

IV-6 One-Hour-Average Ozone Concentrations Measured and Simulated with the Carbon-Bond Mechanism 278

I INTRODUCTION

For the last few years the United States Environmental Protection Agency (EPA) has sponsored a coordinated program comprising fundamental chemical research, smog chamber experimentation, and model development. The objective of this program is to develop a mathematical model capable of simulating the dynamics of the chemical reactions involving gaseous pollutants in the lower troposphere. This model, or kinetic mechanism, is to serve as a component of a more general model, one designed to predict atmospheric ozone concentrations by simulating the transport, dispersion, chemical reactions, and scavenging processes that affect air pollutants.

A kinetic mechanism is simply a set of chemical reactions and rate constants that is intended to describe some chemical process. From a kinetic mechanism for smog chemistry, one can derive a set of coupled, first-order, nonlinear differential equations that describe the rates of change of pollutant concentrations with time. These equations can be solved using a computer to model the changing concentrations of chemical species in a smog chamber. If the concentrations of these species could be accurately measured as a function of time, and the differential equations derived from the theory of gas-phase kinetics could be solved directly, then computer modeling based on kinetic mechanisms would be unnecessary. However, this is not the case; both data and theory are inadequate. Although computer modeling is relatively new and still developing, it can and does provide an important link between theoretical and experimental activities.

SAI began computer modeling with kinetic mechanisms when inadequacies in both data and theory were glaring. SAI's initial efforts, started in 1972 under EPA Contract 68-02-0580, resulted in the development of the Hecht, Seinfeld, and Dodge (HSD) kinetic mechanism (Hecht et al., 1974a). This work is described in three reports to the EPA: a detailed planning document (Seinfeld et al., 1973) and two final reports (Hecht et al., 1973; 1974b). Because the HSD mechanism was to be incorporated in a regional air pollution simulation model, it had to strike a balance between compactness of form and accuracy of prediction. The number of chemical species that could be included in it, and thus the extent of the mathematical description, were limited by the practical considerations of computing time and computer storage requirements. But an overly simplified mechanism might have omitted important reactions steps and thus have been inadequate for accurate prediction over a range of atmospheric conditions.

The HSD mechanism struck a balance by treating the important inorganic smog reactions explicitly, and by treating hydrocarbons in four groups, or "lumps": olefin, paraffin, aromatic, and aldehyde. It incorporated the latest knowledge of smog chemistry, but because of gaps in that knowledge it also incorporated some empirical parameters. The values of these parameters were chosen by fitting predicted concentration-time profiles to a set of smog chamber data.

The HSD mechanism was a significant improvement over the lumped mechanisms then available. The results presented by Hecht et al. (1974a) showed reasonable agreement with smog chamber data. In addition, by combining the numerical sensitivity and estimated uncertainty of each reaction and rate constant in the HSD mechanism, Hecht et al. (1974b) were able to determine which reactions and rate constants produced the greatest uncertainties in predictions, and were thus most in need of further study. Some problems were encountered, however, in attempting to apply the mechanism to situations other than smog chamber experiments and to apply it outside the range of concentrations and hydrocarbon mixes upon which it was based (Demerjian et al., 1974).

These problems stemmed largely from the use of parameters that were based on smog chamber data, not on the fundamental chemistry. Incorrect fundamental chemistry and chamber-dependent phenomena could be compensated for or masked by these parameters. No single set of parameters would fit all smog systems, and there was little theoretical guidance for adjusting the parameters for systems for which no experimental data existed.

Meanwhile, technological progress in smog chamber construction and analytical capabilities was making it possible to obtain more detailed and more reliable data. At the same time, the application of advanced computer hardware and software was reducing both the time and cost of computer modeling. These developments made it possible, at least for simple smog chamber experiments (one, two, or three hydrocarbons present initially), to trace many of the major intermediate oxidation products of carbon and hydrogen atoms from the initial hydrocarbon to carbon dioxide and water. The combination of the need for a better mechanism and the availability of more reliable and detailed data led to a new phase in SAI's work--the development of explicit kinetic mechanisms.

Whereas a lumped mechanism treats hydrocarbons in groups or "lumps," an explicit mechanism attempts to account for the fundamental or elementary reactions of every atom. For example, the explicit mechanism for propylene and NO_x in a smog chamber contains over 70 reactions involving 35 species. Explicit mechanisms are based on studies of the chemical kinetics of individual reactions. The results of many of these studies have been compiled and evaluated [e.g., Hampson and Garvin (1975), Demerjian et al. (1974)]. When data for a particular elementary reaction are insufficient, its rate constant and products can often be estimated from analogous reactions using thermodynamic principles (Benson, 1975). Because explicit mechanisms are based on the fundamental chemistry, a poor fit between predictions and measurements for a given species can sometimes be traced to uncertainties in chemical reactions or inaccuracies in smog chamber experiments. For example, poor fits between predictions and measurements for some propylene/NO_x experiments in the evacuable smog chamber at the University of California at Riverside (UCR) led Durbin et al. (1975) to hypothesize that the intensity from the UV light source in the chamber was decreasing more rapidly at short wavelengths than at long wavelengths. Subsequent measurements on replacement light sources at UCR were consistent with this hypothesis.

In the early stages of SAI's development of explicit mechanisms, smog chamber data could be fitted more closely with the parameterized HSD mechanism than with the explicit mechanisms. As knowledge of smog chemistry increased, this situation was reversed. At present, the explicit mechanisms predict smog chamber data better than the HSD mechanism, and without any adjustment of parameters they fit a much wider range of concentrations than does the HSD mechanism. They provide more detailed insight into the smog formation process. Because they are not as empirical, there is a theoretical justification for applying them outside the range of concentrations and hydrocarbon mixes used in smog chamber experiments. Furthermore, if chamber-dependent reactions are removed and appropriate atmospheric reactions (such as reactions on aerosols and other surfaces) are added, an explicit mechanism can be used as a component of a regional air pollution simulation model.

One might question the usefulness of explicit mechanisms in a regional model. Since the mechanism for propylene and NO_x alone contains over 70 reactions, surely an explicit mechanism for urban smog would contain too many reactions to be of practical use. A condensed version of the explicit mechanisms would combine the advantages of a basis in elementary chemical reactions and speed of computation. Near the end of this contract year, SAI began development of a new condensed mechanism, the carbon-bond mechanism.

Like the HSD mechanism, the carbon-bond mechanism employs lumped chemical species, but there are important differences. The HSD mechanism treats groups of molecules (e.g., aldehydes), whereas the carbon-bond mechanism treats groups of similarly bonded carbon atoms (e.g., carbonyl carbons). The carbon-bond mechanism is far easier to use because it was designed to accept the types of data most commonly reported. But the most important difference is the scientific basis: whereas the HSD mechanism was of necessity somewhat empirical, the carbon-bond mechanism is derived from the fundamental chemical reactions in smog as represented by explicit mechanisms. Thus the carbon-bond mechanism is a condensation of our understanding rather than a parameterization of our uncertainty.

Although the carbon-bond mechanism was developed recently, it has been applied to some smog chamber experiments. Preliminary results, presented in Chapter IV of this report, indicate that it is far more accurate than the HSD mechanism. Under EPA support, SAI is now refining the carbon-bond mechanism and developing guidelines to handle complex mixtures of hydrocarbons and to modify the mechanism as our knowledge of smog chemistry increases.

The actual computer modeling efforts of the past year have concentrated on smog chamber data taken by the Statewide Air Pollution Research Center located at the University of California at Riverside (UCR). The UCR experimental program was supported by EPA Grant No. 800649. In these sets of experiments, which were performed in an evacuable chamber, hydrocarbon and nitrogen oxide ratios and concentrations were varied in accordance with the principles of factorial design. The light source, temperature, and humidity were not varied systematically. Analytical data for every set included measurements at various times of nitrogen dioxide, nitric oxide, ozone, PAN, hydrocarbons, and carbonyl compounds. For some experiments, alkyl nitrate and olefin-oxide data were also supplied. The following sets of data were modeled and are discussed in this report:

- Propylene/NO_x--15 experiments
- Butane/NO_x--7 experiments
- Combined propylene/butane/NO_x--7 experiments
- Toluene/NO_x--10 experiments
- 1-Butene/NO_x--3 experiments.

SAI's initial modeling efforts using explicit mechanisms (Durbin et al., 1975) were based on a small amount of data supplied by UCR in 1975. During the past year more data and continued modeling efforts have made possible significant improvements in these mechanisms. The explicit mechanisms for the experiments listed above, except toluene/NO_x, can reproduce the results of smog chamber experiments with reasonable accuracy. Many improvements to the explicit mechanisms stemmed from recent experimental investigations of fundamental reactions. Changes were also made in the mechanisms to improve the simulations of UCR data. (Some of these changes may not have experimental validation.) Some significant improvements are as follows:

- Formation of peroxyformyl radicals from the formyl radical instead of $HO_2\cdot$ and CO.
- Formation of hydroxyperoxyalkyl radicals from the $OH\cdot$ oxidation of olefins.
- Formation of stable ozonides from the olefin-ozone reactions.
- Formation of alkyl nitrates as measured by UCR.
- The hydrogen rearrangement in an n-butoxyl radical to form a hydroxyperoxyalkyl radical.
- Formation of biacetyl from methylethylketone (MEK) and $OH\cdot$ radical.
- Elimination of most alkoxyl radical decomposition reactions.

The explicit mechanisms and the carbon-bond mechanism can now reproduce the overall pattern of the smog reaction--the hydrocarbon disappearance, NO_x chemistry, and the chemistry of secondary products such as aldehydes and PAN--and at the same time reproduce the maximum ozone concentration within ±20 percent (1σ). The explicit mechanisms are discussed in detail in Chapter III. In Chapter II, we review recent studies of inorganic chemical reactions. The carbon-bond mechanism is presented in Chapter IV. Chapter V contains an overview of the status of mechanism development, a summary of the differences between simulated and measured ozone concentrations for all simulations discussed in this report, except toluene/NO_x, and recommendations for future smog chamber experiments.

II INORGANIC CHEMISTRY

Many of the inorganic reactions have been reviewed by Demerjian et al. (1974) and by Hampson and Garvin (1975). Although some of the rate constants for these inorganic reactions are being refined with more sophisticated measuring techniques, the overall set has become well established. A recent change has been the photolysis of nitrous acid, HNO_2. HNO_2 photolysis can be an important source of hydroxyl radicals, which can initiate the organic reaction mechanisms. Review of the photolysis of HNO_2 and other recent changes in the inorganic reactions are presented in this section.

A. NO-OH· REACTION

Recent studies by Atkinson et al. (1975) and Cox 1974 have shown that the reaction of NO with hydroxyl radicals (OH·) has a rate constant three times faster than the second-order high pressure limit rate constant estimated by Baulch et al. (1973) and recommended by Hampson and Garvin (1975). Changing to the new rate constant of 9.0×10^3 $ppm^{-1}min^{-1}$ by itself slows the rate of smog formation in the mechanism because it is a significant but temporary sink for OH·.

B. HNO_2 PHOTOLYSIS

The photolysis of HNO_2 to form NO and hydroxyl radicals has recently been studied by Johnston and Graham (1973) and by Cox (1975). The absorption cross sections obtained by Graham were used to estimate the photolysis constant for HNO_2 photolysis. Recently, Graham (1975) reported an error in his previous observations of the absorption cross sections. The previous data were low by a factor of three. The faster photolysis rate constant agrees with the work of Cox (1975) and offsets the effect just described above from the faster rate constant for the reaction of NO with OH·. The HNO_2 photolysis rate constants used in the computer simulations are listed in Chapter III.

C. NO_2-OH·-M REACTION

The major sink for NO_x in smog chemistry appears to be this reaction. The reaction is in its falloff region at standard conditions and apparently has a complicated pressure and temperature dependence. Tsang (1973) investigated this reaction and reported extrapolated rate constants as a function of pressure and temperature. The value of the rate constant at 1 atm for the NO_2-OH· reaction is 6.6×10^3 $ppm^{-1}min^{-1}$. Anastasi et al. (1976a, 1976b) have recently reviewed this reaction as well as conducting experiments of their own near room temperature and pressure; they recommended a value of 1.6×10^4 $ppm^{-1}min^{-1}$. We are currently using an intermediate value of 9.2×10^3 $ppm^{-1}min^{-1}$, which was recommended by Cox (1975).

D. $HO_2^{\cdot}$-NO_2 REACTION

Farrow et al. (1975) postulated aerosols as possible nighttime sinks for hydroperoxy radicals ($HO_2^{\cdot}$). Although aerosol chemistry may be a possible sink, we have not included it in the explicit mechanisms. Also, the UCR chamber data do not include any information on aerosols. An alternative nighttime sink may be the reaction of HO_2 with NO_2. Simonaitis and Heicklen (1974) estimated a value for the ratio of rate constants for reaction of HO_2 with NO and NO_2 to be approximately 7:1; Cox and Derwent (1975) estimated a ratio of 10:1.

With a value of 2×10^3 $ppm^{-1}min^{-1}$ for the $HO_2^{\cdot}$-NO reaction, we find the maximum rate constant for $HO_2^{\cdot}$-NO_2 to be near 20 $ppm^{-1}min^{-1}$, if the products are HNO_2 and O_2. Our method for estimating a maximum value in this case was to run simulations with various values of this rate constant. The net effect of this reaction is to convert NO_2 into NO, because the HNO_2 formed rapidly photolyzes. Since this effect is opposite to the overall formation of ozone by conversion of NO into NO_2, our maximum estimate is in reality the value that begins to cut back noticeably on ozone formation. Nevertheless, a value of 20 ppm^{-1}min^{-1} still provides an important nighttime sink for $HO_2^{\cdot}$ radicals. It is noteworthy that 30 ppm^{-1}min^{-1} corresponds to the absolute value reported by Simonaitis and Heicklen (1974) and recommended by Hampson and Garvin (1975). It is below the value of 180 ppm^{-1}min^{-1} suggested by Cox and Derwent (1975). Currently, we are using a value of 20 ppm^{-1}min^{-1} to give better predictions of the smog chamber data.

During the writing of this document, Niki et al. (1976a) proposed that peroxynitric acid is the product of this reaction. They found that it rapidly disappeared in their chamber but its fate is still unknown.

E. $HO_2^{\cdot}$-NO REACTION

In last year's final report, SAI used a value of 800 ppm^{-1}min^{-1} for the reaction of $HO_2^{\cdot}$ with NO. Mabey and Hendry (1974) reported a value of 1.2×10^3 ppm^{-1}min^{-1} for this reaction. Cox and Derwent (1975) reported a value of 2×10^3 ppm^{-1}min^{-1} based on simulations of experimental data. We are currently using a value of 2×10^3 ppm^{-1}min^{-1} for this reaction.

In addition to the major route to produce OH· and NO_2, this reaction may provide a minor pathway to $HONO_2$, as suggested by Cox and Derwent (1975). Their estimate for the rate constant for $HONO_2$ formation was about 10 percent, or 200 ppm^{-1}min^{-1}. The removal of NO_x in smog chemistry is still somewhat uncertain and this reaction suggests not only one more route of removal but the analogous reactions, $RO_2^{\cdot}$-NO, as well. As suggested by Cox and Derwent, this alternate path would presumably require a third body and would be competitive only at high pressure and low temperature, such as those found in the atmosphere. These reactions are not included in the kinetic mechanisms due to their uncertainties.

F. HNO_2 FORMATION

The formation of HNO_2 was discussed by Durbin et al. (1975). The following two reactions may occur:

$$NO + NO_2 + H_2O \rightarrow 2HNO_2 \quad ,$$

$$2HNO_2 \rightarrow NO + NO_2 + H_2O \quad .$$

Chan et al. (1976) reported the following gas-phase rate constants for these reactions:

$$k_{NO-NO_2-H_2O} = 2.2 \times 10^{-9}\ ppm^{-2}min^{-1} \quad ,$$

$$k_{2HNO_2} = 1.3 \times 10^{-3}\ ppm^{-1}min^{-1} \quad .$$

These values have been used in this study. The value of $k_{NO-NO_2-H_2O}$ is approximately 10 times slower than the value recommended by Hampson and Garvin (1975). The new values are two orders of magnitude lower than the heterogeneous values used by Durbin et al. (1975). Therefore, gas-phase production of HNO_2 through the above reaction is slow. Nevertheless, it is noteworthy that Chan et al. (1976) were unable to load their chamber without making substantial amounts of HNO_2. Thus they postulated that either heterogeneous formation occurs during the gas handling and dilution or localized high concentrations in the same steps lead to substantial and irregular amounts formed initially. These suggestions, of course, have rather profound implications for both smog chamber and real atmosphere chemistry. They have led us to assume that initial and possibly irregular amounts of HNO_2 can be found in the loading phase of a smog chamber experiment, or even in the atmosphere, due to localized high concentrations and/or heterogeneous effects. The actual initial amounts of HNO_2 that exist at sunrise in the real atmosphere and at the onset of smog chamber experiments remain important unsolved aspects of smog chemistry. To obtain the proper reactivity in computer simulations, a small amount (usually from 0.001 to 0.03 ppm) of HNO_2 is introduced initially. The initial concentrations of HNO_2 may seem high but no actual measurements of HNO_2 have been reported by UCR. High local HNO_2 concentrations may be possible initially if there are regions in the chamber where NO and NO_2 concentrations are high, e.g., near the area where the NO and NO_2 are introduced into the chamber (Chan et al., 1976). Also, HNO_2 may have come off the walls between experiments at UCR (Bufalini et al., 1972).

G. HNO_3 FORMATION

The reaction of N_2O_5 with H_2O has been shown to have a major effect in smog chemistry--primarily after the NO_2 peak--by Durbin et al. (1975). Morris and Niki (1973) found that for the reaction

$$N_2O_5 + H_2O \rightarrow 2HNO_3$$

the upper limit of the gas-phase rate constant was near 1.5×10^{-5} ppm^{-1} min^{-1}. We have chosen 5×10^{-6} $ppm^{-1}min^{-1}$ for the rate constant of the reaction of N_2O_5 with H_2O. This value was chosen to give an overall optimum prediction of NO_2 behavior. Note that this value is much less than the maximum estimated gas-phase rate. Thus the heterogeneous component of the above reaction may be very small in the UCR chamber.

III ORGANIC CHEMISTRY

Much of SAI's initial work on propylene/NO_x and butane/NO_x systems was documented by Durbin et al. (1975) in last year's final report. Our work this year concentrated mainly on the following:

- Improvement of the mechanisms for propylene/NO_x and butane/NO_x.
- Further efforts in the development of an explicit mechanism for toluene/NO_x chemistry.
- Testing the combined explicit mechanisms on UCR's combined butane/propylene/NO_x data.
- Developing an explicit mechanism for 1-butene/NO_x chemistry.

In this chapter, we discuss the results of these efforts.

A. PROPYLENE/NO_x CHEMISTRY

The explicit propylene mechanism presented last year (Durbin et al., 1975) has been changed in the following ways:

- The addition product of hydroxyl radicals with propylene does not include a hydride shift.
- A higher rate constant has been used for the reaction of propylene with hydroxyl radicals.
- The product of formyl radicals plus molecular oxygen is taken as peroxyformyl radicals.
- Changes have been made in the mechanism of the propylene-O_3 reaction.
- Changes have been made in the mechanism for the unimolecular decomposition of peroxyacetyl nitrate (PAN).
- Propionaldehyde formation from the propylene-O atom reaction has been added.

These changes are discussed in detail below.

A major change in the explicit propylene mechanism involves the treatment of the propylene-OH· reaction. In last year's final report (Durbin et al., 1975), this reaction was assumed to proceed by addition followed by a hydride shift to produce alkoxyl radicals. These radicals then react predominantly with molecular oxygen to produce propionaldehyde and acetone. This treatment has been changed for two reasons. Recent measurements of propionaldehyde at UCR are poorly simulated by this treatment. More importantly, this treatment was developed to simulate high acetone concentrations measured at UCR. Much of this acetone apparently came from the acetone used to clean the smog chamber during construction. Experiments performed recently show much lower acetone concentrations. We now believe that addition of OH· followed by a hydride shift is only a minor pathway for the oxidation of propylene.

Niki et al. (1972) discussed the following mechanism for addition of OH· to propylene:

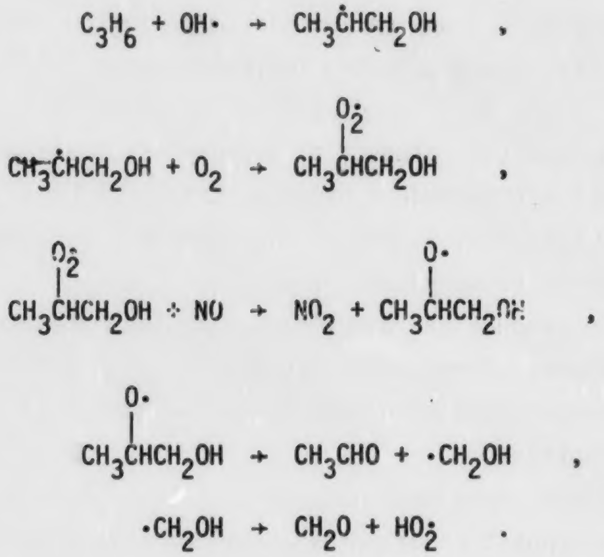

$$C_3H_6 + OH\cdot \rightarrow CH_3\dot{C}HCH_2OH \quad ,$$

$$CH_3\dot{C}HCH_2OH + O_2 \rightarrow CH_3\overset{O_2\cdot}{\overset{|}{C}}HCH_2OH \quad ,$$

$$CH_3\overset{O_2\cdot}{\overset{|}{C}}HCH_2OH + NO \rightarrow NO_2 + CH_3\overset{O\cdot}{\overset{|}{C}}HCH_2OH \quad ,$$

$$CH_3\overset{O\cdot}{\overset{|}{C}}HCH_2OH \rightarrow CH_3CHO + \cdot CH_2OH \quad ,$$

$$\cdot CH_2OH \rightarrow CH_2O + HO_2\cdot \quad .$$

The above reaction scheme has been incorporated into the explicit propylene mechanism as the pathway of oxidation of propylene by hydroxyl radicals. This pathway leads to equal amounts of acetaldehyde and formaldehyde, in keeping with most of the UCR data. However, the most recent data show considerably less acetaldehyde. The lower acetaldehyde data have also introduced a large carbon mass loss in the UCR results. If future studies show that these latest results are correct and all the earlier results with virtually equal amounts of acetaldehyde and formaldehyde were wrong, then the present mechanism is certainly in error.

Besides this mechanism change, a higher rate constant has been measured independently by Davis (1976) and Atkinson and Pitts (1975). The new rate constant for propylene-OH· reaction is 3.8×10^4 $ppm^{-1}min^{-1}$. A review of Davis' work on oxidation of olefins is presented in Table III-1. The new value of 3.8×10^4 $ppm^{-1}min^{-1}$ is 1.5 times higher than the previously accepted value for the reaction of propylene with OH·. Therefore, the modeling of the propylene system with the higher rate constant requires less hydroxyl radicals to fit the decomposition curves for propylene. The initial slope has normally been fitted by using an appropriate amount of nitrous acid, which photolyzes to give the initial hydroxyl radicals. The required amount of HNO_2 has always been near the equilibrium value (Durbin et al., 1975). Using less of this unmeasured species appears to be desirable so as to place more emphasis on the other initial sources of radicals, namely, aldehydes and oxygen atoms from nitrogen dioxide photolysis.

However, the faster olefin-hydroxyl rate constant creates a problem: the disparity between our simulated hydroxyl concentrations and those measured by Wang et al. (1975) is larger and the loss of NO_x to the nitrogen dioxide-hydroxyl reaction is no longer sufficient to match the measured loss. Although the high hydroxyl radical concentrations reported by Wang have been explained by Davis et al. (1976) as resulting from too broad a laser pulse, the inability of the present chemical mechanism to account for NO_x loss is a difficult problem. Davis et al. (1976) have also measured much lower hydroxyl radical concentrations in the troposphere than reported by Wang et al. (1975).

TABLE III-1. RATE CONSTANTS FOR THE OLEFIN-OH· REACTION

Olefin	k ($ppm^{-1}min^{-1}$)
Ethylene	7.9×10^3
Propylene	3.8×10^4
1-Butene	4.8×10^4
cis-2-Butene	7.1×10^4
Tetramethylethylene	8.4×10^4

Source: Davis (1976).

2. Peroxy Radical Chemistry

Production of the hydroxyperoxyalkyl radicals forms the basis for the organic reactions producing ozone and secondary products. Three main areas of organic radical chemistry were investigated in detail:

> Reactions of alkoxyl radicals with molecular oxygen and thermal decomposition.

> Reactions of organic radicals with NO_x (NO, NO_2).

> Sinks of organic radicals.

Each of these areas is discussed below.

a. Reactions of Alkoxyl Radicals with Molecular Oxygen and Thermal Decomposition

Reactions of alkoxyl radicals with molecular oxygen have recently been studied by Barker et al. (1976) and Mendenhall et al. (1975). Their measurement of the rate constant for the reaction

$$CH_3O\cdot + O_2 \rightarrow HCHO + HO_2^{\cdot}$$

is approximately 100 times faster than the 3.9×10^{-3} $ppm^{-1}min^{-1}$ rate constant estimated by Heicklen (1968) and used in the mechanism and the 4.4×10^{-3} $ppm^{-1}min^{-1}$ recommended by Hampson and Garvin (1975). The new value for the rate constant of the $CH_3O\cdot - O_2$ reaction is approximately 0.95 $ppm^{-1}min^{-1}$ as estimated by Mendenhall et al. and Barker et al. We have incorporated this value into the kinetic mechanism.

Bell et al. (1951) investigated the thermal decomposition of methoxyl, ethoxyl, isopropoxyl, n-butoxyl, iso-butoxyl, and t-butoxyl radicals. From measurements of the relative rates of abstraction and decomposition, Bell et al. compared the stabilities of the alkoxyl radicals formed assuming that the rate of hydrogen atom abstraction is the same for all alkoxyl radicals. They found that the shorter chain alkoxyl radicals are more stable than the longer chain alkoxyl radicals. The order of decreasing stability is as follows:

$$CH_3O\cdot > C_2H_5O\cdot > n\text{-}C_4H_9O\cdot > i\text{-}C_3H_7O\cdot > i\text{-}C_4H_9O\cdot \sim t\text{-}C_4H_9O\cdot \quad .$$

The relative ratios of the rates of thermal decomposition measured by this technique were ∼0:1:6:18:70:70. The order of decreasing stabilities as listed above correlates with the minimum enthalpy required for decomposition as discussed by Gray et al. (1967). Table III-2 lists the enthalpy required for decomposition.

TABLE III-2. THERMOCHEMISTRY OF ALKOXYL RADICALS

Radical	Minimum Enthalpy Required for Decomposition (kcal mol^{-1})
$CH_3O\cdot$	22
$C_2H_5O\cdot$	10
n-$C_4H_9O\cdot$	10
i-$C_3H_7O\cdot$	9
i-$C_4H_9O\cdot$	7
t-$C_4H_9O\cdot$	2

Source: Gray et al. (1967).

Gray et al. estimated the rate constant for the decomposition of methoxyl radicals to be comparable to the rate constant for ethyl radical (CH_3CH_2) decomposition, which was estimated to be approximately 2.7 x 10^{-10}min^{-1}. For ethoxyl radical decomposition, Gray et al. estimated a value of 0.26 min^{-1} for the rate constant. Wijnen (1958) estimated a value of approximately 83 min^{-1} for the rate constant of the decomposition of ethoxyl radicals based on photolysis of ethyl propionate. Even though the two estimates differ by a factor of approximately 300, the decomposition of the shorter chain radicals such as ethoxyl and propoxyl is unimportant compared with their reaction with molecular oxygen. This is exemplified by the ratio

$$\frac{\text{Rate}_{(O_2)}}{\text{Rate}_{(\text{decomp})}} = \frac{k_{(O_2)}\,[RO][O_2]}{k_{(\text{decomp})}\,[RO]} \quad ,$$

$$= \frac{k_{(O_2)}}{k_{(\text{decomp})}}\,[O_2] \quad ,$$

$$\sim \frac{2300}{1} \quad .$$

assuming that

$$k_{(O_2)} \sim 0.9\ \mathrm{ppm^{-1}min^{-1}} \quad ,$$

$$k_{(decomp)} \sim 83\ \mathrm{min^{-1}} \quad ,$$

$$[O_2] \sim 2.1 \times 10^5\ \mathrm{ppm} \quad .$$

The stability of the shorter chain alkoxyl radicals has led us to eliminate their decomposition reactions from the kinetic mechanism. In the "explicit" propylene mechanism, the only alkoxyl radicals formed are methoxyl and ethoxyl.

The current mechanism also leads to hydroxy-alkoxyl radicals:

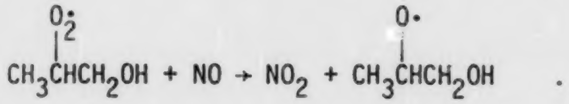

$$\mathrm{CH_3\overset{O_2\cdot}{\overset{|}{C}}HCH_2OH + NO \rightarrow NO_2 + CH_3\overset{O\cdot}{\overset{|}{C}}HCH_2OH} \quad .$$

In this case we have assumed that the unimolecular decomposition occurs exclusively:

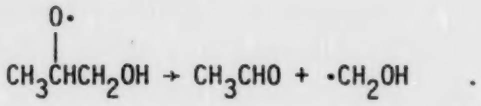

$$\mathrm{CH_3\overset{O\cdot}{\overset{|}{C}}HCH_2OH \rightarrow CH_3CHO + \cdot CH_2OH} \quad .$$

This assumption is based on the fact that until the arrival of the latest UCR data discussed above there was no mass balance loss. Hence the formation of the acyloin,

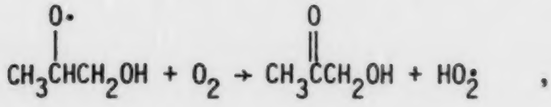

$$\mathrm{CH_3\overset{O\cdot}{\overset{|}{C}}HCH_2OH + O_2 \rightarrow CH_3\overset{O}{\overset{\|}{C}}CH_2OH + HO_2\cdot} \quad ,$$

rather than acetaldehyde was unjustified.

b. Reactions of Organic Radicals with NO_x (NO and NO_2)

The production of ozone from the organic reactions occurs with the conversion of NO to NO_2 through the series of reactions,

$$RO_2^{\cdot} + NO \rightarrow RO\cdot + NO_2 \quad .$$

Only two published laboratory studies of this reaction have been performed, one by Spicer et al. (1973) and the other by Simonaitis and Heicklen (1974). Simonaitis' work disclaimed Spicer's work, both of which were performed at the same laboratory but with different experimental procedures. Simonaitis found that the reaction

$$CH_3O_2^{\cdot} + NO \rightarrow CH_3O\cdot + NO_2$$

leads to the products shown at least 80 percent of the time. From Simonaitis' private communications, Finlayson and Pitts observed this reaction to occur totally through the above pathway. Finlayson and Pitts (1976) in a review article reported later that $RO_2^{\cdot}$ and NO react to produce NO_2 and RO· to a very large extent. Only the quantum yield of NO_2 was reported by Simonaitis and Heicklen (1974). We estimate the rate constant for the series of $RO_2^{\cdot}$-NO reactions to be 2.0×10^3 $ppm^{-1}min^{-1}$, which is the value measured independently for the rate constant of the $HO_2^{\cdot}$-NO reaction by Cox and Derwent (1975) and Hendry (1976). Demerjian et al. (1974) estimated the $RO_2^{\cdot}$-NO rate constant to be 9.1×10^2 ppm^{-1} min^{-1} based on the value they used for the rate constant of the $HO_2^{\cdot}$-NO reaction.

The reactions of peroxyalkyl radicals with nitrogen dioxide were also studied by Simonaitis and Heicklen (1974). They found the ratio of the rate constants was $k_{(RO_2^{\cdot}-NO)}/k_{(RO_2^{\cdot}-NO_2)} = 2.2$. Their conclusions are in agreement with Spicer et al. (1973), who presented the possible pathways for the reaction of $CH_3O_2^{\cdot}$ and NO_2 as:

$$CH_3O_2^{\cdot} + NO_2 \rightarrow CH_3O_2NO_2 \quad ,$$

$$CH_3O_2^{\cdot} + NO_2 \rightarrow HCHO + HNO_3 \quad ,$$

$$CH_3O_2^{\cdot} + NO_2 \rightarrow CH_3O\cdot + NO_3 \quad .$$

The third reaction path was found to be unimportant.

The peroxynitrate formed in the first reaction may react with NO_2 to produce methyl nitrate or with NO to produce methyl nitrite, according to Spicer et al. Simonaitis and Heicklen do not give a definite mechanism for reactions involving the peroxynitrate.

We are not including the $RO_2^{\cdot}$-NO_2 reactions in the kinetic mechanism until more definite evidence is found for these reactions. As in the case of the reaction of $HO_2^{\cdot}$ with NO_2, the peroxyalkyl radical reaction diminishes the formation of ozone. The ozone formation chemistry as presently understood requires a high NO_2/NO ratio to produce ozone. This ratio is thought to be increased by peroxy radicals. Thus, any significant reaction of $RO_2^{\cdot}$ with NO_2 would limit this ratio and demand some other method of producing ozone or some other means of increasing this ratio.

The series of RO·-NO reactions has been studied by Batt et al. (1975). They found that the primary pathway is the formation of an alkyl nitrite:

$$RO\cdot + NO \rightarrow RONO \ , \quad k = 4.9 \times 10^4 \ ppm^{-1}min^{-1} \quad .$$

A second pathway is also discussed by Batt et al.:

$$RO\cdot + NO \rightarrow RCHO + HNO \; , \quad k = 9.8 \times 10^3 \; ppm^{-1}min^{-1} \quad .$$

The activation energies for several different alkyl groups were found to be near zero; there seems to be no dependence on the alkyl group in the alkoxyl radical (RO·). Apparently, the alkyl nitrite formed rapidly photolyzes to form the alkoxyl radical and nitric oxide (Calvert and Pitts, 1966). The rate of photolysis seems uncertain. At moderate photolysis rates, simulations with nitrite chemistry show an irregular bulge in the propylene decay curve that does not correspond to the smooth decay curves reported by UCR. Although some of the NO_x missing from the NO_x mass balance analysis may be in the form of nitrites, we decided to leave the nitrite chemistry out of the mechanism because of the uncertainty in the overall photolysis rate.

The series of reactions involving alkoxyl radicals and NO_2 has recently been studied by Mendenhall et al. (1975) and Barker et al. (1976). Mendenhall et al. found the value of the rate constant for $RO\cdot\text{-}NO_2$ to be 7.8×10^3 $ppm^{-1}min^{-1}$, and Barker et al. found this rate constant to be 1.5×10^4 $ppm^{-1}min^{-1}$. Mendenhall et al. estimated their results from the pyrolysis of n-propyl nitrate and assumed the activation energy to be zero. Barker et al. calculated their results from estimates of the ratio for $k_{(RO\cdot\text{-}NO)}/k_{(RO\cdot\text{-}NO_2)} = 2 \pm 1$, using the value of Batt et al. for the rate constant for $RO\cdot\text{-}NO$ to estimate the $RO\cdot\text{-}NO_2$ rate constant. We are using the value of 2×10^4 $ppm^{-1}min^{-1}$ to improve the fit of the computer simulations to UCR's nitrate data, which are available for experiments EC-60, 95, 96, and 121.

Two reaction paths have been reported for the series of $RO\cdot\text{-}NO_2$ reactions:

$$RO\cdot + NO_2 \xrightarrow{a} RONO_2 \quad ,$$

$$RO\cdot + NO_2 \xrightarrow{b} RCHO + HNO_2 \quad .$$

Barker et al. (1976) estimated the ratio k_b/k_a to be 0.3 from pseudo-steady-state calculations. Baker and Shaw (1965) concluded that k_b/k_a is approximately 0.11. Wiebe et al. (1973) reported a value of 0.11 for the ratio of k_b/k_a. We are using a ratio of 0.11 for the computer simulations in order to be consistent with experimental observations. We have placed the above two reactions in the kinetic mechanism.

c. Sinks of Organic Radicals

For the major sink of peroxyalkyl and peroxyacyl radicals in the kinetic mechanism, we have used the reaction with $HO_2^{\cdot}$,

$$RO_2^{\cdot} + HO_2^{\cdot} \rightarrow ROOH + O_2$$

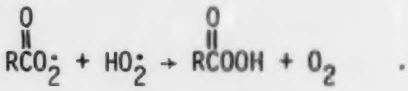

$$R\overset{O}{\overset{\|}{C}}O_2^{\cdot} + HO_2^{\cdot} \rightarrow R\overset{O}{\overset{\|}{C}}OOH + O_2 \quad .$$

We estimated the rate constants for these reactions based on the rate constant for the recombination of $HO_2^{\cdot}$ radicals,

$$HO_2^{\cdot} + HO_2^{\cdot} \rightarrow H_2O_2 + O_2 \quad .$$

Hampson and Garvin (1975) recommended a value of 8.3×10^3 ppm^{-1}min^{-1} for the recombination of $HO_2^{\cdot}$ radicals. In order to fit the highly reactive experiments such as EC-5, we assumed that the $HO_2^{\cdot}$-$HO_2^{\cdot}$ reaction rate constant is 4×10^3 ppm^{-1}min^{-1}, which is the value recommended by Lloyd (1974) and the lower limit recommended by Hampson and Garvin (1975). We also assumed that $RO_2^{\cdot}$ radicals will react at about the same rate as $HO_2^{\cdot}$ radicals.

We have chosen values of 1 x 10^4 and 4.0 x 10^3 $ppm^{-1}min^{-1}$ for the rate constants of the reactions of peroxyacyl and peroxyalkyl radicals with HO_2 radicals as upper limits to simulate the UCR data.

Another possible sink of peroxyalkyl radicals is the formation of alkoxyl radicals through peroxyalkyl radical-peroxyalkyl radical reactions. Simulations using these radical-radical reactions have shown them to be unimportant in the propylene series of experiments, but they could be important in the propylene/butane/NO_x system discussed later. In the propylene system of experiments the highest peroxy radical concentrations in our simulations (9 x 10^{-3} ppm) were found in experiment EC-18. The radical-radical reactions would be unimportant unless their rate constants were at least 1 x 10^4 $ppm^{-1}min^{-1}$. The concentrations of the peroxy radicals are controlled to some extent by their reactions with nitric oxide, for which we have taken rate constants to be 2 x 10^3 $ppm^{-1}min^{-1}$.

Peroxyacyl radicals may not react with $HO_2^{\cdot}$ at the same rate as peroxyalkyl radicals. We lowered the peroxyalkyl radical rate constants to fit the sharp ozone rise seen in EC-5 (and also, to a lesser extent, in EC-11). Using the same constants for peroxyacyl radicals, however, allowed too much PAN to form in the simulations of EC-11 and especially EC-18. Therefore, we have speculated that the peroxyacyl radicals may react with hydroperoxy radicals at a much faster rate, 1 x 10^4 $ppm^{-1}min^{-1}$.

Highly different rates for radical-radical reactions involving peroxy radicals have recently been seen by Whitbeck et al. (1976). Although their combination rate for $CH_3O_2^{\cdot}$ radicals of about 500 $ppm^{-1}min^{-1}$ agreed with Parkes et al. (1973), the combination rate for $(CH_3)_3CO^{\cdot}$ radicals was found to be about three orders of magnitude slower. Demerjian et al. (1974) also discussed the possibility of very divergent radical-radical rate constants based on the liquid-phase work of Bennett et al. (1970).

3. Reactions of Olefins with Nitrate Radicals ($NO_3^{\cdot}$)

Japar and Niki (1975) performed a study of the reactions of $NO_3^{\cdot}$ with a series of olefins. Table III-3 lists their comparisons of the rate constants of the reactions of $NO_3^{\cdot}$, $O(^3P)$, and O_3 with olefins. For the short chain olefins, the rate constants for the reactions with $NO_3^{\cdot}$ are 1000 times lower than the rate constants for the reactions involving $O(^3P)$, yet the rate constants are similar for longer internal olefins. In anticipation of future UCR experiments involving longer chain olefins, we added the reaction of $NO_3^{\cdot}$ with olefins to the kinetic mechanism. The rate constant employed for the reaction of propylene with $NO_3^{\cdot}$ is 8 ppm^{-1} min^{-1}. The products observed by Japar and Niki for this reaction were NO_2 and a compound that absorbs near 1670 cm^{-1} in the infrared region. The significance of this reaction can be completely assessed only after further experimental work is performed by UCR on longer chain olefin/NO_x systems. The nitrate reaction will reduce or eliminate the significance of the formation of nitric acid via the reaction of dinitrogen pentoxide with water:

$$NO_3^{\cdot} + NO_2 \rightleftarrows N_2O_5 \quad ,$$

$$N_2O_5 + H_2O \rightarrow 2HNO_3 \quad .$$

Also, competition for the nitrate radical, which usually reacts with NO,

$$NO_3^{\cdot} + NO \rightarrow 2NO_2 \quad ,$$

could lower the ozone produced from the internal olefins by removing this source of conversion of NO to NO_2.

TABLE III-3. COMPARISON OF THE REACTIVITIES OF $O(^3P)$ ATOMS, OZONE, AND NO_3 TOWARD OLEFINS

Olefin	Rate Constant ($ppm^{-1}min^{-1}$)		
	$k_{O(^3P)}$*	k_{O_3}†	k_{NO_3}
Ethylene	9.2×10^2	2.8×10^{-3}	1.37 ± 0.15
Propylene	5.3×10^3	1.9×10^{-2}	7.82 ± 0.44
Propylene-d_6	--	2.2×10^{-2}	8.71 ± 0.59
1-Butene	5.3×10^3	1.8×10^{-2}	11.5 ± 1.2
Isobutene	2.2×10^4	2.1×10^{-2}	162 ± 14.8
trans-2-Butene	2.7×10^4	3.8×10^{-1}	207 ± 14.8
cis-2-Butene	2.2×10^4	2.4×10^{-1}	266 ± 29.5
2-Methyl-2-butene	7.4×10^4	7.2×10^{-1}	8120 ± 738
2,3-Dimethyl-2-butene	9.6×10^4	2.2	54600 ± 7380

---

*Based on $k(C_3H_6\text{-}O) = 5.3 \times 10^3\ ppm^{-1}min^{-1}$, Stuhl and Niki (1971), and the relative reactivities of Cvetanovic (1963).

†Japar et al. (1974).

Source: Japar and Niki (1975).

4. Formyl Radical Chemistry

Formyl radicals are produced by the photolysis of aldehydes and by reaction of hydroxyl radicals with formaldehyde. Until recently, hydroperoxy radicals ($HO_2^{\cdot}$) and carbon monoxide were the only species produced from the reaction of formyl radicals in air according to our mechanism (Durbin et al., 1975). Formyl radicals undergo the reactions:

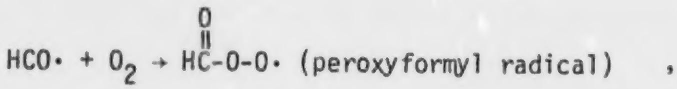

$$HCO\cdot + O_2 \rightarrow H\overset{\overset{\displaystyle O}{\|}}{C}\text{-}O\text{-}O\cdot \text{ (peroxyformyl radical)} \quad ,$$

$$HCO\cdot + O_2 \rightarrow HO_2^{\cdot} + CO \quad .$$

The ratio $k_{HCO_3^{\cdot}}/k_{HO_2^{\cdot}\text{-}CO}$ has been studied by Osif and Heicklen (1975), who found a value of approximately five. Niki et al. (1976a) studied the products of the oxidation of formyl radicals. Using a Fourier-transform infrared spectrometric technique, they found that over 50 percent of the reactions of formyl radicals with molecular oxygen formed peroxyformyl radicals. Therefore, the main reaction path is the formation of $HCO_3^{\cdot}$ radicals. The formation of $HCO_3^{\cdot}$ has an effect on conversion of NO to NO_2 primarily after disappearance of propylene. There is an increase in ozone production because the peroxyformyl radical is assumed to react with NO in the following manner:

$$HCO_3^{\cdot} + NO \rightarrow NO_2 + HO_2^{\cdot} + CO_2 \ , \quad k = 2 \times 10^3 \ ppm^{-1}min^{-1} \quad ,$$

$$HO_2^{\cdot} + NO \rightarrow NO_2 + OH\cdot \quad .$$

The exclusive formation of $HO_2^{\cdot}$ from $HCO\cdot\text{-}O_2$ produces only a single conversion of NO. Including the formation of $HCO_3^{\cdot}$ has led to improved fits of most UCR experiments by the kinetic mechanism.

5. Aldehyde Chemistry

The importance of aldehyde chemistry has been discussed by Hecht et al. (1974b) and by Durbin et al. (1975). The emphasis of the present discussion is on fitting the decay of aldehydes as seen in the UCR data. If the decay of aldehydes is not matched, then the rate of radical production from their decay will be incorrect.

Aldehydes decay in the present mechanism by essentially three paths:

- Photolysis to give radicals.
- Photolysis to give stable products.
- Reaction with hydroxyl radicals to give acyl radicals, which in turn immediately react to give peroxyacyl radicals.

The light intensities and hydroxyl radical concentrations in our simulations of UCR experiments produce comparable decay rates for photolysis and hydroxyl radical reactions. The mechanism itself also tends to equalize the two modes in that the photolysis supplies radicals which, after some radical transfer reactions, produce hydroxyl radicals that react with the aldehydes.

Herron and Penzhorn (1969) estimated the lower limit for the rate of the aldehyde-OH· reaction to be 9.8×10^3 $ppm^{-1}min^{-1}$. We had been using the value of 2.1×10^4 $ppm^{-1}min^{-1}$ measured by Morris and Niki (1971). Volman and Gorse (1972) estimated the rate constant for the reaction of propionaldehyde with hydroxyl radicals to be approximately 5.6×10^3 $ppm^{-1}min^{-1}$. We are currently using a rate constant of 1×10^4 to predict aldehyde decay behavior.

Photolysis of aldehydes was discussed in last year's report (Durbin et al., 1975). It was suggested that more spectral data were needed to account for any changes that might occur in the aldehyde photolysis part of the spectrum (the short wavelength end). These changes might be different from the nitrogen dioxide photolysis part of the ultraviolet spectrum (primarily the long wavelength end). The last few runs from UCR have included spectral measurements.

Two important results of having spectral data and therefore reliable aldehyde photolysis constants data have been the following:

- The decay curves of aldehydes can be fitted by choosing the proper hydroxyl radical rate constant--either the published value (2×10^4) given by Hampson and Garvin (1975) is too high or our model has too many hydroxyl radicals, as indicated by the lower value (1×10^4) discussed above.
- The magnitude of the maintenance source of radicals from aldehydes can be specified with greater accuracy. Some uncertainty still exists here because the quantum yields of the aldehyde photolysis reactions are uncertain.

6. Olefin-O_3 Reactions

There has not been any major change in the mechanism for the reaction of propylene with O_3 The O'Neal-Blumstein mechanism (1973) is still incorporated in the propylene mechanism with a minor change for the production of peroxyformyl radicals and ozonides. The ozone-propylene reactions are as follows;

$$C_3H_6 + O_3 \rightarrow HCO_3^{\cdot} + CH_3CHO + OH\cdot \quad , \quad k = 0.005\ ppm^{-1}min^{-1} \quad ,$$

$$C_3H_6 + O_3 \xrightarrow{O_2} HCHO + CH_3C(O)O_2^{\cdot} + OH\cdot \ , \quad k = 0.005\ ppm^{-1}min^{-1} \quad .$$

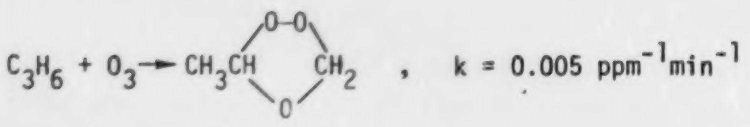

$$C_3H_6 + O_3 \rightarrow CH_3CH(O\text{-}O)(O)CH_2 \quad , \quad k = 0.005\ ppm^{-1}min^{-1} \quad .$$

The injection of radicals from these reactions has a major effect on reactivity. There may be some evidence that these reactions do not give as many radicals as we had previously assumed. At the 1976 ACS national meeting, Niki et al. (1976b) reported seeing stable ozonides from the ozone-propylene reaction with an FTS detector. We have found that a 33 percent pathway from the ozone-olefin reaction gives better predictions of species behavior. Yet, there is still a major uncertainty as to the products of the ozone-olefin reactions. The key points of uncertainty are as follows:

> The extent of stable ozonide formation is not known: it could be either a major or only a trivial fraction of the reaction.
> The need for either reaction path depends on the acetaldehyde/formaldehyde ratio, which has not been consistent in the UCR data.
> The need for a maintenance source of radicals depends on the NO_x sink and whether or not removing NO_x would remove radicals.

7. PAN Chemistry

Recent investigations of peroxyacetyl nitrate (PAN) chemistry by Pate et al. (1976) have led us to change the products of the decomposition of PAN from $NO_3^{\cdot}$, CO_2, and $CH_3O_2^{\cdot}$ to $CH_3CO_3^{\cdot}$ and NO_2. Pate et al. presented a mechanism (listed in Table III-4) to account for the kinetics of PAN decomposition and the observed products. We used the mechanism to model their data presented in Figure III-1. In the Figure III-1 two sets of simulations are presented. The first set (represented by X's) represents our efforts to fit the bottom curve (NO_0 = 26 ppm). When the bottom curve is closely predicted, the top curve (NO_0 = 93 ppm) is

TABLE III-4. MECHANISM FOR PAN DECOMPOSITION

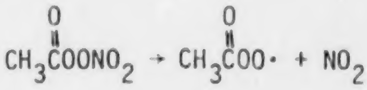

$$\mathrm{CH_3\overset{O}{\overset{\|}{C}}OONO_2 \rightarrow CH_3\overset{O}{\overset{\|}{C}}OO\cdot + NO_2}$$

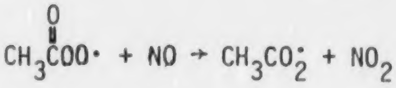

$$\mathrm{CH_3\overset{O}{\overset{\|}{C}}OO\cdot + NO \rightarrow CH_3CO_2^{\cdot} + NO_2}$$

$$\mathrm{CH_3CO_2^{\cdot} \rightarrow CH_3^{\cdot} + CO_2}$$

$$\mathrm{CH_3^{\cdot} + O_2 \rightarrow CH_3O_2^{\cdot}}$$

$$\mathrm{CH_3^{\cdot} + NO \rightarrow CH_3NO}$$

$$\mathrm{CH_3^{\cdot} + NO_2 \rightarrow CH_3NO_2}$$

$$\mathrm{CH_3O_2^{\cdot} + NO \rightarrow CH_3O\cdot + NO_2}$$

$$\mathrm{CH_3O\cdot + NO \rightarrow CH_3ONO}$$

$$\mathrm{CH_3O\cdot + NO_2 \rightarrow CH_3ONO_2}$$

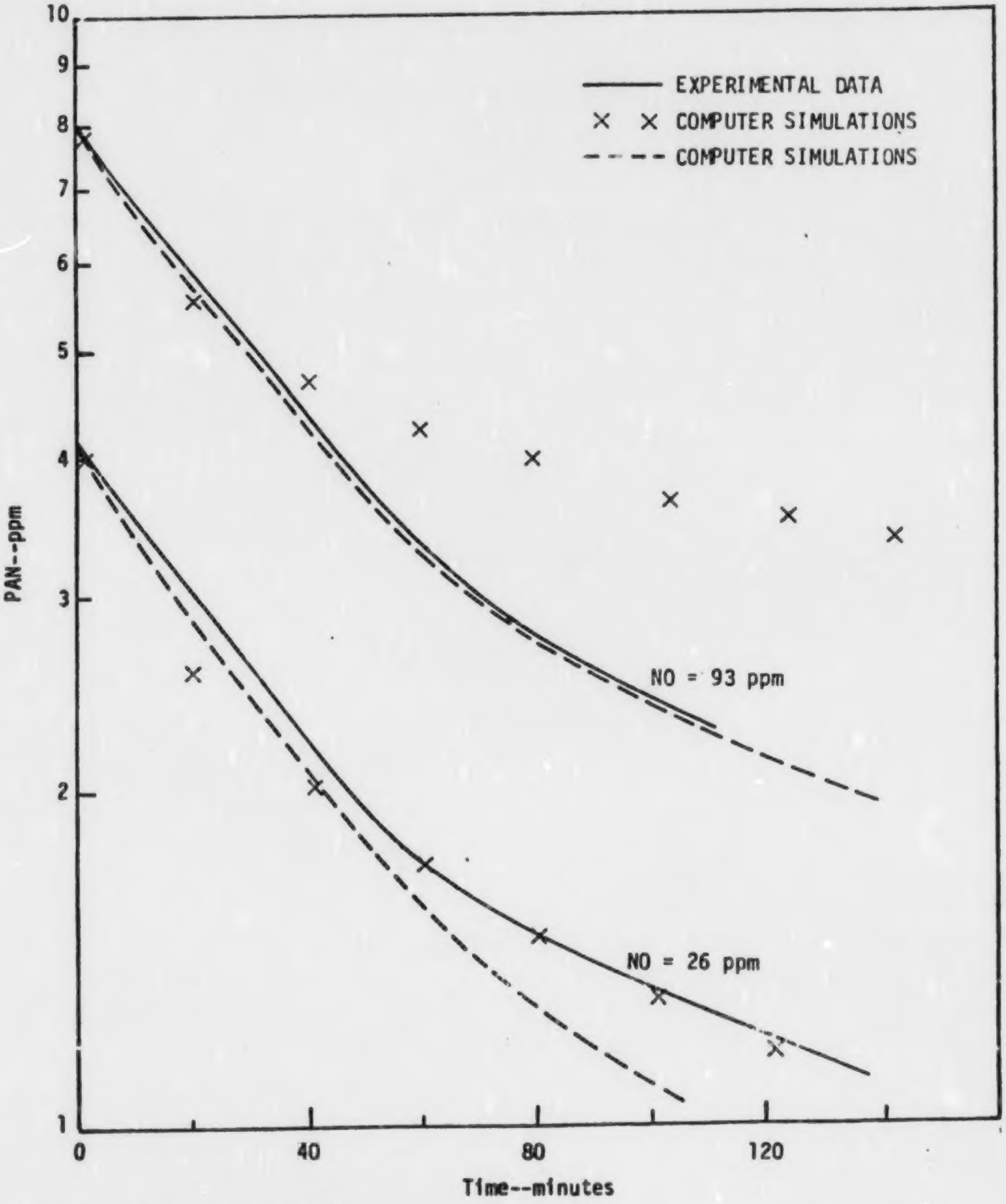

Source: Pate et al. (1975).

FIGURE III-1. PAN CONCENTRATION VERSUS TIME FOR THE REACTION OF PAN WITH NO IN AIR

overpredicted. The second set of simulations (represented by dashes) shows our efforts to simulate the top curve. When the top curve is closely predicted, the bottom curve is underpredicted. Unfortunately we have been unable to successfully simulate their experimental data using any of several combinations of rate constants or extra reactions. The chemistry of PAN in all the systems we have modeled and discussed in this report may be in error. The extent of occurrence of the various pathways for peroxyacyl radical formation, especially in olefin systems, is uncertain. The relative rates of reaction of these radicals with NO and NO_2 are still uncertain. Finally, any alternate paths of reaction for the peroxyacyl radicals other than the ones we have used are not certain. Hence more work is required to clarify the roles of PAN chemistry and peroxyacyl radicals in smog formation.

8. Propylene-O Atom Reaction

In the later UCR runs (EC-95, 96, and 121), propionaldehyde was observed as a minor product. The propylene mechanism did not contain the production of propionaldehyde. To follow the UCR data, we added the following reaction pathway for the propylene-O atom reaction:

$$C_3H_6 + O \rightarrow CH_3CH_2CHO \quad .$$

This reaction is believed to occur (Niki et al., 1972). We assumed that propionaldehyde is produced in one-third of the propylene-O atom reactions. The other two possible pathways for this reaction are:

$$C_3H_6 + O \xrightarrow{2O_2} CH_3CH_2O_2\cdot + H\overset{\overset{O}{\|}}{C}O_2\cdot \quad ,$$

$$C_3H_6 + O \xrightarrow{2O_2} CH_3\overset{\overset{O}{\|}}{C}O_2\cdot + CH_3O_2\cdot \quad .$$

We assumed that each of the pathways accounts for one-third of the total reactions. The overall effect of the propylene-O atom reaction is the initial generation of alkyl radicals required for NO to NO_2 conversion.

9. Simulation Results

Presented in Table III-5 is the explicit propylene mechanism. Table III-6a lists the initial conditions for each simulation, and Table III-6b shows the photolysis rate constants. Figure III-2 shows the factorial block for this system. Figures III-3 to III-64 show the results of our simulations of the propylene/NO_x system.* In the EC-50 series of UCR runs, UCR performed three experiments with the same initial conditions (EC-51, 52, and 57). We performed simulations of an "averaged" run consisting of these three experiments (EC-5127). The data from each of the runs were averaged by taking a simple arithmetic mean for each data point.

In addition to simulating the UCR data, we systematically examined the carbon mass balance in the propylene/NO_x system in an attempt to determine the nature and importance of undetected carbon-containing products in the smog chamber. After correcting the reported concentrations for chamber dilution in the sampling process, we summed and compared the reactant losses and product gains in units of ppmC, the difference being the carbon mass discrepancy. The calculated carbon recoveries for various runs are shown in Table III-7. The decrease of percentage recovery with time in the propylene/NO_x system appears to be accounted for by CO and CO_2 production at later times. The duplicate run (EC-121) produces significantly lower recovery percentages which, when considered with the apparent overprediction of acetaldehyde by our mechanism, could indicate either a systematic error in the new acetaldehyde detection method or a need for changes in the mechanism.

---

*In all figures showing simulations of the UCR data, the symbols *, +, and x are used to represent the experimental data.

TABLE III-5. THE PROPYLENE/NO_x MECHANISM

Reaction	Rate Constant (ppm^{-1} min^{-1})
$NO_2 + h\nu \rightarrow NO + O(^3P)$	Experimental*
$O(^3P) + O_2 + M \rightarrow O_3 + M$	$2.08 \times 10^{-5\dagger}$
$O(^3P) + NO_2 \rightarrow NO + O_2$	1.34×10^4
$O_3 + NO \rightarrow NO_2 + O_2$	25.2
$O(^1D) + H_2O \rightarrow O + M$	8.6×10^4
$O(^1D) + H_2O \rightarrow 2OH\cdot$	5.1×10^5
$O_3 + OH\cdot \rightarrow HO_2\cdot + O_2$	87.0
$O_3 + HO_2\cdot \rightarrow OH\cdot + 2O_2$	1.2
$O_3 + NO_2 \rightarrow NO_3 + O_2$	5×10^{-2}
$O_3 + h\nu \rightarrow O(^1D) + O_2$	Experimental*
$O_3 + h\nu \rightarrow O(^3P) + O_2$	Experimental*
$O_3 \rightarrow wall$	1×10^{-3}
$NO_3 + NO \rightarrow 2NO_2$	1.3×10^4
$NO_3 + NO_2 \rightarrow N_2O_5$	5.6×10^3
$N_2O_5 + H_2O \rightarrow 2HNO_3$	5×10^{-6}
$N_2O_5(+ M) \rightarrow NO_3 + NO_2(+ M)$	24.0*
$NO + NO_2 + H_2O \rightarrow 2HNO_2$	$2.2 \times 10^{-9\dagger}$

TABLE III-5 (Continued)

Reaction	Rate Constant (ppm-1 min-1)
$2HNO_2 \rightarrow NO + NO_2 + H_2O$	1.3×10^{-3}
$HNO_2 + h\nu \rightarrow OH\cdot + NO$	Experimental*
$NO_2 + OH\cdot(+ M) \rightarrow HNO_3(+ M)$	9.2×10^{3}
$NO + OH\cdot \rightarrow HNO_2$	9×10^{3}
$HO_2^{\cdot} + NO \rightarrow OH\cdot + NO_2$	2×10^{3}
$HO_2^{\cdot} + NO_2 \rightarrow HNO_2 + O_2$	20
$H_2O_2 + h\nu \rightarrow 2OH\cdot$	Experimental*
$CH_3CH{=}CH_2 + O \rightarrow CH_3CH_2CHO$	1.77×10^{3}
$CH_3CH{=}CH_2 + O \xrightarrow{2O_2} CH_3O_2^{\cdot} + CH_3C(O)O_2^{\cdot}$	1.77×10^{3}
$CH_3CH{=}CH_2 + O \xrightarrow{2O_2} CH_3CH_2O_2^{\cdot} + HC(O)O_2^{\cdot}$	1.77×10^{3}
$CH_3CH{=}CH_2 + OH\cdot \xrightarrow{O_2} CH_3CH(O_2^{\cdot})CH_2OH$	3.8×10^{4}
$CH_3CH{=}CH_2 + NO_3 \rightarrow NO_2 + \text{Products}$	7.82
$CH_3CH{=}CH_2 + O_3 \xrightarrow{O_2} H_2CO + CH_3C(O)O_2^{\cdot} + OH\cdot$	5×10^{-3}
$CH_3CH{=}CH_2 + O_3 \rightarrow CH_3CHO + HC(O)O_2^{\cdot} + OH\cdot$	5×10^{-3}
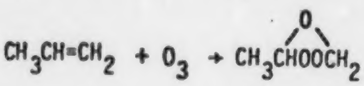 $CH_3CH{=}CH_2 + O_3 \rightarrow CH_3\overset{O}{CHOOCH}_2$	5×10^{-3}
$CH_3CH_2C(O)O_2^{\cdot} + NO \xrightarrow{O_2} NO_2 + CH_3CH_2O_2^{\cdot} + CO_2$	2×10^{3}
$CH_3C(O)O_2^{\cdot} + NO \xrightarrow{O_2} NO_2 + CH_3O_2^{\cdot} + CO_2$	2×10^{3}
$HC(O)O_2^{\cdot} + NO \xrightarrow{O_2} NO_2 + HO_2^{\cdot} + CO_2$	2×10^{3}

TABLE III-5 (Continued)

Reaction	Rate Constant $(ppm^{-1}\ min^{-1})$
$CH_3CH(O_2^{\cdot})CH_2OH + NO \rightarrow NO_2 + CH_3CH(O\cdot)CH_2OH$	2×10^3
$CH_3CH_2O_2^{\cdot} + NO \rightarrow NO_2 + CH_3CH_2O\cdot$	2×10^3
$CH_3O_2^{\cdot} + NO \rightarrow NO_2 + CH_3O\cdot$	2×10^3
$CH_3C(O\cdot)CH_2OH \xrightarrow{O_2} CH_3CHO + H_2CO + HO_2^{\cdot}$	$3 \times 10^{5*}$
$CH_3CH_2O\cdot + O_2 \rightarrow CH_3CHO + HO_2^{\cdot}$	0.95
$CH_3O\cdot + O_2 \rightarrow H_2CO + HO_2^{\cdot}$	0.95
$H_2CO + h\nu \xrightarrow{2O_2} HO_2^{\cdot} + HC(O)O_2^{\cdot}$	Experimental*
$H_2CO + h\nu \rightarrow H_2 + CO$	Experimental*
$CH_3CHO + h\nu \xrightarrow{2O_2} CH_3O_2^{\cdot} + HC(O)O_2$	Experimental*
$CH_3CH_2CHO + h\nu \xrightarrow{2O_2} CH_3CH_2O_2^{\cdot} + HC(O)O_2^{\cdot}$	Experimental*
$H_2CO + OH\cdot \xrightarrow{O_2} HC(O)O_2^{\cdot} + H_2O$	1×10^4
$CH_3CHO + OH\cdot \xrightarrow{O_2} CH_3C(O)O_2^{\cdot} + H_2O$	1×10^4
$CH_3CH_2CHO + OH\cdot \xrightarrow{O_2} CH_3CH_2C(O)O_2^{\cdot} + H_2O$	1×10^4
$CH_3CH_2C(O)O_2^{\cdot} + HO_2^{\cdot} \rightarrow CH_3CH_2C(O)OOH + O_2$	1×10^4
$CH_3C(O)O_2^{\cdot} + HO_2^{\cdot} \rightarrow CH_3C(O)OOH + O_2$	1×10^4
$HC(O)O_2^{\cdot} + HO_2^{\cdot} \rightarrow HC(O)OOH + O_2$	1×10^4
$CH_3CH(O_2^{\cdot})CH_2OH + HO_2^{\cdot} \rightarrow CH_3CH(OOH)CH_2OH + O_2$	4×10^3
$CH_3CH_2O_2^{\cdot} + HO_2^{\cdot} \rightarrow CH_3CH_2OOH + O_2$	4×10^3

TABLE III-5 (Concluded)

Reaction	Rate Constant (ppm^{-1} min^{-1})
$CH_3O_2\cdot + HO_2\cdot \rightarrow CH_3OOH + O_2$	4×10^3
$HO_2\cdot + HO_2\cdot \rightarrow H_2O_2 + O_2$	4×10^3
$CH_3CH_2C(O)O_2\cdot + NO_2 \rightarrow CH_3CH_2C(O)O_2NO_2$	4×10^2
$CH_3C(O)O_2\cdot + NO_2 \rightarrow CH_3C(O)O_2NO_2$	4×10^2
$CH_3C(O)O_2NO_2 \rightarrow NO_2 + CH_3C(O)O_2\cdot$	$1.7 \times 10^{-2*}$
$CH_3CH_2C(O)O_2NO_2 \rightarrow NO_2 + CH_3CH_2C(O)O_2\cdot$	$2 \times 10^{-2*}$
$CH_3O\cdot + NO_2 \rightarrow CH_3ONO_2$	2×10^4
$CH_3O\cdot + NO_2 \rightarrow H_2CO + HNO_2$	2.2×10^3
$CH_3CH_2O\cdot + NO_2 \rightarrow CH_3CH_2ONO_2$	2.0×10^4
$CH_3CH_2O\cdot + NO_2 \rightarrow CH_3CHO + HNO_2$	2.2×10^3
$CO + OH\cdot \xrightarrow{O_2} HO_2 + CO_2$	2.06×10^2
$CH_3CH(O_2\cdot)CH_2OH + CH_3CH(O_2\cdot)CH_2OH \rightarrow CH_3CH(O\cdot)CH_2OH + CH_3CH(O\cdot)CH_2OH + O_2$	4×10^3

---

* Units of min^{-1}.

† Units of $ppm^{-2}min^{-1}$.

TABLE III-6a. INITIAL CONDITIONS FOR SIMULATIONS OF UCR PROPYLENE/NO_x SYSTEMS

Run Number	NO (ppm)	NO_2 (ppm)	Propylene (ppm)	HNO_2 (ppm)	k_1 (min^{-1})
EC-5	0.551	0.047	0.993	0.01	0.223
EC-11	0.115	0.020	0.447	0.003	0.223
EC-13	0.504	0.018	0.500	0.03	0.223
EC-16	1.12	0.156	1.036	0.025	0.223
EC-17	0.105	0.015	0.103	0.005	0.223
EC-18	0.106	0.0142	0.972	0.001	0.223
EC-21	0.558	0.066	0.104	0.02	0.223
EC-5127	0.53	0.06	0.52	0.01	0.213
EC-55	0.48	0.121	0.524	0.02	0.209
EC-56	0.311	0.283	0.511	0.015	0.208
EC-59	0.124	0.481	0.51	0.005	0.204
EC-60	1.11	0.145	1.04	0.02	0.204
EC-95	0.365	0.092	0.504	0.01	0.351
EC-96	0.349	0.09	0.500	0.005	0.351
EC-121	0.41	0.101	0.483	0.03	0.300

TABLE III-6b. PHOTOLYSIS RATE CONSTANTS FOR SIMULATIONS OF PROPYLENE/NO_x SYSTEMS (10^4 min^{-1})

Run Number	$O_3 \rightarrow O^1D$	$O_3 \rightarrow O^3P$	$HNO_2 \rightarrow$	$H_2O_2 \rightarrow$	$HCHO \rightarrow H\cdot + HCO\cdot$	$HCHO \rightarrow CO + H_2$	$CH_3CHO \rightarrow$	$CH_3CH_2CHO \rightarrow$
5 11 13 16 17 18 21	29.7	75	468	7.0	5.5	18.0	3.5	5
5127 55	0.65	63	430	3.8	2.9	12.6	1.6	1.5
56	0.3	55	435	3.4	2.0	12	1.3	1.9
59 60	0.18	52	410	3.0	1.4	10	0.8	1.2
95 96	27	270	670	9.1	11.0	28.0	8.0	8.0
121	39	300	570	6.9	7.5	21.0	5.5	6.0

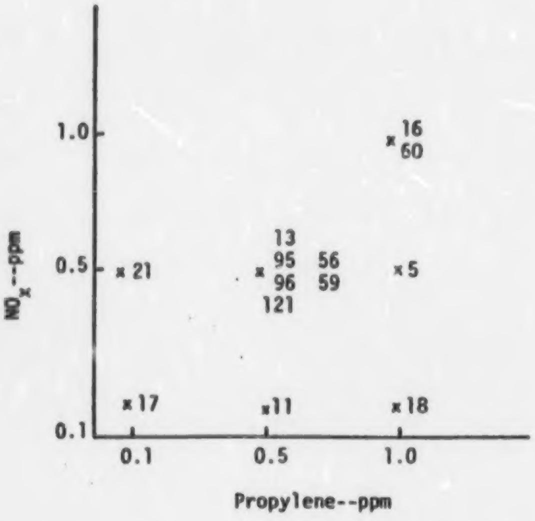

FIGURE III-2. FACTORIAL BLOCK FOR PROPYLENE/NO_x SYSTEMS

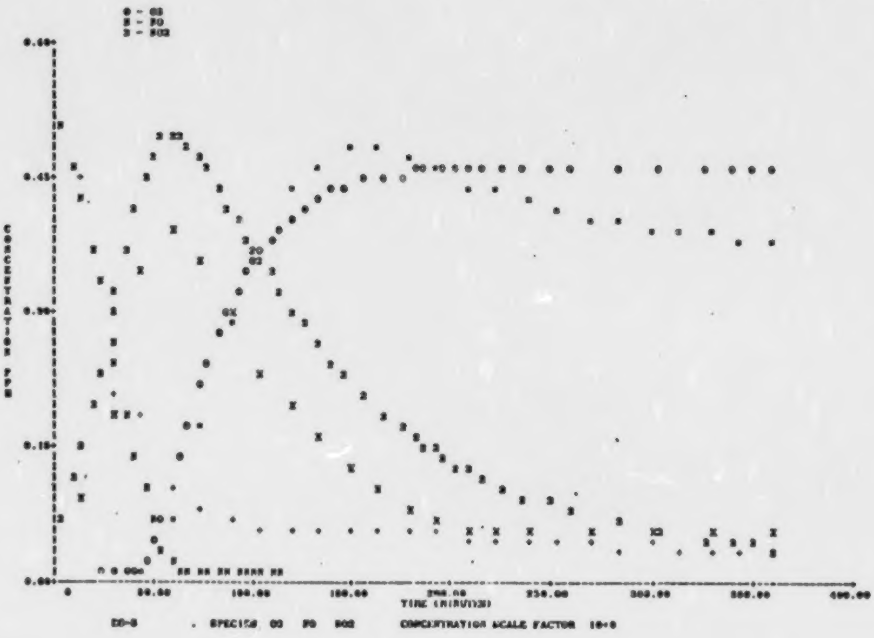

FIGURE III-3

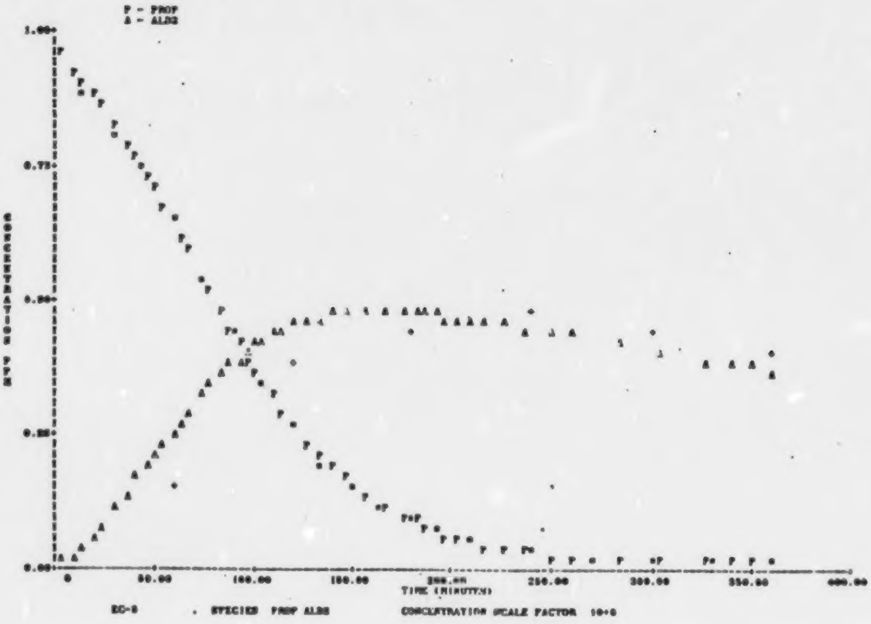

FIGURE III-4

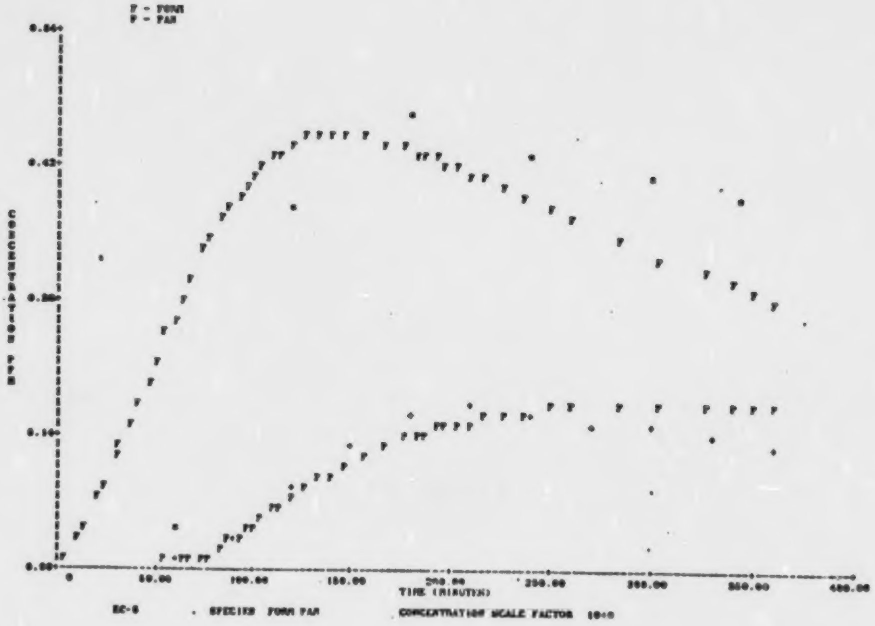
F - FORM
P - PAN
0.56
0.42
0.28
0.14
0.00
CONCENTRATION PPM
0
50.00
100.00
150.00
200.00
250.00
300.00
350.00
400.00
TIME (MINUTES)
EC-6
SPECIES FORM PAN
CONCENTRATION SCALE FACTOR 10+0

FIGURE III-5

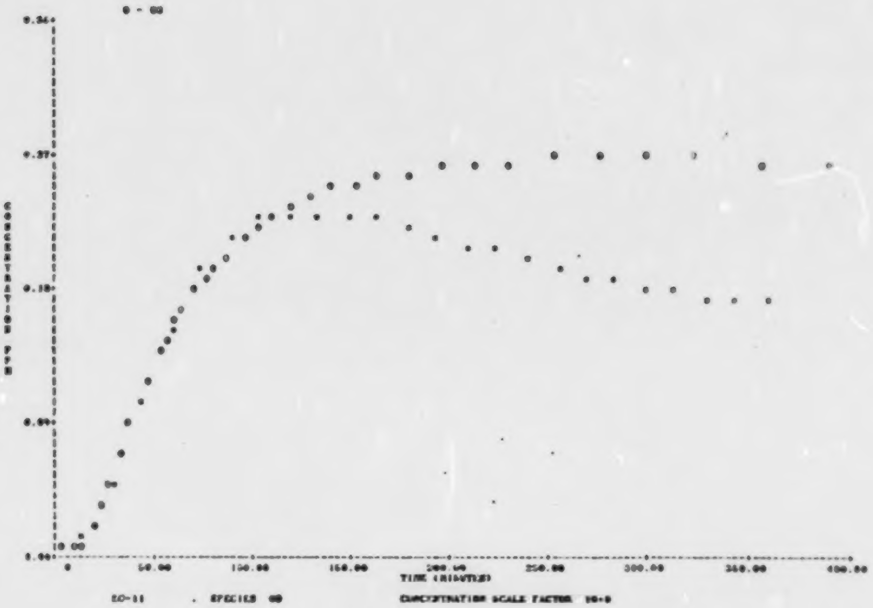

FIGURE III-6

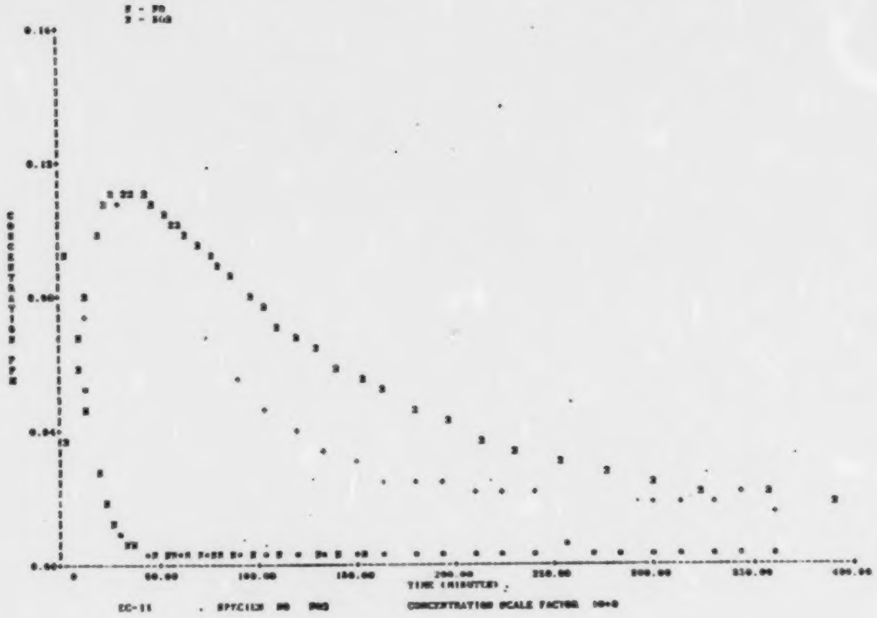

FIGURE III-7

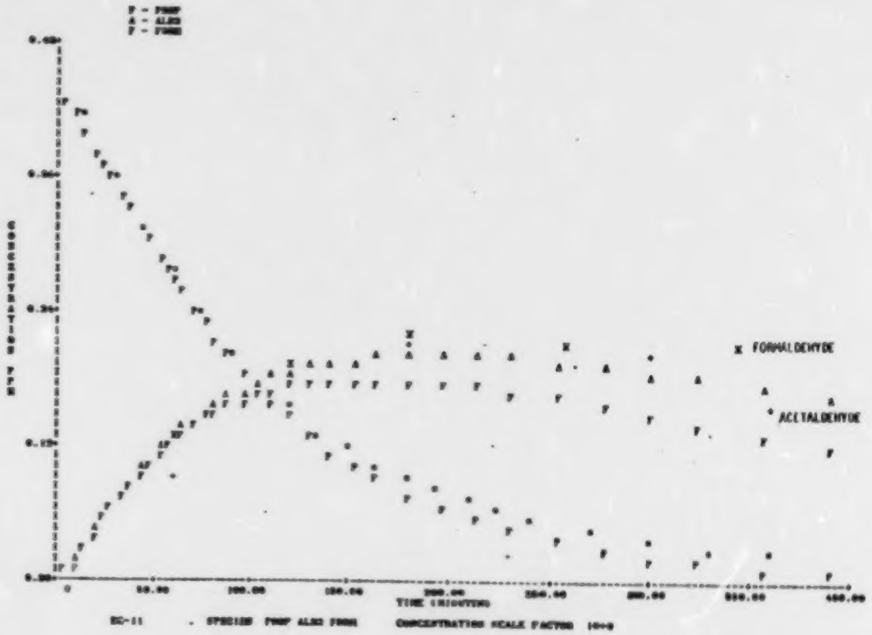

FIGURE III-8

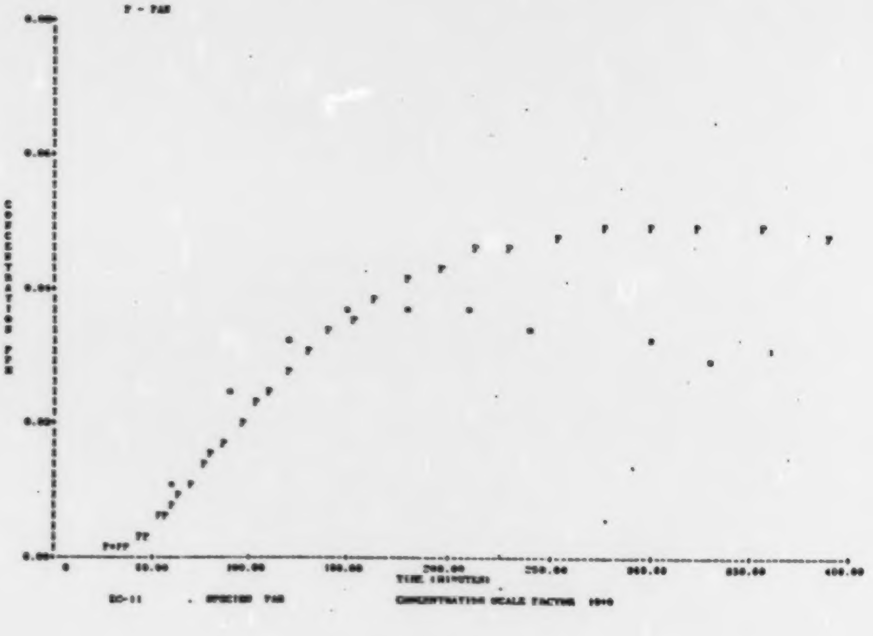

FIGURE III-9

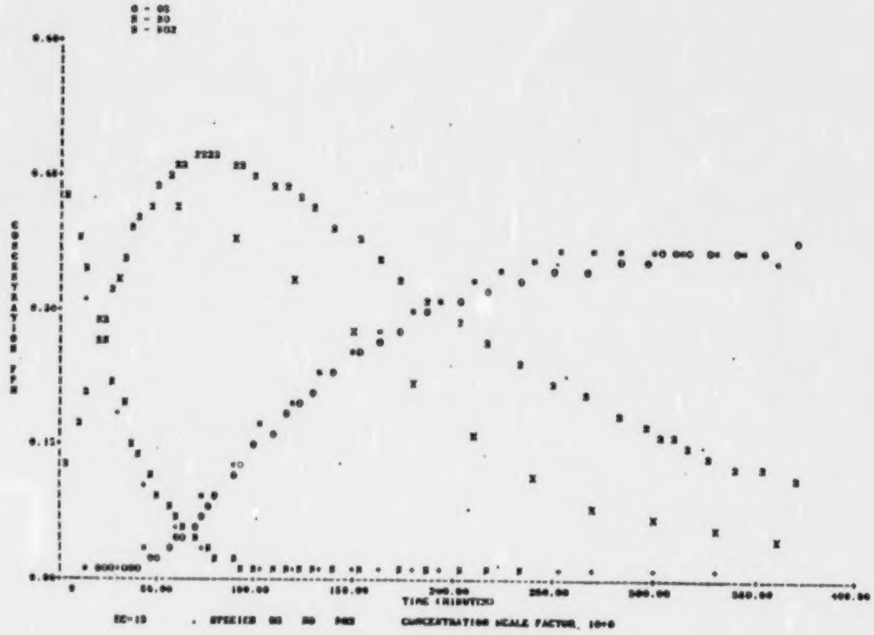

FIGURE III-10

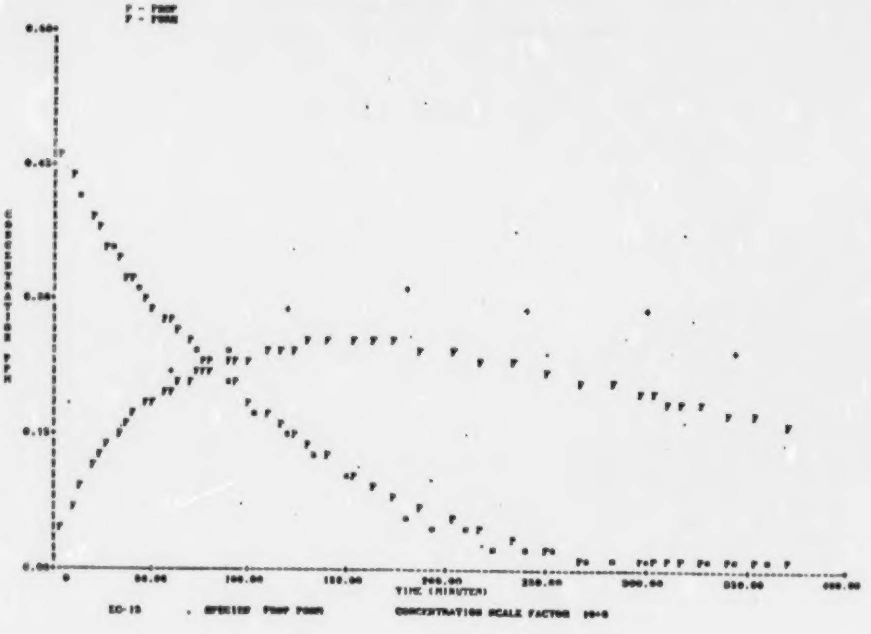

FIGURE III-11

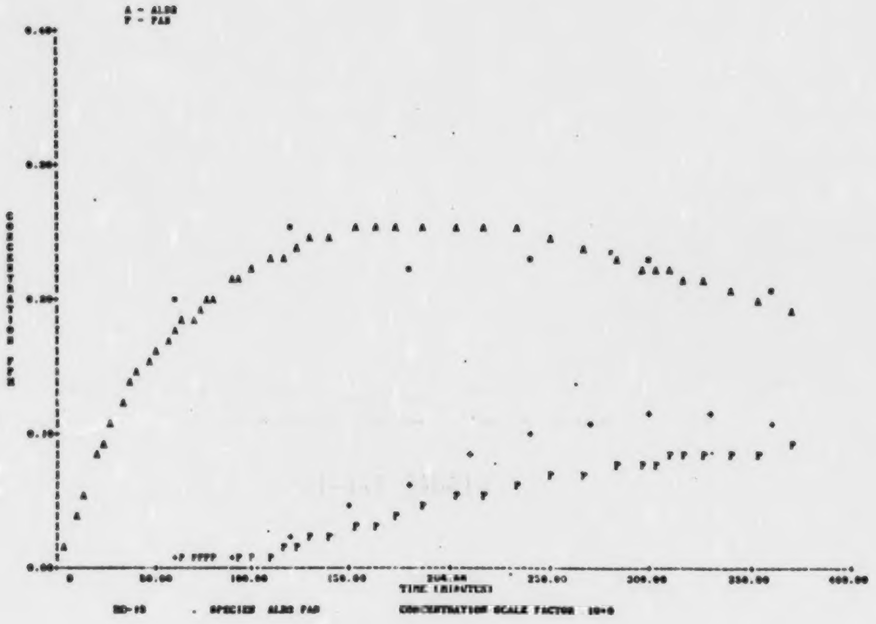

FIGURE III-12

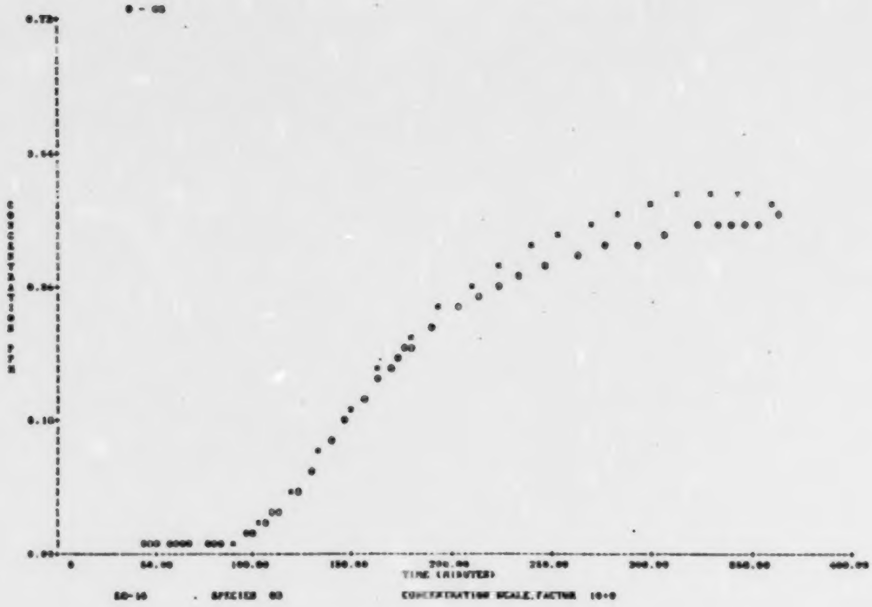

FIGURE III-13

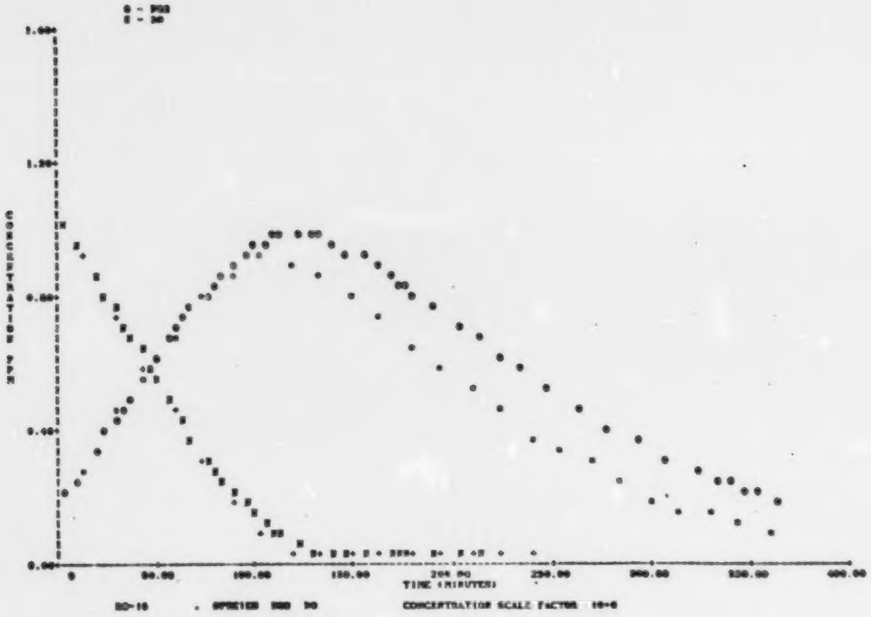

FIGURE III-14

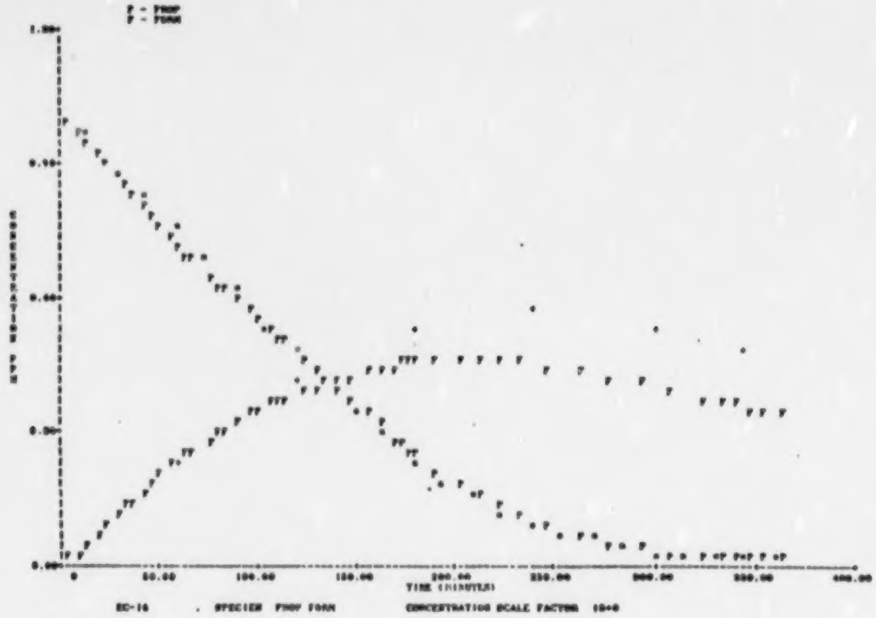

FIGURE III-15

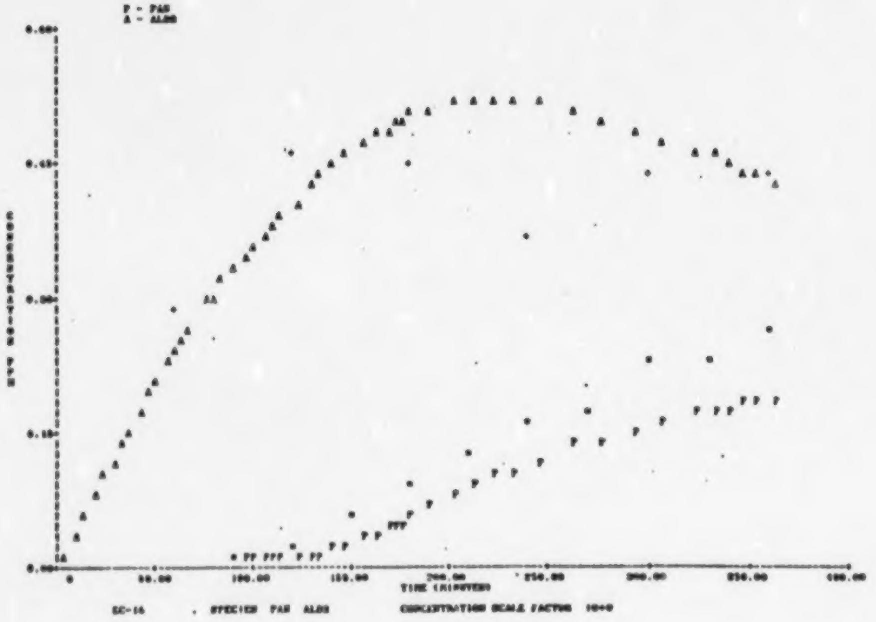

FIGURE III-16

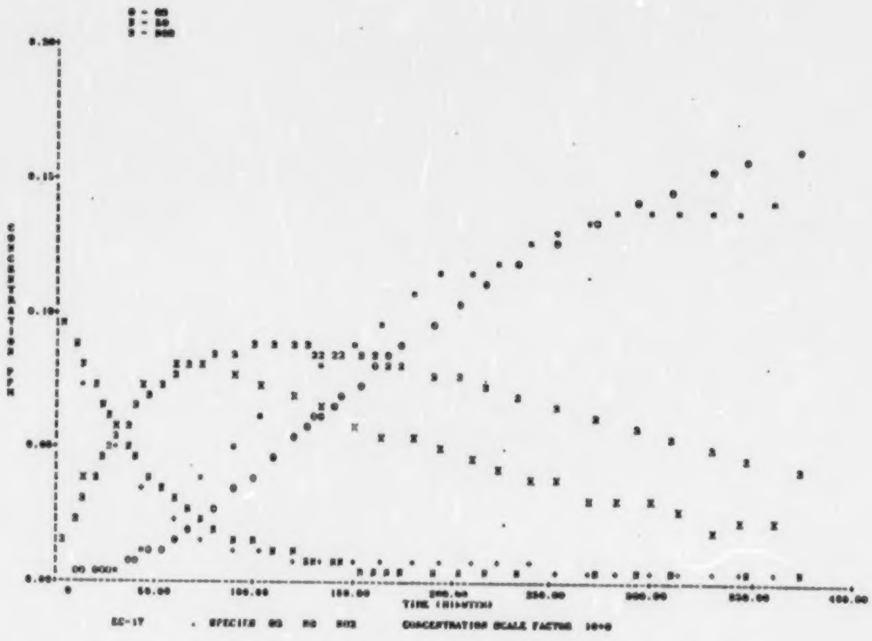

FIGURE III-17

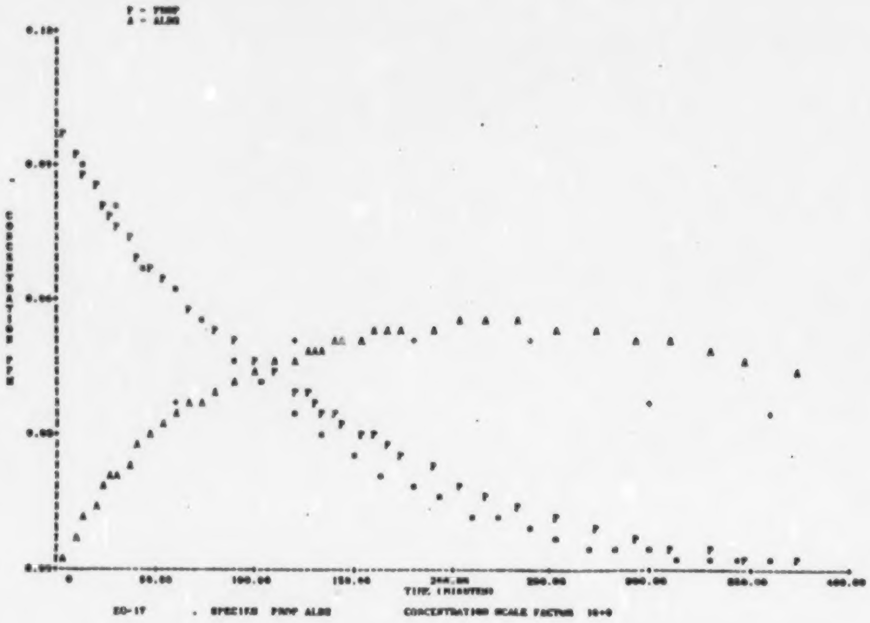

FIGURE III-18

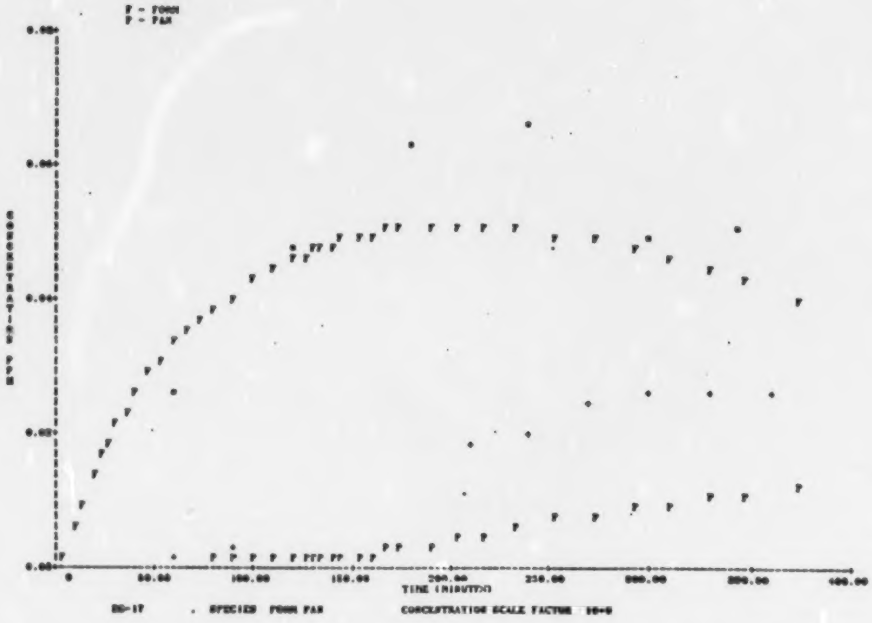

FIGURE III-19

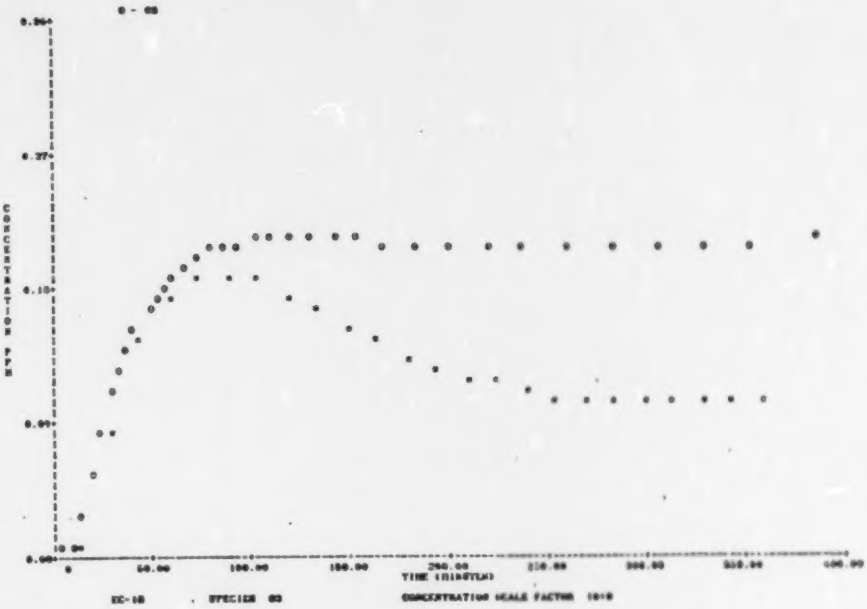

FIGURE III-20

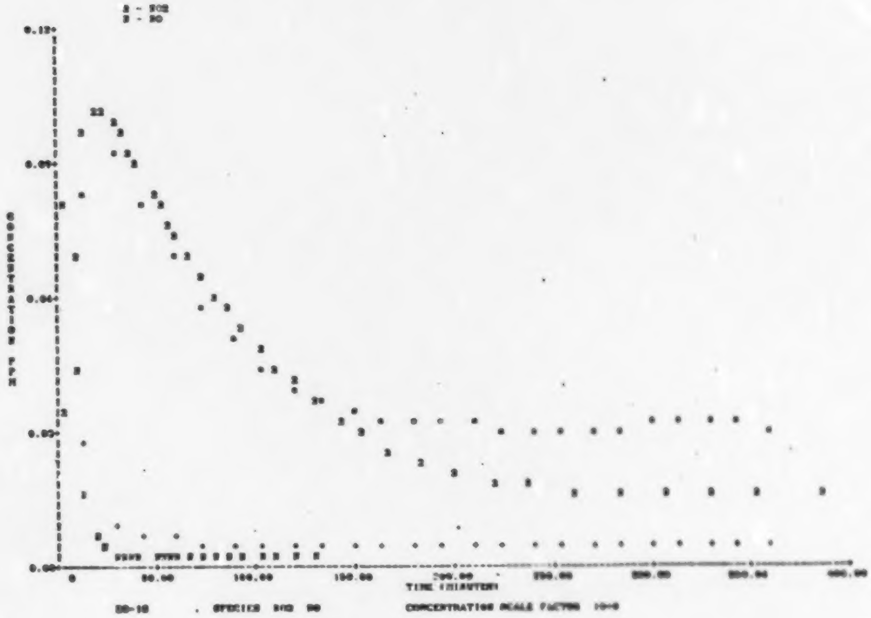

FIGURE III-21

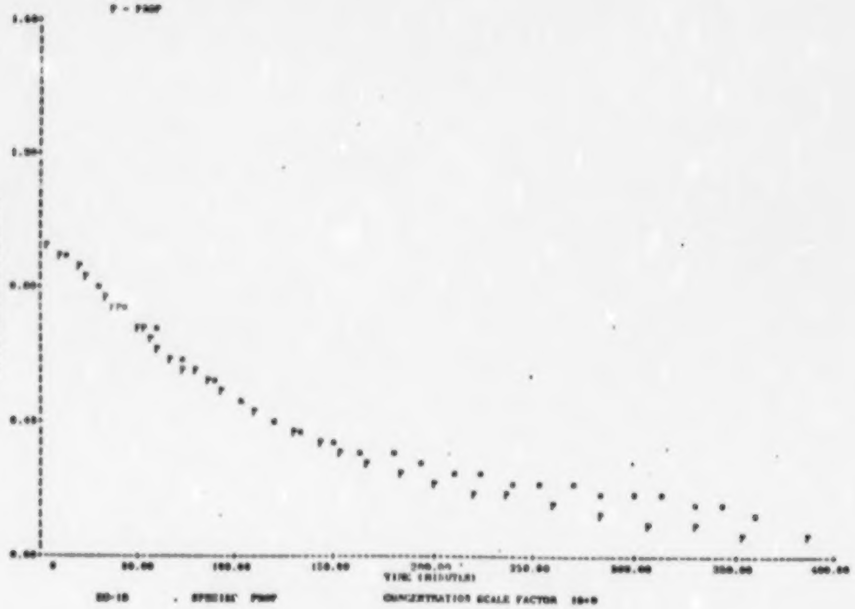

FIGURE III-22

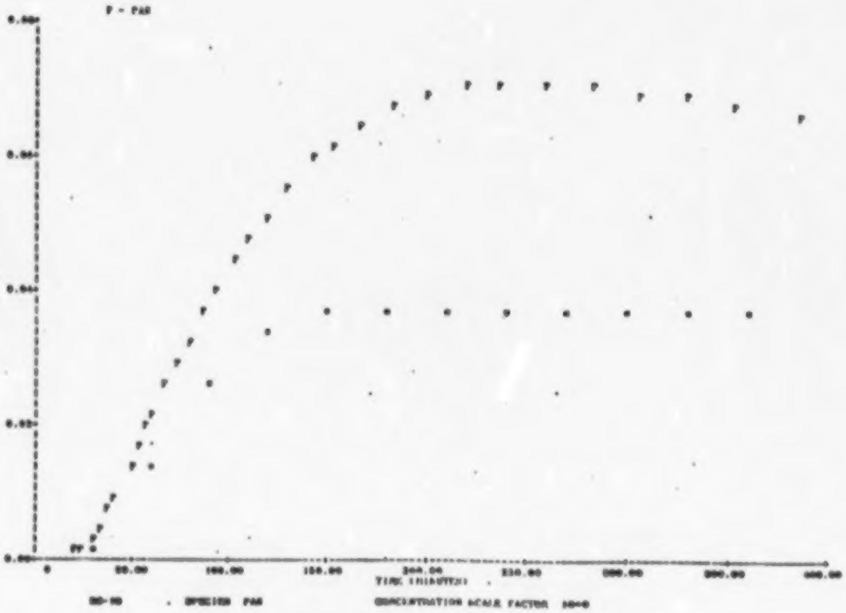

FIGURE III-23

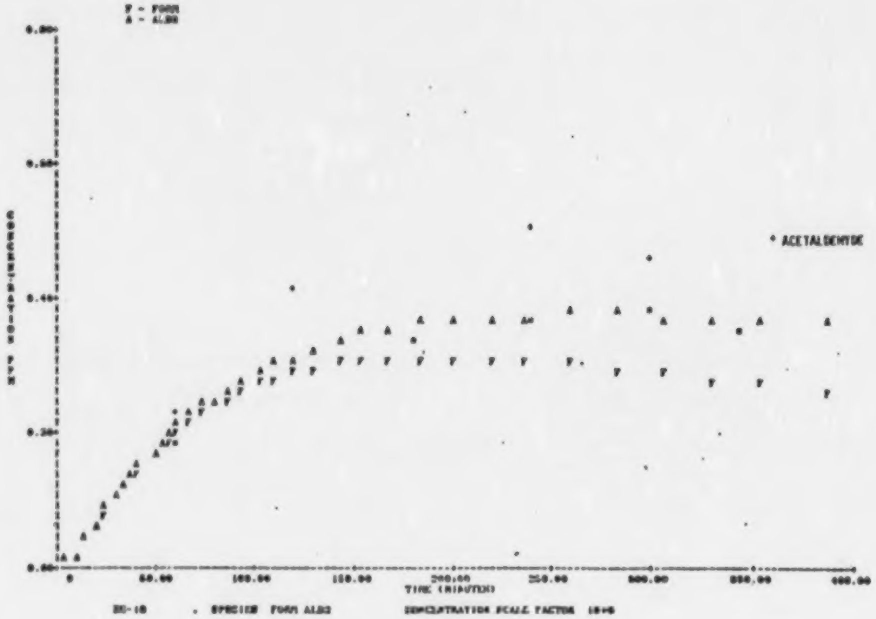

FIGURE III-24

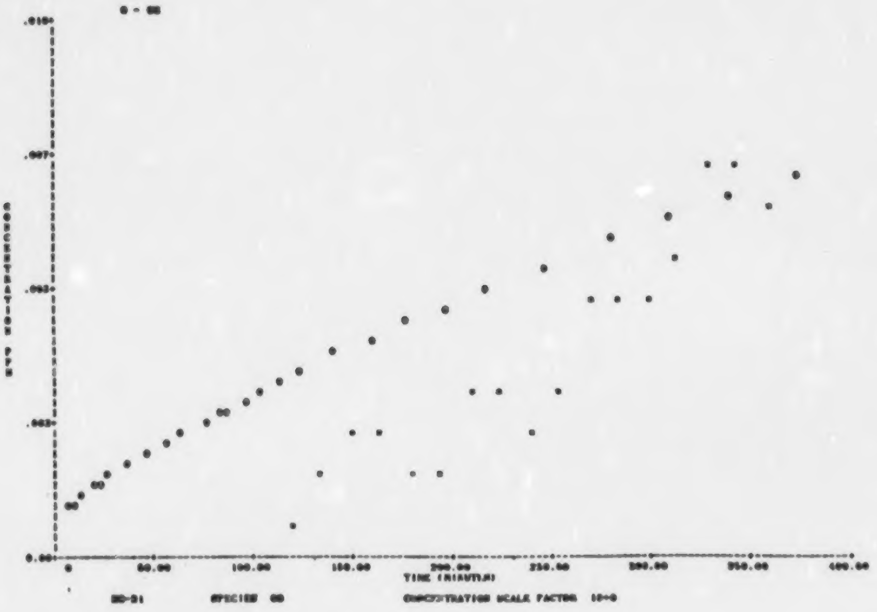

FIGURE III-25

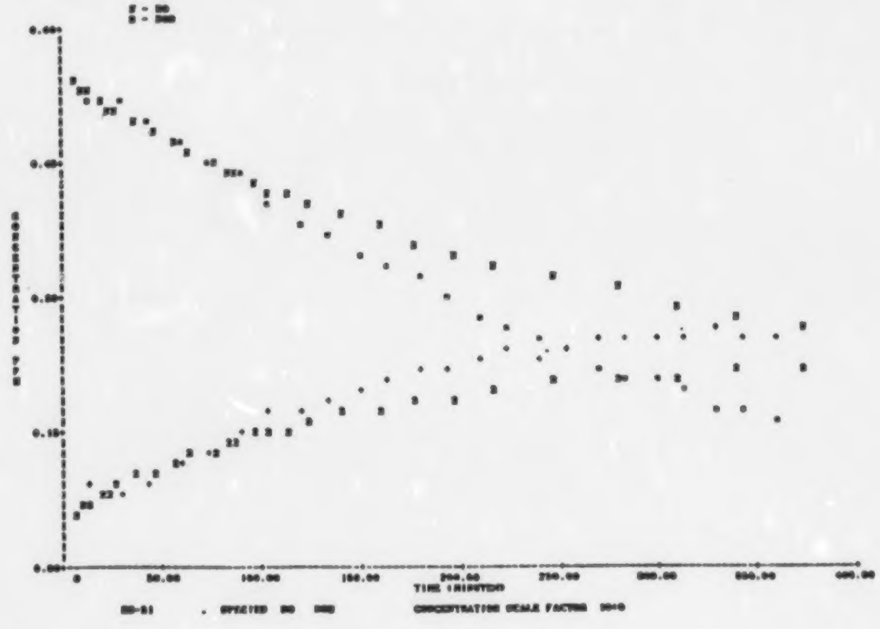

FIGURE III-26

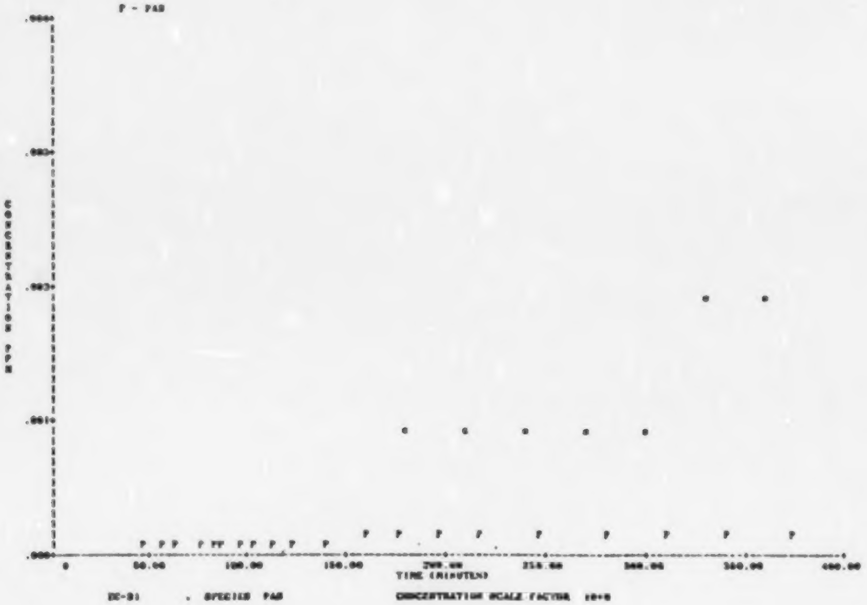

FIGURE III-27

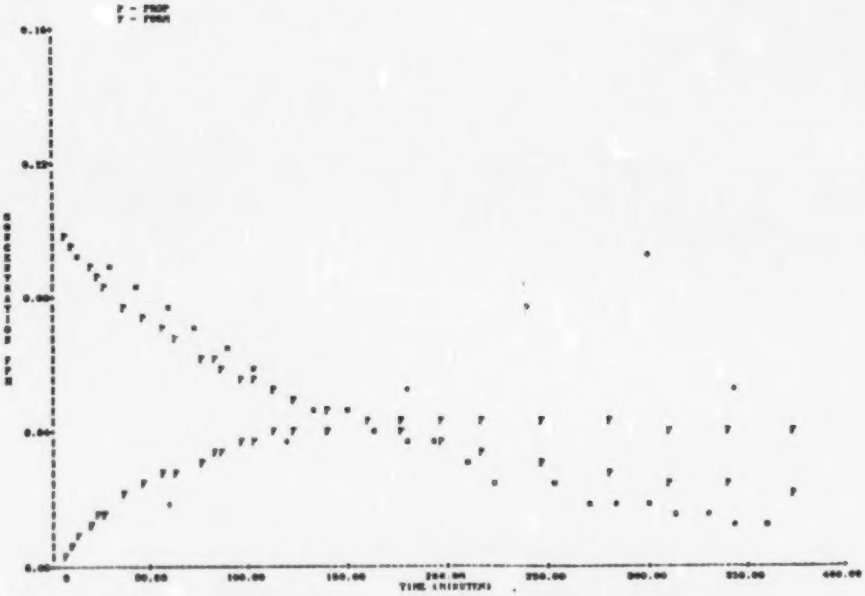

FIGURE III-28

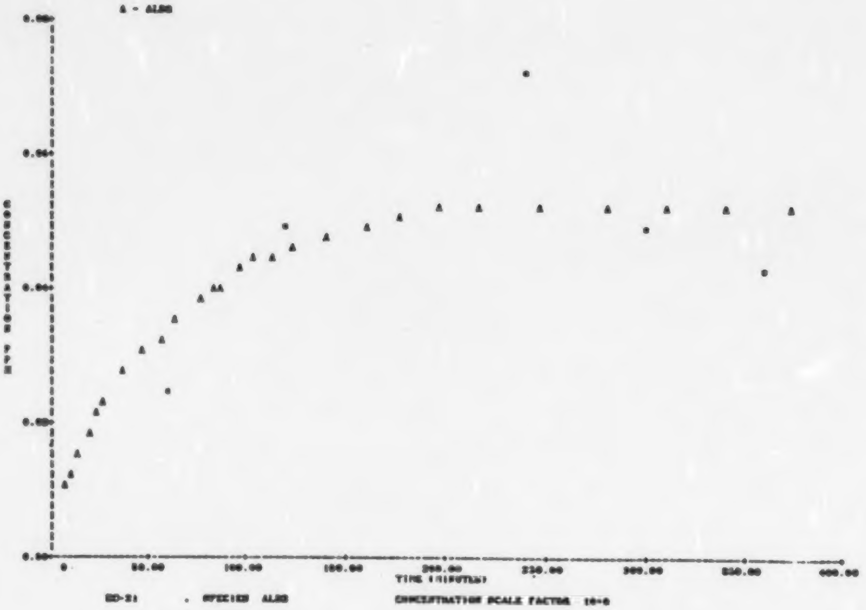

FIGURE III-29

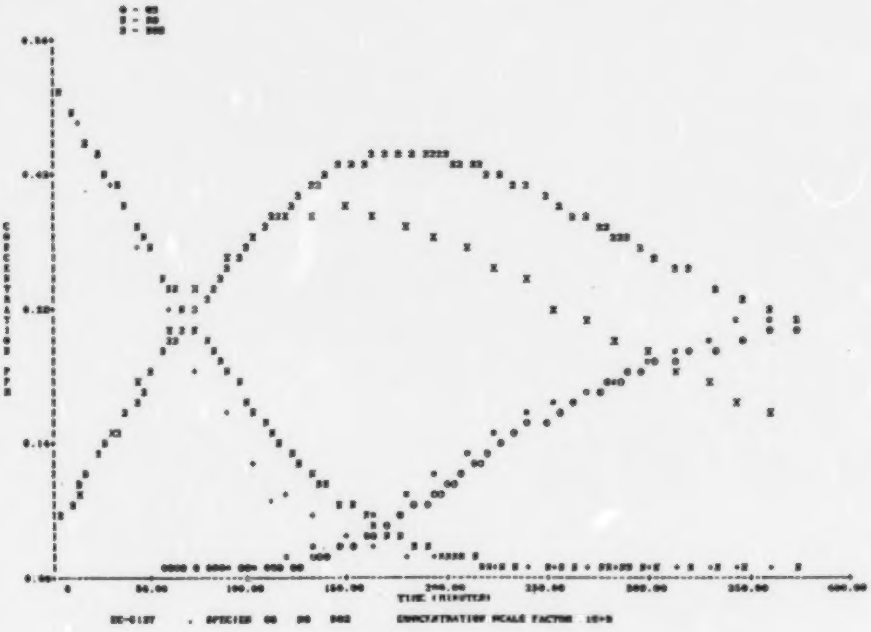

FIGURE III-30

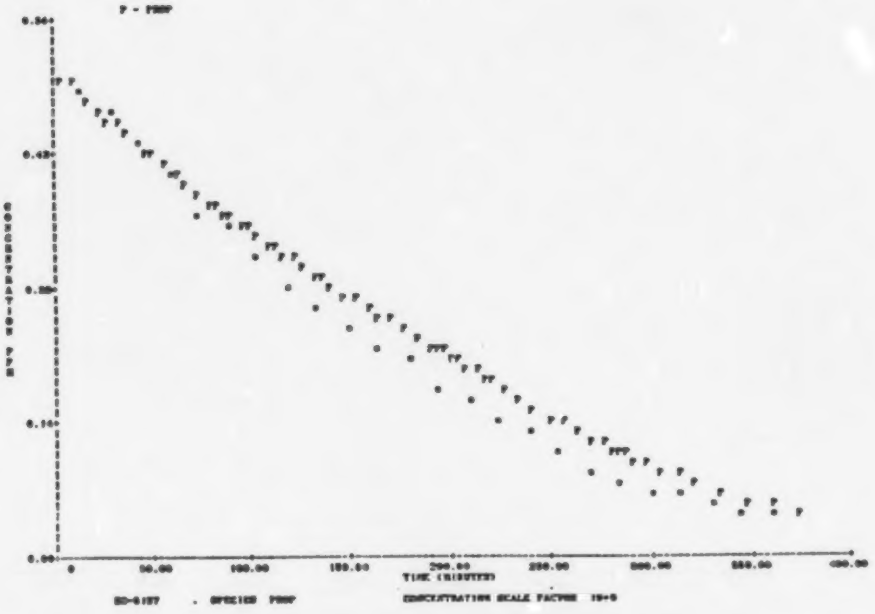

FIGURE III-31

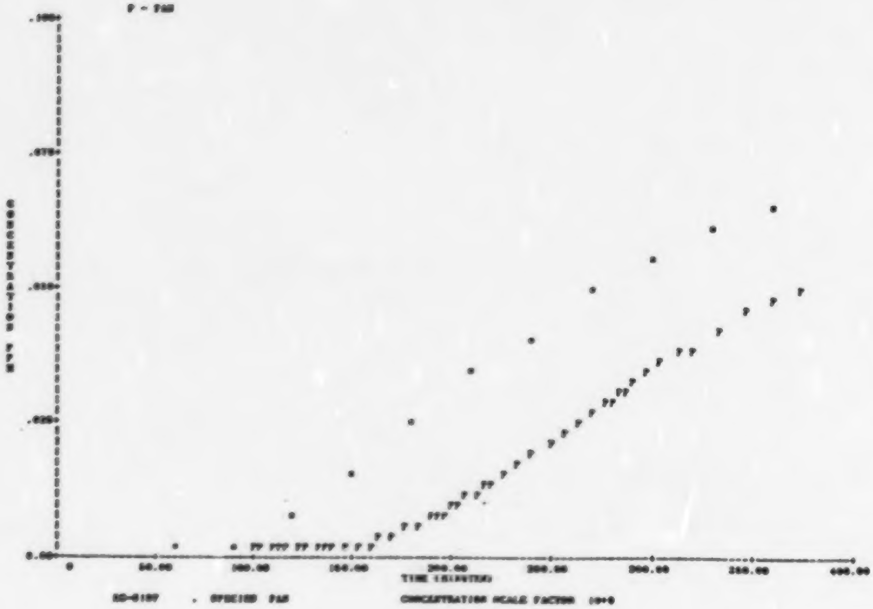

FIGURE III-32

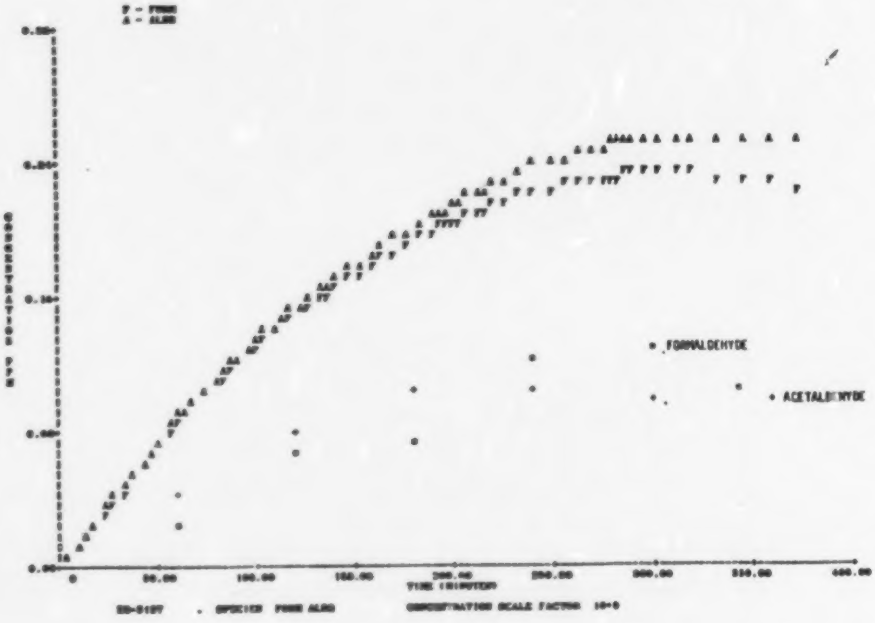

FIGURE III-33

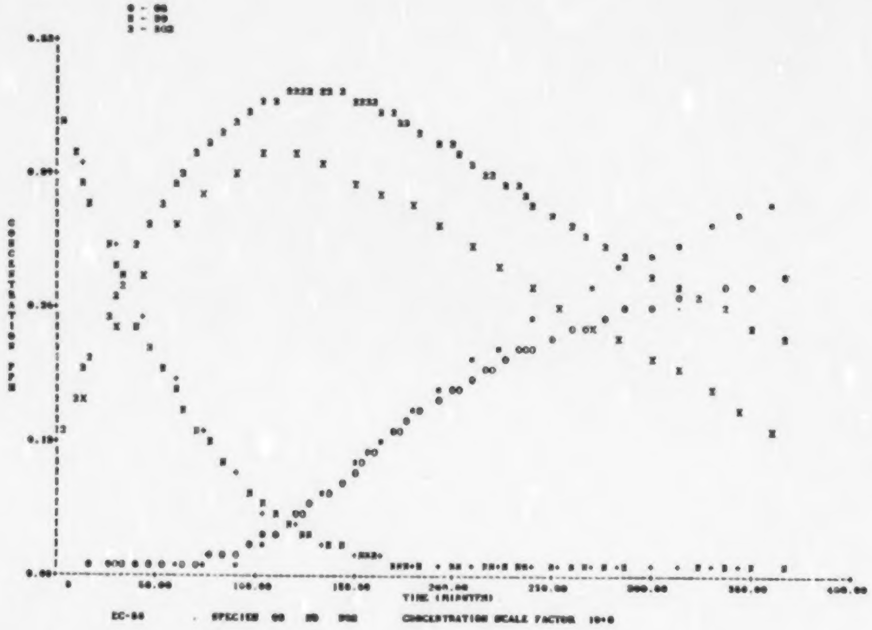

FIGURE III-34

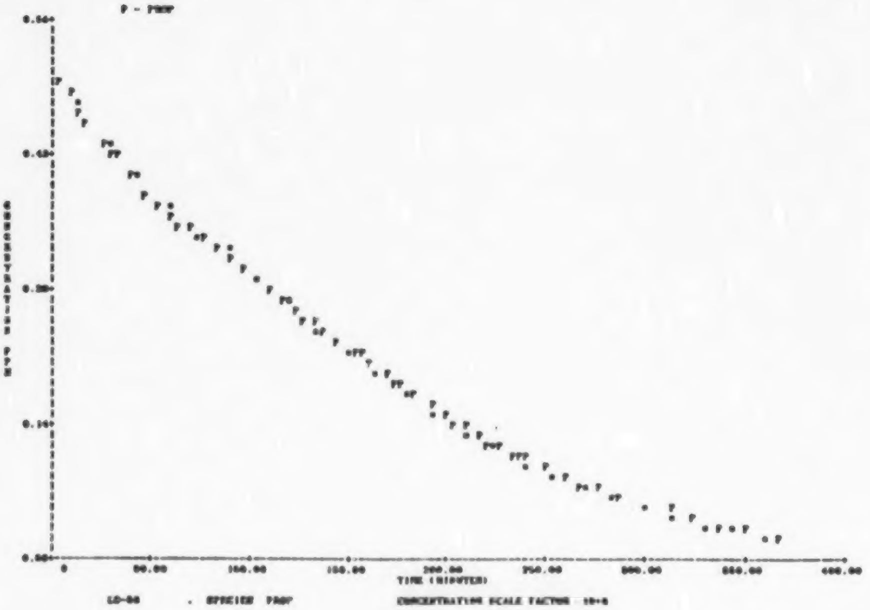

FIGURE III-35

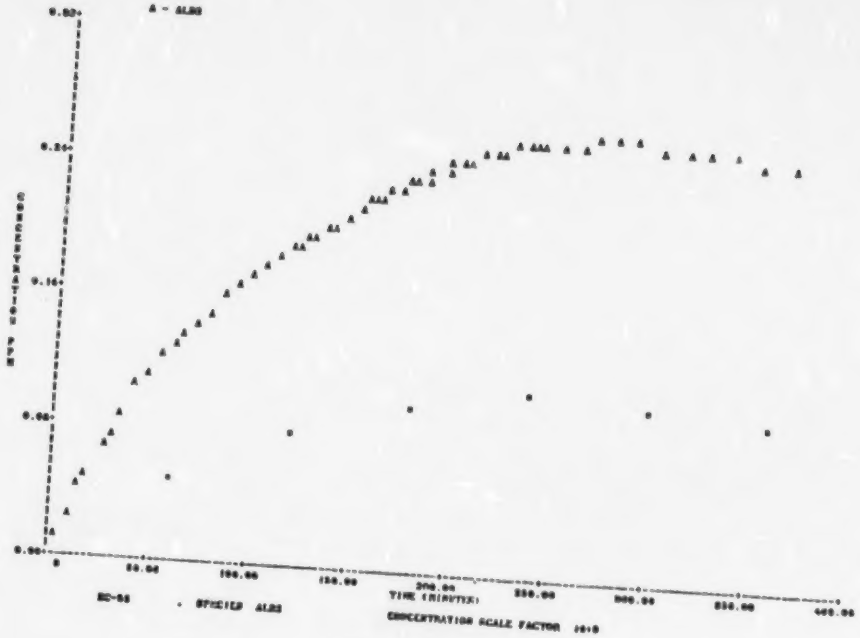

FIGURE III-36

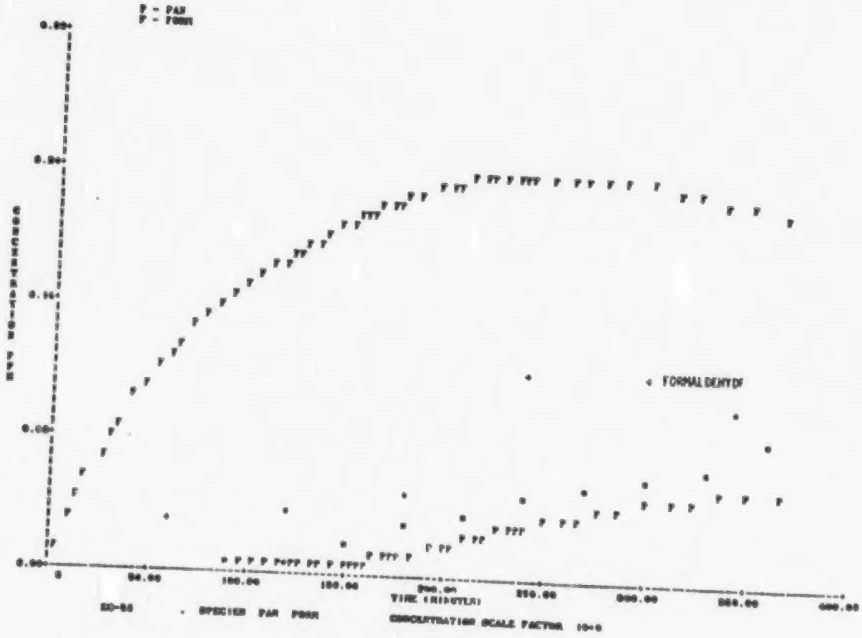

FIGURE III-37

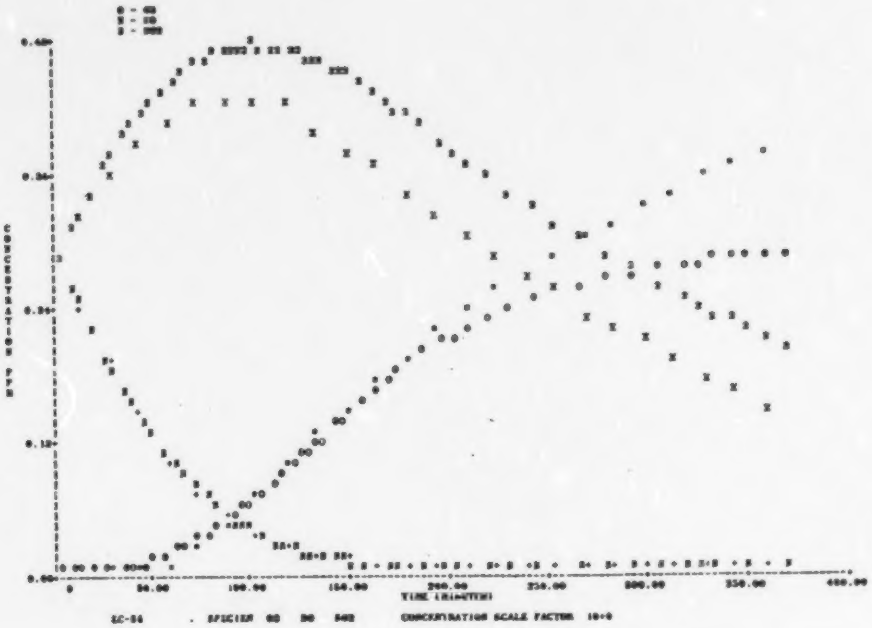

FIGURE III-38

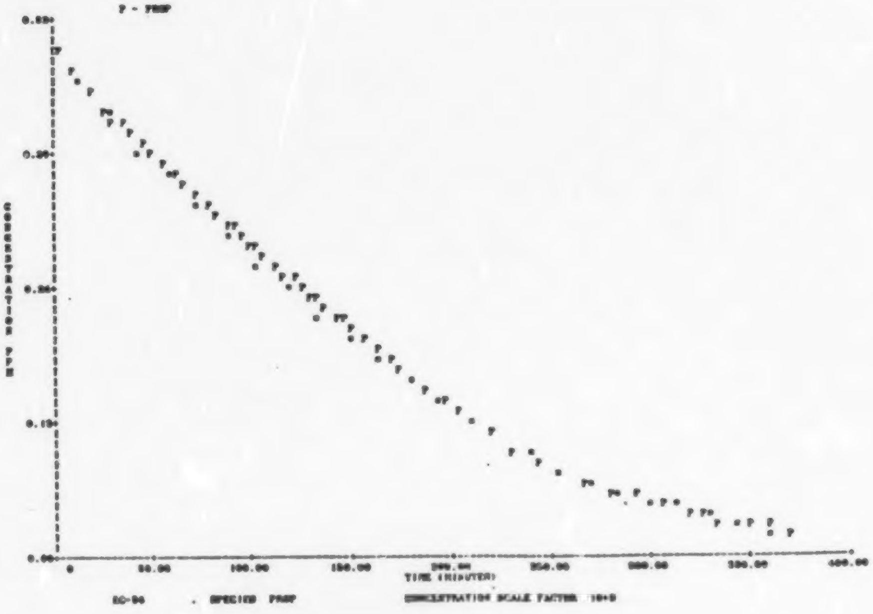

FIGURE III-39

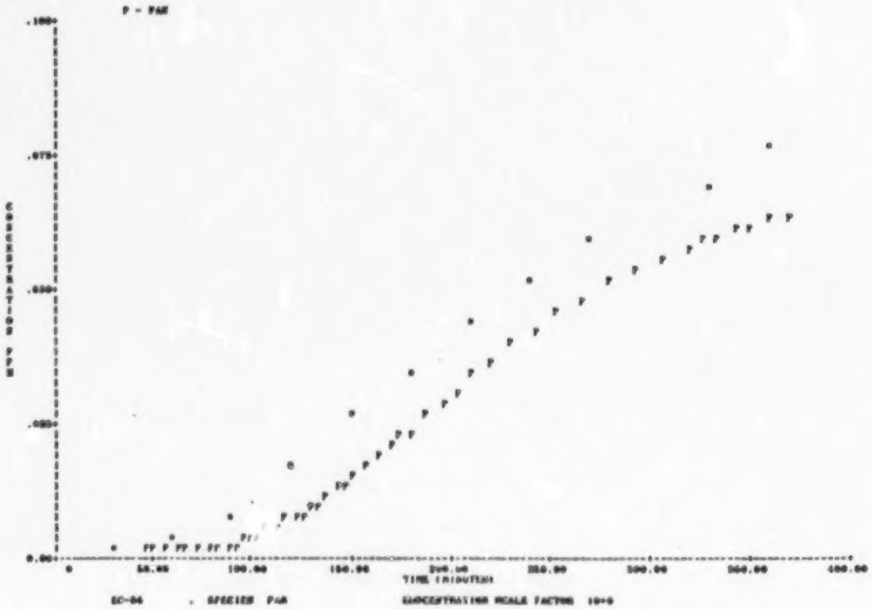

FIGURE III-40

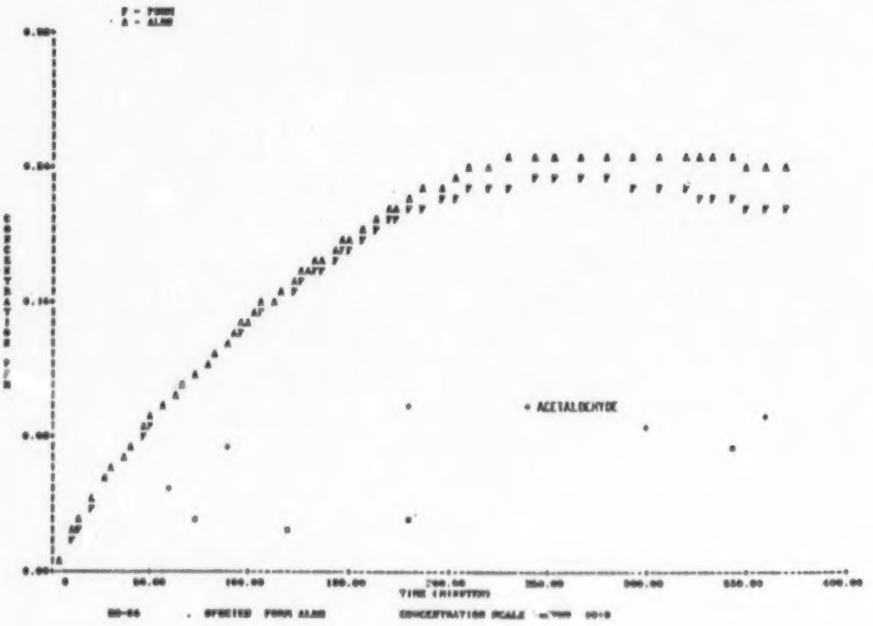

FIGURE III-41

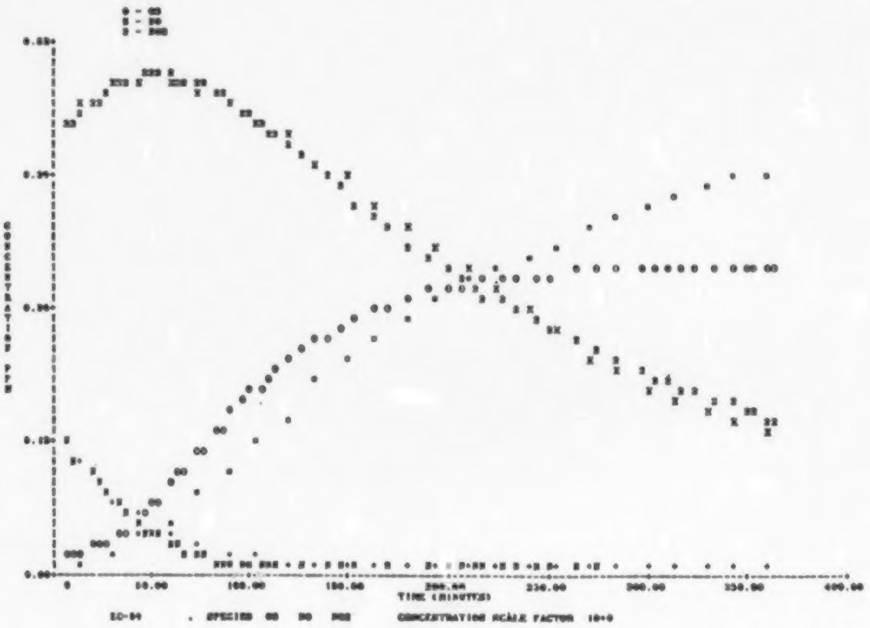

FIGURE III-42

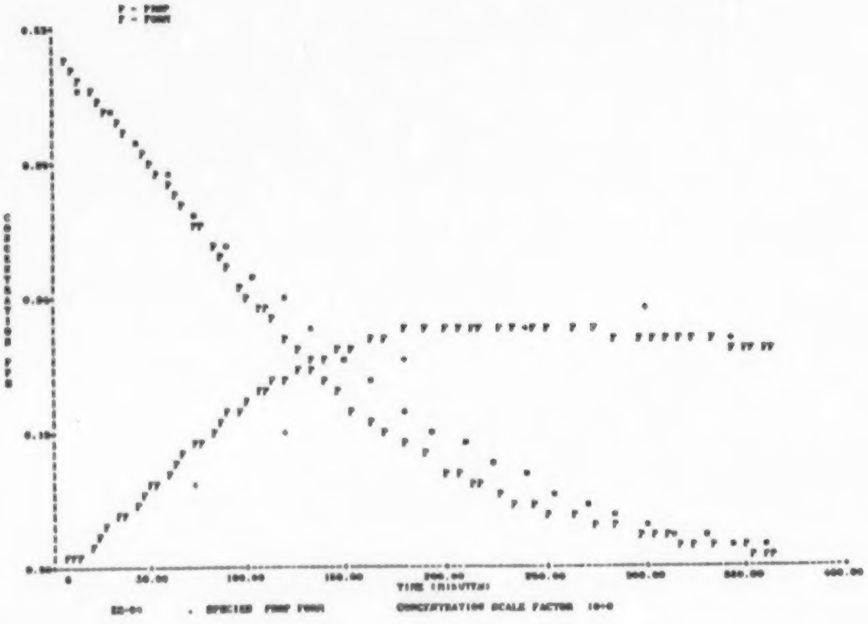

FIGURE III-43

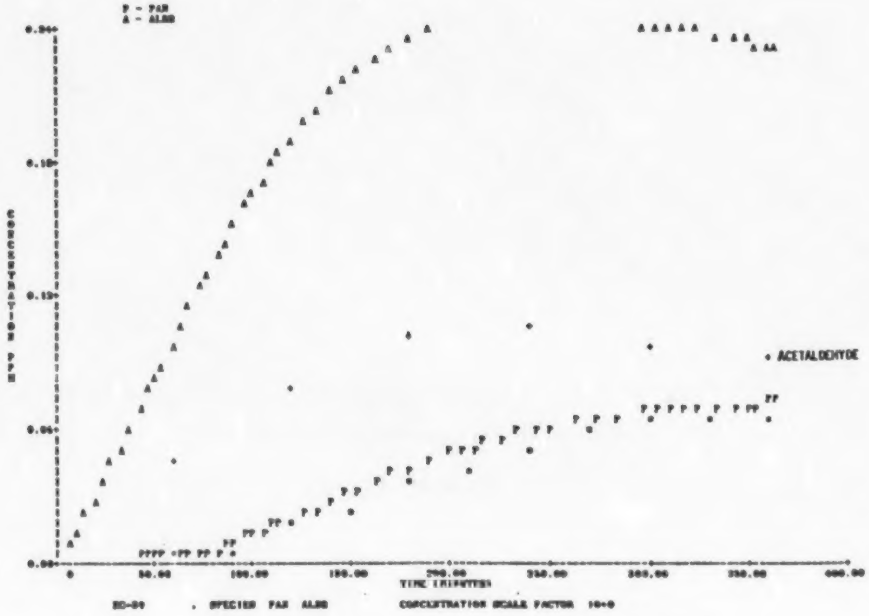

FIGURE III-44

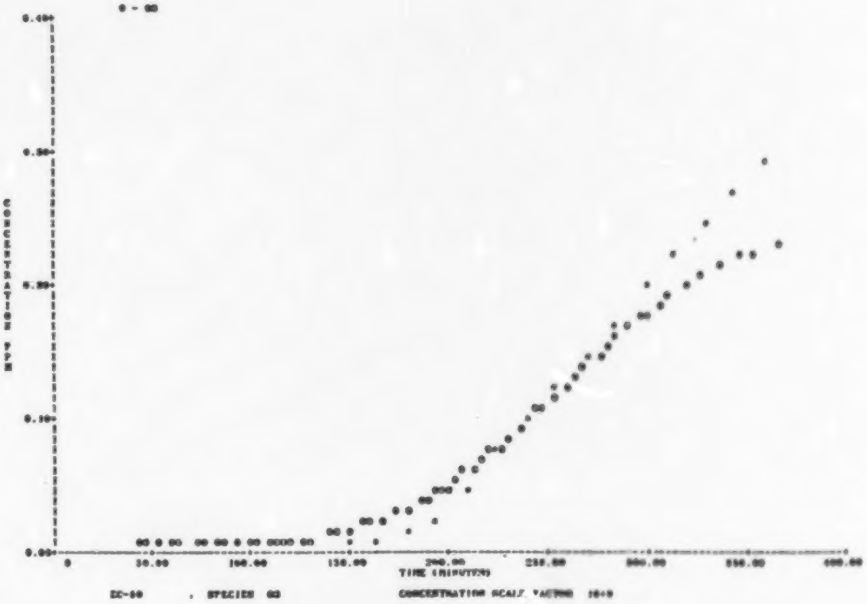

FIGURE III-45

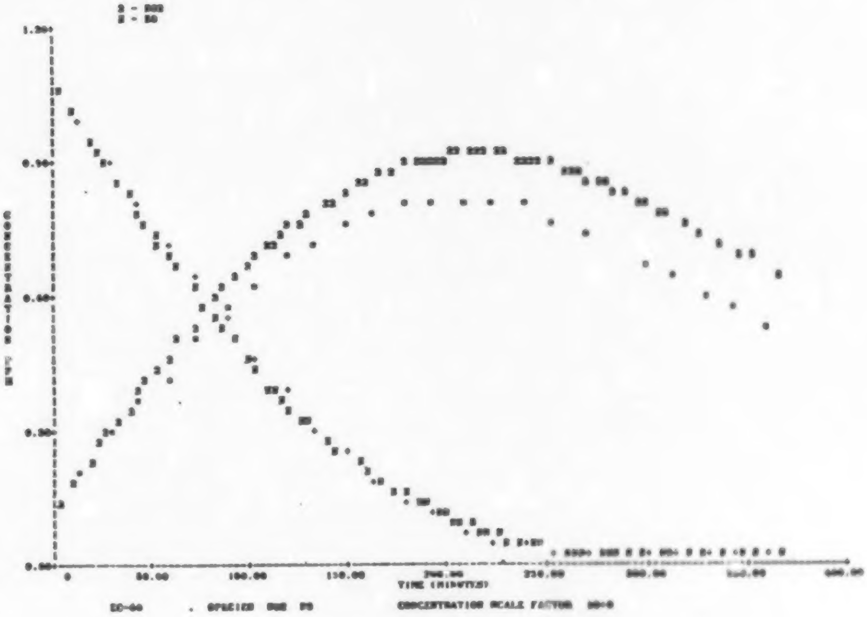

FIGURE III-46

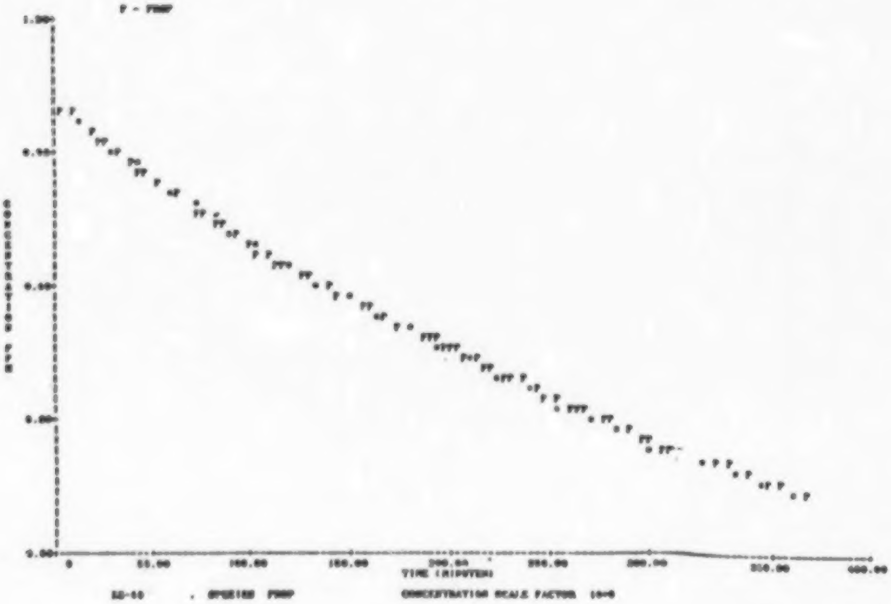

FIGURE III-47

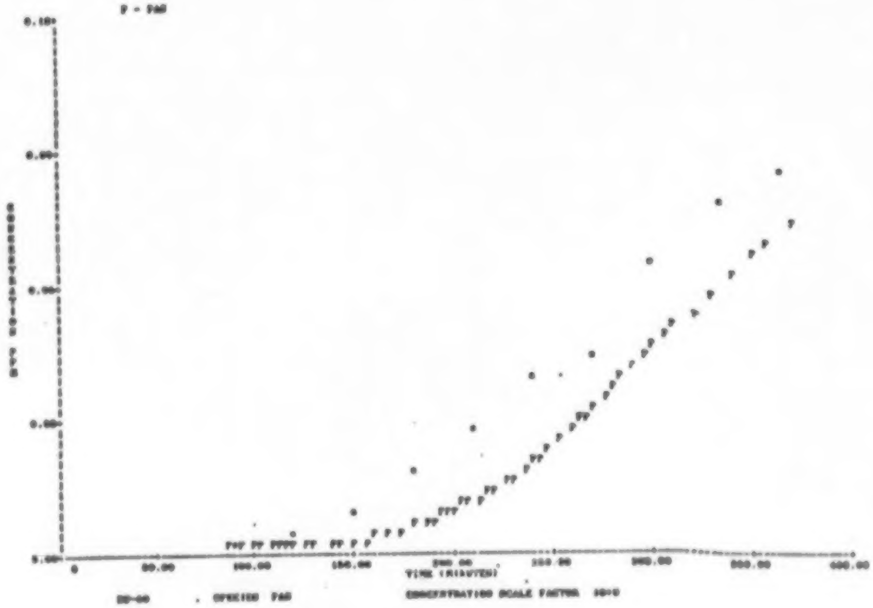

FIGURE III-48

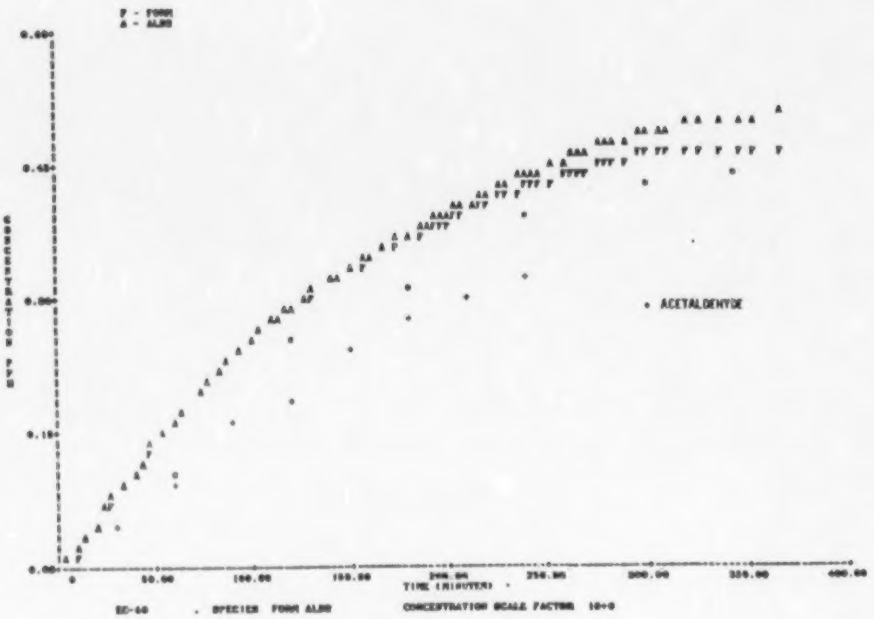

FIGURE III-49

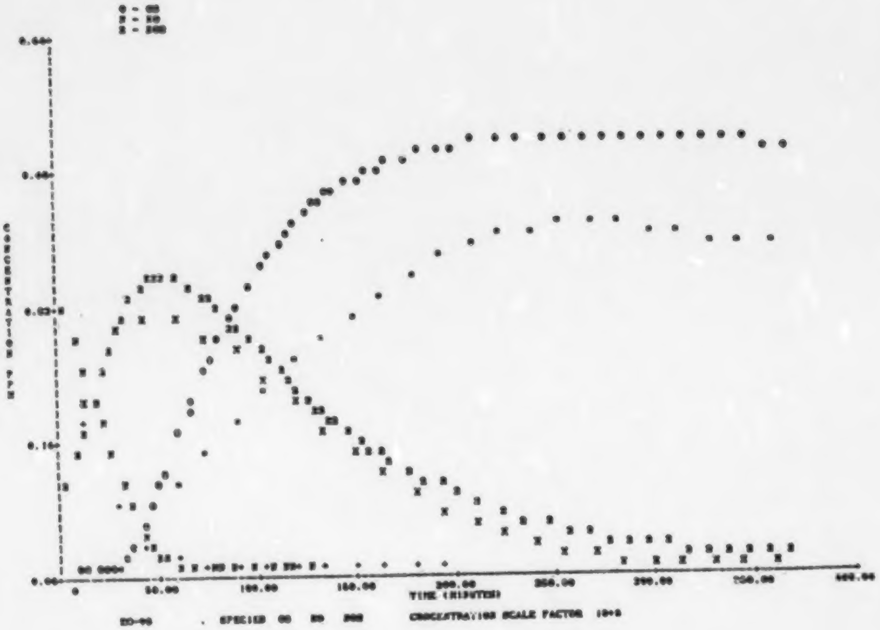

FIGURE III-50

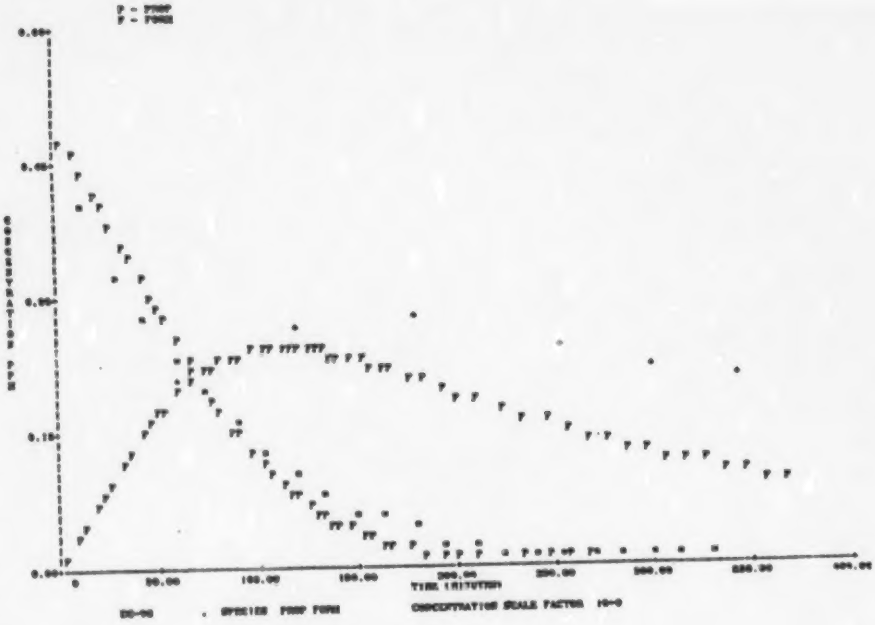

FIGURE III-51

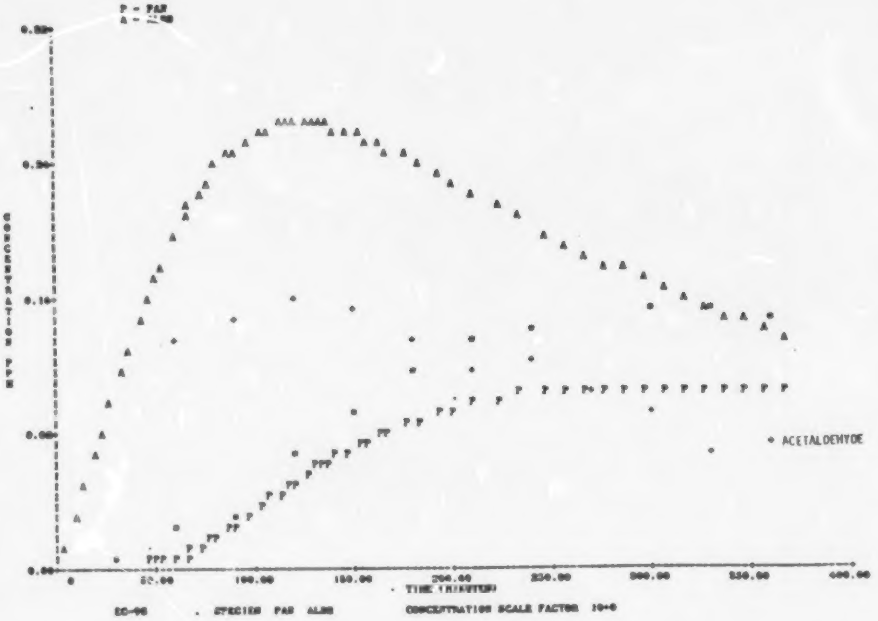

FIGURE III-52

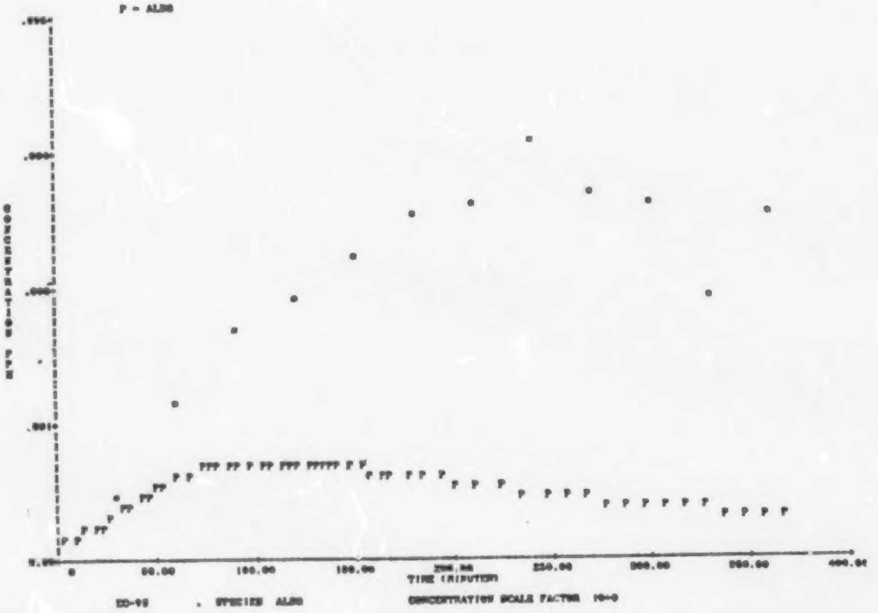

FIGURE III-53

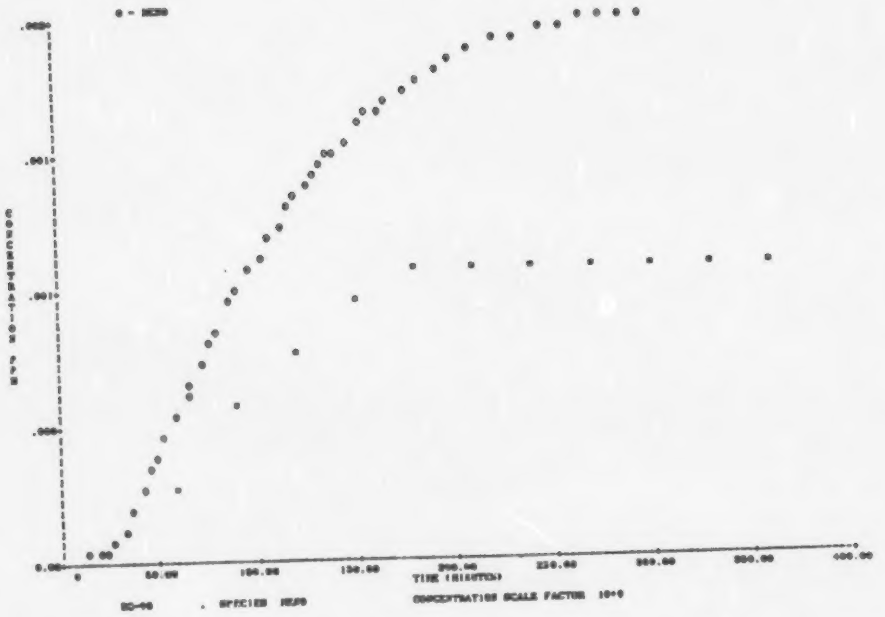

FIGURE III-54

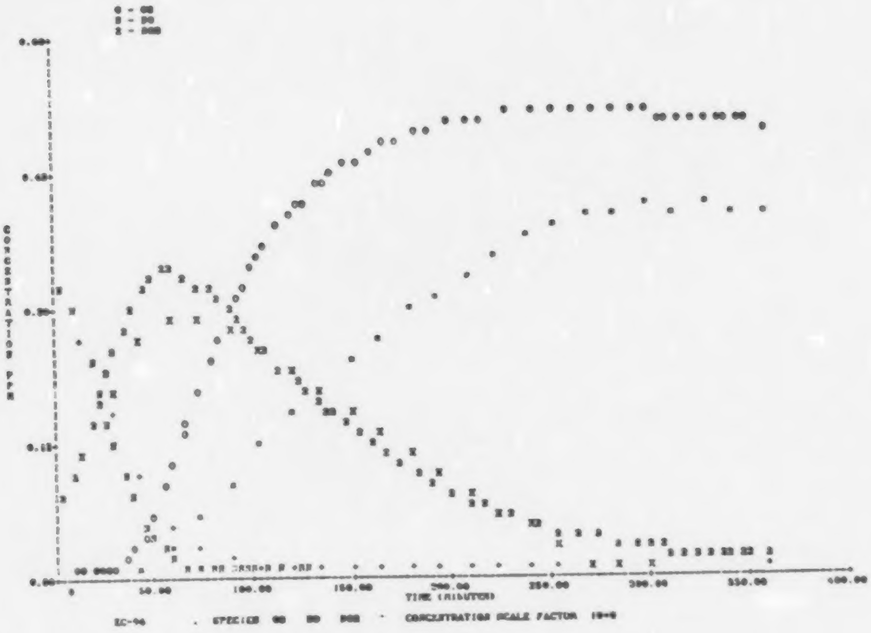

FIGURE III-55

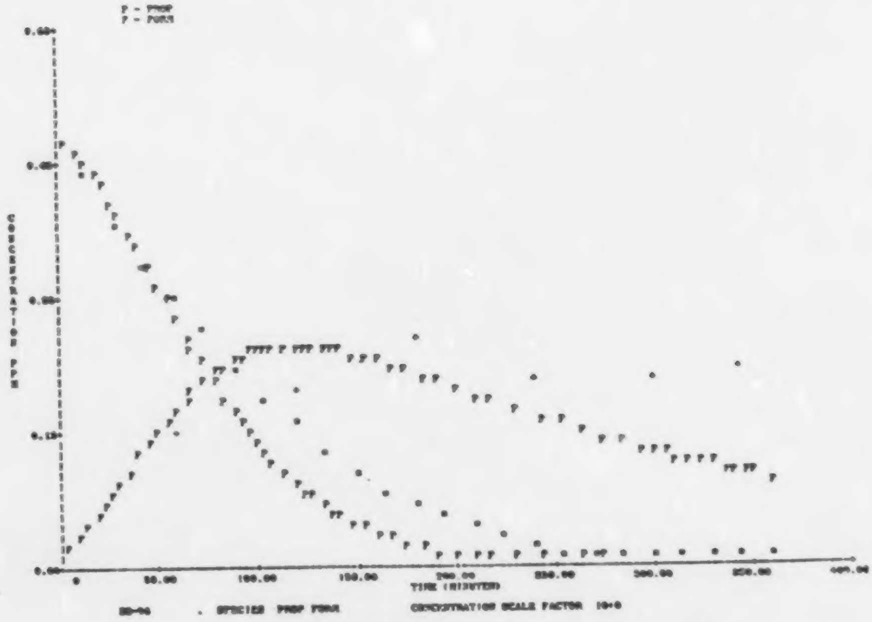

FIGURE III-56

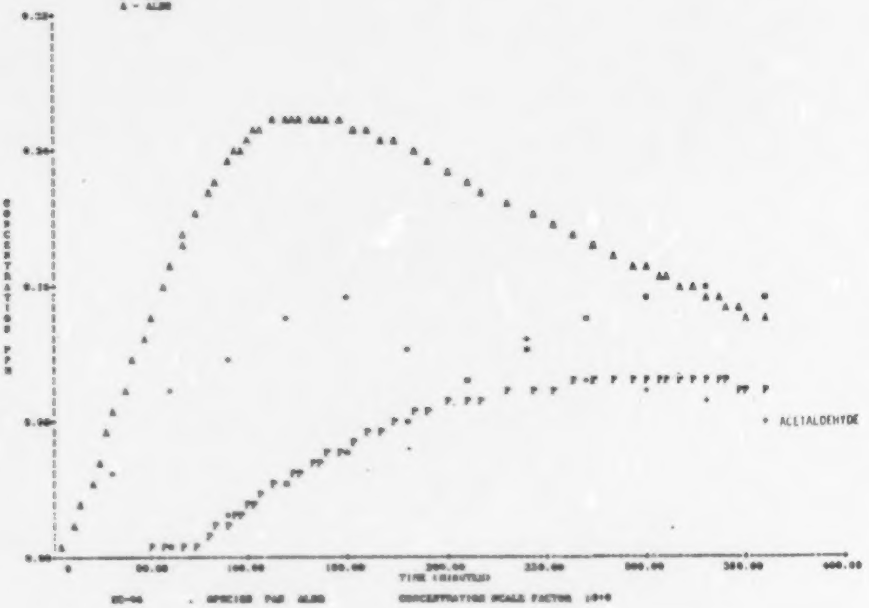

FIGURE III-57

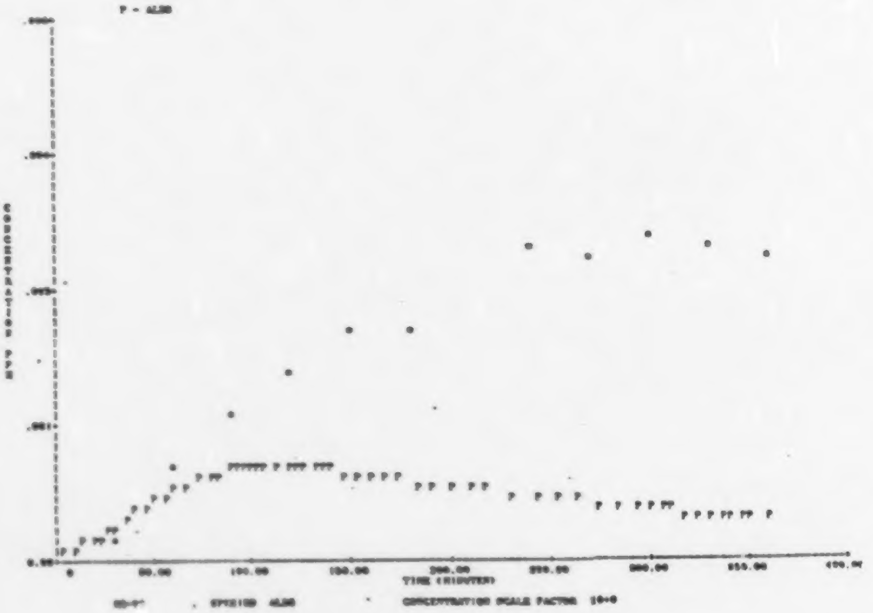

FIGURE III-58

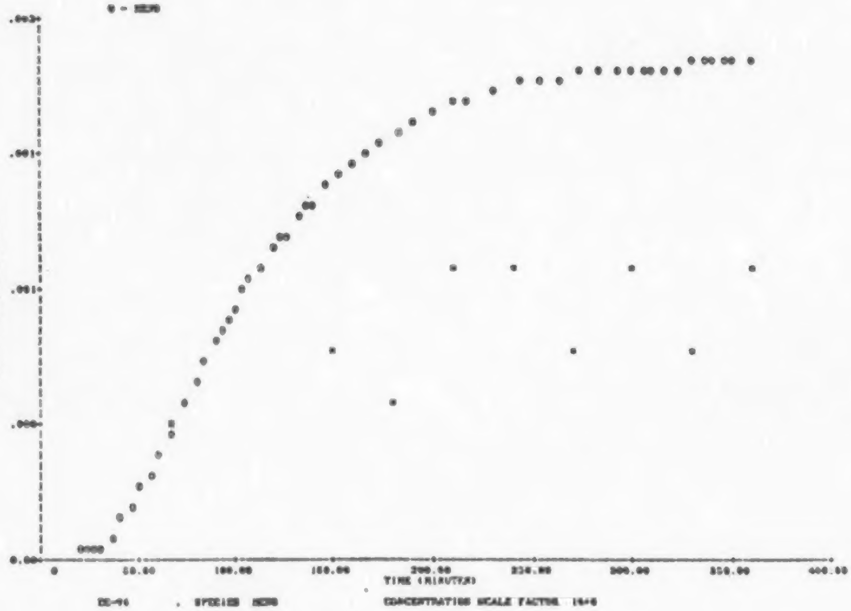

FIGURE III-59

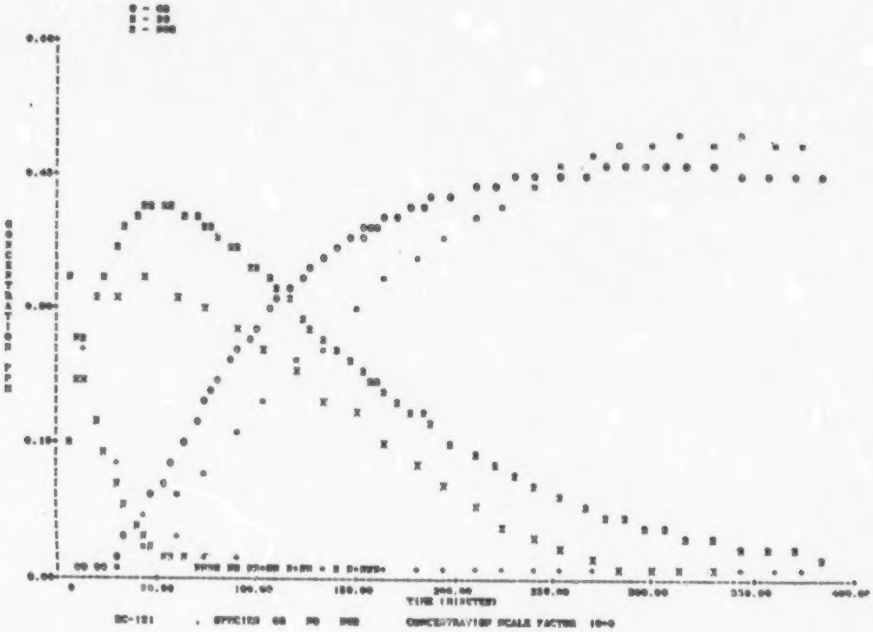

FIGURE III-60

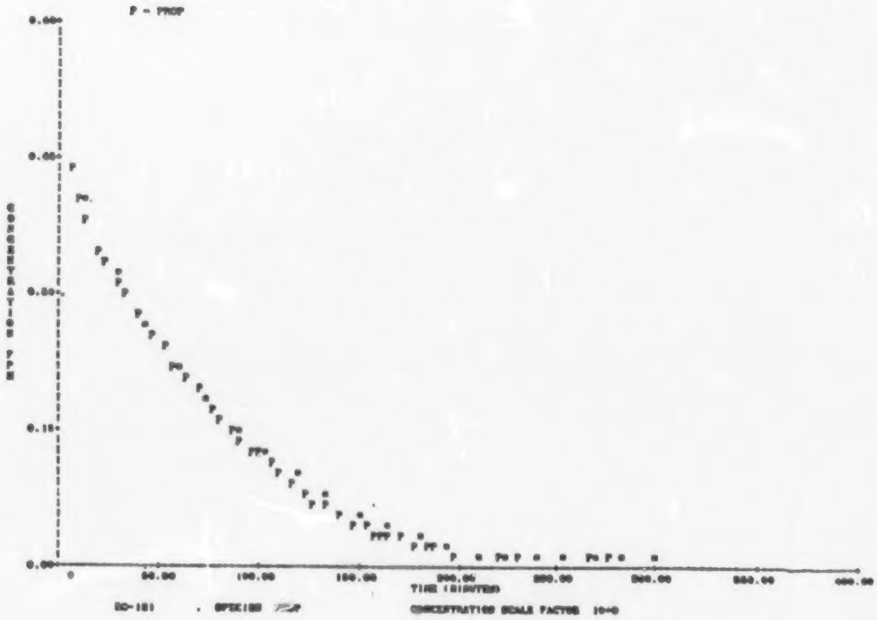

FIGURE III-61

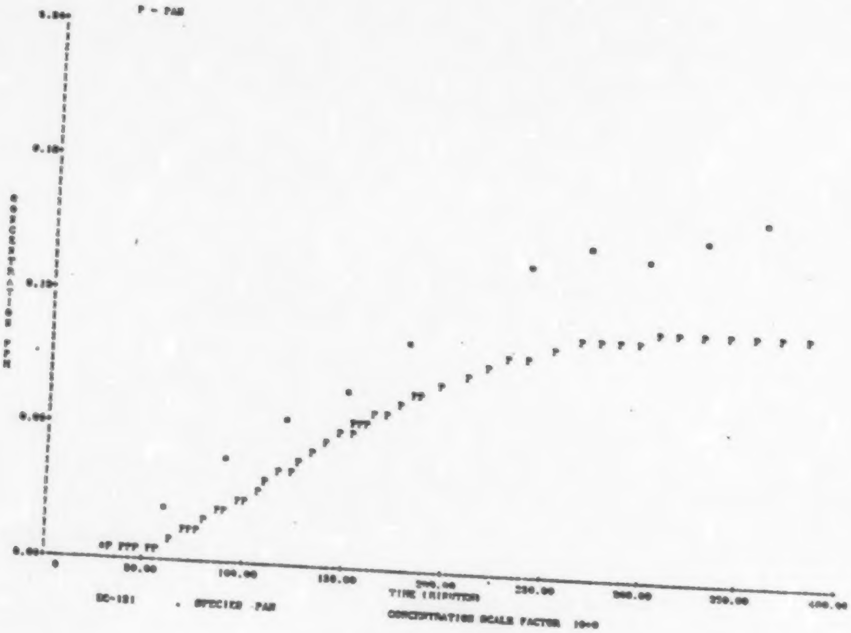

FIGURE III-62

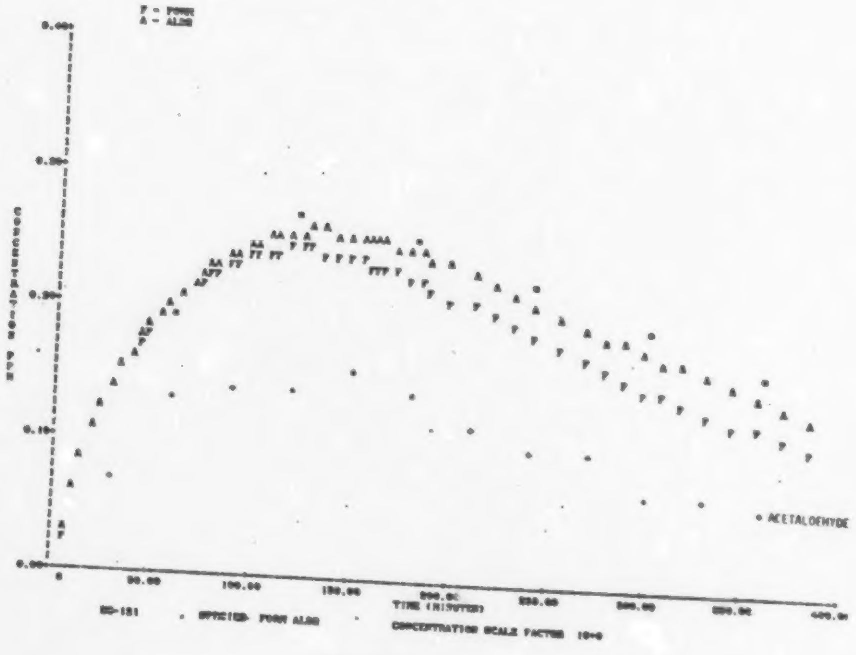

FIGURE III-63

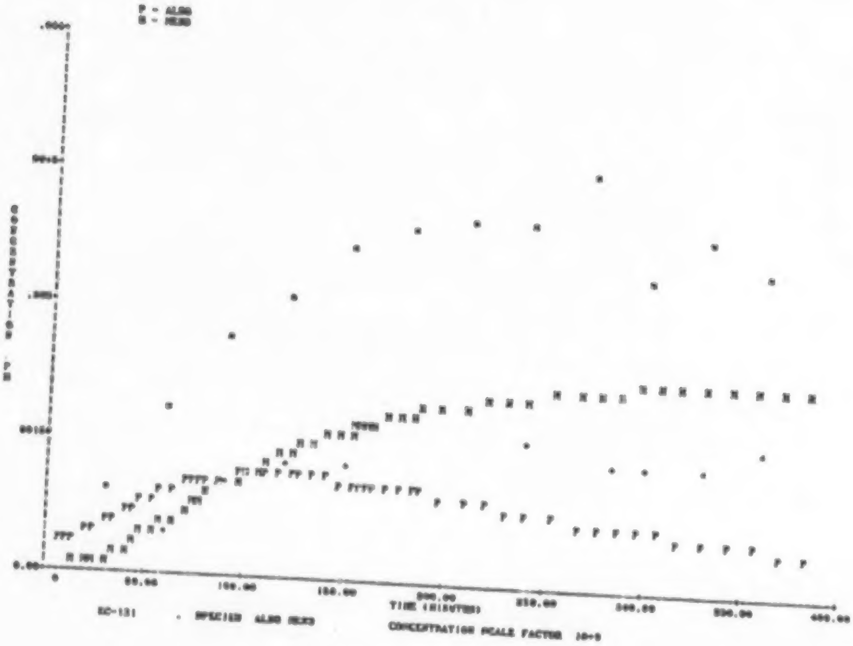

FIGURE III-64

TABLE III-7. PERCENT CARBON RECOVERY FOR PROPYLENE/NO_x SYSTEMS

EC Run Number	Elapsed Time (minutes) 60	120	180	240	300
5	57%	76%	76%	75%	70%
11	82	81	80	*	*
13	*	88	75	76	77
16	99	90	73	63	70
17	97	*	*	87	72
18	93	85	*	81	73
21	91	*	*	76	83
5127	43	42	42	43	39
55	35	36	35	41	39
56	*	*	35	38	*
59	*	52	52	52	49
60	*	*	69	68	60
95	73	68	64	*	55
96	*	*	58	57	56
121	*	53	*	38	27

---

* Data not available.

10. Discussion of the Propylene/NO_x Systems

The set of propylene experiments was performed at UCR over a period of some 25 months, in contrast to the other sets discussed below, each of which was completed within a few weeks. Propylene runs EC-5 to EC-21, however, were performed in a short time period, and later runs were mostly repeats of the standard run, EC-13. During the next year we will analyze these repeat runs more closely as part of a computer modeling study to seek out and explain chamber effects. In this report we present what we consider our best simulations of these runs, using the same overall mechanism throughout and varying only the light spectrum and initial HNO_2 concentration. As explained in Section III-B-5, the light spectrum was varied in a systematic way and only when spectral data were not available. The initial HNO_2 concentration used in the simulations was usually about one-third of the equilibrium concentration possible from the reaction of H_2O, NO, and NO_2.

In our final fitting procedure we began with propylene runs EC-95, EC-96, and EC-121, because detailed spectral measurements were available for these runs. We used our photolysis constant program to calculate the carbonyl photolysis constants (relative to NO_2 photolysis). We then varied the percent of ozonide formation in the mechanism until the total maintenance source of radicals from aldehydes, propylene-O atom reactions, and ozone-propylene reactions gave a good fit to the UCR data. Note that the percent of ozonide formation is only a fitting parameter. If the quantity is measured, many other parameters or added reactions could be used as fitting parameters. Some of these are as follows:

> Reactions of ozonides with radicals to act as sinks, or reactions that produce or release radicals.

> A slower or faster rate constant for the ozone-propylene reaction.
> Larger or smaller quantum yields for carbonyl photolysis.
> Fundamental changes in the mechanism, such as PAN chemistry, NO_x loss chemistry, and aldehyde formation.

During the fitting procedure for propylene runs, we discovered that the photolysis constants calculated from the spectral data for runs EC-95 and EC-121 differed. (Of course, it was still possible to produce good fits by arbitrarily varying the photolysis constants in the simulations of these runs.) The reported relative spectral data lead to a formaldehyde photolysis constant for radical production of 1.1×10^{-3} min^{-1} for EC-95 and 7.5×10^{-4} min^{-1} for EC-121.

On one hand, both of these values are rather high. In the simulations this causes an abundance of maintenence radicals from the photolysis of formaldehyde and other aldehydes. Thus, we had to lower radical production from the ozone-propylene reaction by setting the tuning parameter, the fraction of ozonide formation, to a high value, 0.33. This high value in turn makes the kinetic mechanism more sensitive to carbonyl photolysis than to the ozone-olefin reaction. On the other hand, the formaldehyde photolysis constants for EC-95 and EC-121 are quite different--the EC-95 constants are almost 50 percent larger than those of EC-121. Despite this outcome, the data from EC-95 and EC-121 are very similar. Therefore, the amounts of maintenance radicals required in simulating these runs must be similar. At this point we examined the reported spectral data for the period between runs EC-95 and EC-124. These are plotted in Figure III-65, which shows that some experimental scatter may be possible. Therefore, we chose the EC-120 curve to select the optimum value of the fitting parameter and used the value in all simulations. Figure III-66 shows the product of the acetaldehyde absorption spectrum and the reported relative spectral data for run EC-120. This figure shows that the region of the spectrum having the largest effect on radical production from aldehyde photolysis is from 300 nm to 340 nm. The same region shows the most apparent scatter in the UCR spectral data. Figures III-50 to III-59 show measurements and predictions for runs EC-95 and EC-96. These simulations used photolysis constants calculated from the relative spectral data reported by UCR. From the decay curves for propylene it is evident that too many radicals are present in the simulation.

We continued the fitting procedure by studying earlier experiments for butane as well as propylene to ensure that the spectra and HNO_2 concentrations required for different simulations were consistent. At this time we lowered the photolysis quantum yield for aldehydes larger than formaldehyde to 0.5. This change produced consistency between the butane, propylene, and 1-butene simulations.

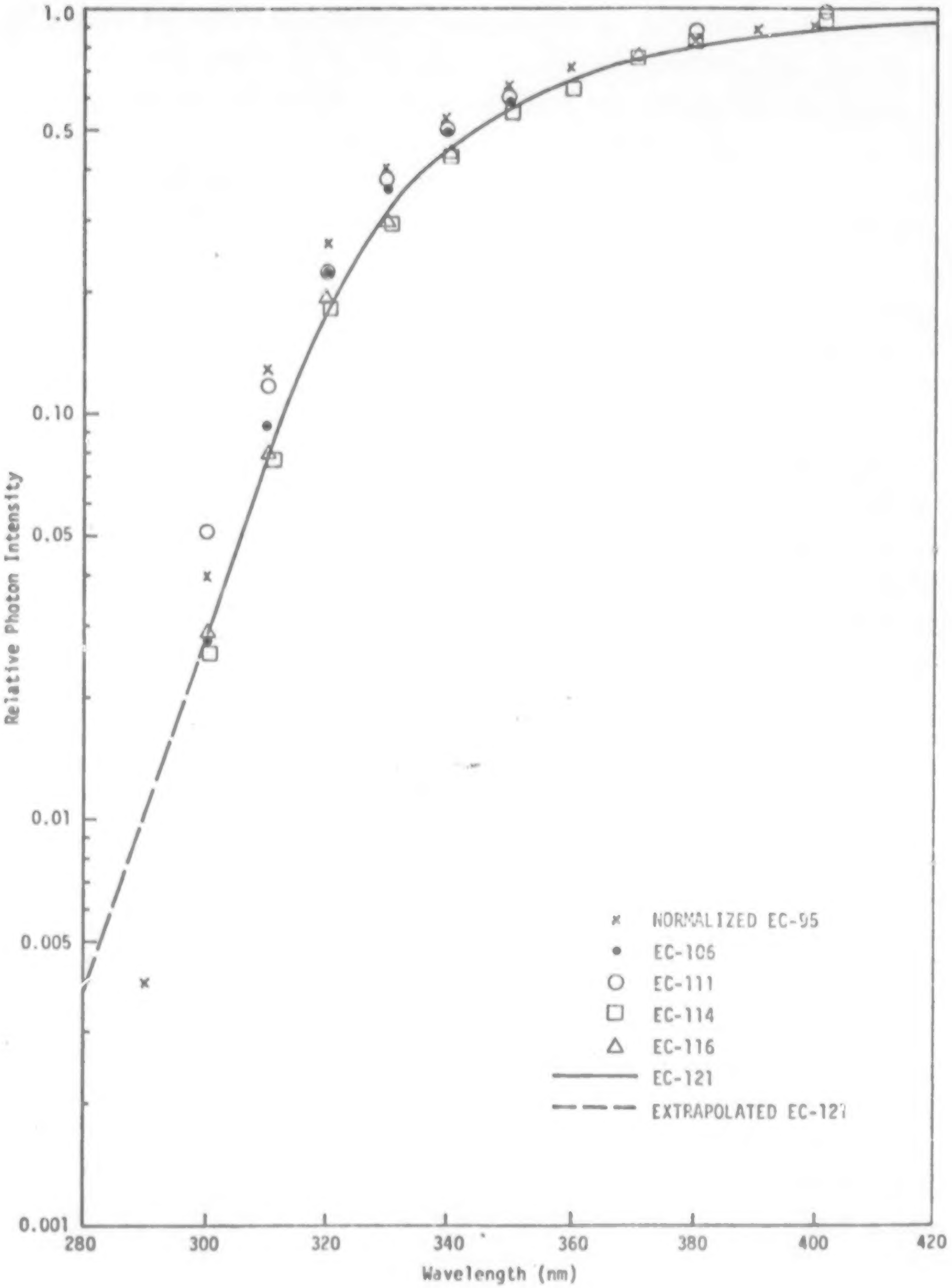

FIGURE III-65. RELATIVE INTENSITY FOR DIFFERENT UCR RUNS

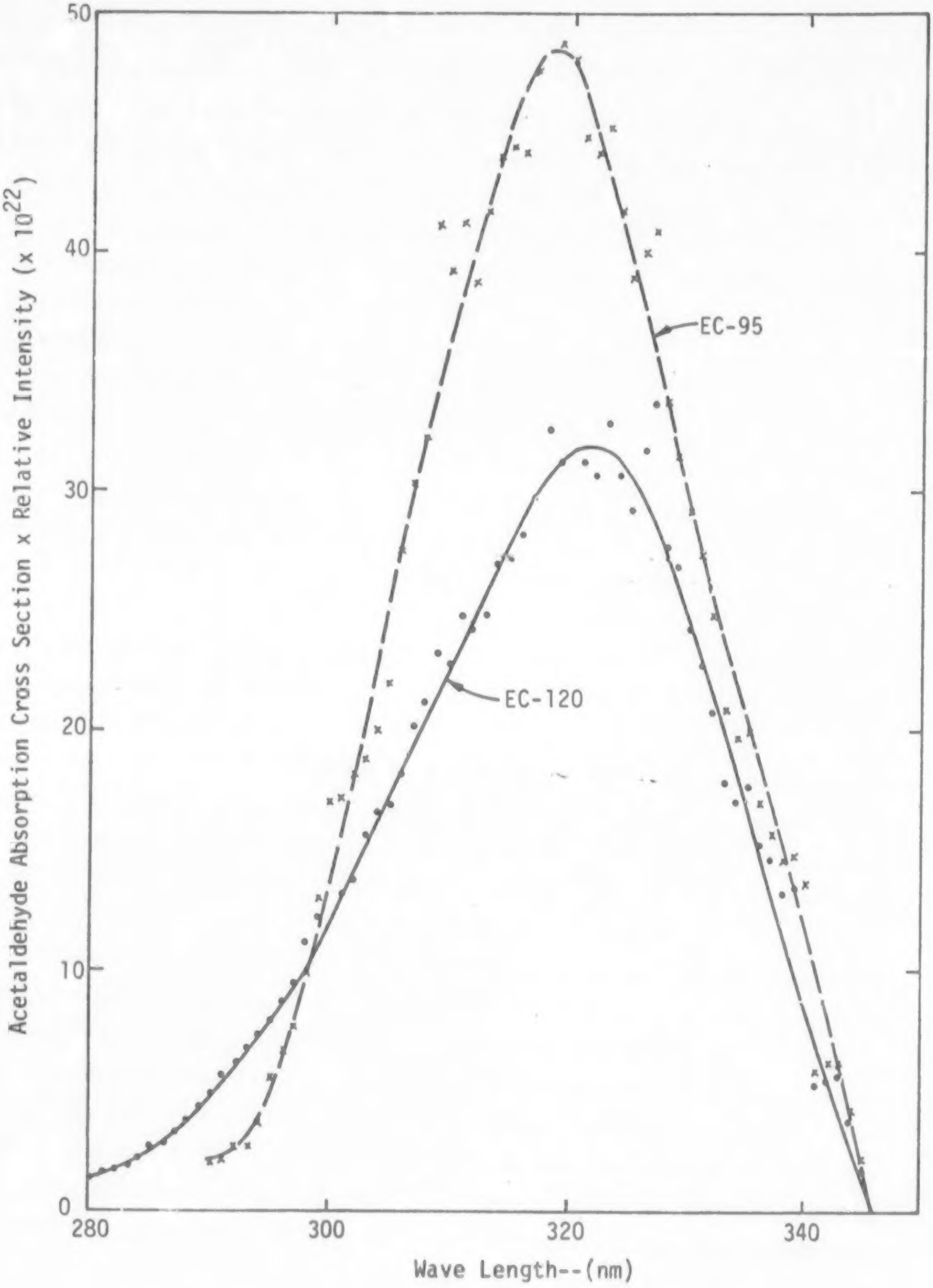

FIGURE III-66. ACETALDEHYDE PHOTOLYSIS CROSS SECTIONS FOR TWO DIFFERENT SIMULATIONS

As with all simulations, the total NO_x loss is not duplicated. The overall smog chemistry is dominated by conversion of NO to NO_2, and this conversion has been accurately simulated by providing a combination of chemical reactions and rate parameters. As discussed in the butane section above, we feel that our worst simulation is for EC-21. The mechanism does not provide enough maintenence radicals to sustain the rate of chemical reactivity observed at UCR. The compound most poorly simulated is PAN. PAN concentrations can be simulated in runs with high concentrations of NO_x and propylene, such as EC-5, EC-13, and EC-16. For the low NO_x runs (EC-17, EC-11, and EC-18), however, the predicted PAN concentrations vary from too low (EC-17) to too high (EC-18) as the hydrocarbon concentration increases. We feel that the shapes of the simulated ozone curves will more closely resemble the observed data when the NO_x loss and PAN chemistry are elucidated.

The shapes of some ozone curves can be partially explained by loss of ozone to the walls and the use of the controversial reaction of HO_2 and NO_2. In the original simulations of EC runs 55, 56, 59, and 60 the predicted ozone concentrations fit the observations through most of the experiments but were too low at the ends of the experiments. In repeat simulations, the removal of these two reactions from the mechanism improved the fit at the ends of the experiments without degrading the remainder. The rate of ozone loss to the smog chamber walls is treated as a constant in the mechanism, although it is probably not constant in reality. However, we did not feel justified in using different ozone loss rates for different experiments because this quantity is infrequently measured at UCR. Therefore, we continued to use a constant ozone loss rate as reported by Hecht et al. (1974b). The rate constant for the reaction of HO_2 and NO_2 was arbitarily adjusted to give a minimal effect, but the slowness of smog formation in runs EC-50 to EC-60, which is presumably due to a severe deterioration in the light source, exaggerates the overall effect of this reaction.

In Table III-8 we present a comparison between the predicted and measured maximum one-hour-average ozone concentrations. Percent differences are calculated relative to the observed data. The overall average of +0.93 percent represents the average difference between predictions and measurements. This average difference does not signify a bias because the standard deviation is much larger (15.9 percent in the propylene system).

The measured ozone concentrations for EC runs 5, 11, and 18 all peak and then decrease, but the predicted ozone concentrations do not. We found that a much better fit could be obtained by using different PAN chemistry, but the different chemistry caused a poorer fit between measurements and predictions for PAN and NO_2. The simulations shown were chosen for their overall resemblance to the data, not necessarily for the best fit to ozone

B. BUTANE/NO_x CHEMISTRY

Subsequent to our report of last year (Durbin et al., 1975), we revised the "explicit" butane mechanism to improved the simulations of UCR data for the butane/NO_x system. The following areas were studied:

> Butane oxidation.
> Alkoxyl radical chemistry.
> Secondary products important in overall reactivity
(butyraldehyde, methylethylketone).

These areas are discussed below.

TABLE III-8. PREDICTED AND MEASURED MAXIMUM ONE-HOUR-AVERAGE OZONE CONCENTRATIONS FOR PROPYLENE/NO_x SYSTEMS

	Maximum One-Hour-Average Ozone Concentration (ppm)		
EC Run Number	Measured	Predicted	Percent Difference
5	0.46	0.47	2
11	0.23	0.27	17
13	0.37	0.374	1.1
16	0.50	0.45	-10
17	0.14	0.16	14.3
18	0.18	0.21	16.7
21	0.006	0.0067	11.7
5127	0.26	0.245	-5.8
55	0.33	0.28	-15.2
56	0.36	0.285	-20.8
59	0.38	0.31	-18.4
60	0.25	0.21	-16
95	0.41	0.51	24
96	0.413	0.513	24
121	0.503	0.45	-10.5

Note: Average difference +0.93 percent; standard deviation 15.9 percent.

1. Hydrogen Abstraction from Butane by Hydroxyl Radicals

The products of the hydrogen abstraction from butane in air by hydroxyl radicals are a peroxyalkyl radical and water. Hydroxyl radicals can abstract a hydrogen from either the terminal carbon or the secondary carbon as follows:

$$C_4H_{10} + OH\cdot \xrightarrow{O_2} CH_3CH_2CH_2CH_2OO\cdot + H_2O \quad ,$$

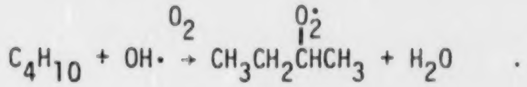

$$C_4H_{10} + OH\cdot \xrightarrow{O_2} CH_3CH_2\overset{O_2^{\cdot}}{\overset{|}{C}}HCH_3 + H_2O \quad .$$

A ratio of 6:1 for secondary to primary attack was determined from the empirical formula developed by Greiner (1970) for

$$\text{Alkane} + OH\cdot \rightarrow \text{Products} \quad .$$

The rate constant is:

$$k = [1.0 \exp(-820/T)N_P + 2.3 \exp(-430/T)N_S$$

$$+ 2.1 \exp(95/T)N_T] \times 1.476 \times 10^3 \text{ ppm}^{-1}\text{min}^{-1} \quad ,$$

where N_P, N_S, N_T are the number of primary, secondary, and tertiary hydrogens, respectively. The initial alkyl radicals immediately react with molecular oxygen to form the peroxyalkyl radicals shown, which will react with nitric oxide (NO) to produce alkoxyl radicals and NO_2. From here on, the chemistry of the alkoxyl radicals plays a central role in the overall system.

2. Alkoxyl Radical Chemistry

a. Decomposition Versus Reaction with Molecular Oxygen

In the propylene/NO_x system, alkoxyl radicals are not as important as they are in the butane/NO_x system because the hydroxyl-alkoxyl radicals that form in the propylene system are apparently less stable than the alkoxyl radicals in the butane system. After reviewing the literature and studying the thermokinetics of the decomposition of the alkoxyl radicals, we have concluded that the decomposition pathways are unimportant (except for sec-butoxyl radical) compared with their reactions with molecular oxygen to form carbonyl compounds. This is discussed in the propylene chemistry section.

Formation of butyraldehyde occurs from only one reaction, that of n-butoxyl radicals with molecular oxygen. Therefore, we need to consider the unimolecular decomposition of sec-butoxyl radicals over the reaction with molecular oxygen in order to limit the formation of methylethylketone,

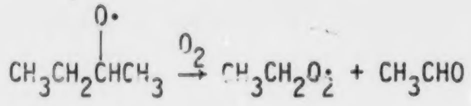

$$\mathrm{CH_3CH_2\overset{O\cdot}{\overset{|}{C}}HCH_3 \xrightarrow{O_2} CH_3CH_2O_2\cdot + CH_3CHO} \quad ,$$

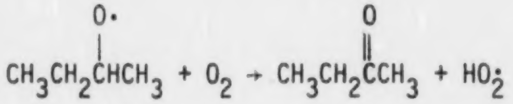

$$\mathrm{CH_3CH_2\overset{O\cdot}{\overset{|}{C}}HCH_3 + O_2 \rightarrow CH_3CH_2\overset{O}{\overset{\|}{C}}CH_3 + HO_2\cdot} \quad ,$$

due to the difference in secondary to primary ratios between the initial attack ratio (from Greiner's formula) and the product ratio measured at UCR. UCR data show the need for a ratio of 18:1 of secondary to primary products, that is, the ratio of MEK to butyraldehyde.

Although neither of these ratios is highly certain, it appears that they are not equal. Additional evidence for some other path to make the products ratio different from the production ratio comes from the results of trial calculations with all the alkoxyl radicals reacting with molecular oxygen. In these experiments we found that too much MEK was formed, not enough acetaldehyde was formed, and far too much butyraldehyde was formed. Adding the unimolecular decomposition of secondary butoxyl radicals to the mechanism is therefore very tempting because the main stable product is acetaldehyde (Benson and O'Neal, 1970). However, the ratio of MEK to butyraldehyde is then even lower than the 6:1 production ratio. If the decomposition of the primary butoxyl radicals is postulated, then the production of propyl radicals must be accepted based on thermokinetic considerations:

$$CH_3CH_2CH_2CH_2O\cdot \rightarrow CH_3CH_2CH_2^{\cdot} + HCHO \quad .$$

Then one would have:

$$CH_3CH_2CH_2^{\cdot} + O_2 \rightarrow CH_3CH_2CH_2O_2^{\cdot} \quad ,$$

$$CH_3CH_2CH_2O_2^{\cdot} + NO \rightarrow CH_3CH_2CH_2O\cdot + NO_2 \quad ,$$

$$CH_3CH_2CH_2O\cdot + O_2 \rightarrow CH_3CH_2CHO + HO_2^{\cdot} \quad ,$$

$$CH_3CH_2CH_2O\cdot \rightarrow CH_3CH_2^{\cdot} + HCHO \quad .$$

In other words, the formation of more formaldehyde and propionaldehyde is predicted. In all the UCR butane experiments, propionaldehyde was never reported, yet acetaldehyde and butyraldehyde were seen. In some propylene experiments, very low amounts of propionaldehyde were reported in the presence of substantial amounts of acetaldehyde. For instance, in run EC-121, propionaldehyde was reported at 0.003 ppm in the presence of 0.14 ppm acetaldehyde. We feel that the negative UCR experimental results for propionaldehyde imply that little, if any, primary butoxyl radicals were thermally decomposing in the butane system. Also there is supporting evidence from our trial calculations with exclusive decomposition that the decomposition chemistry would lead to greatly enhanced formaldehyde production, a result that is not in keeping with the low amounts reported in the UCR data.

As we reported last year, for alkoxyl radicals the rates of unimolecular decomposition and reaction with molecular oxygen span several orders of magnitude. Recently, Barker et al. (1976) have shown that most reactions with molecular oxygen proceed at similar rates virtually independent of the size of the radical. However, thermokinetic and experimental evidence suggests that unimolecular decomposition rates increase rapidly with increasing molecular weight. Thus somewhere in the alkyl chain-length progression, unimolecular decomposition would be competitive with reaction with molecular oxygen. Future smog chamber experiments with longer chain alkanes, such as n-hexane and n-octane, are necessary to help elucidate this chemistry.

In this study we tried to test the assumption that either one or the other process is dominant in the butane system. Our finding is that, overall, the dominance of reaction with oxygen is more in keeping with the UCR data. The one unimolecular decomposition that seems necessary to retain at this time is that of the secondary butoxyl radical.

b. Internal Isomerization of the Alkoxyl Radicals

The information above suggests that reaction with oxygen may dominate the alkoxyl radical chemistry of butane. However, the observed product ratio of MEK to butyraldehyde and especially the carbon mass loss in the butane experiments cannot be fitted by this conclusion alone. A carbon mass loss could be explained by formation of bifunctional compounds, such as hydroxy-carbonyls, which would have long retention times for chromatographic analysis as used at UCR.

Carter et al. (1976) have suggested that internal hydrogen rearrangement may occur via a six-member cyclic intermediate for n-butoxy radicals:

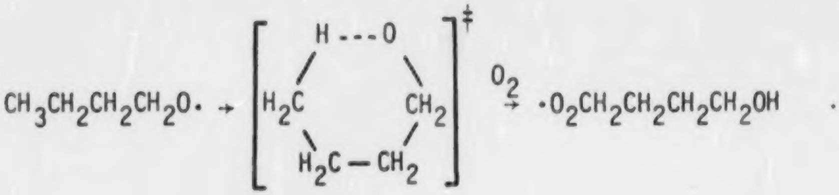

The hydroxyperoxybutyl radical would then react with NO:

$$\cdot O_2CH_2CH_2CH_2CH_2OH + NO \rightarrow NO_2 + \cdot OCH_2CH_2CH_2CH_2OH \quad ,$$

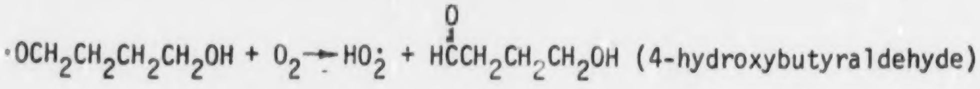

$$\cdot OCH_2CH_2CH_2CH_2OH + O_2 \rightarrow HO_2^{\cdot} + H\overset{\overset{O}{\|}}{C}CH_2CH_2CH_2OH \text{ (4-hydroxybutyraldehyde)}$$

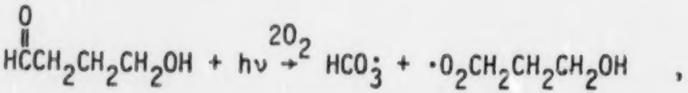

$$H\overset{\overset{O}{\|}}{C}CH_2CH_2CH_2OH + h\nu \xrightarrow{2O_2} HCO_3^{\cdot} + \cdot O_2CH_2CH_2CH_2OH \quad ,$$

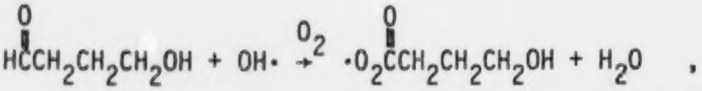

$$H\overset{\overset{O}{\|}}{C}CH_2CH_2CH_2OH + OH\cdot \xrightarrow{O_2} \cdot O_2\overset{\overset{O}{\|}}{C}CH_2CH_2CH_2OH + H_2O \quad ,$$

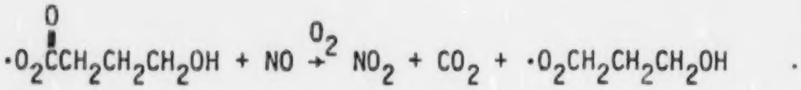

$$\cdot O_2\overset{\overset{O}{\|}}{C}CH_2CH_2CH_2OH + NO \xrightarrow{O_2} NO_2 + CO_2 + \cdot O_2CH_2CH_2CH_2OH \quad .$$

3-Peroxy-1-propanol radicals may also form; these would undergo reactions similar to the above:

$$\cdot O_2CH_2CH_2CH_2OH + NO \rightarrow NO_2 + \cdot OCH_2CH_2CH_2OH \quad ,$$

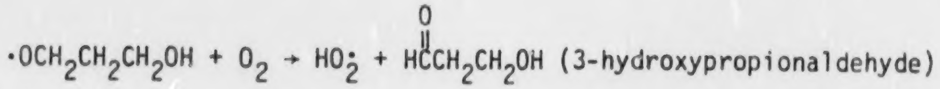

$$\cdot OCH_2CH_2CH_2OH + O_2 \rightarrow HO_2^{\cdot} + H\overset{\overset{O}{\|}}{C}CH_2CH_2OH \text{ (3-hydroxypropionaldehyde)} \quad ,$$

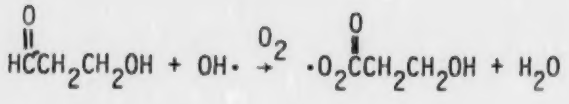

$$H\overset{\overset{O}{\|}}{C}CH_2CH_2OH + OH\cdot \xrightarrow{O_2} \cdot O_2\overset{\overset{O}{\|}}{C}CH_2CH_2OH + H_2O \quad ,$$

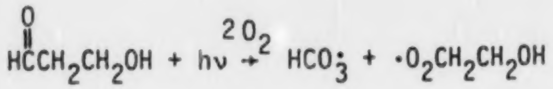

$$H\overset{\overset{O}{\|}}{C}CH_2CH_2OH + h\nu \xrightarrow{2O_2} HCO_3^{\cdot} + \cdot O_2CH_2CH_2OH \quad ,$$

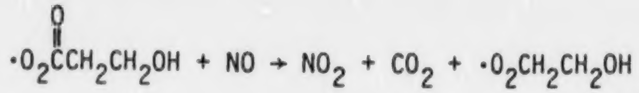

$$\cdot O_2\overset{\overset{O}{\|}}{C}CH_2CH_2OH + NO \rightarrow NO_2 + CO_2 + \cdot O_2CH_2CH_2OH \quad ,$$

The 2-peroxyethanol radicals formed might then react with NO:

$$\cdot O_2CH_2CH_2OH + NO \rightarrow NO_2 + \cdot OCH_2CH_2OH \quad ,$$

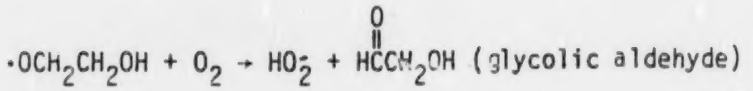

$$\cdot OCH_2CH_2OH + O_2 \rightarrow HO_2^{\cdot} + H\overset{\overset{O}{\|}}{C}CH_2OH \text{ (glycolic aldehyde)} \quad ,$$

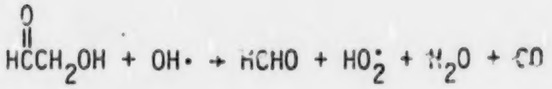

$$H\overset{\overset{O}{\|}}{C}CH_2OH + OH\cdot \rightarrow HCHO + HO_2^{\cdot} + H_2O + CO \quad ,$$

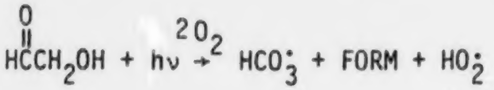

$$H\overset{\overset{O}{\|}}{C}CH_2OH + h\nu \xrightarrow{2O_2} HCO_3^{\cdot} + FORM + HO_2^{\cdot} \quad ,$$

The sec-butoxyl radical may also undergo rearrangement processes. These processes would occur more slowly than for the n-butoxyl radical, however, because five-membered ring intermediates probably form more slowly than six-membered ring intermediates (Hendry, 1976):

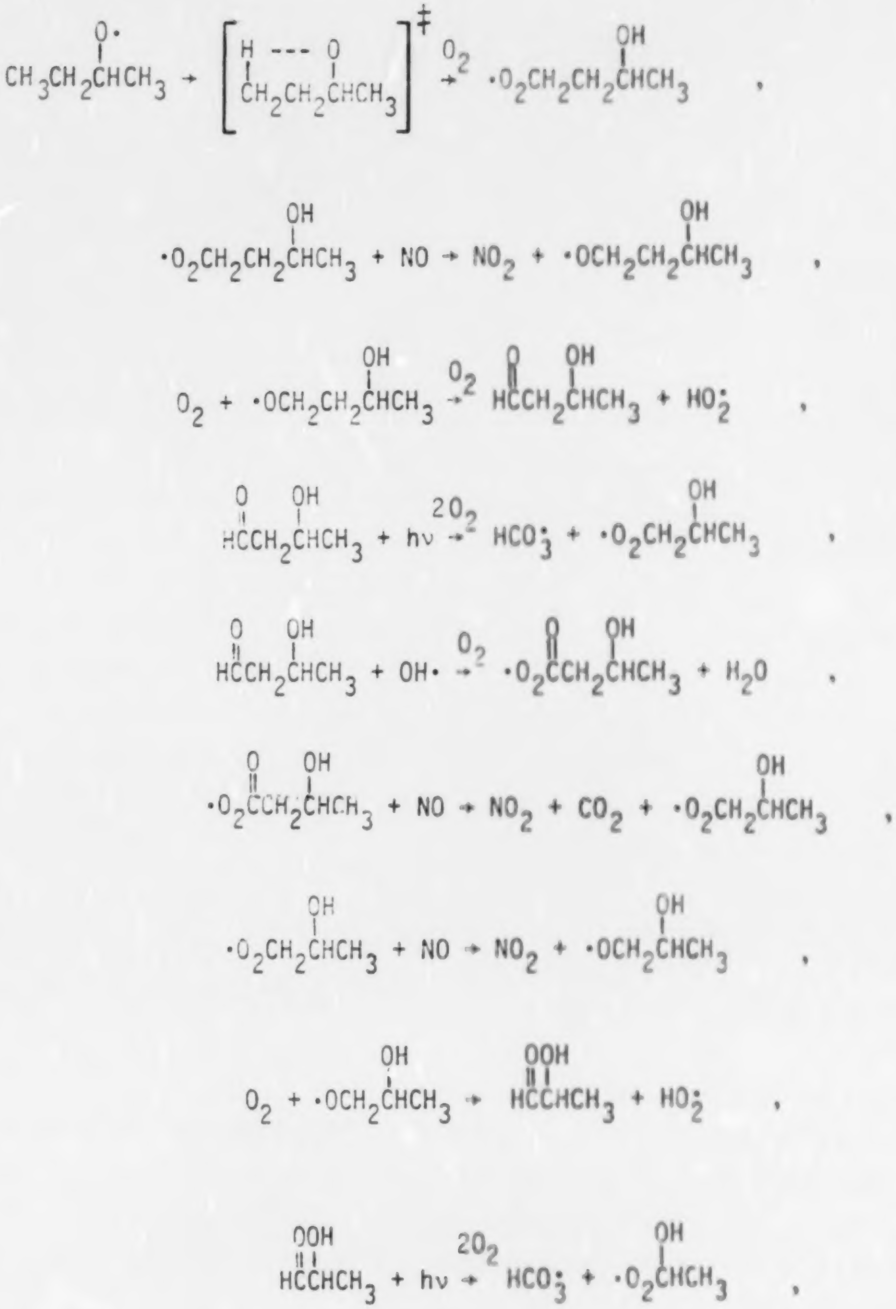

$$CH_3CH_2\overset{O\cdot}{\overset{|}{C}}HCH_3 \rightarrow \left[\begin{matrix}H \text{ --- } O\\ | \qquad\quad | \\ CH_2CH_2CHCH_3\end{matrix}\right]^{\ddagger} \xrightarrow{O_2} \cdot O_2CH_2CH_2\overset{OH}{\overset{|}{C}}HCH_3 \quad ,$$

$$\cdot O_2CH_2CH_2\overset{OH}{\overset{|}{C}}HCH_3 + NO \rightarrow NO_2 + \cdot OCH_2CH_2\overset{OH}{\overset{|}{C}}HCH_3 \quad ,$$

$$O_2 + \cdot OCH_2CH_2\overset{OH}{\overset{|}{C}}HCH_3 \xrightarrow{O_2} H\overset{O}{\overset{\|}{C}}CH_2\overset{OH}{\overset{|}{C}}HCH_3 + HO_2^{\cdot} \quad ,$$

$$H\overset{O}{\overset{\|}{C}}CH_2\overset{OH}{\overset{|}{C}}HCH_3 + h\nu \xrightarrow{2O_2} HCO_3^{\cdot} + \cdot O_2CH_2\overset{OH}{\overset{|}{C}}HCH_3 \quad ,$$

$$H\overset{O}{\overset{\|}{C}}CH_2\overset{OH}{\overset{|}{C}}HCH_3 + OH\cdot \xrightarrow{O_2} \cdot O_2\overset{O}{\overset{\|}{C}}CH_2\overset{OH}{\overset{|}{C}}HCH_3 + H_2O \quad ,$$

$$\cdot O_2\overset{O}{\overset{\|}{C}}CH_2\overset{OH}{\overset{|}{C}}HCH_3 + NO \rightarrow NO_2 + CO_2 + \cdot O_2CH_2\overset{OH}{\overset{|}{C}}HCH_3 \quad ,$$

$$\cdot O_2CH_2\overset{OH}{\overset{|}{C}}HCH_3 + NO \rightarrow NO_2 + \cdot OCH_2\overset{OH}{\overset{|}{C}}HCH_3 \quad ,$$

$$O_2 + \cdot OCH_2\overset{OH}{\overset{|}{C}}HCH_3 \rightarrow H\overset{O}{\overset{\|}{C}}\overset{OH}{\overset{|}{C}}HCH_3 + HO_2^{\cdot} \quad ,$$

$$H\overset{O}{\overset{\|}{C}}\overset{OH}{\overset{|}{C}}HCH_3 + h\nu \xrightarrow{2O_2} HCO_3^{\cdot} + \cdot O_2\overset{OH}{\overset{|}{C}}HCH_3 \quad ,$$

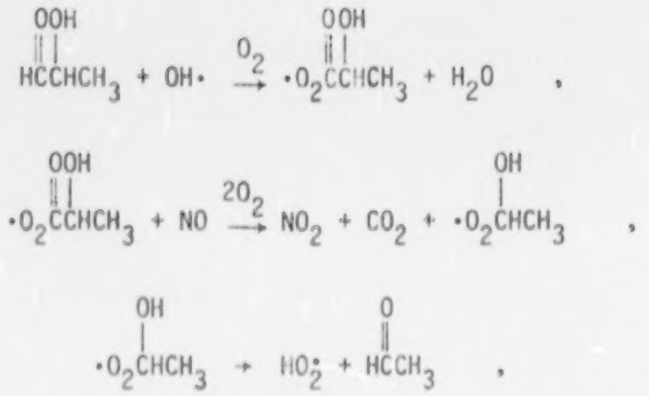

$$H\overset{O}{\overset{\|}{C}}\overset{OH}{\overset{|}{C}}HCH_3 + OH\cdot \xrightarrow{O_2} \cdot O_2\overset{O}{\overset{\|}{C}}\overset{OH}{\overset{|}{C}}HCH_3 + H_2O \quad ,$$

$$\cdot O_2\overset{O}{\overset{\|}{C}}\overset{OH}{\overset{|}{C}}HCH_3 + NO \xrightarrow{2O_2} NO_2 + CO_2 + \cdot O_2\overset{OH}{\overset{|}{C}}HCH_3 \quad ,$$

$$\cdot O_2\overset{OH}{\overset{|}{C}}HCH_3 \rightarrow HO_2^{\cdot} + H\overset{O}{\overset{\|}{C}}CH_3 \quad ,$$

Private communications with K. Darnell of UCR confirmed the existence of some peaks in their GC analyses that are consistent with hydroxyaldehydes. Mill and Montorsi (1973) found the major products of gas-phase oxidation of n-pentane and higher homologs to be cyclic ethers. The corresponding reaction of the 1-butoxy radical to form tetrahydrofuran is probably slower, since the transition state is a strained five-membered ring, but intramolecular hydrogen abstraction, as discussed above, is reported to occur with facility in the liquid phase. Furthermore, Carter et al. (1976) have reported evidence for alkoxyl radical isomerization occurring in C_4-C_6 alkanes in NO_x/air systems in smog chambers. We have chosen the rate constant for the reaction:

$$CH_3CH_2CH_2CH_2O\cdot \rightarrow \cdot O_2CH_2CH_2CH_2CH_2OH$$

to fit UCR's butyraldehyde data.

A carbon mass balance, as described earlier in this chapter, was performed on UCR's butane data (Table III-9). The carbon mass balance in general showed approximately a 40 percent loss early in each run. In the butane/NO_x system the reactive losses are proportionally smaller than in the other systems. Since butane is a four-carbon molecule, the error in its measurement is a

TABLE III-9. PERCENT CARBON MASS RECOVERY FOR BUTANE/NO_x SYSTEMS

Time (minutes)	UCR Run Number						
	EC-39	EC-41	EC-42	EC-43	EC-44	EC-45	EC-48
60	37%	55%	*	*	53%	33%	79%
120	79	62	83%	53%	*	48	44
180	*	57	80	46	*	*	*
240	81	57	*	54	*	*	73
300	77	54	84	54	62	54	79

---

*Data not available.

large contributor to error in the mass balance calculation. Table III-10 indicates this effect in EC-44, in which the reported initial concentration of butane seems anomalously high. Included in the table are mass balances calculated using a gross extrapolation and a semi-log least-squares fit to the data. The reactive loss of butane results almost exclusively from oxidation by the hydroxy radical, which is present in steady-state amounts. The assumption that its concentration is fairly constant during the run appears justified by the more reasonable carbon recoveries and the high correlation coefficients for the least-squares fit, which are usually 0.99 or larger. The qualitative and quantitative differences of the

TABLE III-10. PERCENT CARBON MASS RECOVERY FOR RUN EC-44

Time (minutes)	Initial Butane Concentration		
	3.92 ppm (reported)	3.80 ppm (extrapolated)	3.90 ppm (fitted)
60	25%	759%	53%
300	49	76	62

recovery in the butane/NO_x system indicate an undetected carbon-containing species other than CO or CO_2. The early and fairly constant loss of carbon implicates a primary product of butane oxidation as the prodigal species.

The mass loss expressed in ppmC is shown in Figure III-67. It is closely similar in shape and magnitude to the MEK data (uncorrected for dilution) plotted as ppmC in Figure III-68. All carbon products measured in the butane/NO_x system exhibit similar concentration-time profiles, so that systematic gross underestimation of one or more of these carbon containing product concentrations (such as MEK) is a possibility. Concentrations of the four-carbon nitrates (which undoubtedly form a portion of the lost carbon) in the propylene/butane runs are about 20 percent of the MEK concentration. However, these data, which also show a similar carbon loss from butane, are more recent and presumably have improved analytical calibration, thus confirming the large mass loss in the butane system. The production of hydroxyaldehydes could account for some of the undetected carbon mass.

3. Formation and Destruction of Methylethylketone

Our initial mechanism for the formation and destruction of MEK was presented by Durbin et al. (1975):

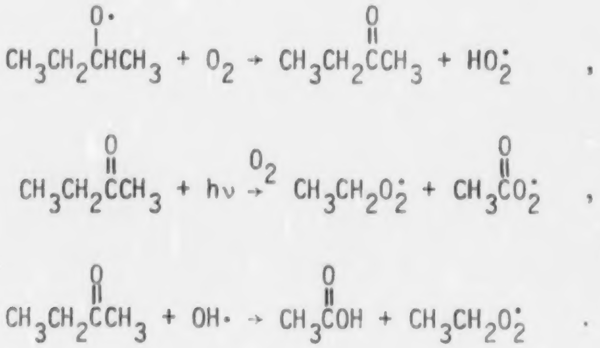

$$CH_3CH_2\overset{O\cdot}{\overset{|}{C}}HCH_3 + O_2 \rightarrow CH_3CH_2\overset{O}{\overset{\|}{C}}CH_3 + HO_2^{\cdot} \quad ,$$

$$CH_3CH_2\overset{O}{\overset{\|}{C}}CH_3 + h\nu \xrightarrow{O_2} CH_3CH_2O_2^{\cdot} + CH_3\overset{O}{\overset{\|}{C}}O_2^{\cdot} \quad ,$$

$$CH_3CH_2\overset{O}{\overset{\|}{C}}CH_3 + OH\cdot \rightarrow CH_3\overset{O}{\overset{\|}{C}}OH + CH_3CH_2O_2^{\cdot} \quad .$$

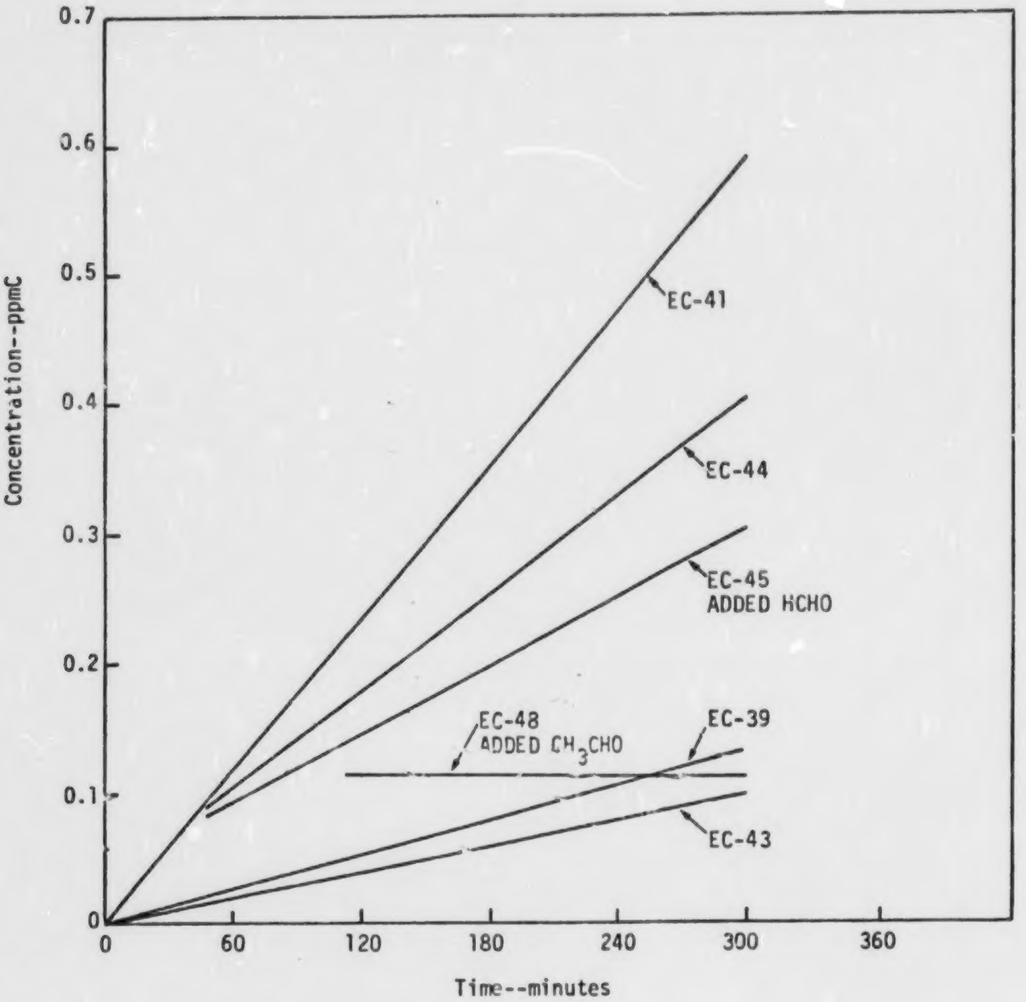

FIGURE III-67. UNRECOVERED CARBON AS A FUNCTION OF TIME FOR VARIOUS RUNS (NOT CORRECTED FOR DILUTION)

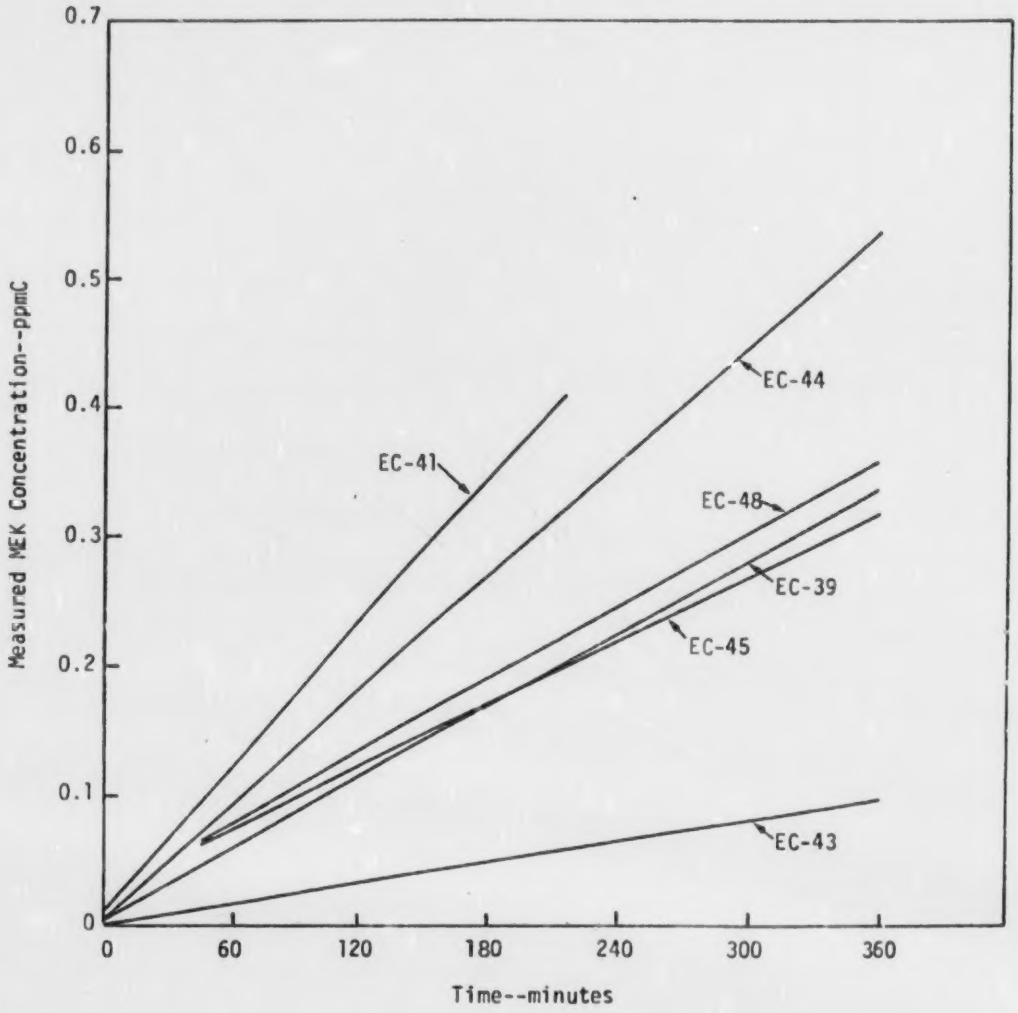

FIGURE III-68. MEASURED MEK CONCENTRATION AS A FUNCTION OF TIME FOR VARIOUS RUNS

We now believe that OH· radicals will not attack the carbonyl part of the molecule to give acetic acid, but rather that OH• radicals will abstract the secondary hydrogen:

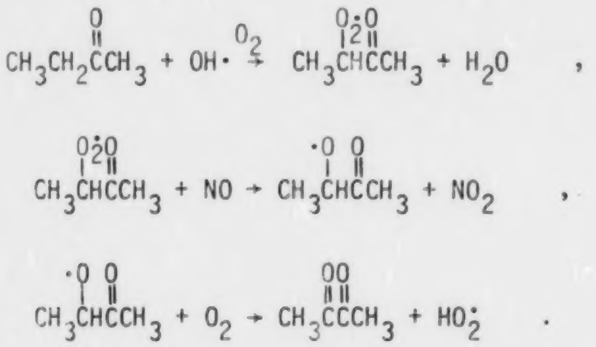

$$\mathrm{CH_3CH_2\overset{\overset{O}{\|}}{C}CH_3 + OH\cdot \xrightarrow{O_2} CH_3\overset{\overset{O_2\cdot}{|}}{C}H\overset{\overset{O}{\|}}{C}CH_3 + H_2O} \quad ,$$

$$\mathrm{CH_3\overset{\overset{O_2\cdot}{|}}{C}H\overset{\overset{O}{\|}}{C}CH_3 + NO \rightarrow CH_3\overset{\overset{\cdot O}{|}}{C}H\overset{\overset{O}{\|}}{C}CH_3 + NO_2} \quad ,$$

$$\mathrm{CH_3\overset{\overset{\cdot O}{|}}{C}H\overset{\overset{O}{\|}}{C}CH_3 + O_2 \rightarrow CH_3\overset{\overset{O}{\|}}{C}\overset{\overset{O}{\|}}{C}CH_3 + HO_2\cdot} \quad .$$

This mechanism has been postulated by Demerjian et al. (1974). The rate of the hydroxyl radical reaction has recently been reviewed by Lloyd et al. (1976), and we have used their recommended value of 5.2 x 10[illegible] ppm^{-1} min^{-1}. The biacetyl formed from the above reaction will photolyze rapidly to give two radicals:

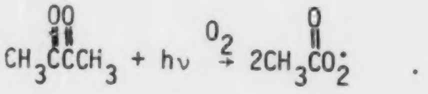

$$\mathrm{CH_3\overset{\overset{O}{\|}}{C}\overset{\overset{O}{\|}}{C}CH_3 + h\nu \xrightarrow{O_2} 2CH_3\overset{\overset{O}{\|}}{C}O_2\cdot} \quad .$$

The formation of these two radicals may lead to increased reactivity in the latter stages of simulation of the butane system (see Figure III-69). Introduction of this reaction leads to approximately 25 percent more ozone with approximately a 45 percent increase in PAN concentrations for EC-39.

4. Simulation Results

The explicit butane mechanism is presented in Table III-11. Simulations were performed on UCR runs EC-39 through EC-48 with the initial conditions listed in Table III-12a and the photolysis rate constants

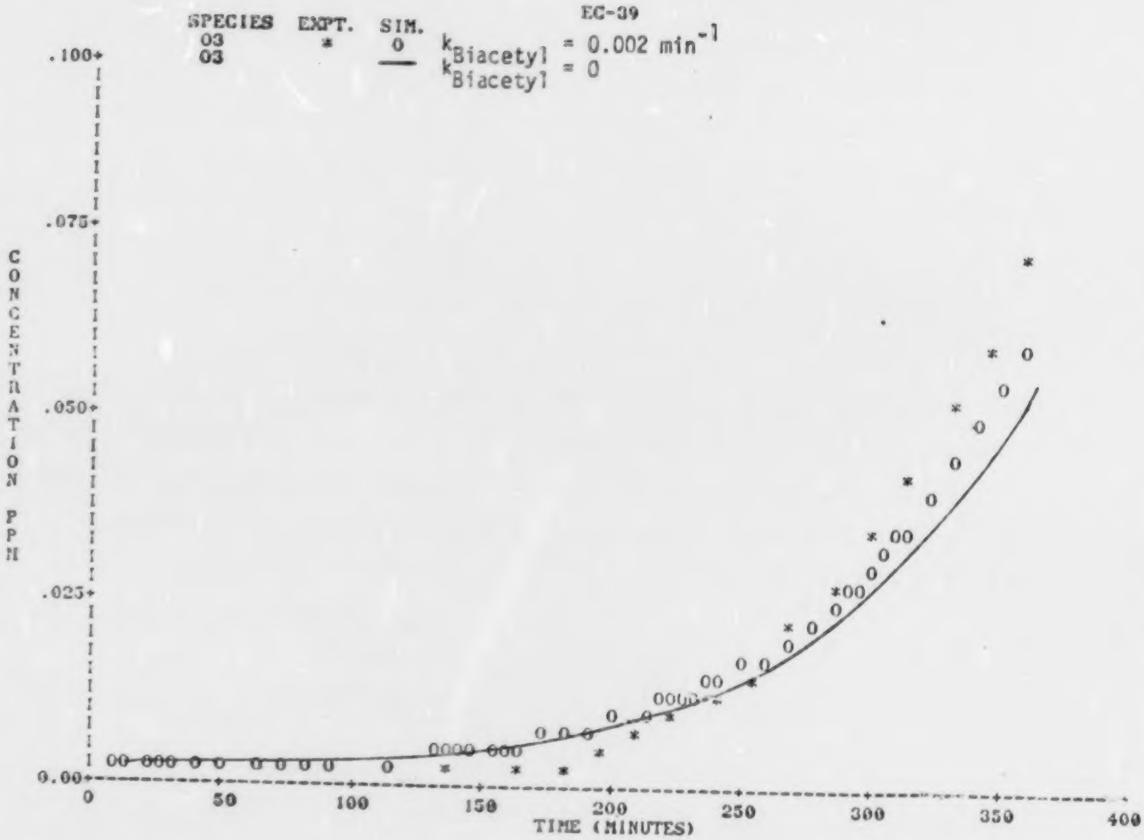

FIGURE III-69. EFFECT OF INCLUDING BIACETYL PHOTOLYSIS

TABLE III-11. THE BUTANE/NO_x MECHANISM

Reaction	Rate Constant (ppm^{-1} min^{-1})
$NO_2 + h\nu \rightarrow NO + O(^3P)$	Experimental*
$O(^3P) + O_2 + M \rightarrow O_3 + M$	$2.08 \times 10^{-5\dagger}$
$O(^3P) + NO_2 \rightarrow NO + O_2$	1.34×10^4
$O_3 + NO \rightarrow NO_2 + O_2$	25.2
$O(^1D) + M \rightarrow O + M$	8.6×10^4
$O(^1D) + H_2O \rightarrow 2OH\cdot$	5.1×10^5
$O_3 + OH\cdot \rightarrow HO_2^{\cdot} + O_2$	87.0
$O_3 + HO_2^{\cdot} \rightarrow OH\cdot + 2O_2$	1.2
$O_3 + NO_2 \rightarrow NO_3 + O_2$	5×10^{-2}
$O_3 + h\nu \rightarrow O(^1D) + O_2$	Experimental*
$O_3 + h\nu \rightarrow O(^3P) + O_2$	Experimental*
$O_3 \rightarrow$ wall	1×10^{-3}
$NO_3 + NO \rightarrow 2NO_2$	1.3×10^4
$NO_3 + NO_2 \rightarrow N_2O_5$	5.6×10^3
$N_2O_5 + H_2O \rightarrow 2HNO_3$	5×10^{-6}
$N_2O_5(+ M) \rightarrow NO_3 + NO_2(+ M)$	24.0*
$NO + NO_2 + H_2O \rightarrow 2HNO_2$	$2.2 \times 10^{-9\dagger}$
$2HNO_2 \rightarrow NO + NO_2 + H_2O$	1.3×10^{-3}

TABLE III-11 (Continued)

Reaction	Rate Constant (ppm^{-1} min^{-1})
$HNO_2 + h\nu \rightarrow OH\cdot + NO$	Experimental*
$NO_2 + OH\cdot(+ M) \rightarrow HNO_3(+ M)$	9.2×10^3
$NO + OH\cdot \rightarrow HNO_2$	9×10^3
$HO_2\cdot + NO \rightarrow OH\cdot + NO_2$	2×10^3
$HO_2\cdot + NO_2 \rightarrow HNO_2 + O_2$	20
$H_2O_2 + h\nu \rightarrow 2OH\cdot$	Experimental*
$CH_3CH_2CH_2CH_3 + O \xrightarrow{O_2} CH_3CH_2CH(O_2\cdot)CH_3 + OH\cdot$	64.0
$CH_3CH_2CH_2CH_3 + OH\cdot \xrightarrow{O_2} CH_3CH_2CH_2CH_2O_2\cdot + H_2O$	5.0×10^2
$CH_3CH_2CH_2CH_3 + OH\cdot \xrightarrow{O_2} CH_3CH_2CH(O_2\cdot)CH_3 + H_2O$	2.9×10^3
$HOCH_2CH_2CH_2C(O)O_2\cdot + NO \rightarrow NO_2 + HOCH_2CH_2CH_2O_2\cdot + CO_2$	2×10^3
$HOCH_2CH_2C(O)O_2\cdot + NO \rightarrow NO_2 + HOCH_2CH_2O_2\cdot + CO_2$	2×10^3
$CH_3CH_2CH_2C(O)O_2\cdot + NO \xrightarrow{O_2} NO_2 + CH_3CH_2CH_2O_2\cdot + CO_2$	2×10^3
$CH_3CH_2C(O)O_2\cdot + NO \xrightarrow{O_2} NO_2 + CH_3CH_2O_2\cdot + CO_2$	2×10^3
$CH_3C(O)O_2\cdot + NO \xrightarrow{O_2} NO_2 + CH_3O_2\cdot + CO_2$	2×10^3
$HC(O)O_2\cdot + NO \xrightarrow{O_2} NO_2 + HO_2\cdot + CO_2$	2×10^3
$HOCH_2CH_2CH_2CH_2O_2\cdot + NO \rightarrow NO_2 + HO_2\cdot + HOCH_2CH_2CH_2CH_2CHO$	2×10^3
$CH_3CH(O_2\cdot)C(O)CH_3 + NO \rightarrow NO_2 + HO_2\cdot + CH_3C(O)C(O)CH_3$	2×10^3
$CH_3CH(O_2\cdot)CH_2CH_3 + NO \rightarrow NO_2 + CH_3CH(O\cdot)CH_2CH_3$	2×10^3

TABLE III-11 (Continued)

Reaction	Rate Constant (ppm^{-1} min^{-1})
$CH_3CH_2CH_2CH_2O_2^{\cdot} + NO \rightarrow NO_2 + CH_3CH_2CH_2CH_2O\cdot$	2×10^3
$HOCH_2CH_2CH_2O_2^{\cdot} + NO \rightarrow NO_2 + HO_2 + HOCH_2CH_2CHO$	2×10^3
$HOCH_2CH_2O_2^{\cdot} + NO \rightarrow NO_2 + HO_2 + HOCH_2CHO$	2×10^3
$CH_3CH_2CH_2O_2^{\cdot} + NO \rightarrow NO_2 + CH_3CH_2CH_2O\cdot$	2×10^3
$CH_3CH_2O_2^{\cdot} + NO \rightarrow NO_2 + CH_3CH_2O\cdot$	2×10^3
$CH_3O_2^{\cdot} + NO \rightarrow NO_2 + CH_3O\cdot$	2×10^3
$CH_3CH_2CH(O\cdot)CH_3 \xrightarrow{O_2} CH_3CH_2O_2^{\cdot} + CH_3CHO$	$6.7 \times 10^{4*}$
$CH_3CH_2CH_2CH_2O\cdot \xrightarrow{O_2} HOCH_2CH_2CH_2CH_2O_2^{\cdot}$	$7.5 \times 10^{5*}$
$CH_3CH_2CH(O\cdot)CH_3 + O_2 \rightarrow CH_3CH_2C(O)CH_3 + HO_2^{\cdot}$	0.95
$CH_3CH_2CH_2CH_2O\cdot + O_2 \rightarrow CH_3CH_2CH_2CHO + HO_2^{\cdot}$	0.95
$CH_3CH_2CH_2O\cdot + O_2 \rightarrow CH_3CH_2CHO + HO_2^{\cdot}$	0.95
$CH_3CH_2O\cdot + O_2 \rightarrow CH_3CHO + HO_2^{\cdot}$	0.95
$CH_3O\cdot + O_2 \rightarrow H_2CO + HO_2^{\cdot}$	0.95
$H_2CO + h\nu \xrightarrow{2O_2} HO_2^{\cdot} + HC(O)O_2^{\cdot}$	Experimental*
$H_2CO + h\nu \rightarrow H_2 + CO$	Experimental*
$CH_3CHO + h\nu \xrightarrow{2O_2} CH_3O_2^{\cdot} + HC(O)O_2$	Experimental*
$CH_3CH_2CHO + h\nu \xrightarrow{2O_2} CH_3CH_2O_2^{\cdot} + HC(O)O_2^{\cdot}$	Experimental*
$CH_3CH_2CH_2CHO + h\nu \xrightarrow{2O_2} CH_3CH_2CH_2O_2^{\cdot} + HC(O)O_2^{\cdot}$	Experimental*

TABLE III-11 (Continued)

Reaction	Rate Constant (ppm^{-1} min^{-1})
$CH_3CH_2CH_2CHO + h\nu \rightarrow CH_3CHO + C_2H_4$	Experimental*
$CH_3CH_2C(O)CH_3 + h\nu \rightarrow CH_3C(O)O_2^{\cdot} + CH_3CH_2O_2^{\cdot}$	Experimental*
$HOCH_2CHO + h\nu \rightarrow HC(O)O_2^{\cdot} + H_2CO + HO_2^{\cdot}$	1×10^{-3}
$HOCH_2CH_2CHO + h\nu \rightarrow HC(O)O_2^{\cdot} + HOCH_2CH_2O_2$	1×10^{-3}
$HOCH_2CH_2CH_2CHO + h\nu \rightarrow HC(O)O_2^{\cdot} + HOCH_2CH_2CH_2O_2^{\cdot}$	1×10^{-3}
$CH_3C(O)C(O)CH_3 + h\nu \xrightarrow{2O_2} 2CH_3C(O)O_2^{\cdot}$	2×10^{-3}
$H_2CO + OH\cdot \xrightarrow{O_2} HC(O)O_2^{\cdot} + H_2O$	1×10^{4}
$CH_3CHO + OH\cdot \xrightarrow{O_2} CH_3C(O)O_2^{\cdot} + H_2O$	1×10^{4}
$CH_3CH_2CHO + OH\cdot \xrightarrow{O_2} CH_3CH_2C(O)O_2^{\cdot} + H_2O$	1×10^{4}
$CH_3CH_2CH_2CHO + OH\cdot \xrightarrow{O_2} CH_3CH_2CH_2C(O)O_2^{\cdot} + H_2O$	1×10^{4}
$CH_3CH_2C(O)CH_3 + OH\cdot \rightarrow CH_3CH(O_2^{\cdot})C(O)CH_3 + H_2O$	5.2×10^{3}
$HOCH_2CH_2CH_2CHO + OH\cdot \rightarrow HOCH_2CH_2CH_2C(O)O_2^{\cdot} + H_2O$	1×10^{4}
$HOCH_2CH_2CHO + OH\cdot \rightarrow HOCH_2CH_2C(O)O_2^{\cdot} + H_2O$	1×10^{4}
$HOCH_2CHO + OH\cdot \rightarrow H_2CO + HO_2^{\cdot}$	1×10^{4}
$HOCH_2CH_2CH_2C(O)O_2^{\cdot} + HO_2^{\cdot} \rightarrow HOCH_2CH_2CH_2C(O)OOH + O_2$	1×10^{4}
$HOCH_2CH_2C(O)O_2^{\cdot} + HO_2^{\cdot} \rightarrow HOCH_2CH_2C(O)OOH + O_2$	1×10^{4}
$CH_3CH_2CH_2C(O)O_2^{\cdot} + HO_2^{\cdot} \rightarrow CH_3CH_2CH_2C(O)OOH + O_2$	1×10^{4}

TABLE III-11 (Continued)

Reaction	Rate Constant (ppm-1 min-1)
$CH_3CH_2C(O)O_2^{\cdot} + HO_2^{\cdot} \rightarrow CH_3CH_2C(O)OOH + O_2$	1×10^4
$CH_3C(O)O_2^{\cdot} + HO_2^{\cdot} \rightarrow CH_3C(O)OOH + O_2$	1×10^4
$HC(O)O_2^{\cdot} + HO_2^{\cdot} \rightarrow HC(O)OOH + O_2$	1×10^4
$HOCH_2CH_2CH_2CH_2O_2^{\cdot} + HO_2^{\cdot} \rightarrow HOCH_2CH_2CH_2CH_2OOH + O_2$	4×10^3
$CH_3CH(O_2^{\cdot})C(O)CH_3 + HO_2^{\cdot} \rightarrow CH_3CH(OOH)C(O)CH_3 + O_2$	4×10^3
$CH_3CH_2CH(O_2^{\cdot})CH_3 + HO_2^{\cdot} \rightarrow CH_3CH_2CH(CH_3)OOH + O_2$	4×10^3
$CH_3CH_2CH_2CH_2O_2^{\cdot} + HO_2^{\cdot} \rightarrow CH_3CH_2CH_2CH_2OOH + O_2$	4×10^3
$CH_3CH_2CH_2O_2^{\cdot} + HO_2^{\cdot} \rightarrow CH_3CH_2CH_2OOH + O_2$	4×10^3
$CH_3CH_2O_2^{\cdot} + HO_2^{\cdot} \rightarrow CH_3CH_2OOH + O_2$	4×10^3
$CH_3O_2^{\cdot} + HO_2^{\cdot} \rightarrow CH_3OOH + O_2$	4×10^3
$HO_2^{\cdot} + HO_2^{\cdot} \rightarrow H_2O_2 + O_2$	4×10^3
$CH_3CH_2CH_2C(O)O_2^{\cdot} + NO_2 \rightarrow CH_3CH_2CH_2C(O)O_2NO_2$	4×10^2
$CH_3CH_2C(O)O_2^{\cdot} + NO_2 \rightarrow CH_3CH_2C(O)O_2NO_2$	4×10^2
$CH_3C(O)O_2^{\cdot} + NO_2 \rightarrow CH_3C(O)O_2NO_2$	4×10^2
$CH_3C(O)O_2NO_2 \rightarrow NO_2 + CH_3C(O)O_2^{\cdot}$	$1.7 \times 10^{-2*}$
$CH_3CH_2C(O)O_2NO_2 \rightarrow NO_2 + CH_3CH_2C(O)O_2^{\cdot}$	$2 \times 10^{-2*}$
$CH_3CH_2CH_2C(O)O_2NO_2 \rightarrow NO_2 + CH_3CH_2CH_2C(O)O_2^{\cdot}$	$2.5 \times 10^{-2*}$

TABLE III-11 (Concluded)

Reaction	Rate Constant (ppm^{-1} min^{-1})
$CH_3O\cdot + NO_2 \rightarrow CH_3ONO_2$	2×10^4
$CH_3O\cdot + NO_2 \rightarrow H_2CO + HNO_2$	2.2×10^3
$CH_3CH_2O\cdot + NO_2 \rightarrow CH_3CH_2ONO_2$	2.0×10^4
$CH_3CH_2O\cdot + NO_2 \rightarrow CH_3CHO + HNO_2$	2.2×10^3
$CH_3CH_2CH_2O\cdot + NO_2 \rightarrow CH_3CH_2CH_2ONO_2$	2.0×10^4
$CH_3CH_2CH_2O\cdot + NO_2 \rightarrow CH_3CH_2CHO + HNO_2$	2.2×10^3
$CH_3CH_2CH_2CH_2O\cdot + NO_2 \rightarrow CH_3CH_2CH_2CH_2ONO_2$	2×10^4
$CH_3CH_2CH_2CH_2O\cdot + NO_2 \rightarrow CH_3CH_2CH_2CHO + HNO_2$	2.2×10^3
$CH_3CH_2CH(O\cdot)CH_3 + NO_2 \rightarrow CH_3CH_2CH(ONO_2)CH_3$	2×10^4
$CH_3CH_2CH(O\cdot)CH_3 + NO_2 \rightarrow CH_3CH_2C(O)CH_3 + HNO_2$	2.2×10^4
$CO + OH\cdot \xrightarrow{O_2} HO_2 + CO_2$	2.06×10^2

---

† Units of $ppm^{-2}min^{-1}$.

* Units of min^{-1}.

TABLE III-12a. INITIAL CONDITIONS FOR SIMULATIONS OF BUTANE/NO_x SYSTEMS

Run Number	NO (ppm)	NO_2 (ppm)	Butane (ppm)	HNO_2 (ppm)	k1 (min^{-1})
EC-39	0.547	0.06	2.2	0.01	0.24
EC-41	0.542	0.068	4.03	0.01	0.238
EC-42	0.542	0.059	0.385	0.03	0.235
EC-43	0.126	0.013	0.38	0.01	0.233
EC-44	1.14	0.132	3.92	0.03	0.23
EC-45	0.552	0.062	1.94	0.006	0.227
EC-48	0.535	0.059	1.94	0.0	0.221

---

* HNO_2 data and aldehyde photolysis rate constants were chosen to provide the best fit of predicted concentrations to measured concentrations; all other data are UCR measurements.

TABLE III-12b. PHOTOLYSIS RATE CONSTANTS FOR SIMULATIONS OF BUTANE/NO_x SYSTEMS

($10^{-4} min^{-1}$)

EC Run Number	$O_3 \to O^1D$	$O_3 \to O^3P$	$HNO_2 \to$	$H_2O_2 \to$	$HCHO \to H\cdot + HCO\cdot$	$HCHO \to CO + H_2$	$CH_3CHO \to$	$CH_3CH_2CHO \to$	$CH_3CH_2CH_2CHO \to$	MEK→
39 41 42 43 44	31.0	82	500	7.4	9.6	24.0	7.2	16.0	12.0	5.8
45	22.0	82	500	6.9	8.4	24.0	6.5	14.0	10.0	5.0
48	14.0	81	500	6.7	7.4	21.0	5.5	11.0	12.0	3.6

listed in Table III-12b. The factorial block for this system is presented in Figure III-70. Figures III-71 through III-103 show the simulation results for the butane/NO_x system.

5. Discussion of the Butane/NO_x Systems

In the butane/NO_x and propylene/NO_x systems, we assumed that the light source at UCR was deteriorating, especially in the short-wavelength end of the spectrum. This is consistent with UCR data that show a decay in nitrogen dioxide photolysis during these experiments. Unfortunately, no spectral data were taken; so in the simulations of runs EC-39 to EC-60 we varied the intensity of the short wavelengths using an exponential decay function. This function was reported by UCR for the Pyrex filter used in conjunction with its light source. This procedure was reported by Durbin et al. (1975). The filter function was merely shifted to longer wavelengths for later experiments, thus progressively attenuating the light intensity between 300 and 350 nm. This procedure affects the simulations by producing a consistent decrease in the amount of radicals arising from photolysis of carbonyl compounds.

As mentioned in the preceding sections on butane mechanism development, a considerable uncertainty is associated with the butane system because of the substantial carbon mass not accounted for in the UCR data. Another unfortunate aspect of the data is that in none of the experiments did ozone reach a peak concentration. In all the experiments the concentrations of products such as MEK and the aldehydes increased continuously to the end of the experiment. Runs EC-42 and EC-43 show the largest relative reaction of butane, about 35 percent. We therefore recommend more experiments that run longer, to 12 hours instead of 6; that use low NO_x to hydrocarbon ratios, (e.g., 0.1 ppm NO_x to 2 ppm butane) for faster ozone production; or that use even less hydrocarbon than the 0.4 ppm butane used in EC-42 and EC-43, for more complete reaction of butane.

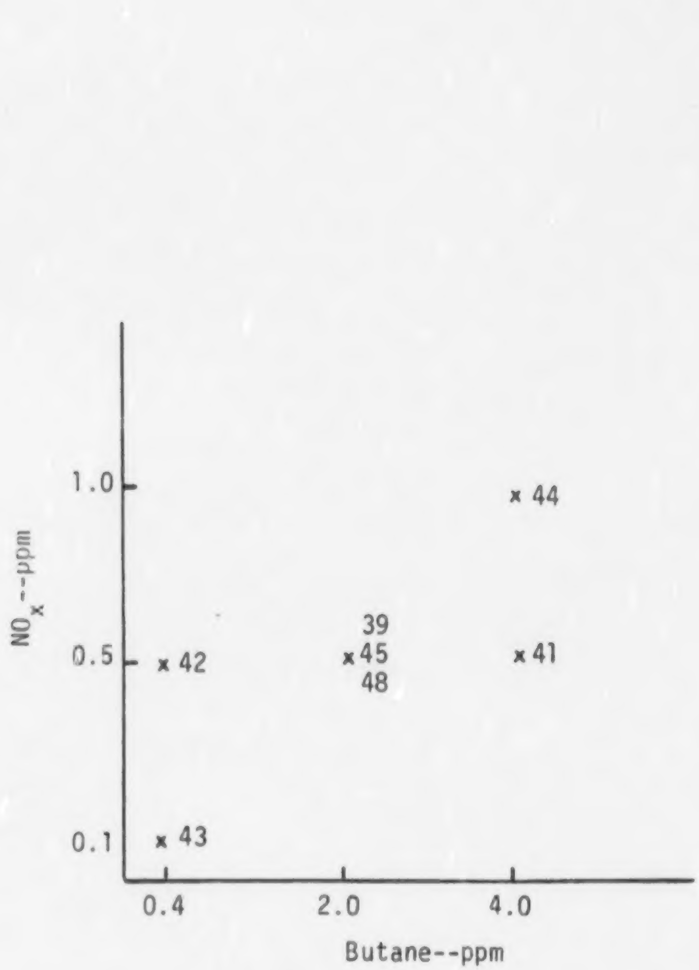

FIGURE III-70. FACTORIAL BLOCK FOR BUTANE/NO_x SYSTEMS

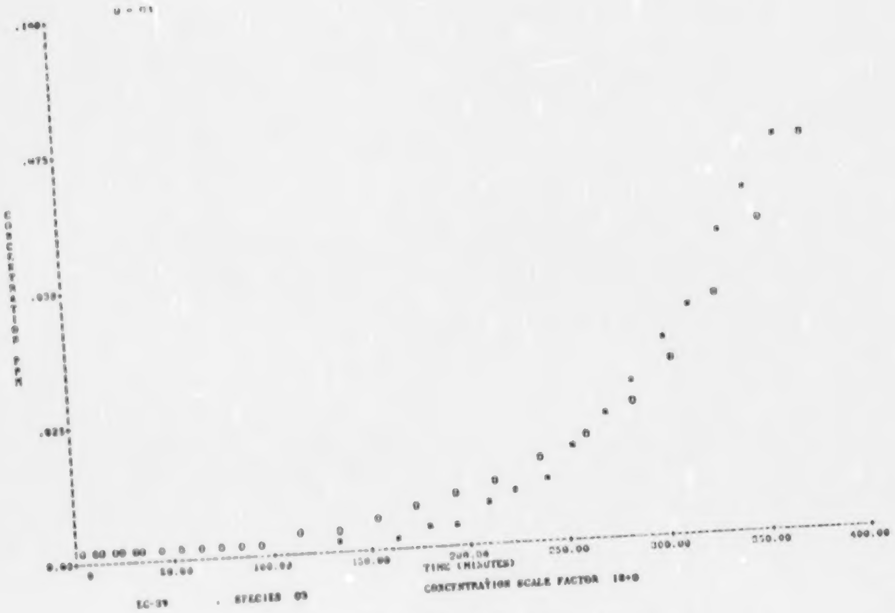

FIGURE III-71

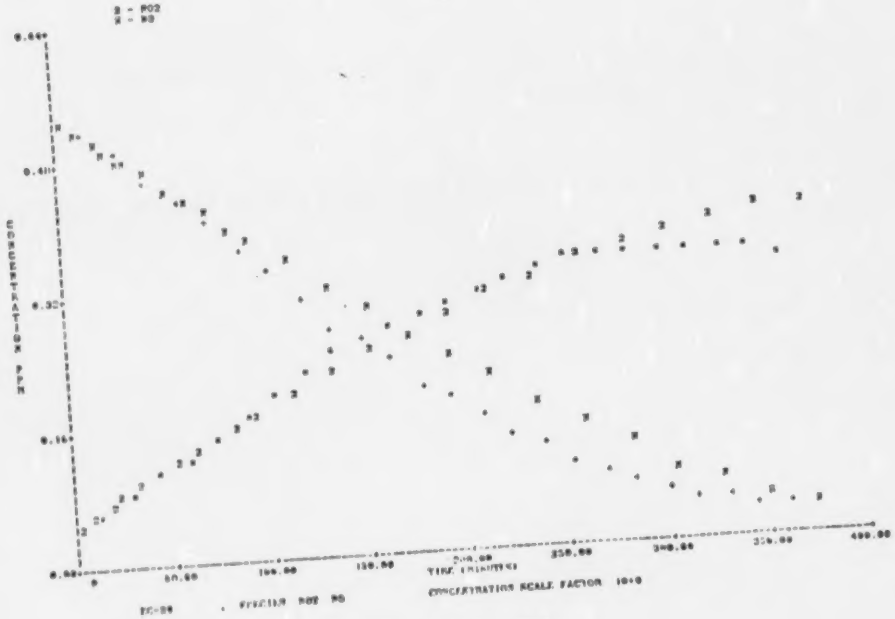

FIGURE III-72

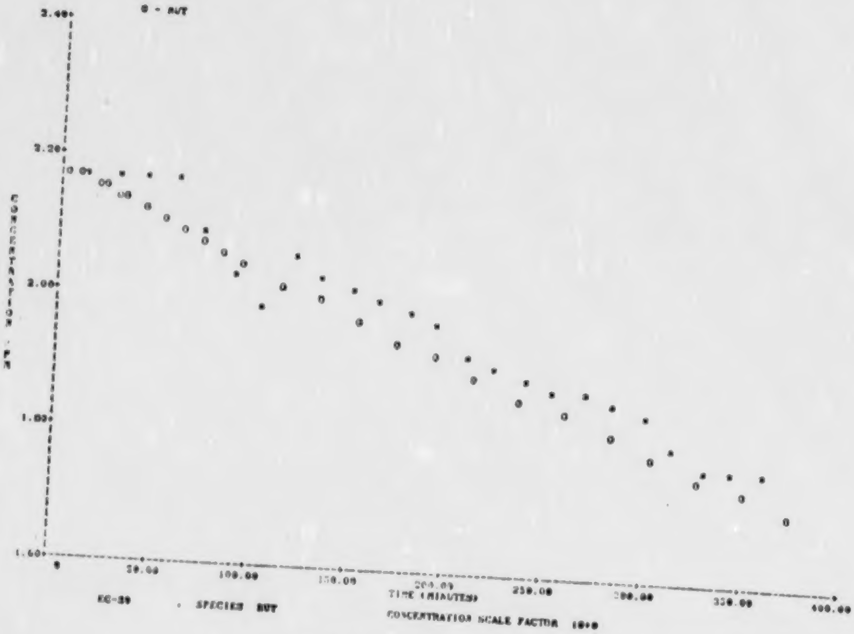

FIGURE III-73

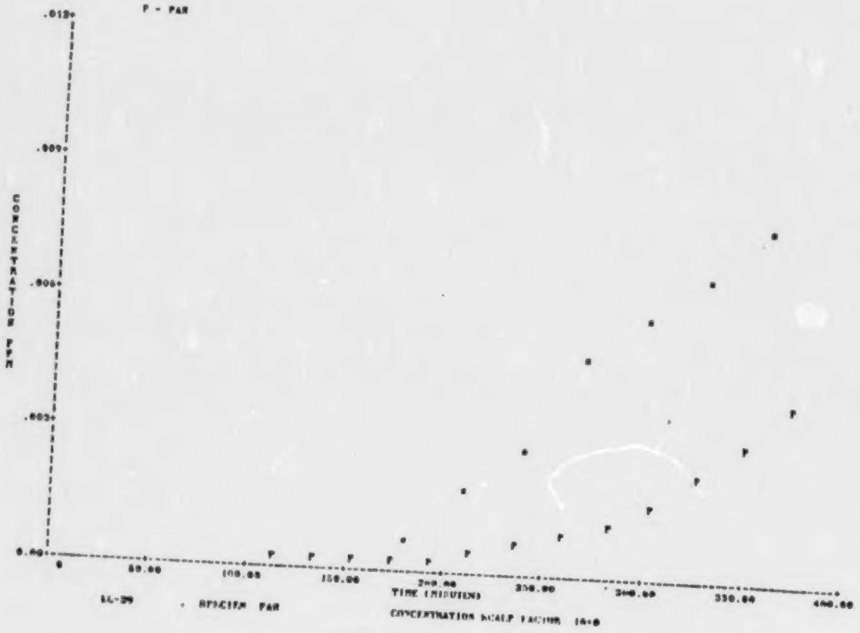

FIGURE III-74

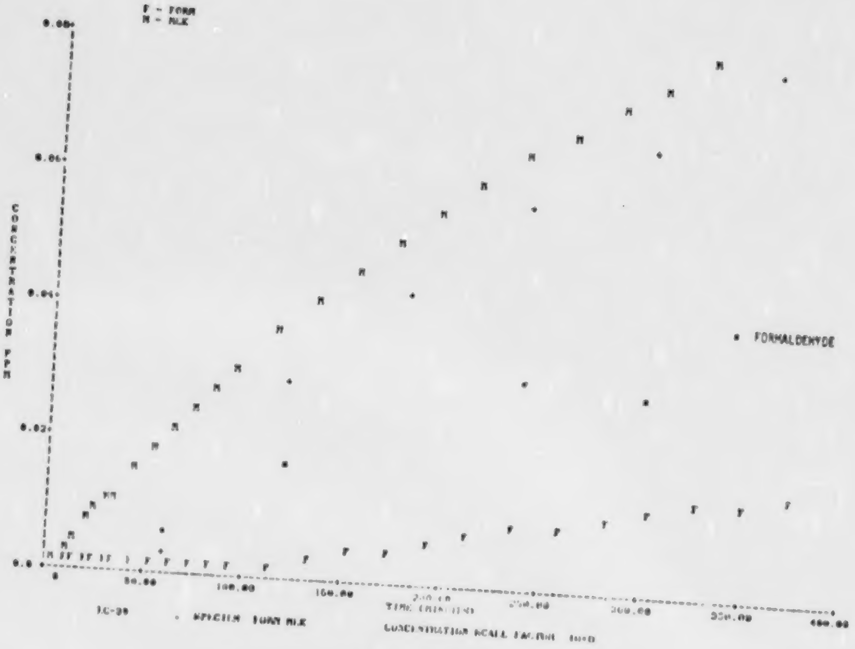

FIGURE III-75

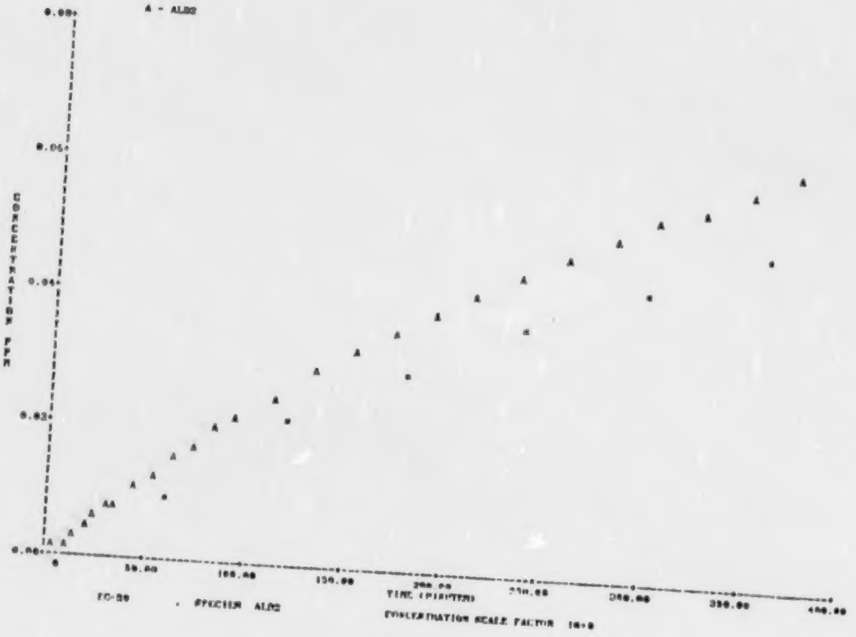

FIGURE III-76

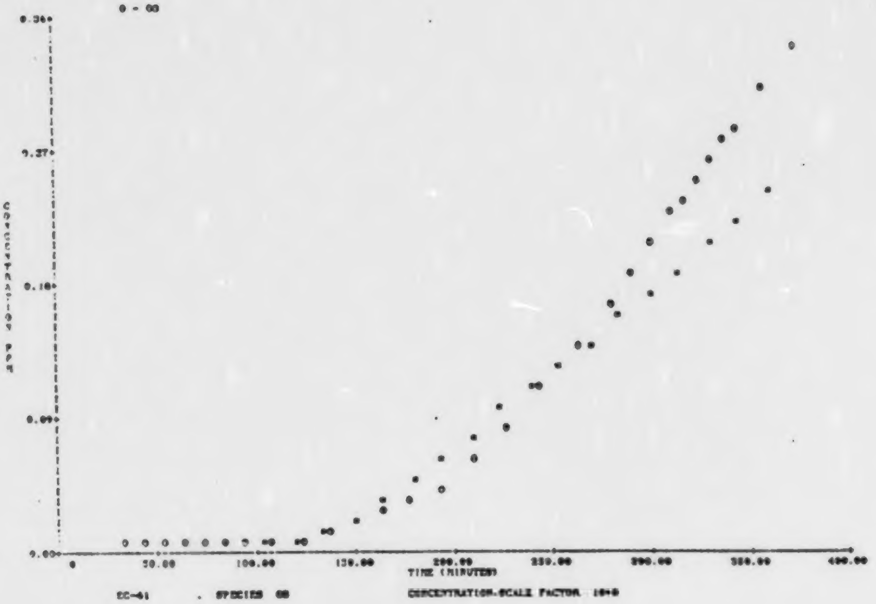

FIGURE III-77

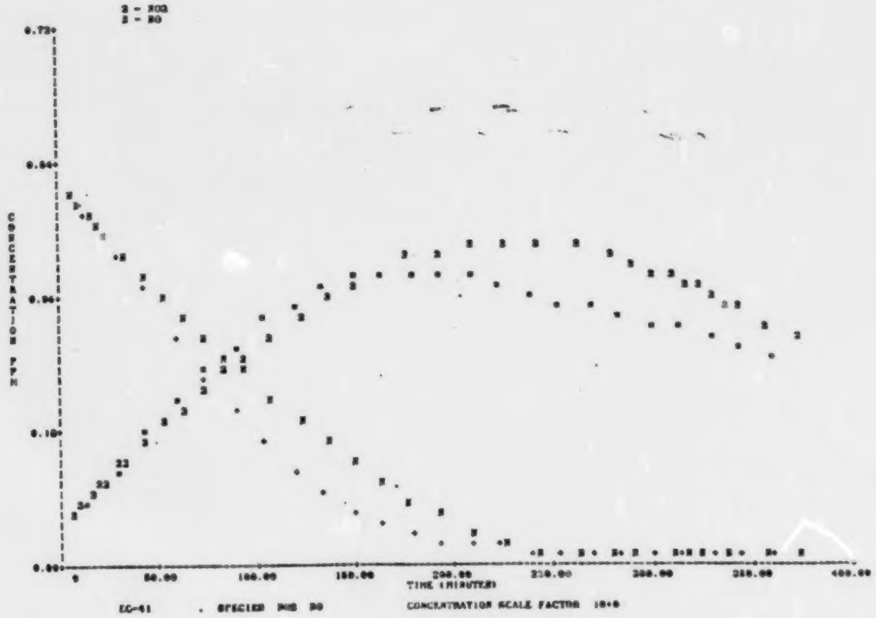

FIGURE III-78

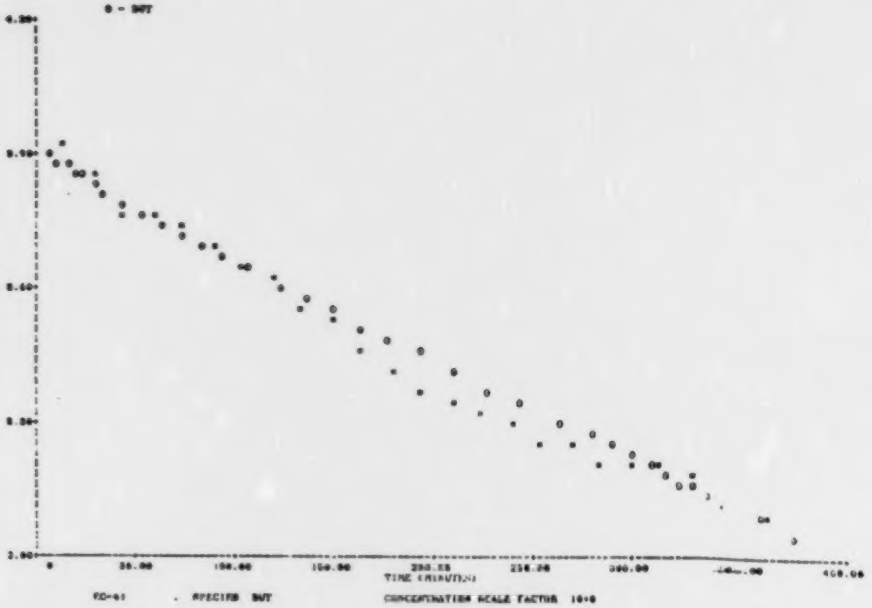

FIGURE III-79

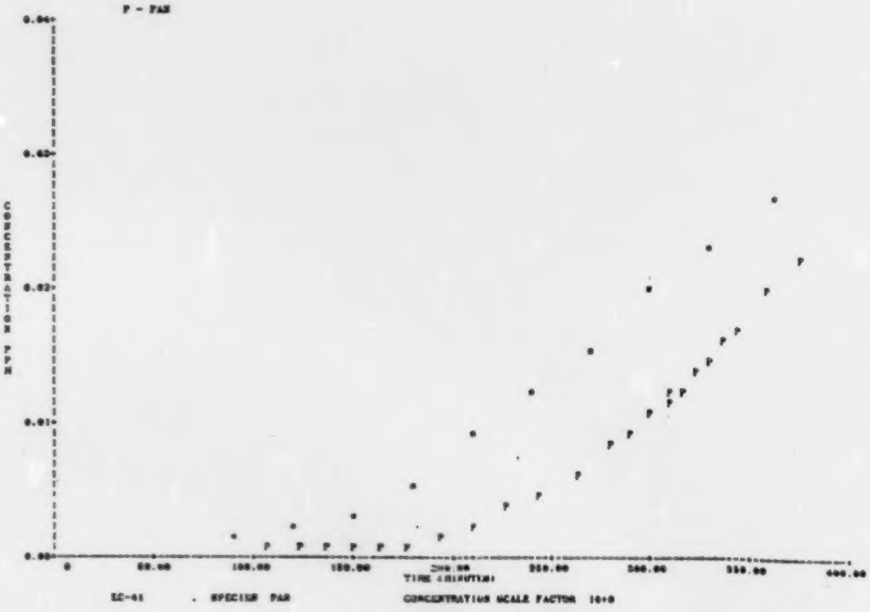

FIGURE III-80

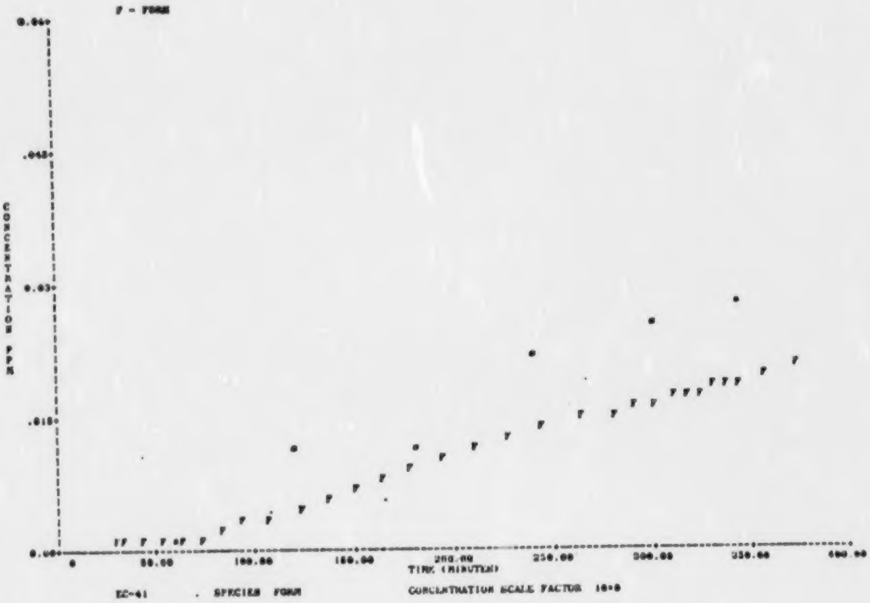

FIGURE III-81

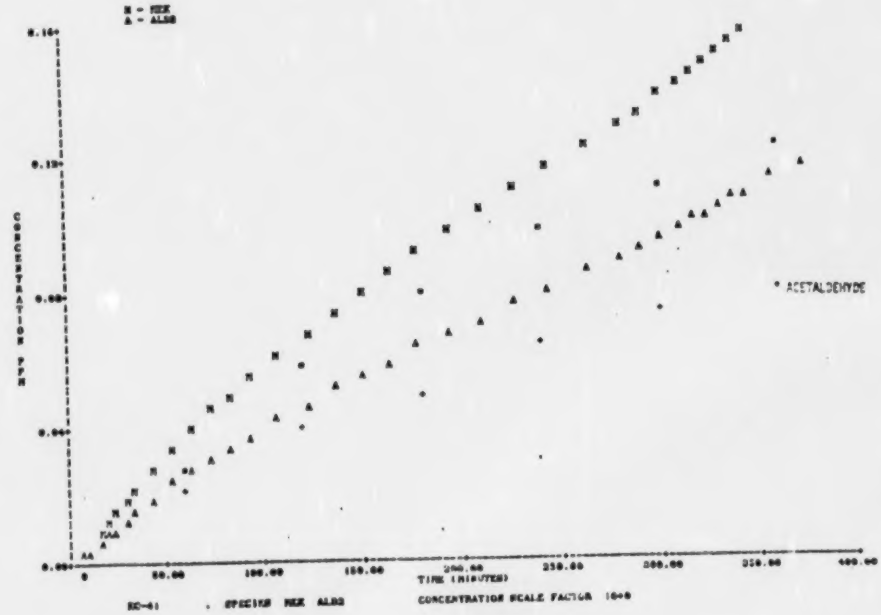

FIGURE III-82

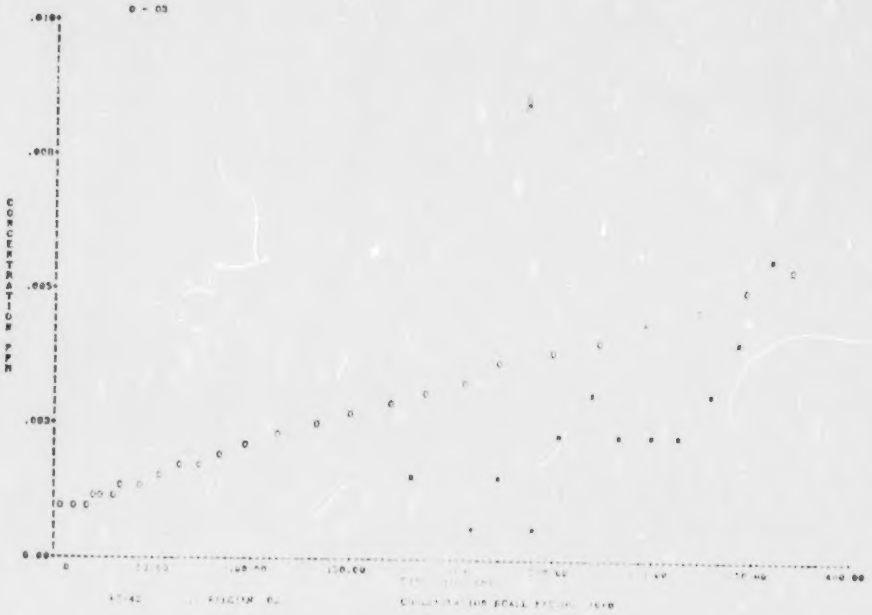

FIGURE III-83

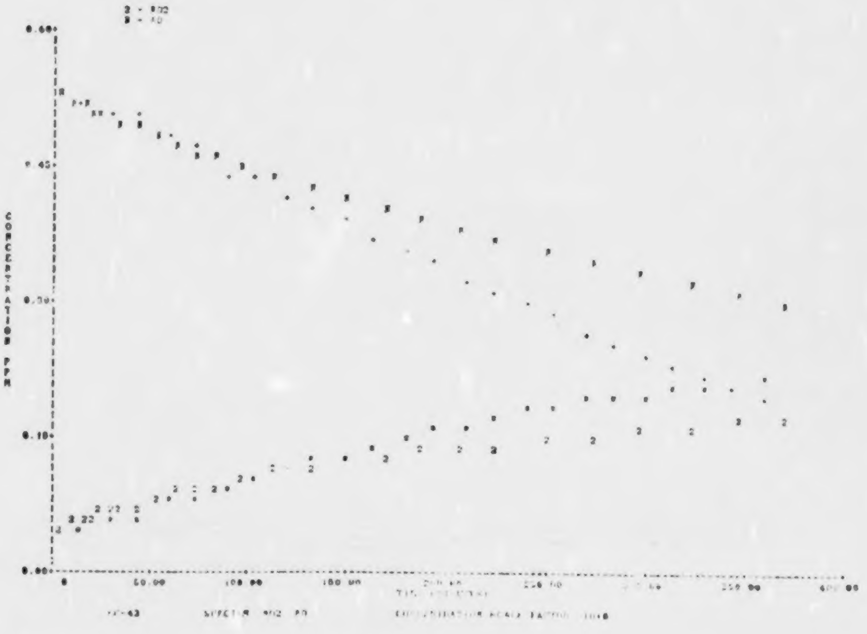

FIGURE III-84

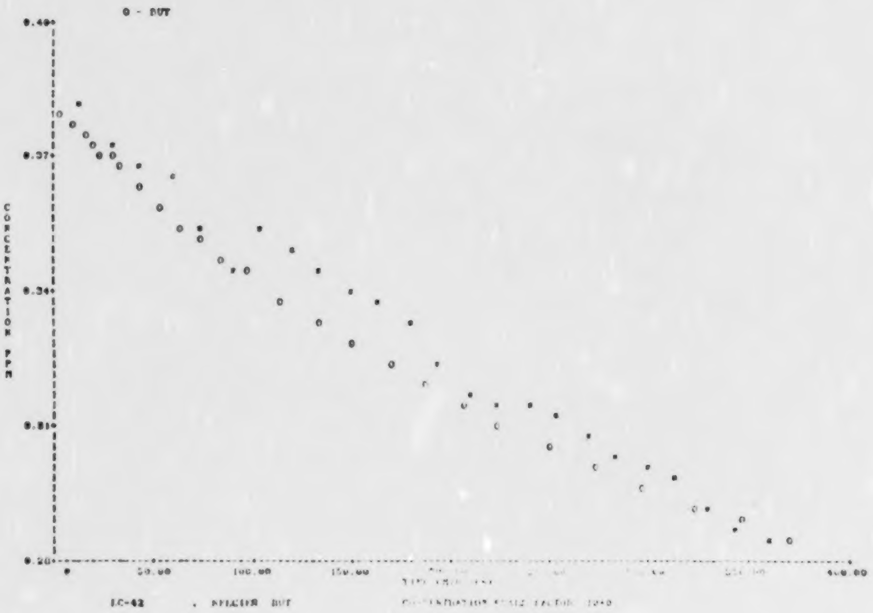

FIGURE III-85

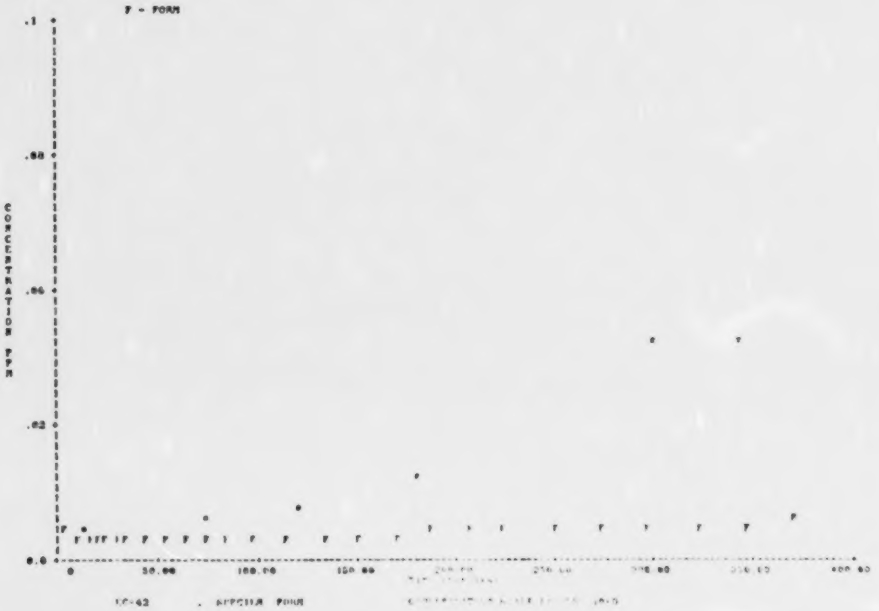

FIGURE III-86

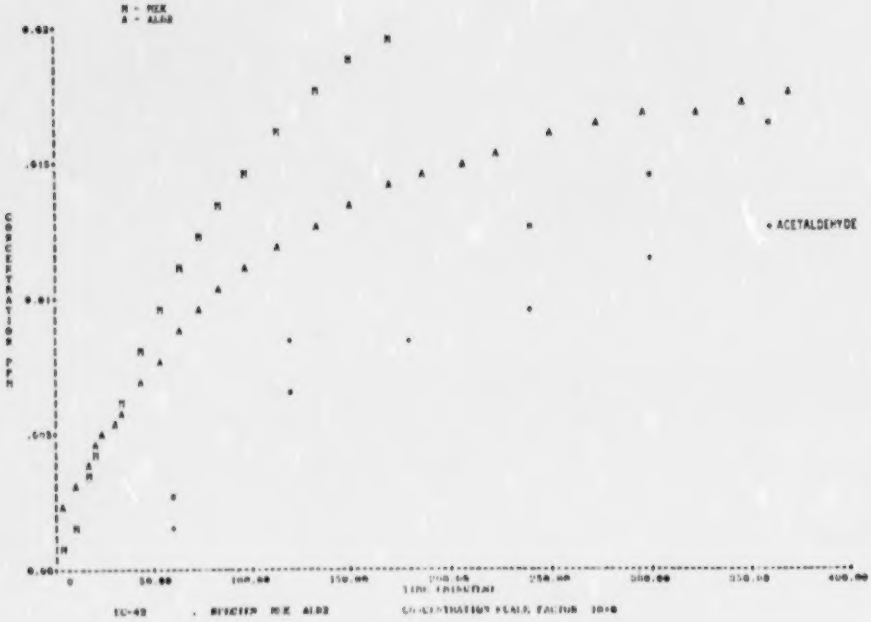

FIGURE III-87

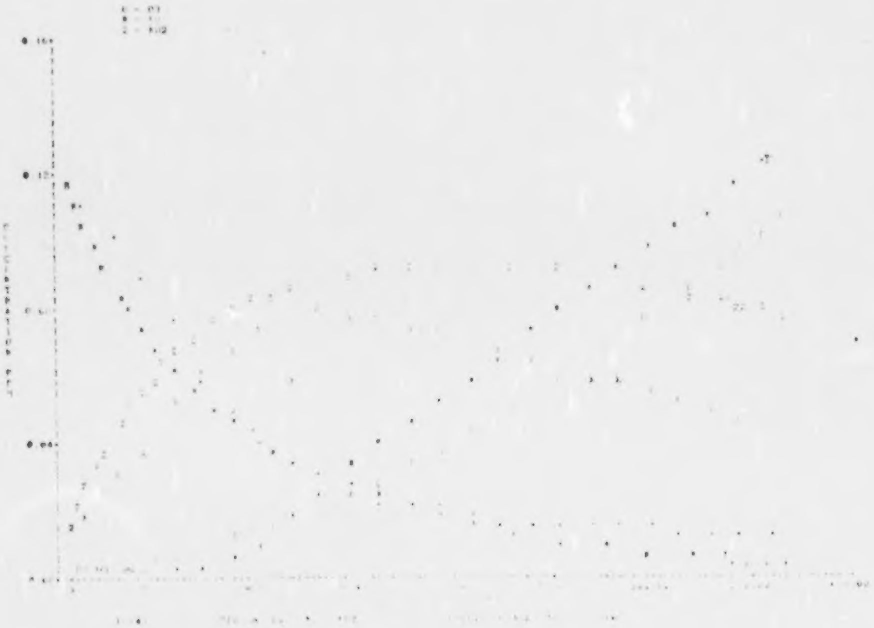

FIGURE III-88

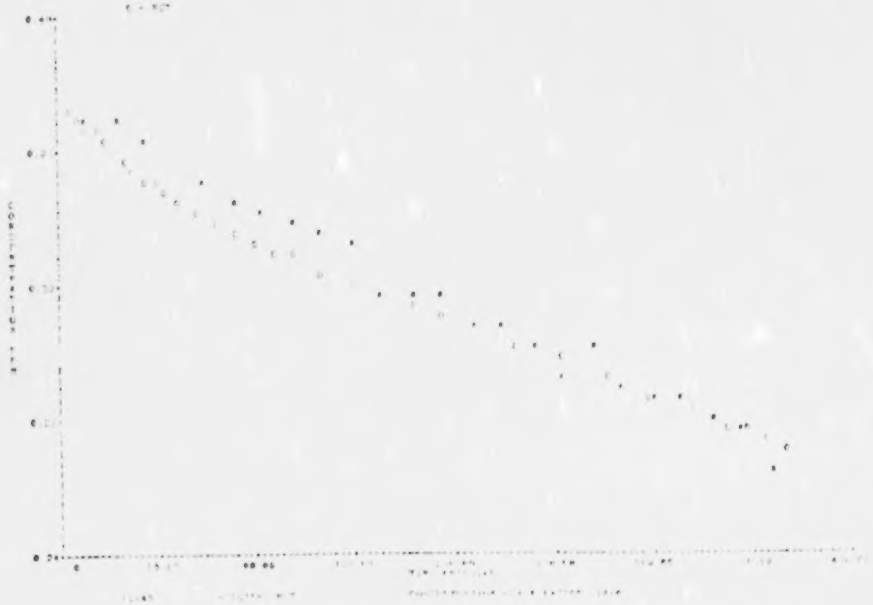

FIGURE III-89

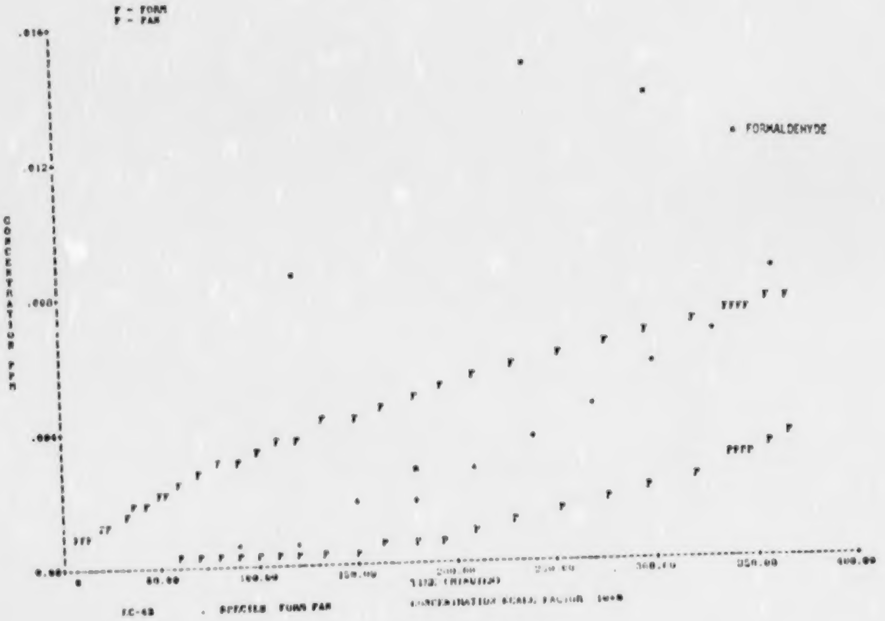

FIGURE III-90

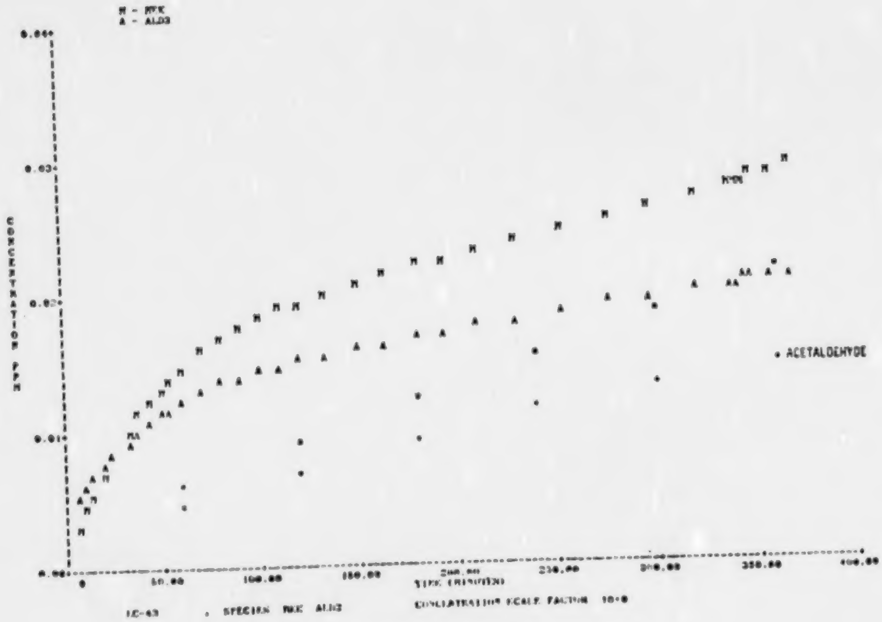

FIGURE III-91

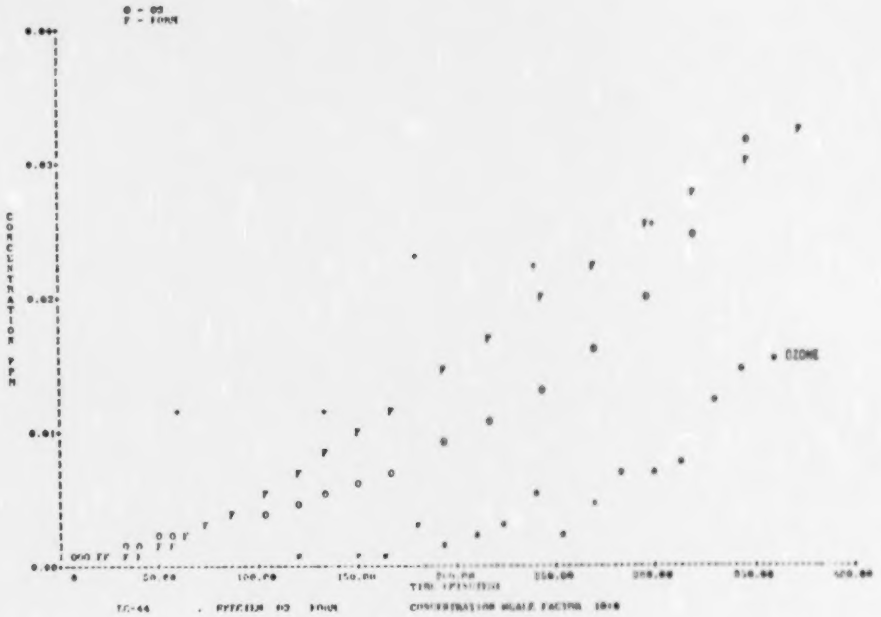

FIGURE III-92

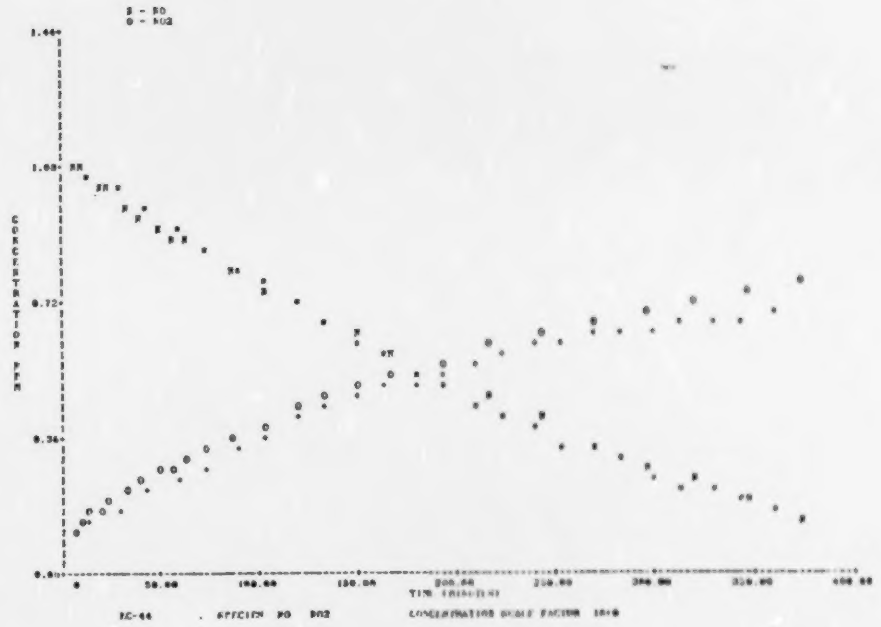

FIGURE III-93

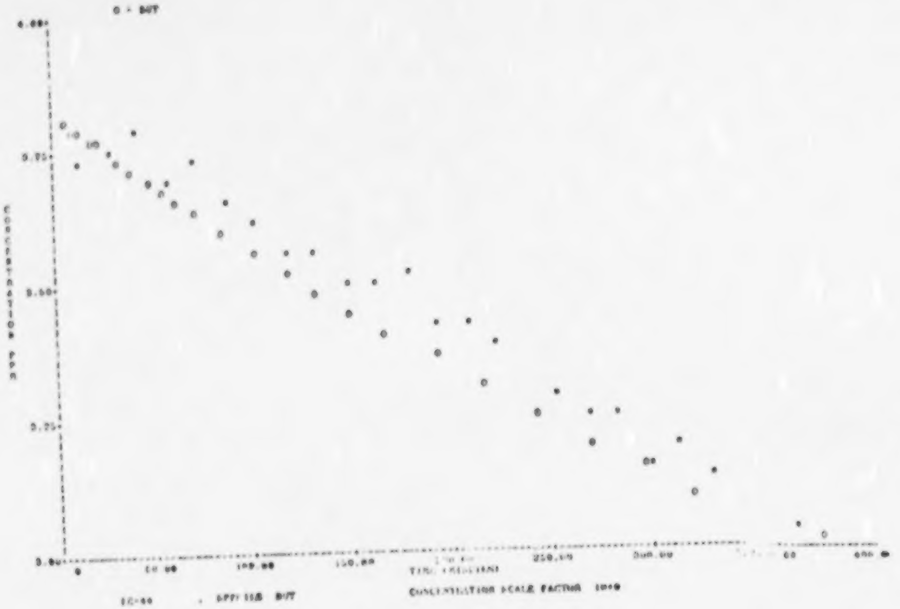

FIGURE III-94

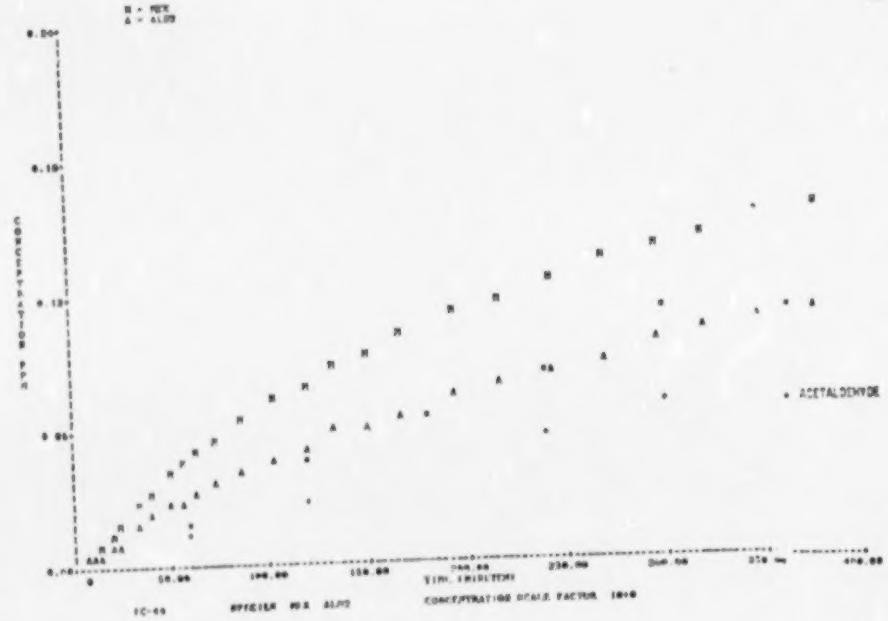

FIGURE III-95

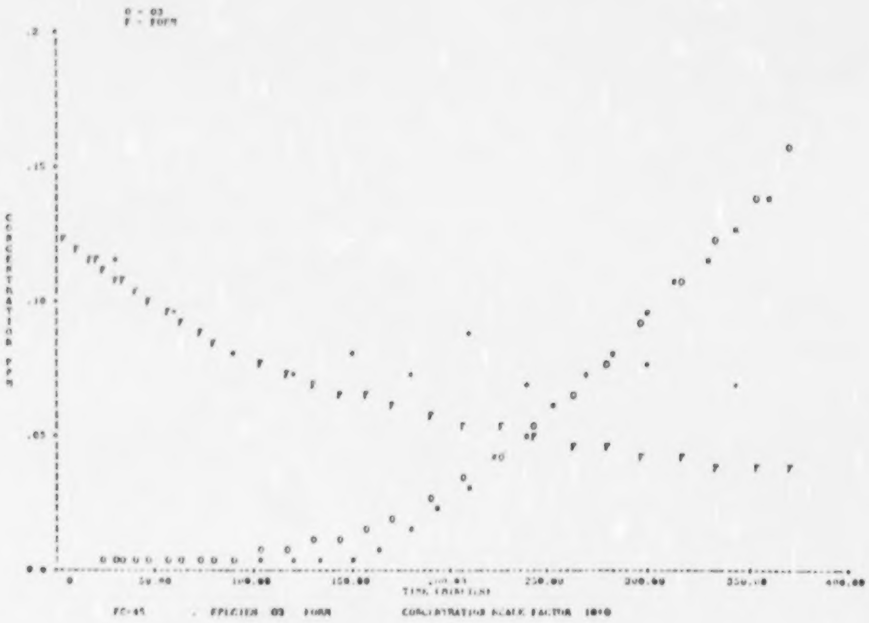

FIGURE III-96

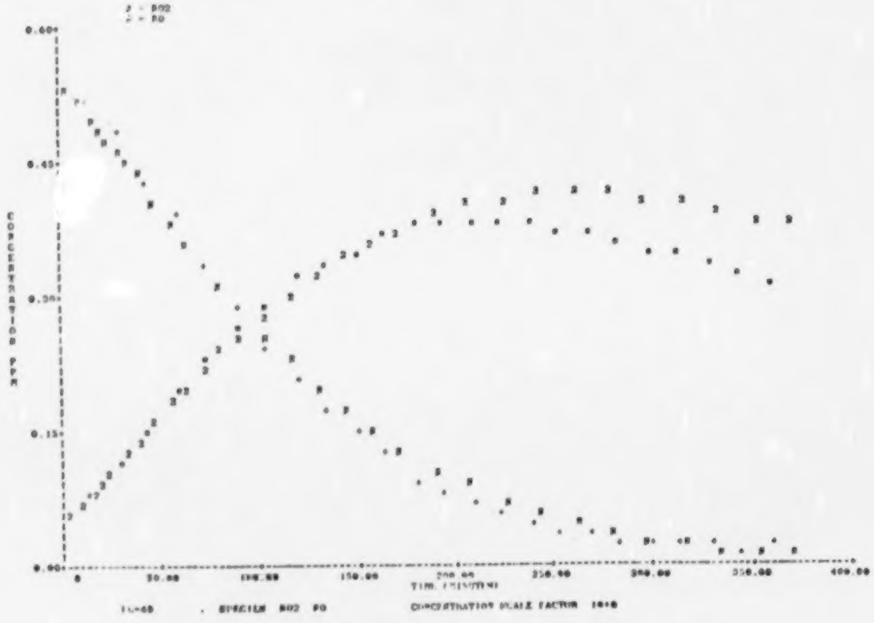

FIGURE III-97

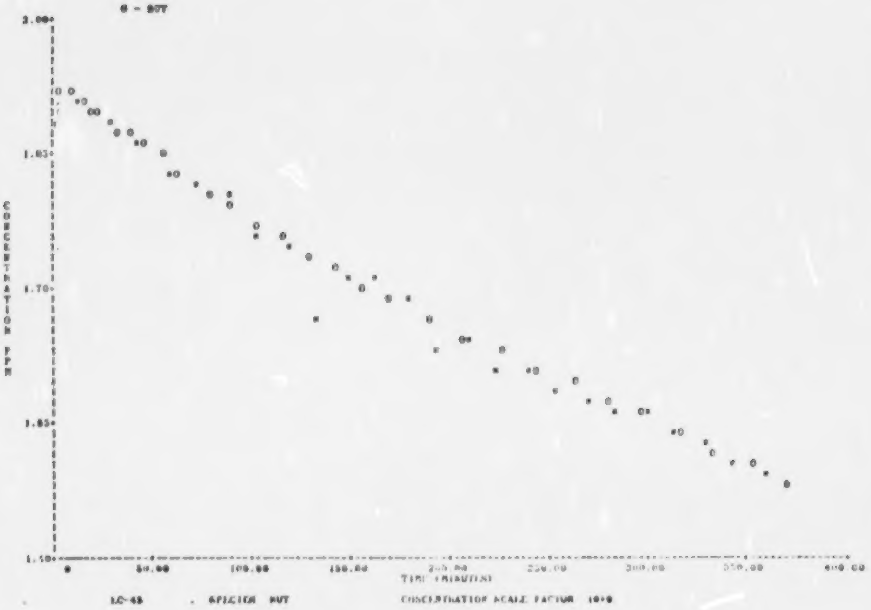

FIGURE III-98

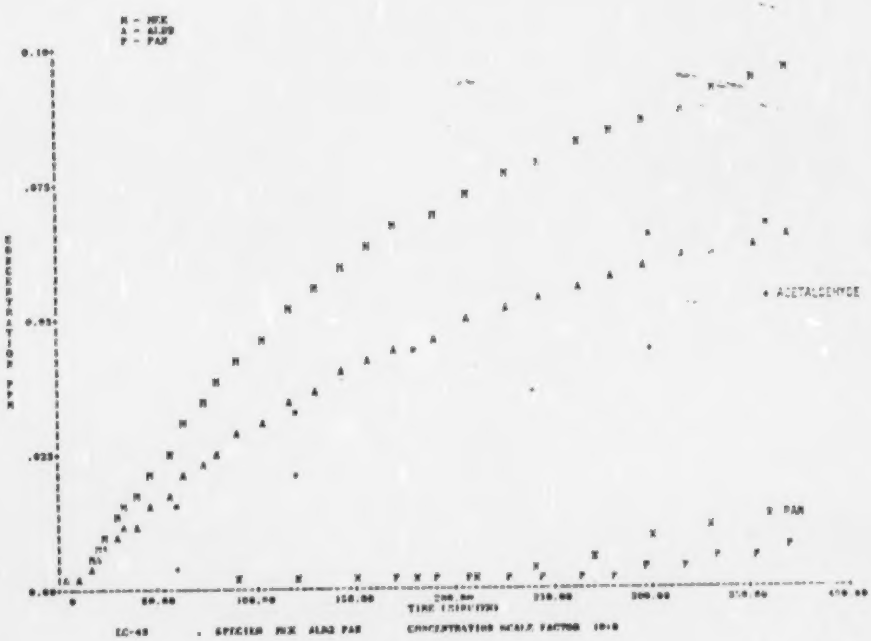

FIGURE III-99

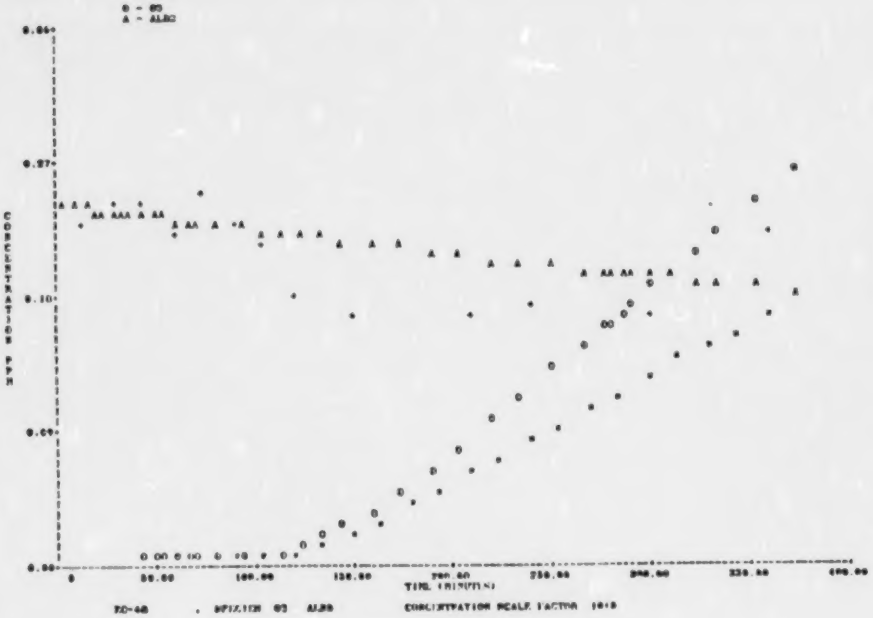

FIGURE III-100

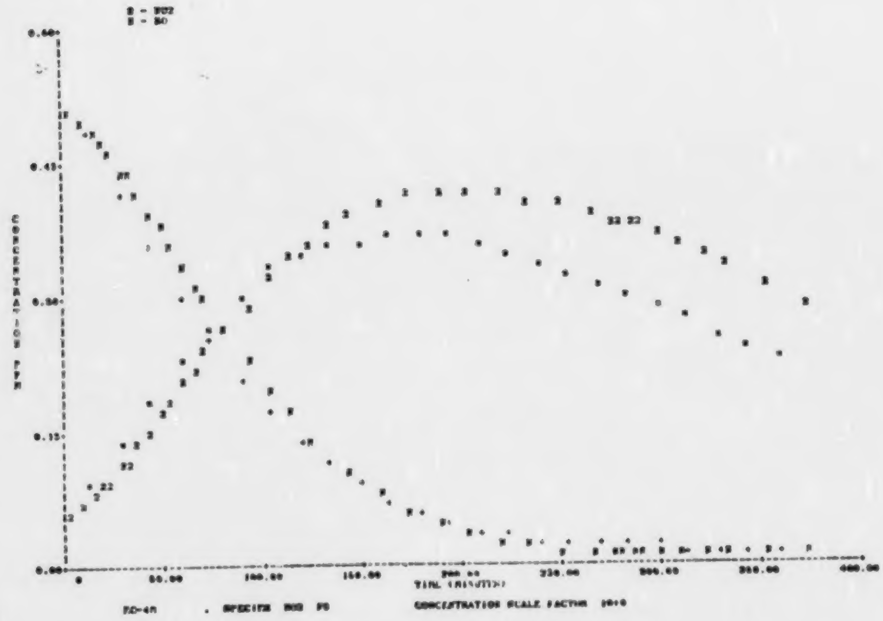

FIGURE III-101

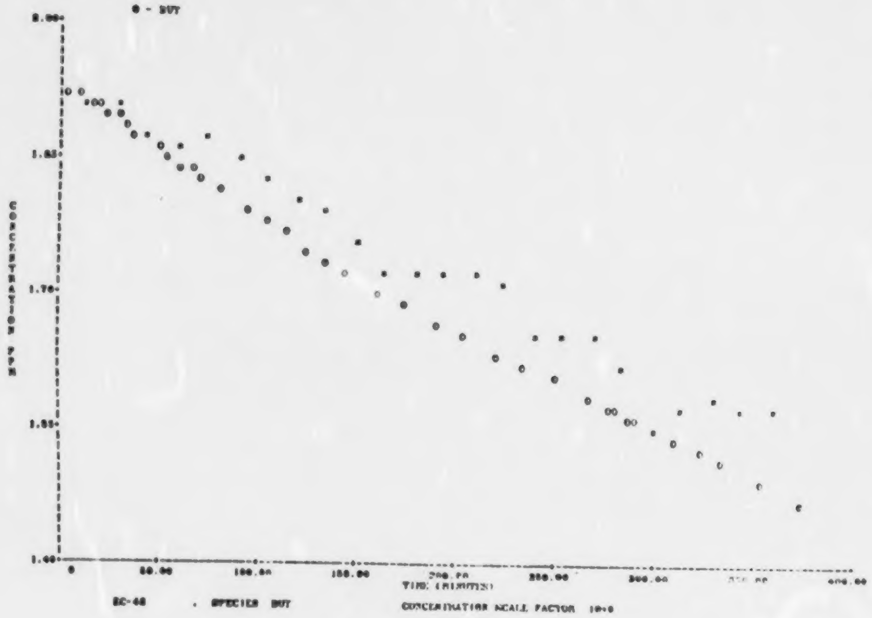

FIGURE III-102

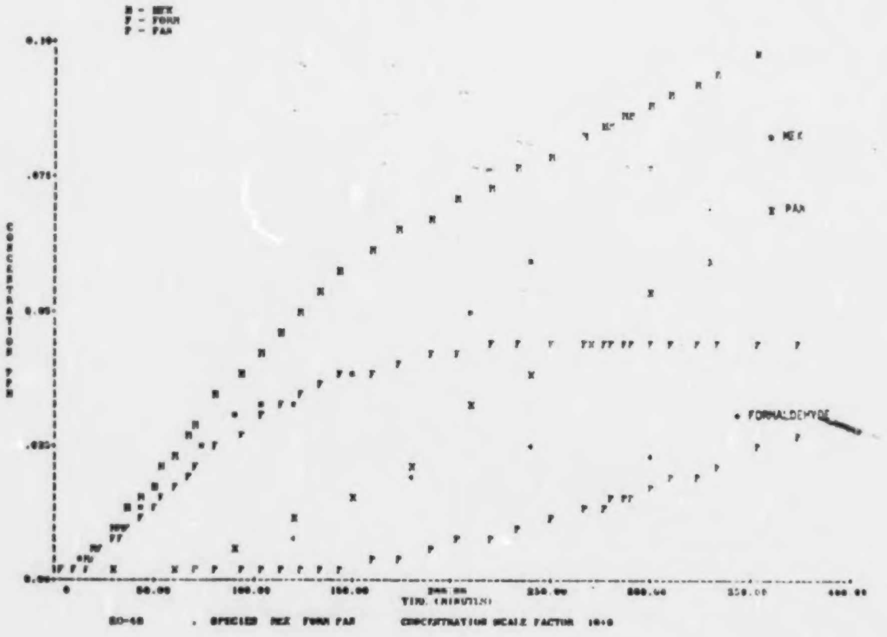

FIGURE III-103

Table III-13 presents a comparison of the experimental and simulated maximum one-hour-average ozone concentrations. (In all UCR butane/NO_x experiments, the highest ozone concentration was measured in the last hour.) The average difference is approximately +17 percent with a standard deviation of 34 percent. These estimates are made excluding EC-44. Including EC-44, the average difference is +36.7 percent with a standard deviation of 60 percent.

TABLE III-13. PREDICTED AND MEASURED MAXIMUM ONE-HOUR-AVERAGE OZONE CONCENTRATIONS FOR THE BUTANE/NO_x SYSTEMS

EC Run No.	Maximum One-Hour Average Ozone Concentration (ppm)		Percent Difference
	Measured	Predicted	
39	0.056	0.048	-14.3
41	0.21	0.33	57.1
42	0.0042	0.005	-19.8
43	0.113	0.097	-14.7
44	0.011	0.028	154.5
45	0.12	0.13	8.3
48	0.14	0.22	57.1

In our opinion the poorest fit to the data is the simulation for EC-42, even though EC-44 has the worst fit to the ozone behavior (Table III-13). This experiment is discussed in the section on development of the carbon-bond mechanism (Section IVC-1). It has the highest NO_x to hydrocarbon ratio and the six-hour experiment shows development of smog formation only to the NO/NO_2 crossover point. Either the mechanism lacks the proper number of NO to NO_2 conversions per butane reacted when the NO_x to hydrocarbon ratio is this high, or some other source of reactivity is present. In simulations of the propylene system, run EC-21, a similar problem exists. In both EC-42 and EC-21 we have shown simulations in which we used the maximum initial HNO_2 concentration possible from the equilibrium between NO, NO_2, and H_2O. In both cases it is obvious that too many radicals are present initially and that the maintenance source of radicals in the mechanism is inadequate. We could not justify changing the light spectrum for these two simulations without changing the light source for adjacent experiments. We speculate that the walls of the chamber in some way supply radicals to the peroxy-oxyl radical pool. The effect of such a process would be greatest when the concentration of normal radicals was the lowest--in a low activity and low hydrocarbon experiment such as EC-42 or EC-21. That the walls are supplying radicals is supported by the similar need for high HNO_2 (relative to equilibrium) to simulate the overall chemistry of EC-43 and EC-17. In EC-43 as in EC-42 it is clear that the initial radical pool in our simulations is too high compared with the rate of reactions seen in the data.

We feel that the worst aspect of the butane simulations in general is associated with the PAN chemistry. The PAN chemistry in the various mechanisms was adjusted to give the best overall fit to the measurements of the olefin systems, where PAN is more abundant than in butane systems. PAN is formed from the reaction of peroxyacetyl radicals and NO_2:

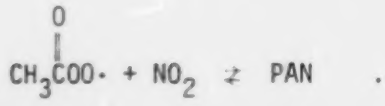

$$CH_3\overset{\overset{O}{\|}}{C}OO\cdot + NO_2 \rightleftarrows PAN \quad .$$

In the butane mechanism a major source of these radicals is the transfer reaction of hydroxyl radicals and acetaldehyde in air:

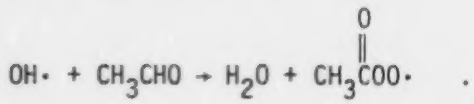

$$OH\cdot + CH_3CHO \rightarrow H_2O + CH_3\overset{\overset{O}{\|}}{C}OO\cdot \quad .$$

According to our present formulation, these radicals compete primarily with NO_2, as shown above, and with NO:

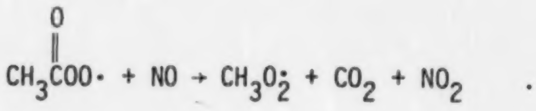

$$CH_3\overset{\overset{O}{\|}}{C}OO\cdot + NO \rightarrow CH_3O_2^{\cdot} + CO_2 + NO_2 \quad .$$

The reaction with NO leads to formaldehyde formation via the following reactions:

$$CH_3O_2^{\cdot} + NO \rightarrow CH_3O\cdot + NO_2 \quad ,$$

$$CH_3O\cdot + O_2 \rightarrow HCHO + HO_2^{\cdot} \quad .$$

The simulation of EC-48 clearly shows that our PAN chemistry is incorrect and suggests what can be changed during our efforts in the near future. Acetaldehyde and formaldehyde were added initially to systems otherwise similar to EC-39 to make up EC-48 and EC-45, respectively. In our simulation of EC-48, far too much formaldehyde is formed, too little PAN is formed (even though it is much more than in EC-45), and too much ozone is formed. If the rate constants in the mechanism were changed so that the reaction of peroxyacetyl radicals with NO was much slower or their reaction with NO_2 was much faster or both, the mechanism would simulate the measurements of formaldehyde, PAN, and ozone more closely. However, this change would result in poorer simulations of olefin systems. This is discussed in the preceding section on propylene chemistry. Another implication of this change is that formaldehyde predictions would be lower than at present; many of the formaldehyde predictions are already much lower than measurements.

In summary, the explicit mechanism for butane provides simulations that follow the observed NO to NO_2 conversions per butane reacted. PAN and formaldehyde are exceptions--the predicted concentrations of those species are generally low. As discussed above, the PAN chemistry in the mechanism is probably incorrect.

C. PROPYLENE/BUTANE/NO_x CHEMISTRY

UCR performed a set of experiments on a propylene/butane/NO_x system. To simulate this system, we combined the explicit propylene mechanism and the explicit butane mechanism. Initial simulations with the "combined" mechanism showed a rapid loss of NO_x during the simulation.

The experiments with propylene and butane have a high hydrocarbon to NO_x ratio and, because of the propylene, a high reactivity. Such a combination rapidly produces peroxy radicals in the presence of relatively low concentrations of nitrogen oxides. If the peroxy radical concentrations get too high, the NO concentration is driven so low (through the reaction $RO_2^{\cdot}$ + NO) that $NO_3^{\cdot}$ then reacts exclusively with NO_2 to give N_2O_5. The increasing N_2O_5 concentration in turn drives NO_x out of the system via the reaction with H_2O producing nitric acid (HNO_3).

Owing to such high concentrations of peroxy radicals, the radical-radical reactions

$$RO_2^{\cdot} + R'O_2^{\cdot} \rightarrow \text{Products}$$

may be significant reactions in this system. The reaction rates and products are not certain. Demerjian et al. (1974) estimated relative rates for primary and secondary radicals based on some liquid phase data by Bennett et al. (1970). In our mechanism, the values for the radical-radical reaction rate constants estimated by Demerjian et al. ($\sim$100 $ppm^{-1}min^{-1}$) seem too low to account for the observed removal of the peroxyalkyl radicals. These rate constants lead to unrealistically high levels of peroxyalkyl radicals ($\sim 10^{-2}$ ppm) and unrealistically low NO_x levels ($\sim 10^{-5}$ ppm). Faster rate constants for radical-radical reactions must be used in our mechanism because the peroxy radical reactions with nitric oxide have a faster rate constant in our mechanism (2000 $ppm^{-1}min^{-1}$) than in Demerjian's mechanism (100-500 $ppm^{-1}min^{-1}$). We are using a value of 4×10^3 $ppm^{-1}min^{-1}$ for the peroxy-peroxy radical reactions, which gives adequate fits to the observed data. However, the products of these reactions are unclear. For hydroperoxy radicals the formation of hydrogen peroxide is accepted, but the reactions of peroxyalkyl and peroxyacyl radicals might lead to different radicals:

$$HO_2^{\cdot} + HO_2^{\cdot} \rightarrow H_2O_2 \quad ,$$

$$HO_2^{\cdot} + RO_2^{\cdot} \rightarrow ROOH + O_2 \quad ,$$

$$RO_2^{\cdot} + RO_2^{\cdot} \rightarrow RO\cdot + RO\cdot + O_2 \quad .$$

An alternate pathway for this last reaction is the formation of an alcohol and an aldehyde. Weaver et al. (1975) suggested approximately an equal split between these paths; they also have data for the alkoxyl path occurring between 18 and 75 percent of the time. (See Chapter IV for further discussion of these reactions.)

1. Simulation Results

We performed carbon mass balance analysis on UCR's propylene/butane/NO_x system. Results of the analysis are presented in Table III-14. The carbon recovery values for the propylene/butane/NO_x system fall logically between the results for the propylene/NO_x and the butane/NO_x systems. The better balance of EC-114 is expected from its larger propylene/butane ratio.

Simulations of the propylene/butane/NO_x system were performed on UCR runs EC-97, 99, 106, 113, 114, 115, and 116 with the initial conditions listed in Table III-15a and the photolysis rate constants for these simulations listed in Table III-15b. The factorial block for this system is shown in Figure III-104. The kinetic mechanism for the simulation is presented in Table III-16. Simulation results for this system are shown in Figures III-105 through III-167.

TABLE III-14. PERCENT CARBON MASS RECOVERY FOR PROPYLENE/BUTANE/NO_x SYSTEMS

Time (minutes)	UCR Run Number						
	EC-97	EC-99	EC-106	EC-113	EC-114	EC-115	EC-116
60	65%	81%	86%	85%	*	*	76%
120	*	75	82	74	87%	*	64
180	74	75	76	66	88	*	75
240	73	77	72	58	80	*	72
300	67	73	*	*	*	*	66
360	*	*	*	*	*	74%	*
390	*	*	*	*	*	68	*

---

*Data not available.

TABLE III-15a. INITIAL CONDITIONS FOR SIMULATIONS OF PROPYLENE/BUTANE/NO_x SYSTEMS*

Run Number	NO (ppm)	NO_2 (ppm)	Propylene (ppm)	Butane (ppm)	HNO_2 (ppm)	k_1 (min^{-1})
EC-97	0.397	0.088	0.5	2.1	0.005	0.351
EC-99	0.407	0.09	0.4	2.0	0.01	0.351
EC-106	0.401	0.102	0.402	2.0	0.001	0.351
EC-113	0.091	0.02	0.41	2.08	0.001	0.351
EC-114	0.794	0.204	0.766	3.66	0.005	0.351
EC-115	0.402	0.104	0.310	2.94	0.002	0.351
EC-116	0.391	0.104	0.824	4.00	0.002	0.351

---

* HNO_2 data and aldehyde photolysis rate constants are chosen to provide the best fit of predicted concentrations to measured concentrations; all other data are UCR measurements.

TABLE III-15b. PHOTOLYSIS RATE CONSTANTS FOR SIMULATIONS OF PROPYLENE/BUTANE/NO_x SYSTEMS

(10^4 min^{-1})

EC Run Number	$O_3 \rightarrow O^1D$	$O_3 \rightarrow O^3P$	$HNO_2 \rightarrow$	$H_2O_2 \rightarrow$	$HCHO \rightarrow H \cdot + HCO \cdot$	$HCHO \rightarrow CO + H_2$	$CH_3CHO \rightarrow$	$CH_3CH_2CHO \rightarrow$	$CH_3CH_2CH_2CHO \rightarrow$	MEK→
97	46	350	670	8.1	8.8	25.0	6.65	7.4	10.5	5.2
99										
106										
113										
114										
115										
116										

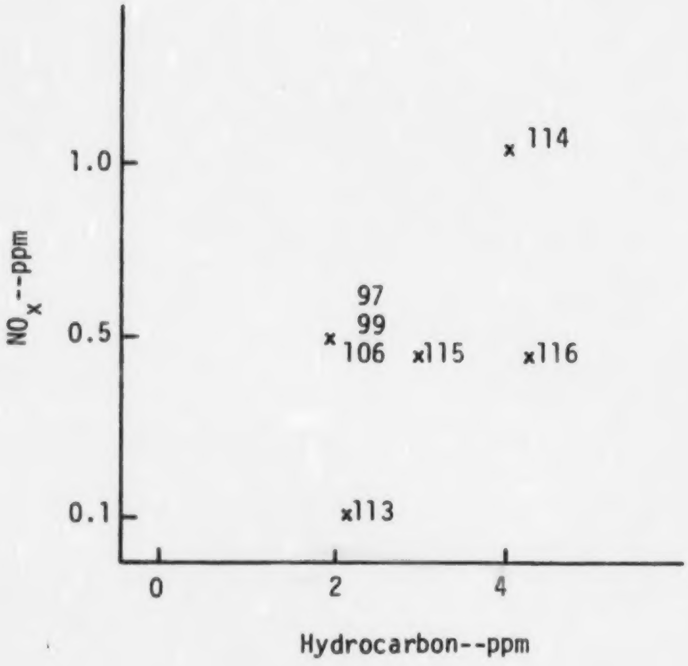

FIGURE III-104. FACTORIAL BLOCK FOR PROPYLENE/BUTANE/NO_x SYSTEMS

TABLE III-16. THE PROPYLENE/BUTANE/NO$_x$ MECHANISM

Reaction	Rate Constant (ppm-1 min-1)
$NO_2 + h\nu \rightarrow NO + O(^3P)$	Experimental *
$O(^3P) + O_2 + M) \rightarrow O_3 + M$	2.08×10^{-5} †
$O(^3P) + NO_2 \rightarrow NO + O_2$	1.34×10^4
$O_3 + NO \rightarrow NO_2 + O_2$	25.2
$O(^1D) + M \rightarrow O + M$	8.6×10^4
$O(^1D) + H_2O \rightarrow 2OH\cdot$	5.1×10^5
$O_3 + OH\cdot \rightarrow HO_2^{\cdot} + O_2$	87.0
$O_3 + HO_2^{\cdot} \rightarrow OH\cdot + 2O_2$	1.2
$O_3 + NO_2 \rightarrow NO_3 + O_2$	5×10^{-2}
$O_3 + h\nu \rightarrow O(^1D) + O_2$	Experimental *
$O_3 + h\nu \rightarrow O(^3P) + O_2$	Experimental *
$O_3 \rightarrow$ wall	1×10^{-3}
$NO_3 + NO \rightarrow 2NO_2$	1.3×10^4
$NO_3 + NO_2 \rightarrow N_2O_5$	5.6×10^3
$N_2O_5 + H_2O \rightarrow 2HNO_3$	5×10^{-6}
$N_2O_5(+ M) \rightarrow NO_3 + NO_2(+ M)$	24.0 *
$NO + NO_2 + H_2O \rightarrow 2HNO_2$	2.2×10^{-9} †

Table III-16 (Continued)

Reaction	Rate Constant (ppm^{-1} min^{-1})
$2HNO_2 \rightarrow NO + NO_2 + H_2O$	1.3×10^{-3}
$HNO_2 + h\nu \rightarrow OH\cdot + NO$	Experimental *
$NO_2 + OH\cdot(+ M) \rightarrow HNO_3(+ M)$	9.2×10^3
$NO + OH\cdot \rightarrow HNO_2$	9×10^3
$HO_2^{\cdot} + NO \rightarrow OH\cdot + NO_2$	2×10^3
$HO_2^{\cdot} + NO_2 \rightarrow HNO_2 + O_2$	20
$H_2O_2 + h\nu \rightarrow 2OH\cdot$	Experimental *
$CH_3CH_2CH_2CH_3 + O \xrightarrow{O_2} CH_3CH_2CH(O_2^{\cdot})CH_3 + OH\cdot$	64.0
$CH_3CH{=}CH_2 + O \rightarrow CH_3CH_2CHO$	1.77×10^3
$CH_3CH{=}CH_2 + O \rightarrow CH_3O_2^{\cdot} + CH_3C(O)O_2^{\cdot}$	1.77×10^3
$CH_3CH{=}CH_2 + O \xrightarrow{2O_2} CH_3CH_2O_2^{\cdot} + HC(O)O_2^{\cdot}$	1.77×10^3
$CH_3CH_2CH_2CH_3 + OH\cdot \xrightarrow{O_2} CH_3CH_2CH_2CH_2O_2^{\cdot} + H_2O$	5.0×10^2
$CH_3CH_2CH_2CH_3 + OH\cdot \xrightarrow{O_2} CH_3CH_2CH(O_2^{\cdot})CH_3 + H_2O$	2.9×10^3
$CH_3CH{=}CH_2 + OH\cdot \xrightarrow{O_2} CH_3CH(O_2^{\cdot})CH_2OH$	3.8×10^4
$CH_3CH{=}CH_2 + NO_3 \rightarrow NO_2$ + Products	7.82
$CH_3CH{=}CH_2 + O_3 \xrightarrow{O_2} H_2CO + CH_3C(O)O_2^{\cdot} + OH\cdot$	0.005
$CH_3CH{=}CH_2 + O_3 \rightarrow CH_3CHO + HC(O)O_2^{\cdot} + OH\cdot$	0.005
$CH_3CH{=}CH_2 + O_3 \rightarrow$ 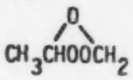 $CH_3CHOOCH_2$	0.005

TABLE III-16 (Continued)

Reaction	Rate Constant (ppm^{-1} min^{-1})
$HOCH_2CH_2CH_2C(O)O_2\cdot + NO \rightarrow NO_2 + HOCH_2CH_2CH_2O_2\cdot + CO_2$	2×10^3
$CH_3CH(OH)CH_2C(O)O_2\cdot + NO \rightarrow NO_2 + CH_3CH(OH)CH_2O_2\cdot + CO_2$	2×10^3
$HOCH_2CH_2C(O)O_2\cdot + NO \rightarrow NO_2 + HOCH_2CH_2O_2\cdot + CO_2$	2×10^3
$CH_3CH_2CH_2C(O)O_2\cdot + NO \xrightarrow{O_2} NO_2 + CH_3CH_2CH_2O_2\cdot + CO_2$	2×10^3
$CH_3CH_2C(O)O_2\cdot + NO \xrightarrow{O_2} NO_2 + CH_3CH_2O_2\cdot + CO_2$	2×10^3
$CH_3C(O)O_2\cdot + NO \xrightarrow{O_2} NO_2 + CH_3O_2\cdot + CO_2$	2×10^3
$HC(O)O_2\cdot + NO \xrightarrow{O_2} NO_2 + HO_2\cdot + CO_2$	2×10^3
$HOCH_2CH_2CH_2CH_2O_2\cdot + NO \rightarrow NO_2 + HO_2\cdot + HOCH_2CH_2CH_2CHO$	2×10^3
$CH_3CH(O_2\cdot)C(O)CH_3 + NO \rightarrow NO_2 + HO_2\cdot + CH_3C(O)C(O)CH_3$	2×10^3
$CH_3CH(O_2\cdot)CH_2CH_3 + NO \rightarrow NO_2 + CH_3CH(O\cdot)CH_2CH_3$	2×10^3
$CH_3CH_2CH_2CH_2O_2\cdot + NO \rightarrow NO_2 + CH_3CH_2CH_2CH_2O\cdot$	2×10^3
$CH_3CH(O_2\cdot)CH_2OH + NO \rightarrow NO_2 + CH_3CH(O\cdot)CH_2OH$	2×10^3
$HOCH_2CH_2CH_2O_2\cdot + NO \rightarrow NO_2 + HO_2 + HOCH_2CH_2CHO$	2×10^3
$HOCH_2CH_2O_2\cdot + NO \rightarrow NO_2 + HO_2 + HOCH_2CHO$	2×10^3
$CH_3CH_2CH_2O_2\cdot + NO \rightarrow NO_2 + CH_3CH_2CH_2O\cdot$	2×10^3
$CH_3CH_2O_2\cdot + NO \rightarrow NO_2 + CH_3CH_2O\cdot$	2×10^3
$CH_3O_2\cdot + NO \rightarrow NO_2 + CH_3O\cdot$	2×10^3
$CH_3CH_2CH(O\cdot)CH_3 \xrightarrow{O_2} CH_3CH_2O_2\cdot + CH_3CHO$	6.7×10^4 *

TABLE III-16 (Continued)

Reaction	Rate Constant (ppm^{-1} min^{-1})
$CH_3C(O\cdot)CH_2OH \xrightarrow{O_2} CH_3CHO + H_2CO + HO_2^{\cdot}$	3×10^5 *
$CH_3CH_2CH_2CH_2O\cdot \xrightarrow{O_2} HOCH_2CH_2CH_2CH_2O_2^{\cdot}$	7.5×10^5 *
$CH_3CH_2CH(O\cdot)CH_3 + O_2 \rightarrow CH_3CH_2C(O)CH_3 + HO_2^{\cdot}$	0.95
$CH_3CH_2CH_2CH_2O\cdot + O_2 \rightarrow CH_3CH_2CH_2CHO + HO_2^{\cdot}$	0.95
$CH_3CH_2CH_2O\cdot + O_2 \rightarrow CH_3CH_2CHO + HO_2^{\cdot}$	0.95
$CH_3CH_2O\cdot + O_2 \rightarrow CH_3CHO + HO_2^{\cdot}$	0.95
$CH_3O\cdot + O_2 \rightarrow H_2CO + HO_2^{\cdot}$	0.95
$H_2CO + h\nu \xrightarrow{2O_2} HO_2^{\cdot} + HC(O)O_2^{\cdot}$	Experimental*
$H_2CO + h\nu \rightarrow H_2 + CO$	Experimental*
$CH_3CHO + h\nu \xrightarrow{2O_2} CH_3O_2^{\cdot} + HC(O)O_2$	Experimental*
$CH_3CH_2CHO + h\nu \xrightarrow{2O_2} CH_3CH_2O_2^{\cdot} + HC(O)O_2^{\cdot}$	Experimental*
$CH_3CH_2CH_2CHO + h\nu \xrightarrow{2O_2} CH_3CH_2CH_2O_2^{\cdot} + HC(O)O_2^{\cdot}$	Experimental*
$CH_3CH_2CH_2CHO + h\nu \rightarrow CH_3CHO + C_2H_4$	Experimental*
$CH_3CH_2C(O)CH_3 + h\nu \rightarrow CH_3C(O)O_2^{\cdot} + CH_3CH_2O_2^{\cdot}$	Experimental*
$HOCH_2CHO + h\nu \rightarrow HC(O)O_2^{\cdot} + H_2CO + HO_2^{\cdot}$	1×10^{-3}
$HOCH_2CH_2CHO + h\nu \rightarrow HC(O)O_2^{\cdot} + HOCH_2CH_2O_2$	1×10^{-3}
$HOCH_2CH_2CH_2CHO + h\nu \rightarrow HC(O)O_2^{\cdot} + HOCH_2CH_2CH_2O_2^{\cdot}$	1×10^{-3}
$CH_3C(O)C(O)CH_3 + h\nu \xrightarrow{2O_2} 2CH_3C(O)O_2^{\cdot}$	2×10^{-3}

TABLE III-16 (Continued)

Reaction	Rate Constant (ppm^{-1} min^{-1})
$H_2CO + OH\cdot \xrightarrow{O_2} HC(O)O_2^{\cdot} + H_2O$	1×10^4
$CH_3CHO + OH\cdot \xrightarrow{O_2} CH_3C(O)O_2^{\cdot} + H_2O$	1×10^4
$CH_3CH_2CHO + OH\cdot \xrightarrow{O_2} CH_3CH_2C(O)O_2^{\cdot} + H_2O$	1×10^4
$CH_3CH_2CH_2CHO + OH\cdot \xrightarrow{O_2} CH_3CH_2CH_2C(O)O_2^{\cdot} + H_2O$	1×10^4
$CH_3CH_2C(O)CH_3 + OH\cdot \rightarrow CH_3CH(O_2^{\cdot})C(O)CH_3 + H_2O$	5.2×10^3
$HOCH_2CH_2CH_2CHO + OH\cdot \rightarrow HOCH_2CH_2CH_2C(O)O_2^{\cdot} + H_2O$	1×10^4
$HOCH_2CH_2CHO + OH\cdot \rightarrow HOCH_2CH_2C(O)O_2^{\cdot} + H_2O$	1×10^4
$HOCH_2CHO + OH\cdot \rightarrow H_2CO + HO_2^{\cdot}$	1×10^4
$HOCH_2CH_2CH_2C(O)O_2^{\cdot} + HO_2^{\cdot} \rightarrow HOCH_2CH_2CH_2C(O)OOH + O_2$	1×10^4
$HOCH_2CH_2C(O)O_2^{\cdot} + HO_2^{\cdot} \rightarrow HOCH_2CH_2C(O)OOH + O_2$	1×10^4
$CH_3CH_2CH_2C(O)O_2^{\cdot} + HO_2^{\cdot} \rightarrow CH_3CH_2CH_2C(O)OOH + O_2$	1×10^4
$CH_3CH_2C(O)O_2^{\cdot} + HO_2^{\cdot} \rightarrow CH_3CH_2C(O)OOH + O_2$	1×10^4
$CH_3C(O)O_2^{\cdot} + HO_2^{\cdot} \rightarrow CH_3C(O)OOH + O_2$	1×10^4
$HC(O)O_2^{\cdot} + HO_2^{\cdot} \rightarrow HC(O)OOH + O_2$	1×10^4
$HOCH_2CH_2CH_2CH_2O_2^{\cdot} + HO_2^{\cdot} \rightarrow HOCH_2CH_2CH_2CH_2OOH + O_2$	4×10^3
$CH_3CH(O_2^{\cdot})C(O)CH_3 + HO_2^{\cdot} \rightarrow CH_3CH(OOH)C(O)CH_3 + O_2$	4×10^3
$CH_3CH_2CH(O_2^{\cdot})CH_3 + HO_2^{\cdot} \rightarrow CH_3CH_2CH(CH_3)OOH + O_2$	4×10^3
$CH_3CH_2CH_2CH_2O_2^{\cdot} + HO_2^{\cdot} \rightarrow CH_3CH_2CH_2CH_2OOH + O_2$	4×10^3

TABLE III-16 (Continued)

Reaction	Rate Constant (ppm^{-1} min^{-1})
$CH_3CH(O_2^{\cdot})CH_2OH + HO_2^{\cdot} \rightarrow CH_3CH(OOH)CH_2OH + O_2$	4×10^3
$CH_3CH_2CH_2O_2^{\cdot} + HO_2^{\cdot} \rightarrow CH_3CH_2CH_2OOH + O_2$	4×10^3
$CH_3CH_2O_2^{\cdot} + HO_2^{\cdot} \rightarrow CH_3CH_2OOH + O_2$	4×10^3
$CH_3O_2^{\cdot} + HO_2^{\cdot} \rightarrow CH_3OOH + O_2$	4×10^3
$HO_2^{\cdot} + HO_2^{\cdot} \rightarrow H_2O_2 + O_2$	4×10^3
$CH_3CH_2CH_2C(O)O_2^{\cdot} + NO_2 \rightarrow CH_3CH_2CH_2C(O)O_2NO_2$	4×10^2
$CH_3CH_2C(O)O_2^{\cdot} + NO_2 \rightarrow CH_3CH_2C(O)O_2NO_2$	4×10^2
$CH_3C(O)O_2^{\cdot} + NO_2 \rightarrow CH_3C(O)O_2NO_2$	4×10^2
$CH_3C(O)O_2NO_2 \rightarrow NO_2 + CH_3C(O)O_2^{\cdot}$	1.7×10^{-2} *
$CH_3CH_2C(O)O_2NO_2 \rightarrow NO_2 + CH_3CH_2C(O)O_2^{\cdot}$	2×10^{-2} *
$CH_3CH_2CH_2C(O)O_2NO_2 \rightarrow NO_2 + CH_3CH_2CH_2C(O)O_2^{\cdot}$	2.5×10^{-2} *
$CH_3O\cdot + NO_2 \rightarrow CH_3ONO_2$	2×10^4
$CH_3O\cdot + NO_2 \rightarrow H_2CO + HNO_2$	2.2×10^3
$CH_3CH_2O\cdot + NO_2 \rightarrow CH_3CH_2ONO_2$	2.0×10^4
$CH_3CH_2O\cdot + NO_2 \rightarrow CH_3CHO + HNO_2$	2.2×10^3
$CH_3CH_2CH_2O\cdot + NO_2 \rightarrow CH_3CH_2CH_2ONO_2$	2.0×10^4
$CH_3CH_2CH_2O\cdot + NO_2 \rightarrow CH_3CH_2CHO + HNO_2$	2.2×10^3
$CH_3CH_2CH_2CH_2O\cdot + NO_2 \rightarrow CH_3CH_2CH_2CH_2ONO_2$	2×10^4

TABLE III-16 (Continued)

Reaction	Rate Constant (ppm^{-1} min^{-1})
$CH_3CH_2CH_2CH_2O\cdot + NO_2 \rightarrow CH_3CH_2CH_2CHO + HNO_2$	2.2×10^3
$CH_3CH_2CH(O\cdot)CH_3 + NO_2 \rightarrow CH_3CH_2CH(ONO_2)CH_3$	2×10^4
$CH_3CH_2CH(O\cdot)CH_3 + NO_2 \rightarrow CH_3CH_2C(O)CH_3 + HNO_2$	2.2×10^4
$CO + OH\cdot \xrightarrow{O_2} HO_2 + CO_2$	2.06×10^2
$2CH_3O_2\cdot \rightarrow 2CH_3O\cdot + O_2$	4×10^3
$2CH_3CH_2O_2\cdot \rightarrow 2CH_3CH_2O\cdot + O_2$	4×10^3
$2CH_3CH_2CH_2O_2\cdot \rightarrow 2CH_3CH_2CH_2O\cdot + O_2$	4×10^3
$2CH_3CH_2CH_2CH_2O_2\cdot \rightarrow 2CH_3CH_2CH_2CH_2O\cdot + O_2$	4×10^3
$2CH_3CH_2CH(O_2\cdot)CH_3 \rightarrow 2CH_3CH_2CH(O\cdot)CH_3 + O_2$	4×10^3
$CH_3O_2\cdot + CH_3CH_2O_2\cdot \rightarrow CH_3O\cdot + CH_3CH_2O\cdot + O_2$	4×10^3
$CH_3O_2\cdot + CH_3CH_2CH_2O_2\cdot \rightarrow CH_3O\cdot + CH_3CH_2CH_2O\cdot + O_2$	4×10^3
$CH_3O_2\cdot + CH_3CH_2CH_2CH_2O_2\cdot \rightarrow CH_3O\cdot + CH_3CH_2CH_2CH_2O\cdot$	4×10^3
$CH_3O_2\cdot + CH_3CH_2CH(O_2\cdot)CH_3 \rightarrow CH_3O\cdot + CH_3CH_2CH(O\cdot)CH_3 + O_2$	4×10^3
$CH_3CH_2O_2\cdot + CH_3CH_2CH_2O_2\cdot \rightarrow CH_3CH_2O\cdot + CH_3CH_2CH_2O\cdot + O_2$	4×10^3
$CH_3CH_2O_2\cdot + CH_3CH_2CH_2CH_2O_2\cdot \rightarrow CH_3CH_2O\cdot + CH_3CH_2CH_2CH_2O\cdot + O_2$	4×10^3
$CH_3CH_2O_2\cdot + CH_3CH_2CH(O_2\cdot)CH_3 \rightarrow CH_3CH_2O\cdot + CH_3CH_2CH(O\cdot)CH_3 + O_2$	4×10^3
$CH_3CH_2CH_2O_2\cdot + CH_3CH_2CH_2CH_2O_2\cdot \rightarrow CH_3CH_2CH_2O\cdot + CH_3CH_2CH_2CH_2O\cdot + O_2$	4×10^3
$CH_3CH_2CH_2O_2\cdot + CH_3CH_2CH(O_2\cdot)CH_3 \rightarrow CH_3CH_2CH_2O\cdot + CH_3CH_2CH(O\cdot)CH_3 + O_2$	4×10^3

TABLE III-16 (Concluded)

Reaction	Rate Constant (ppm^{-1} min^{-1})
$CH_3CH_2CH(O_2^{\cdot})CH_3 + CH_3CH(O_2^{\cdot})CH_2OH \rightarrow CH_3CH_2CH(O\cdot)CH_3 + CH_3CH(O\cdot)CH_2OH + O_2$	4×10^3
$CH_3CH(O_2^{\cdot})CH_2OH + CH_3CH(O_2^{\cdot})CH_2OH \rightarrow CH_3CH(O\cdot)CH_2OH + CH_3CH(O\cdot)CH_2OH + O_2$	4×10^3

---

† Units of ppm^{-2}min^{-1}.

* Units of min^{-1}.

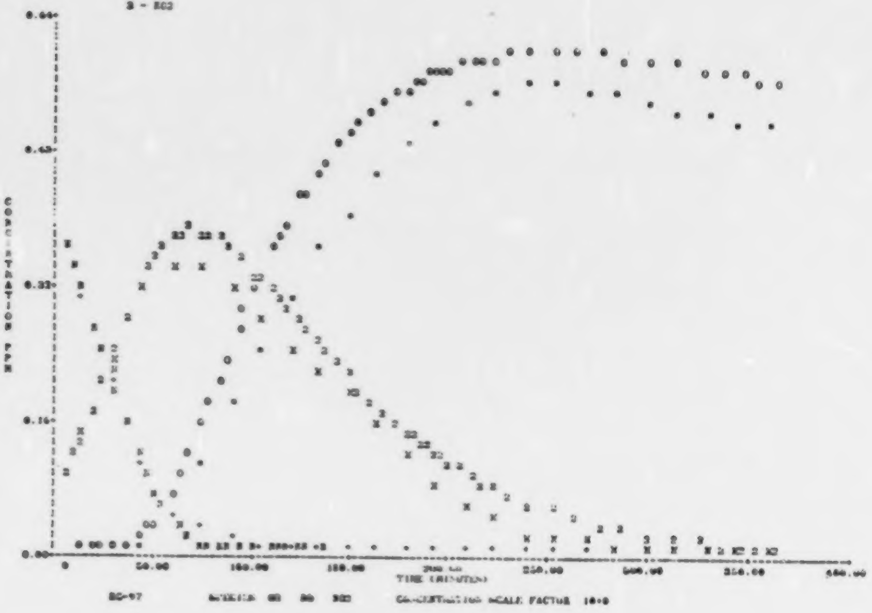

FIGURE III-105

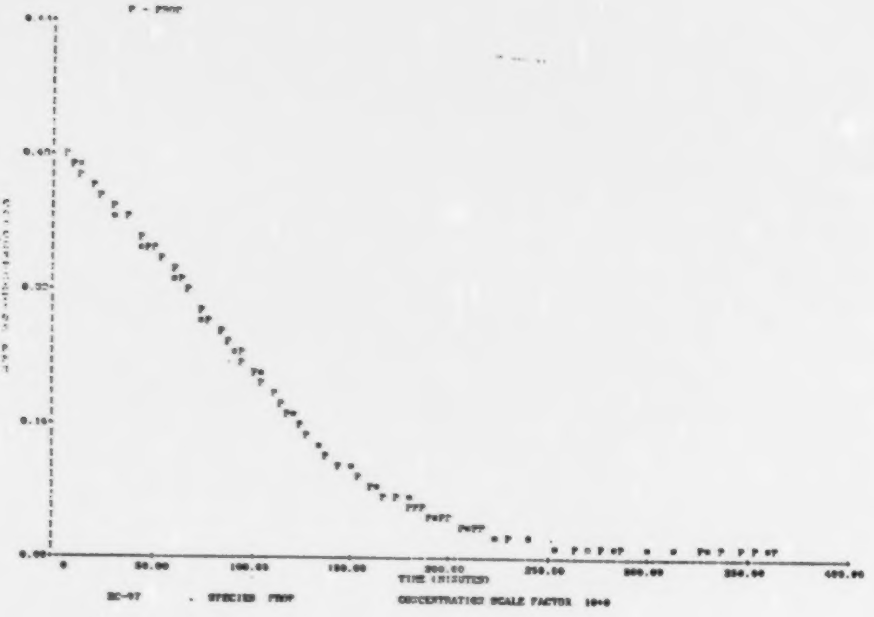

FIGURE III-106

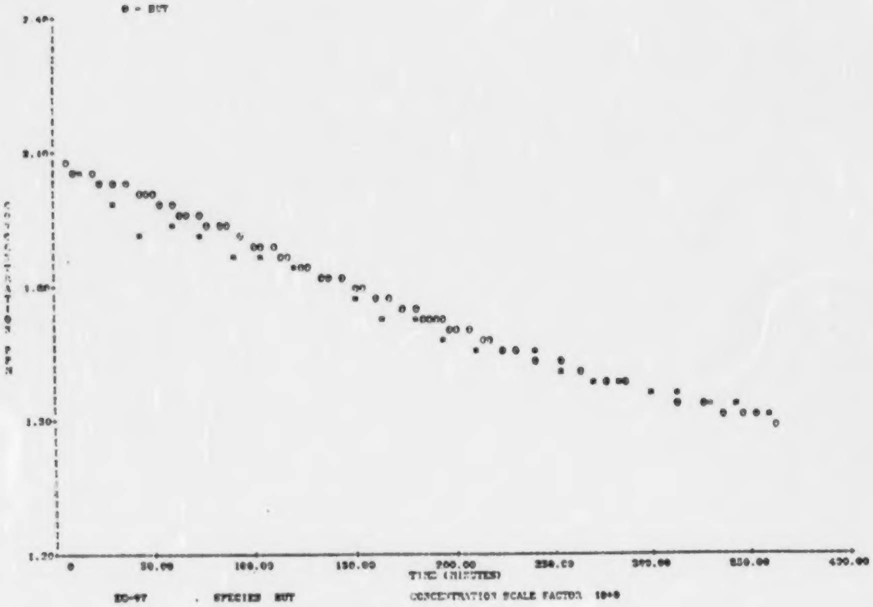

FIGURE III-107

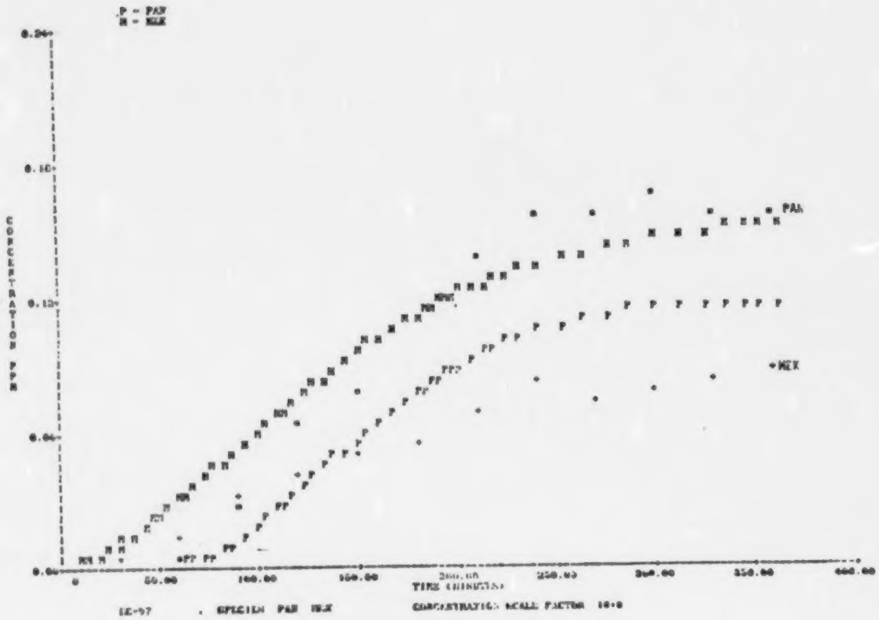

FIGURE III-108

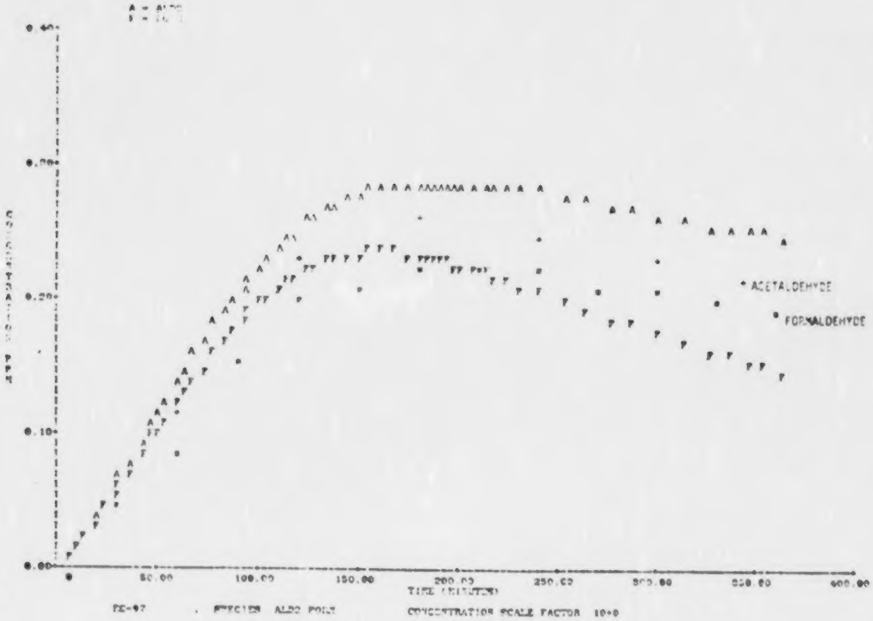

FIGURE III-109

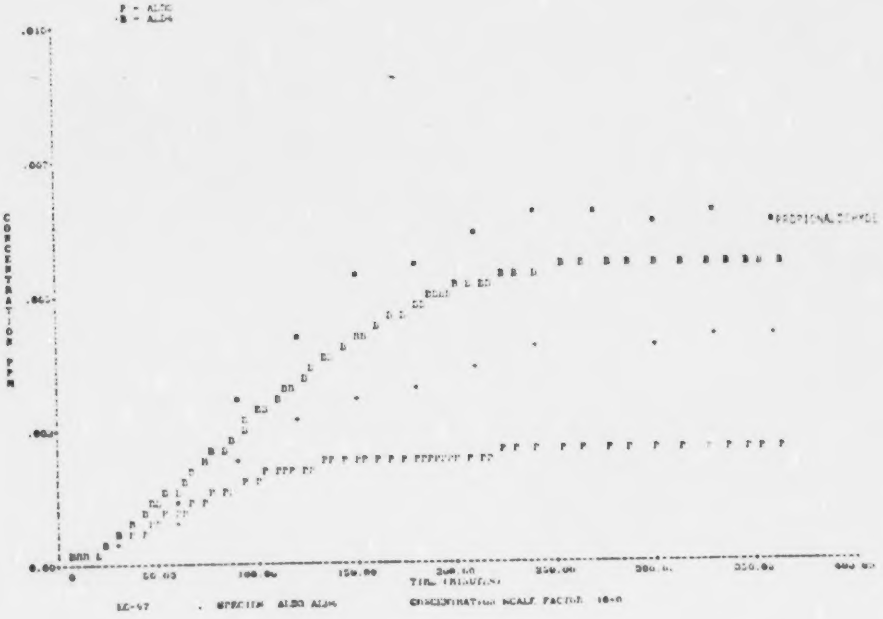

FIGURE III-110

Reproduced from best available copy.

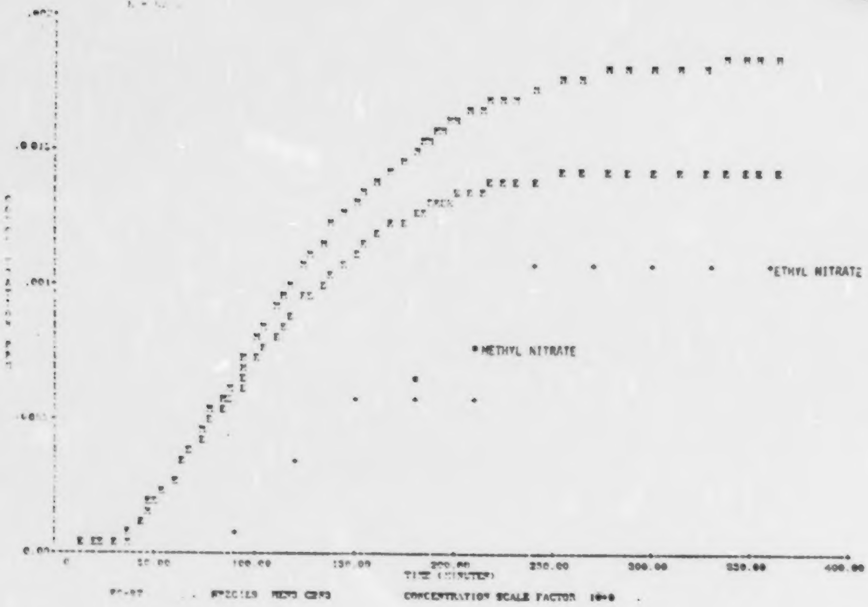

FIGURE III-111

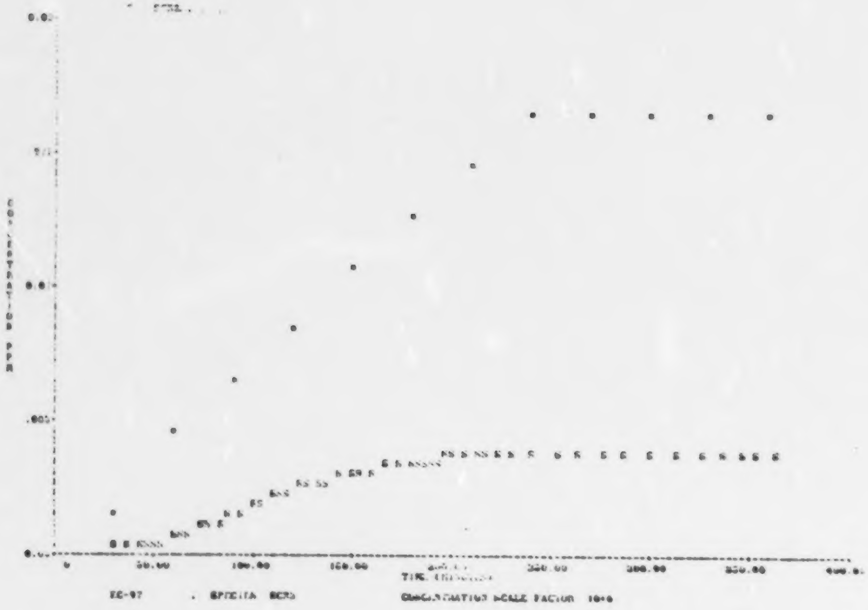

FIGURE III-112

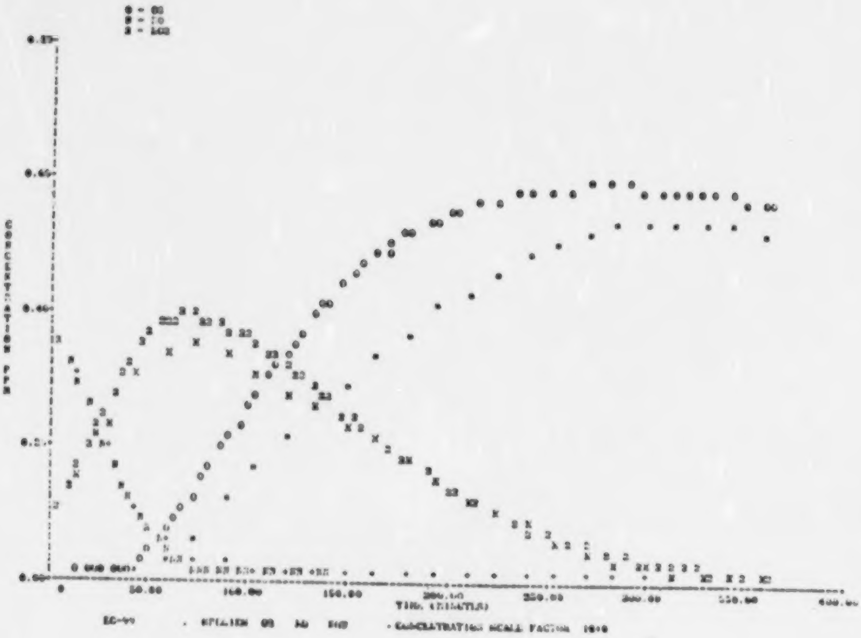

FIGURE III-113

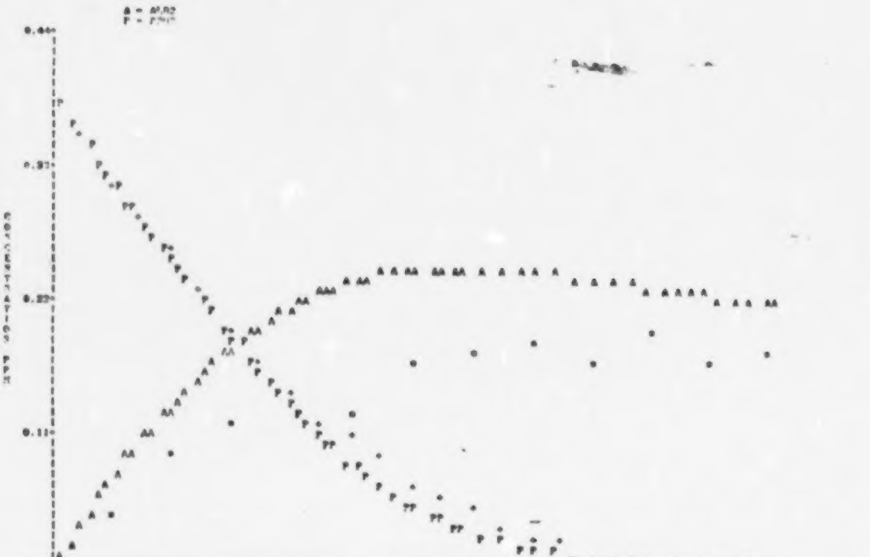

FIGURE III-114

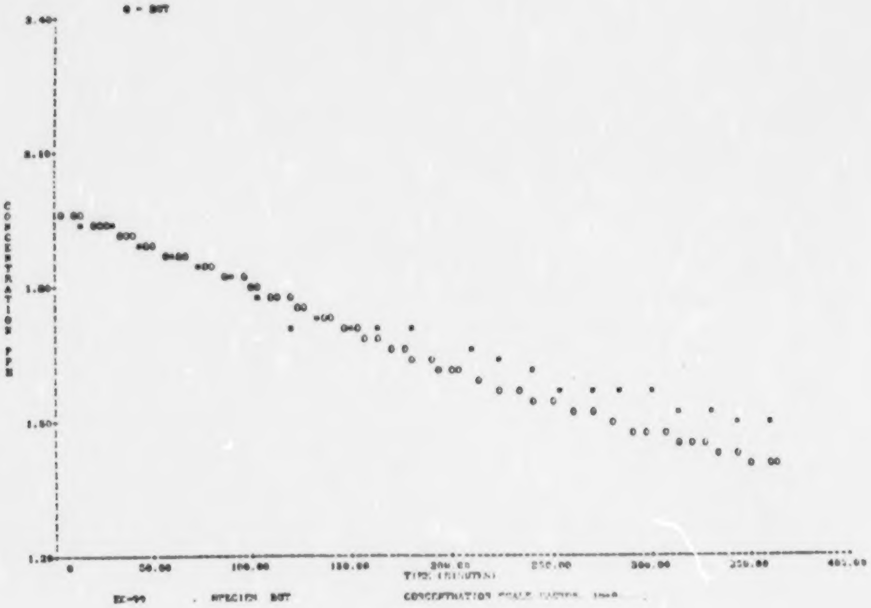

FIGURE III-115

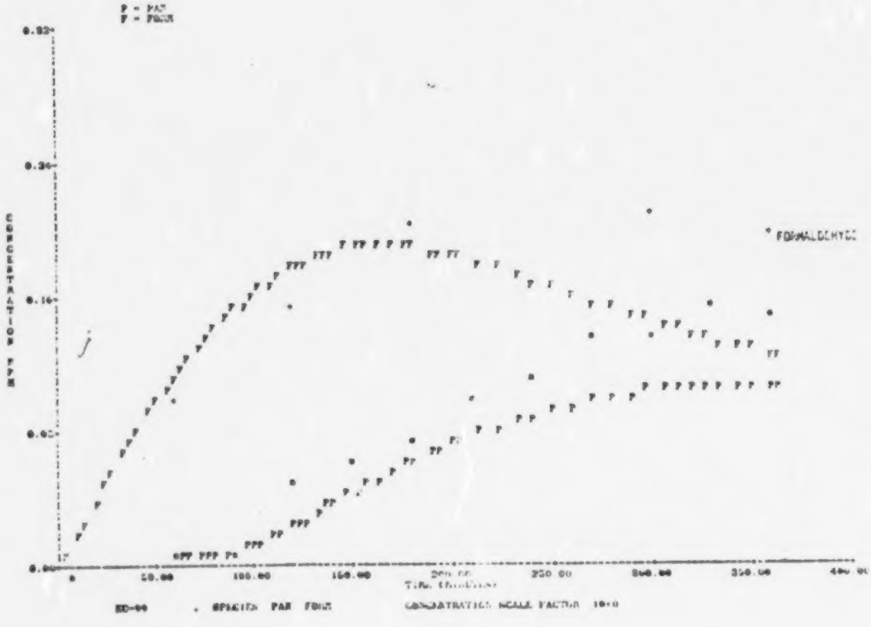

FIGURE III-116

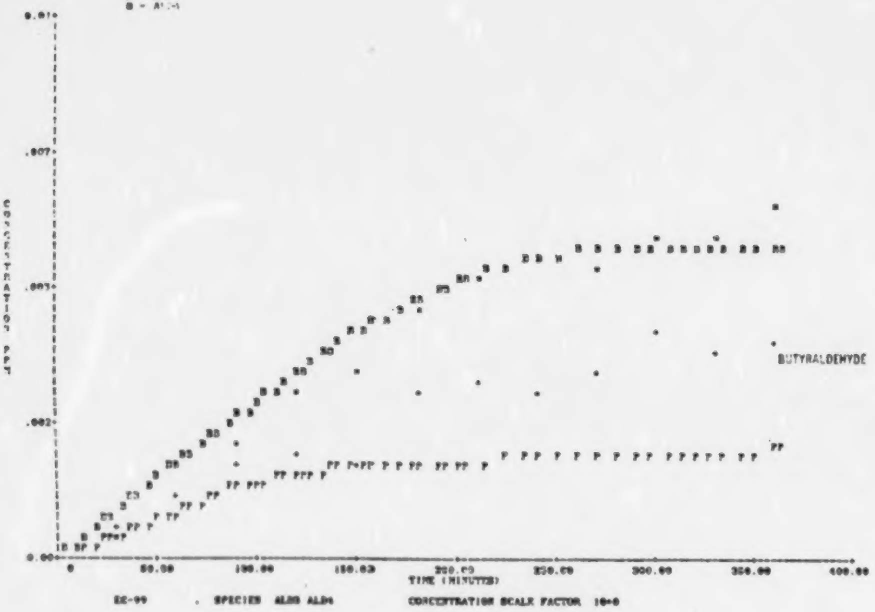

FIGURE III-117

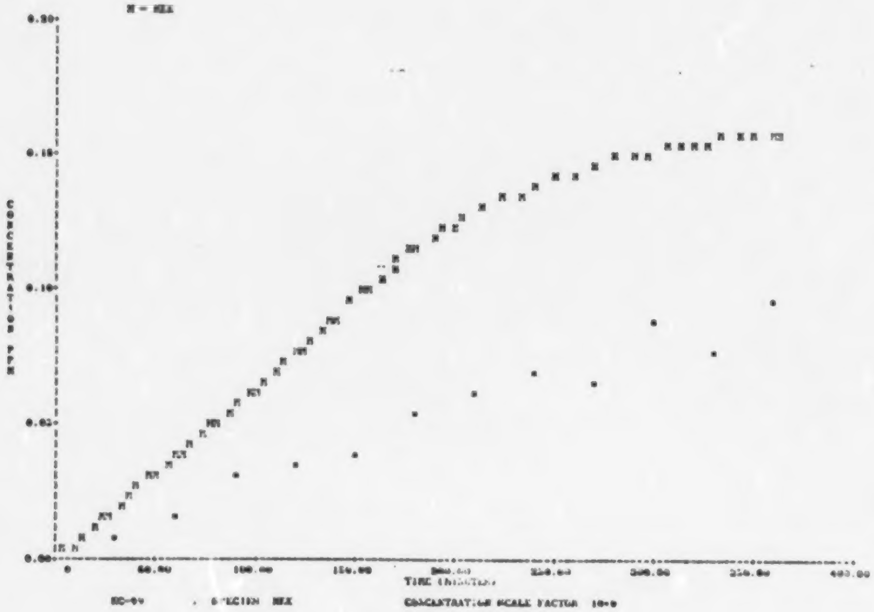

FIGURE III-118

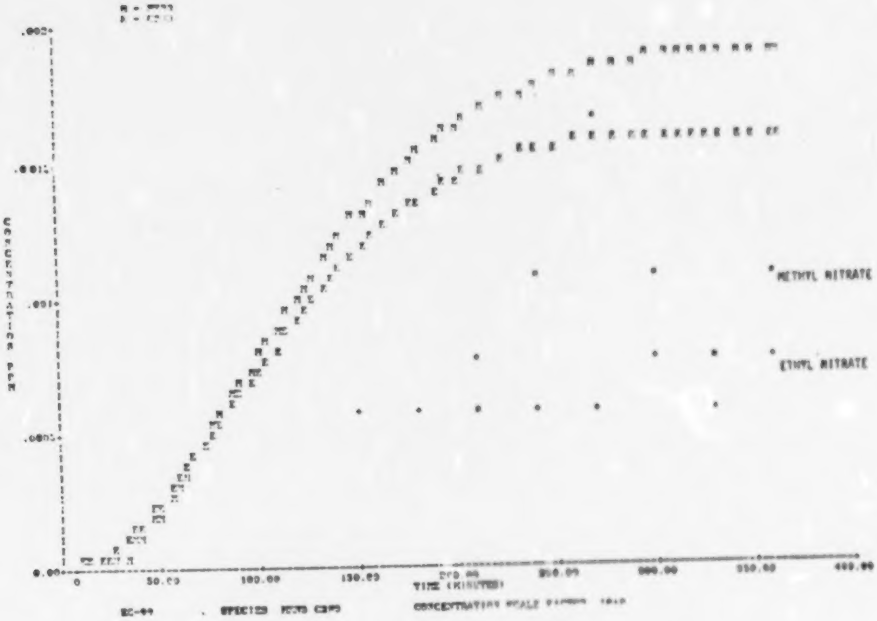

FIGURE III-119

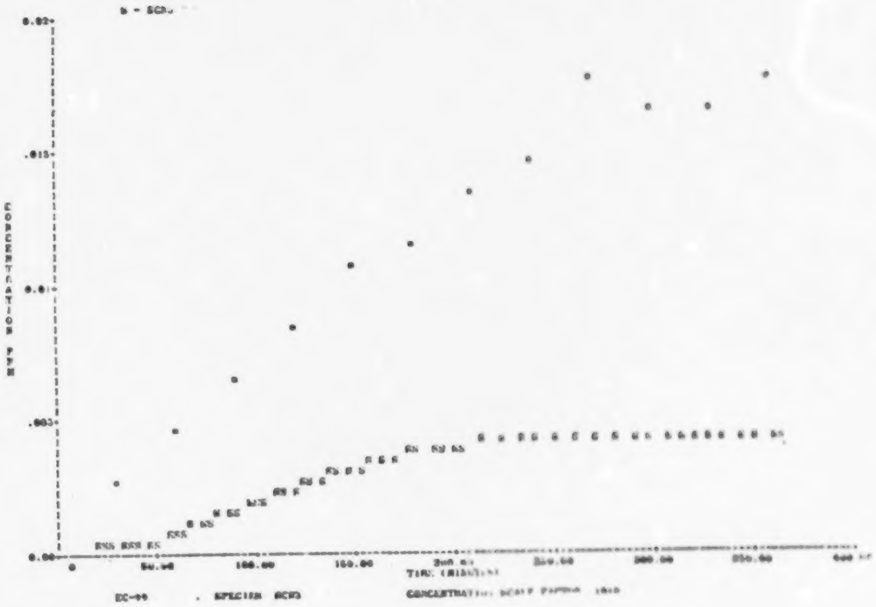

FIGURE III-120

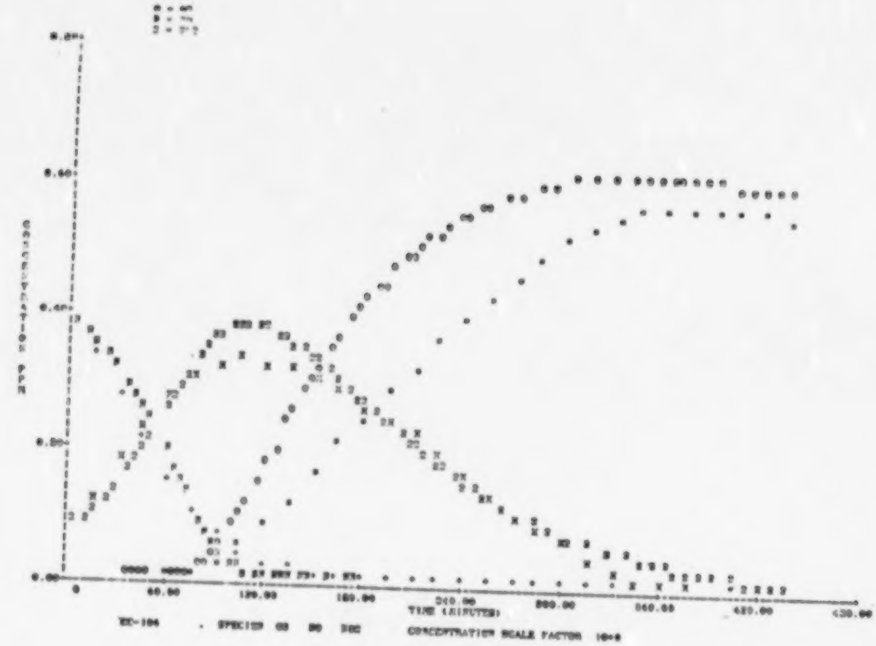

FIGURE III-121

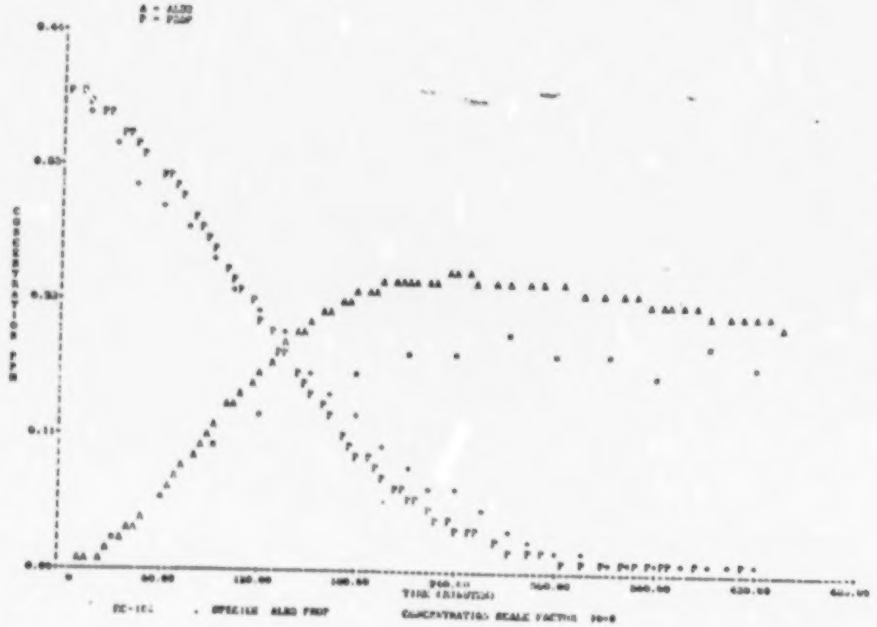

FIGURE III-122

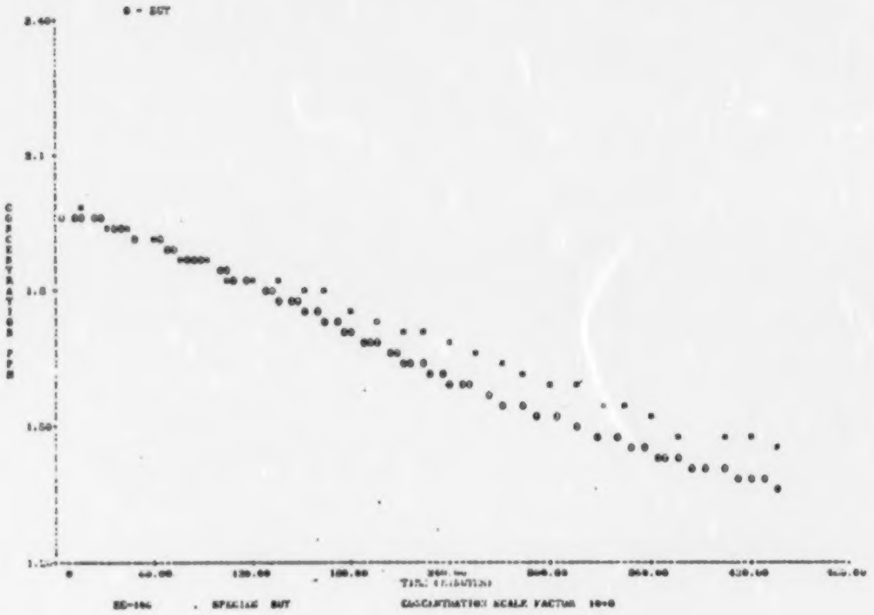

FIGURE III-123

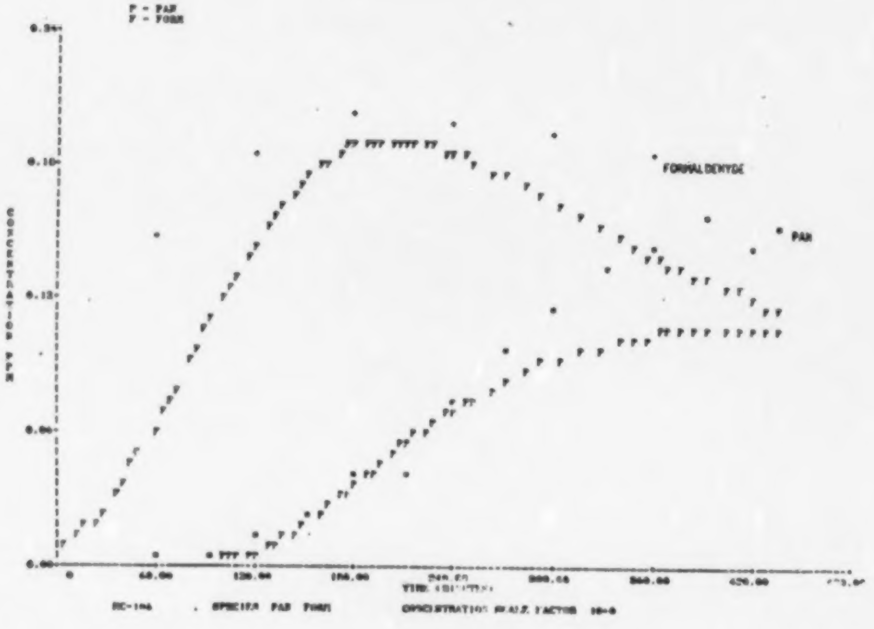

FIGURE III-124

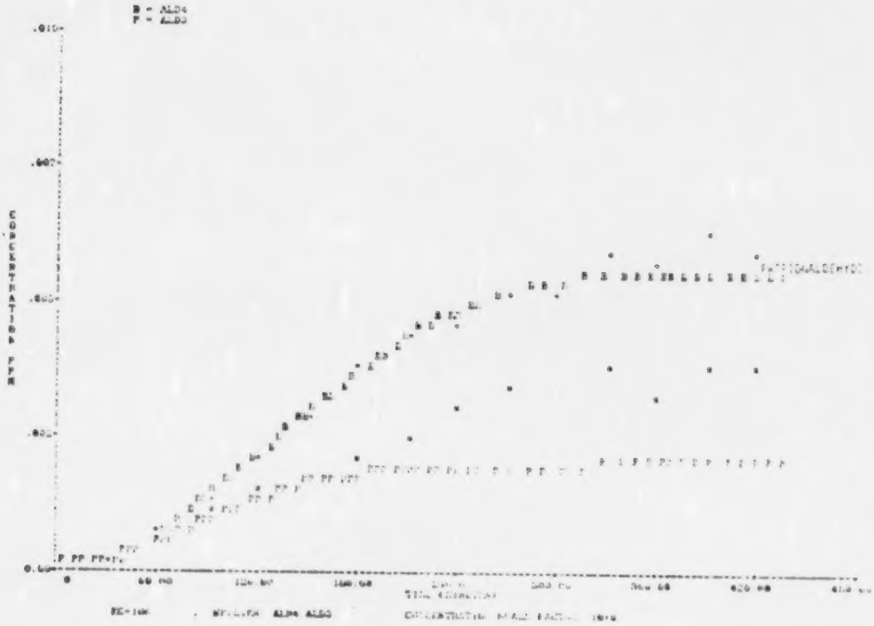

FIGURE III-125

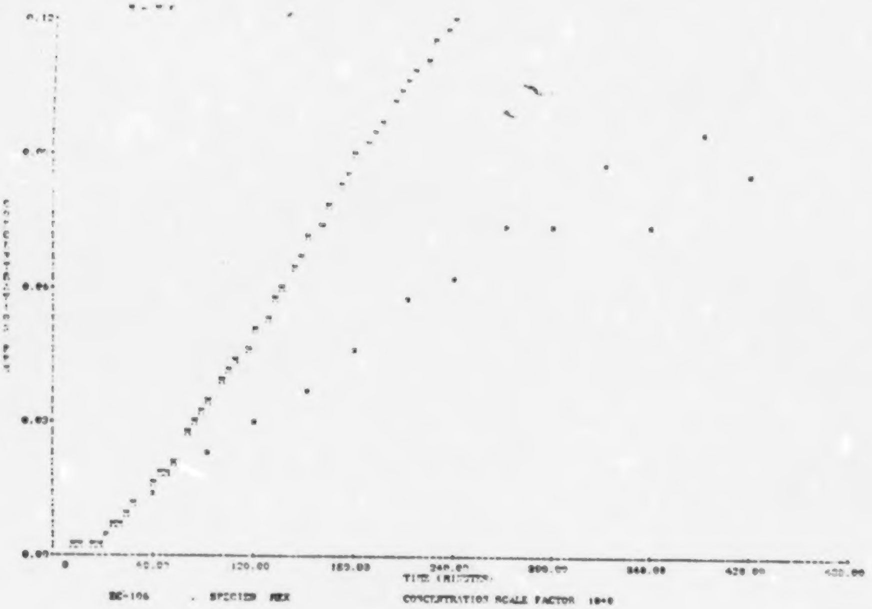

FIGURE III-126

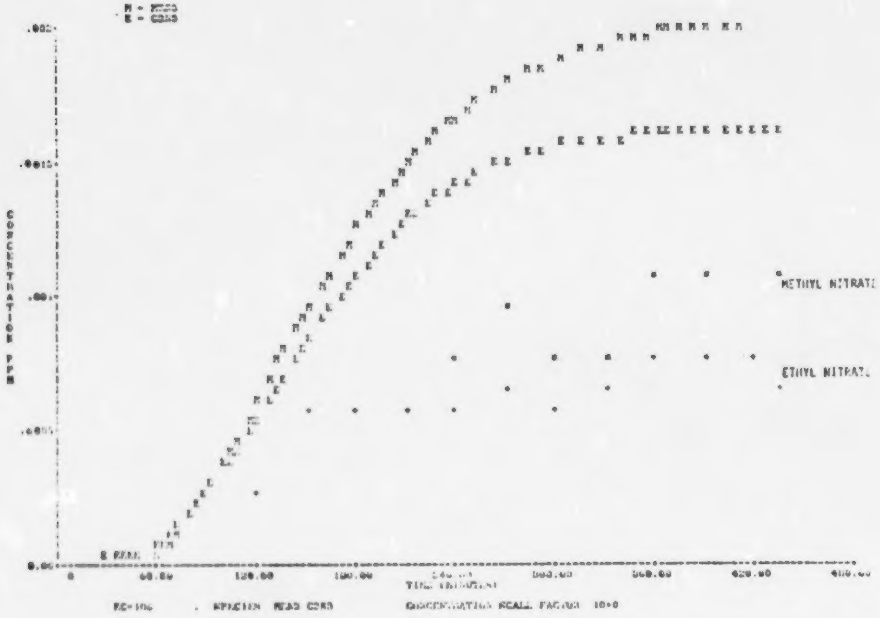

FIGURE III-127

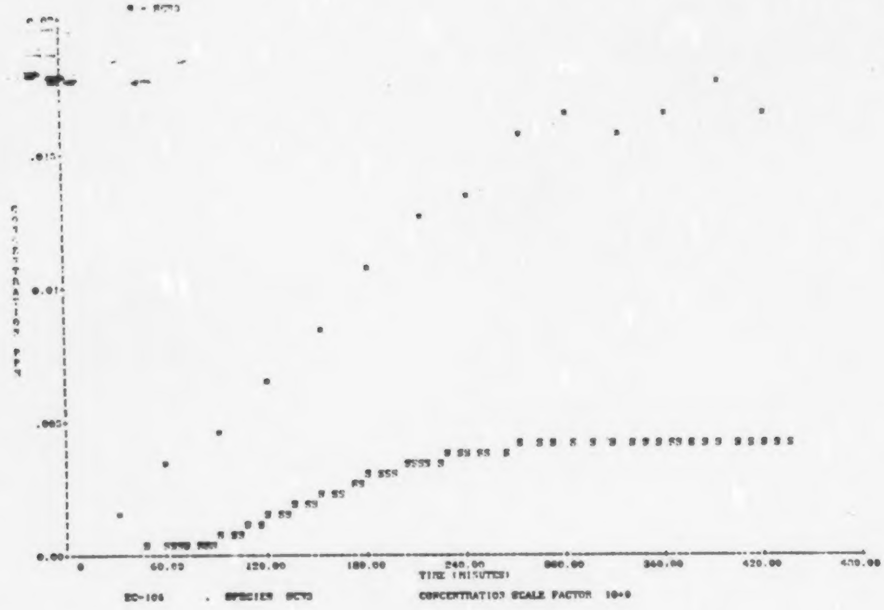

FIGURE III-128

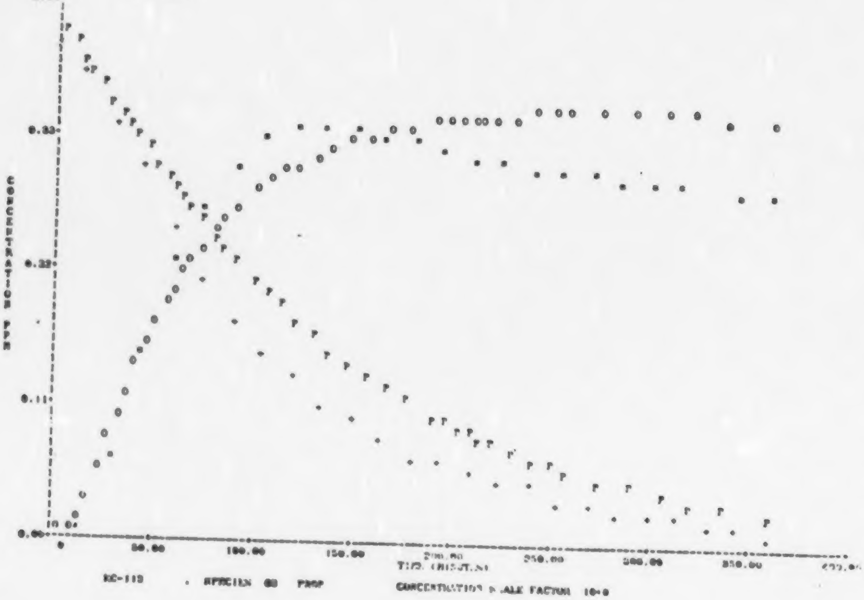

FIGURE III-129

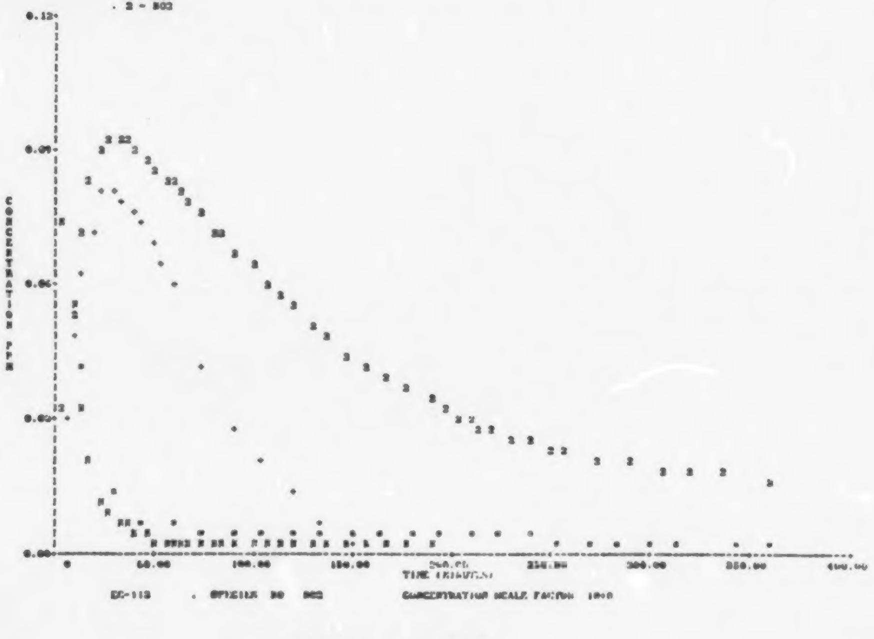

FIGURE III-130

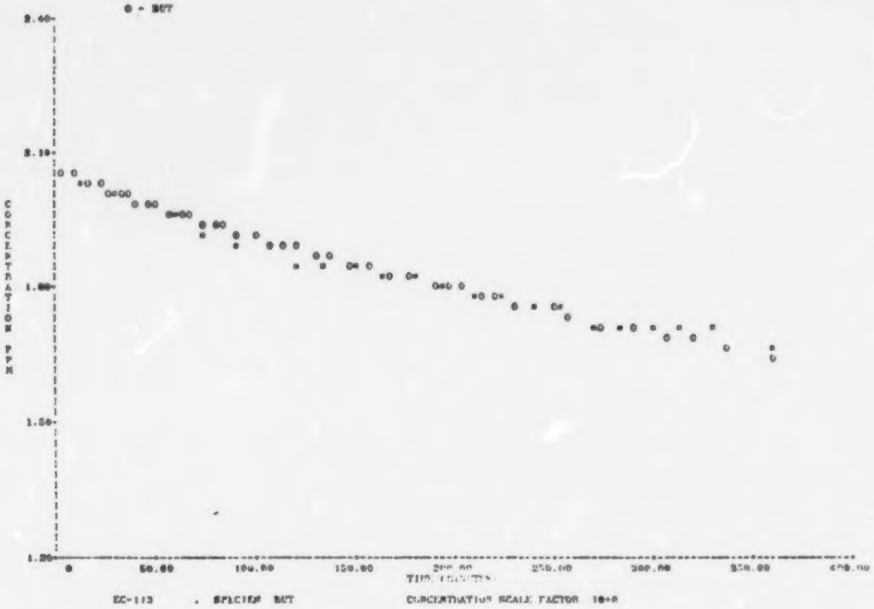

FIGURE III-131

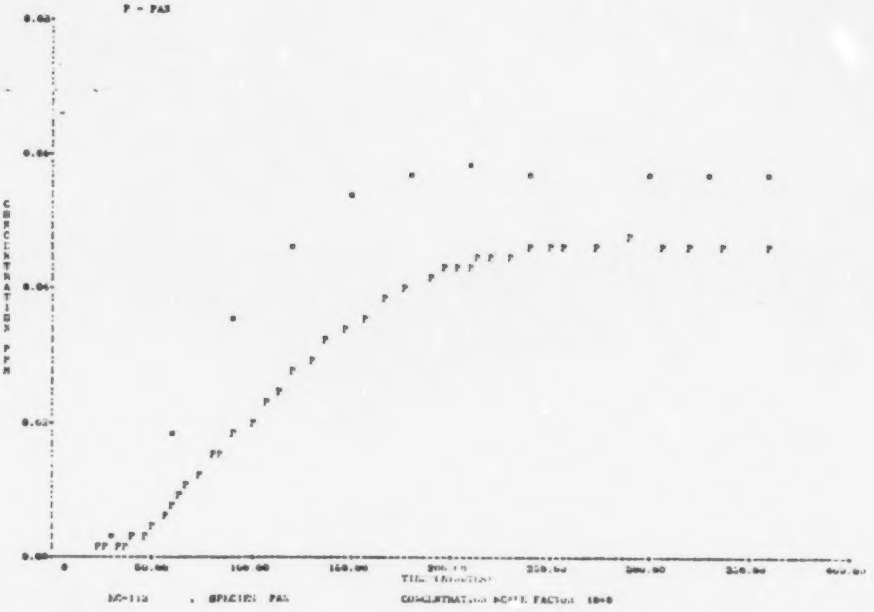

FIGURE III-132

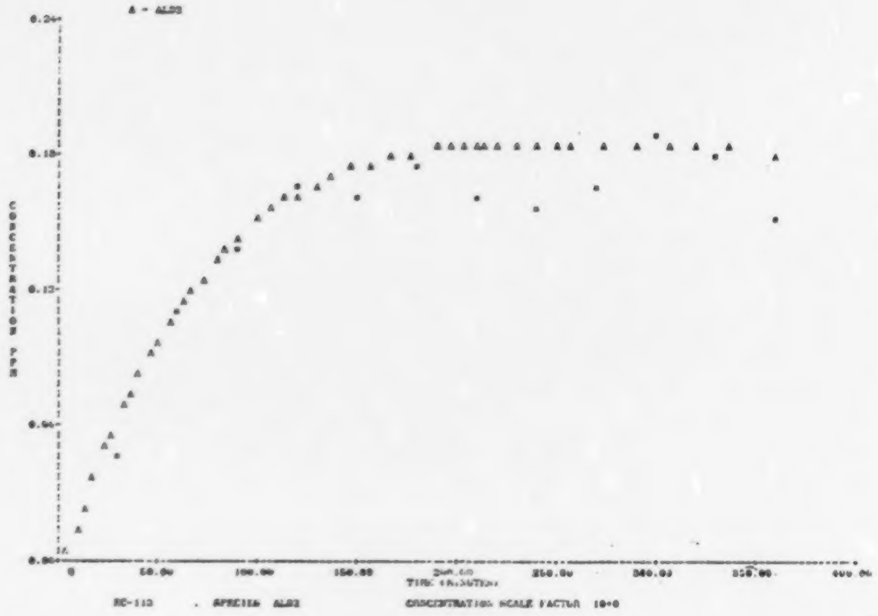

FIGURE III-133

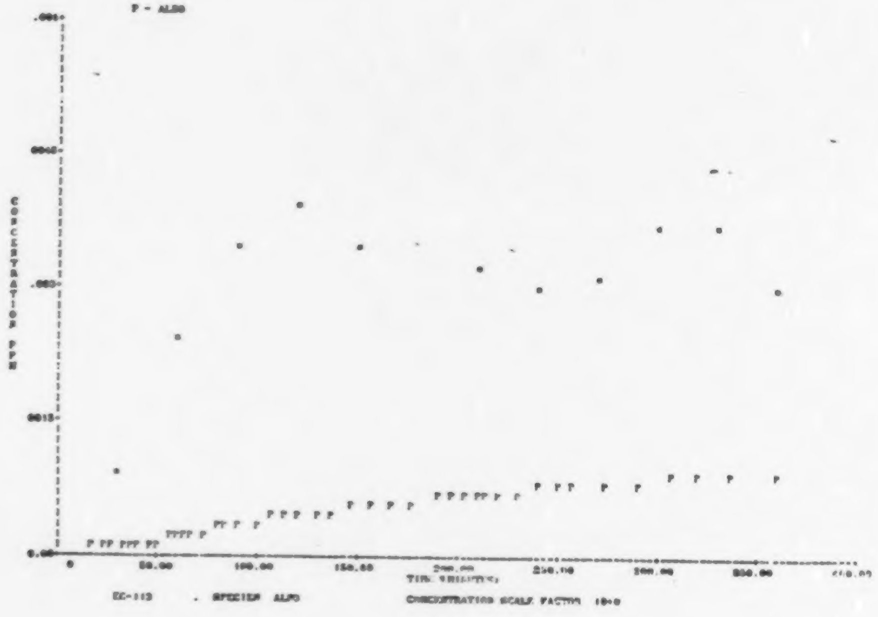

FIGURE III-134

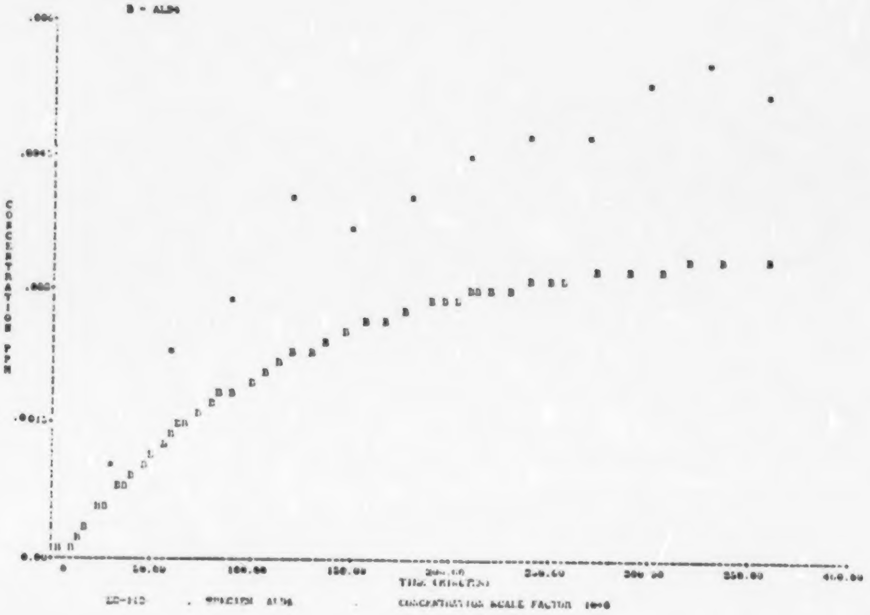

FIGURE III-135

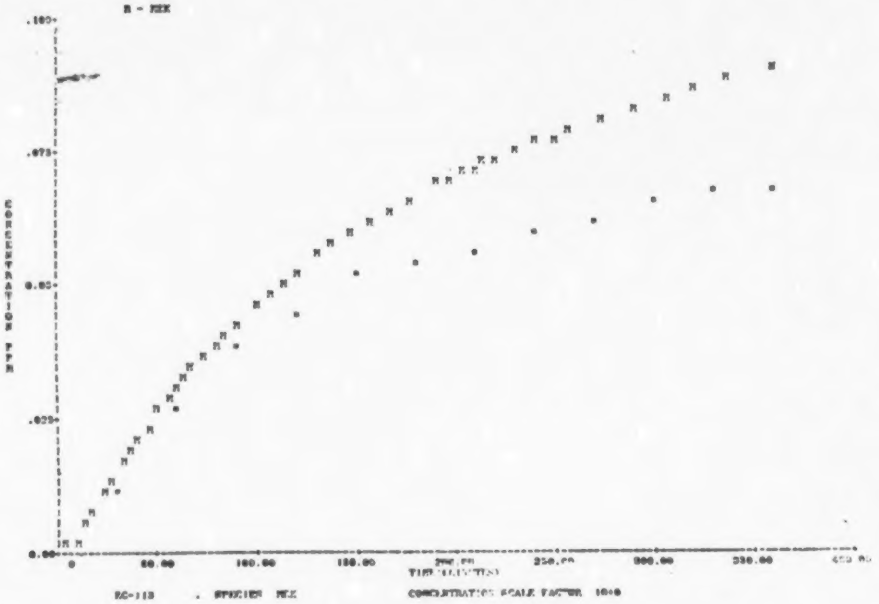

FIGURE III-136

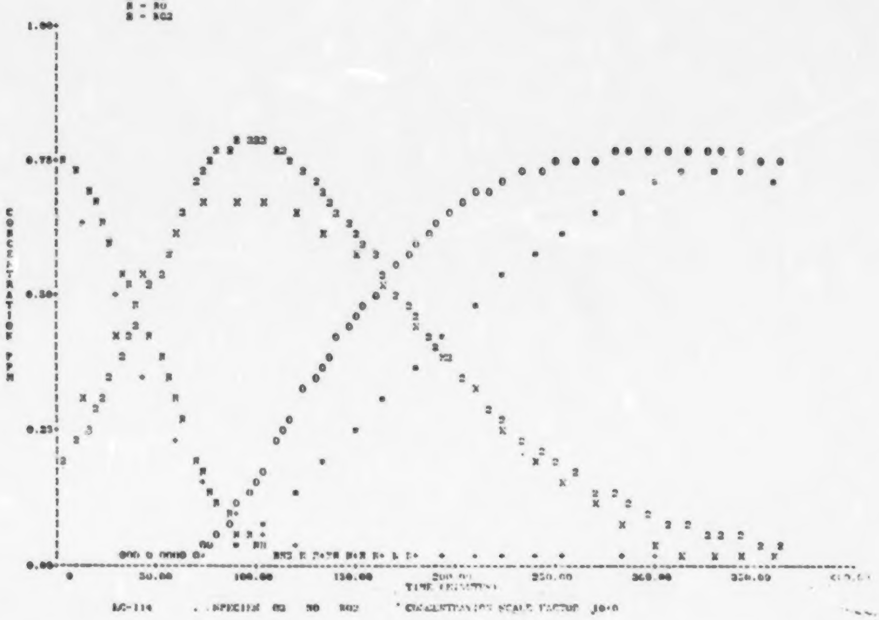

FIGURE III-137

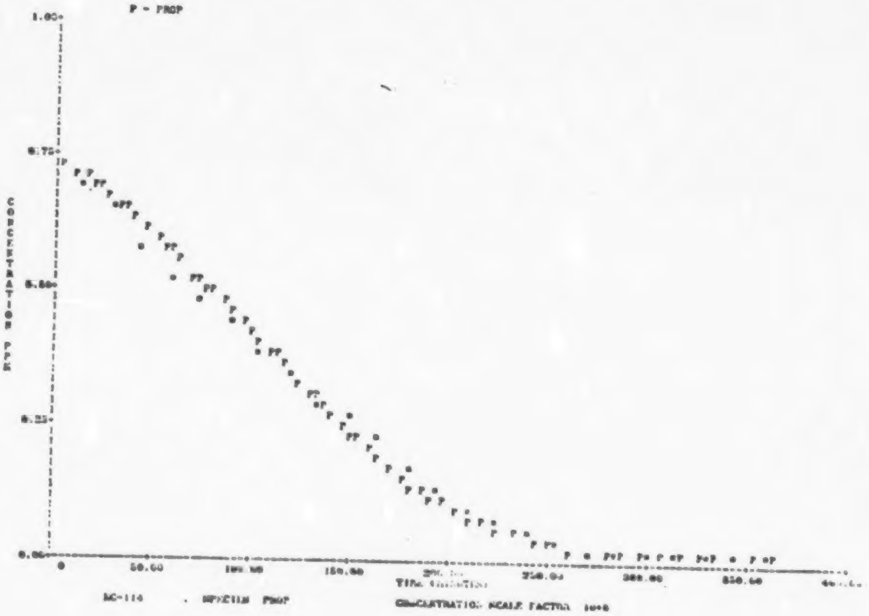

FIGURE III-138

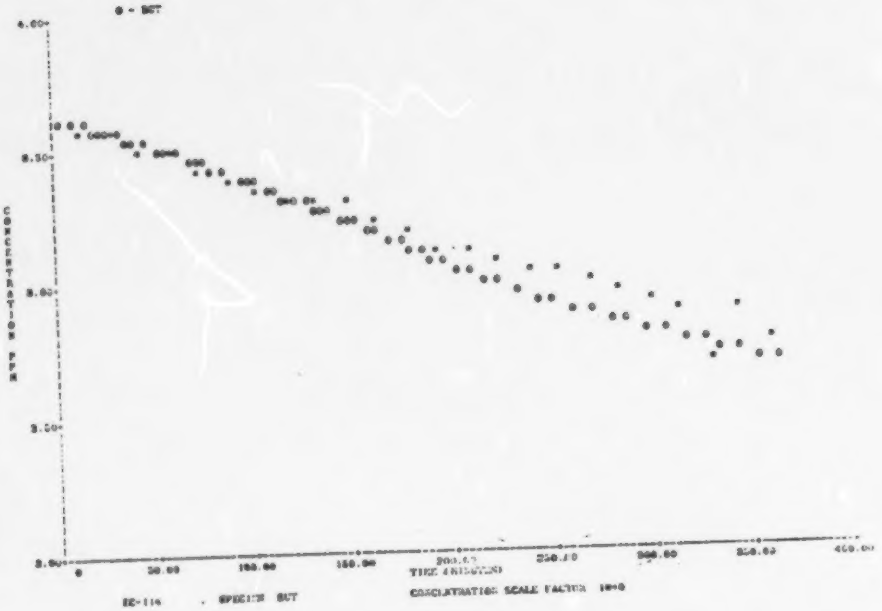

FIGURE III-139

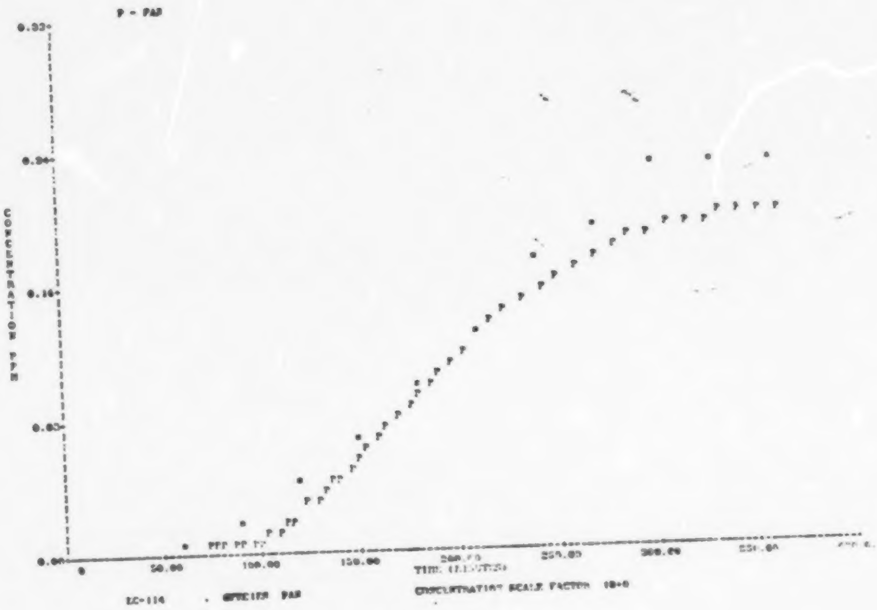

FIGURE III-140

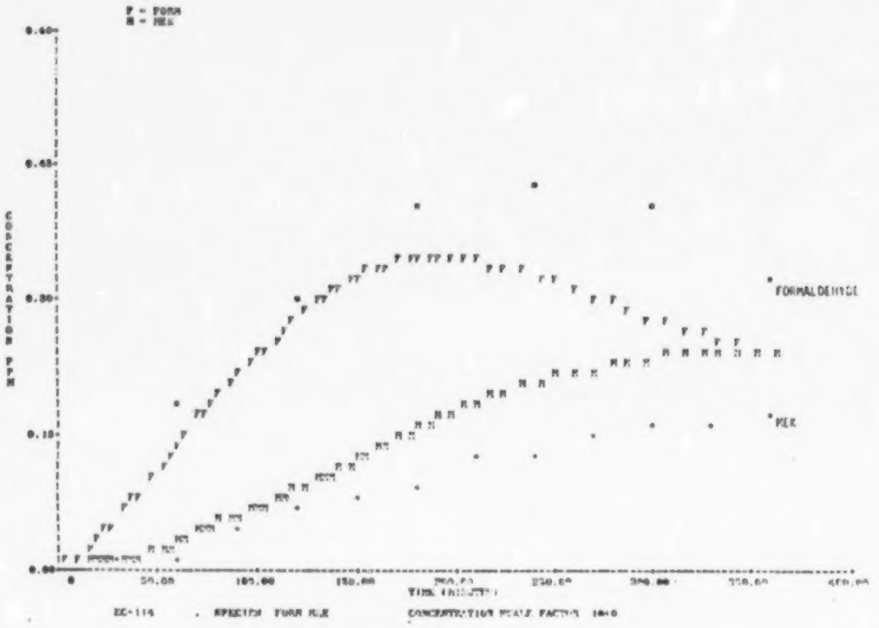

FIGURE III-141

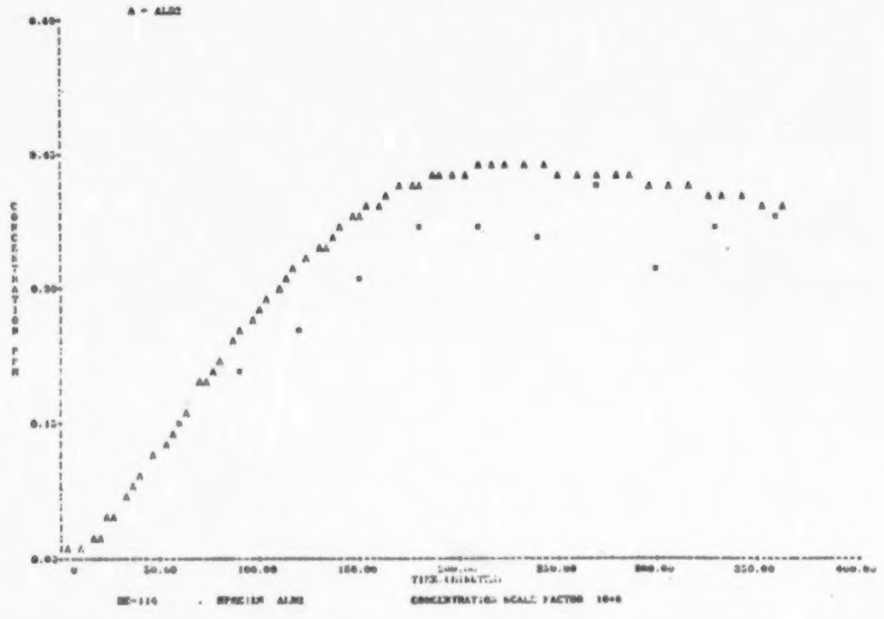

FIGURE III-142

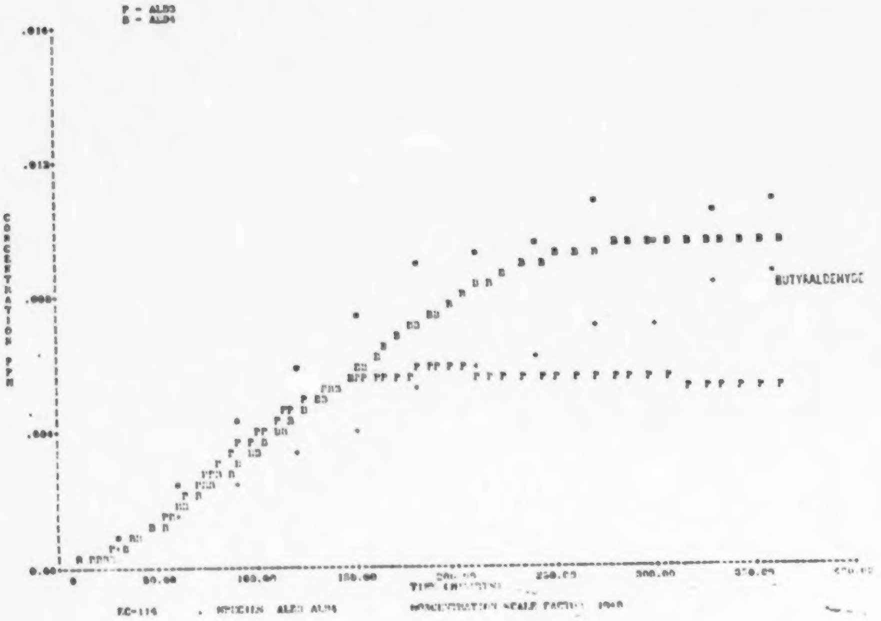

FIGURE III-143

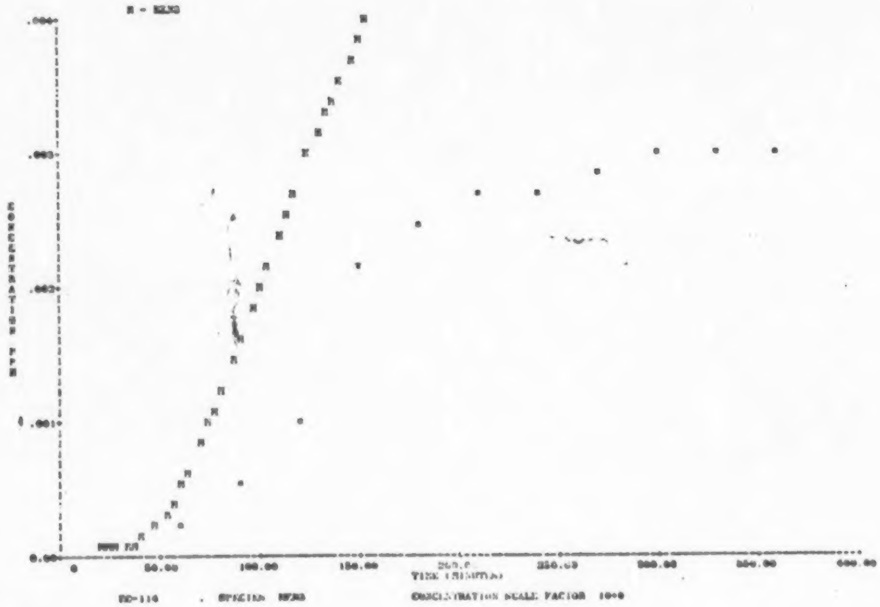

FIGURE III-144

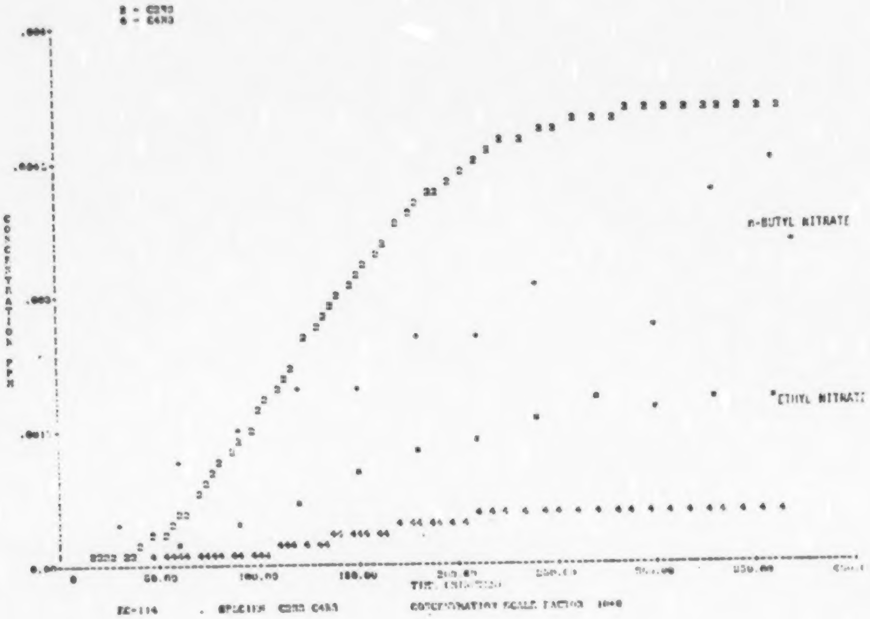

FIGURE III-145

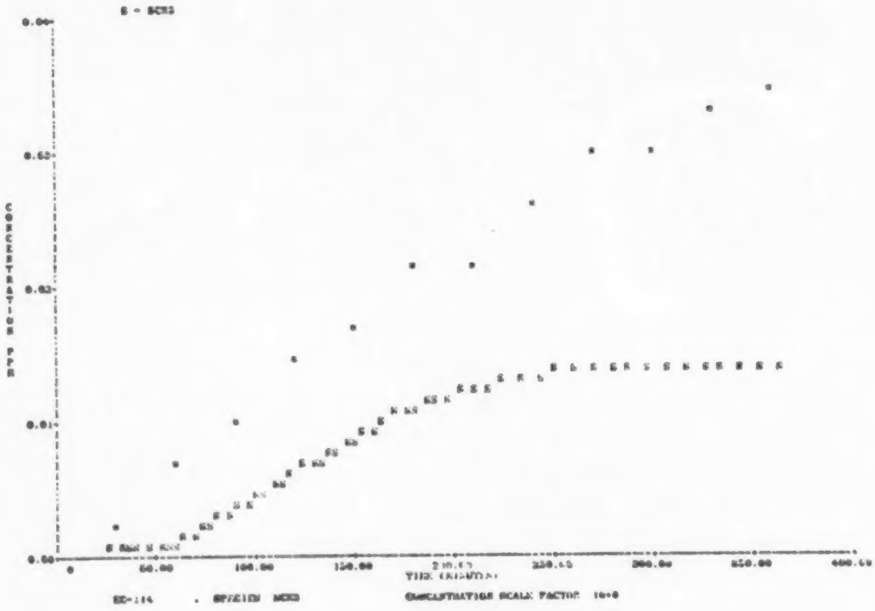

FIGURE III-146

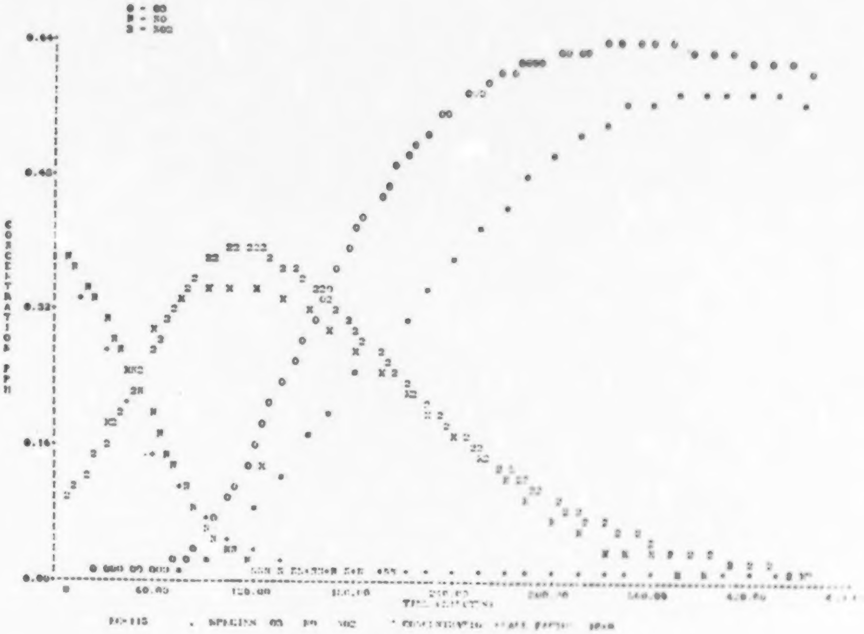

FIGURE III-147

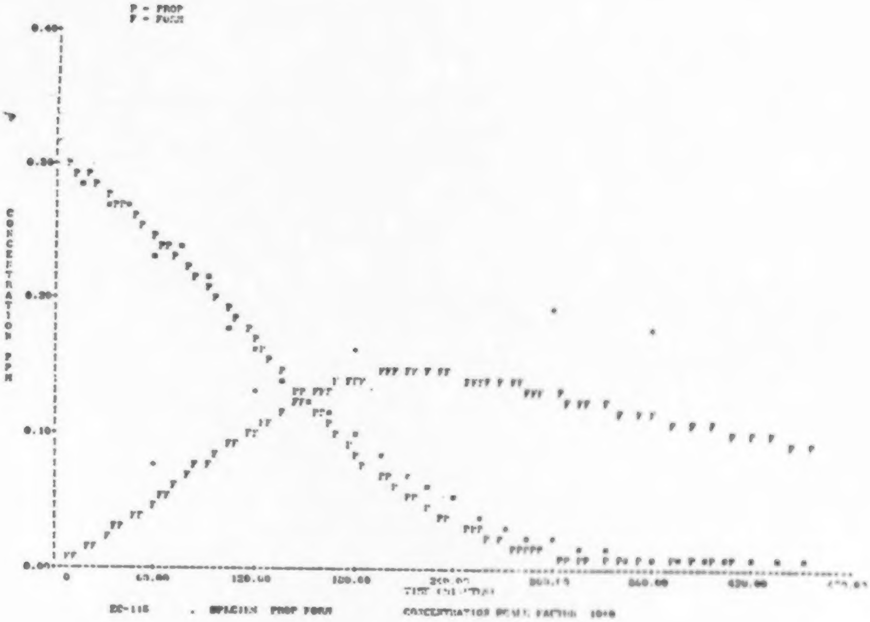

FIGURE III-148

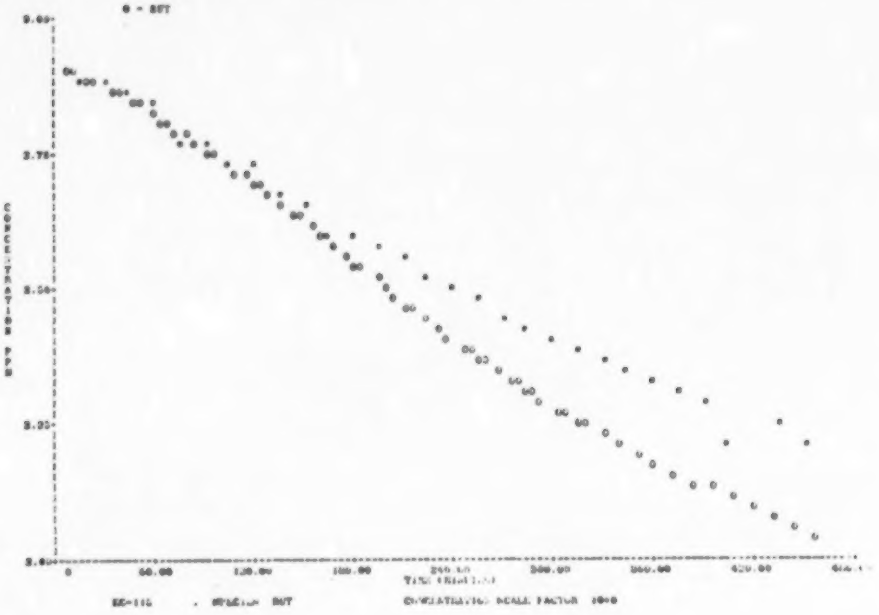

FIGURE III-149

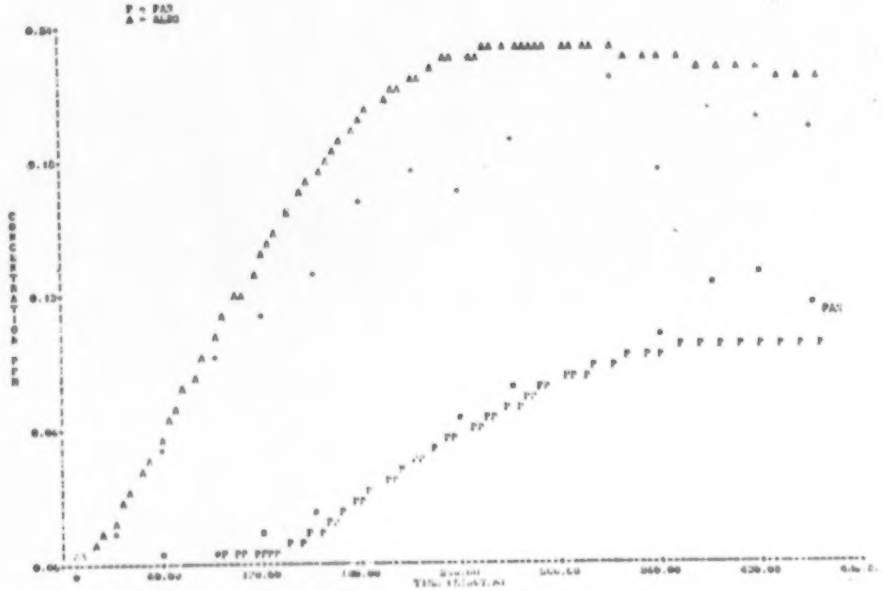

FIGURE III-150

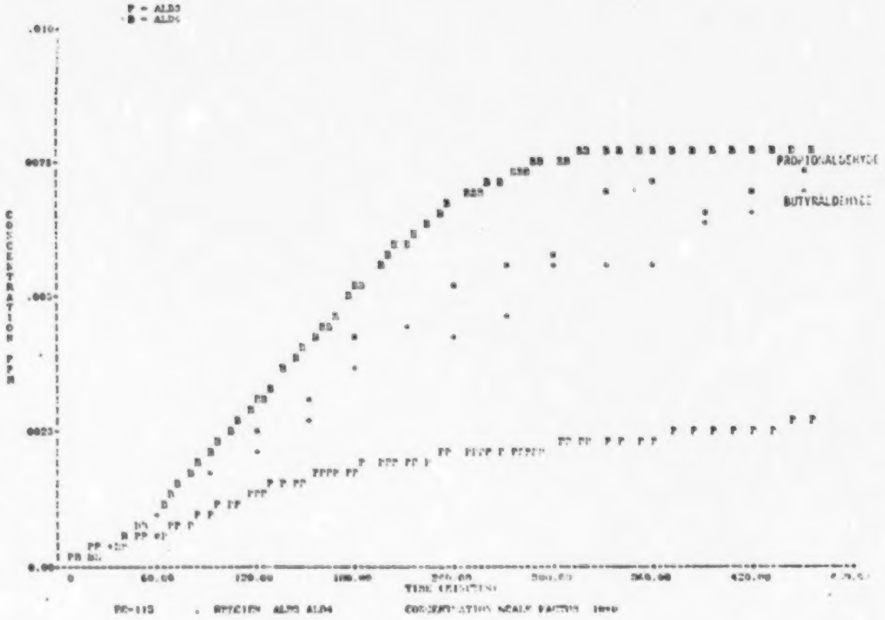

FIGURE III-151

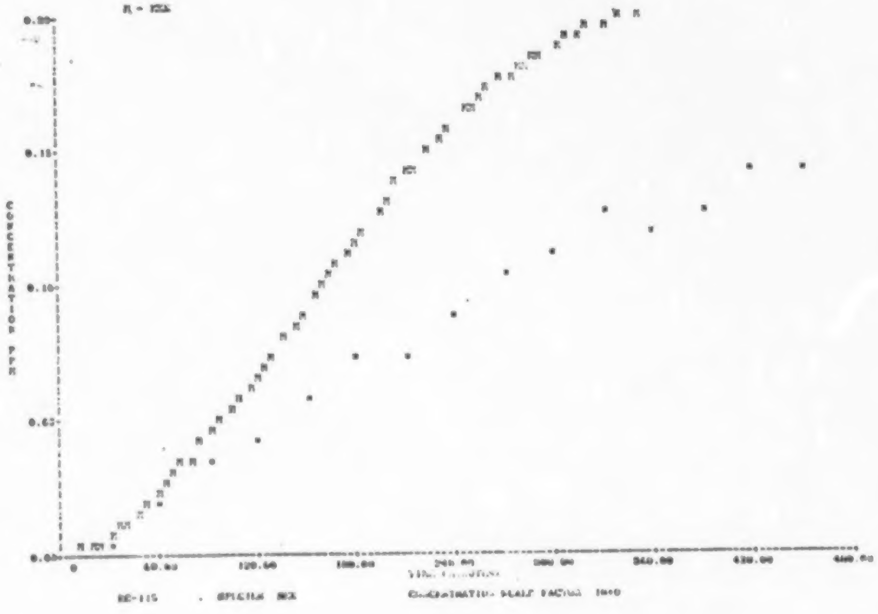

FIGURE III-152

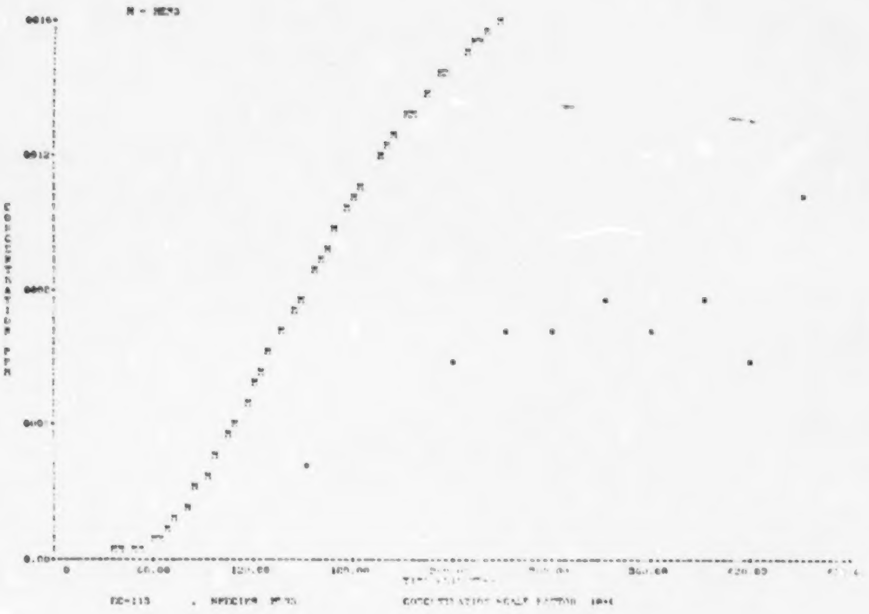

FIGURE III-153

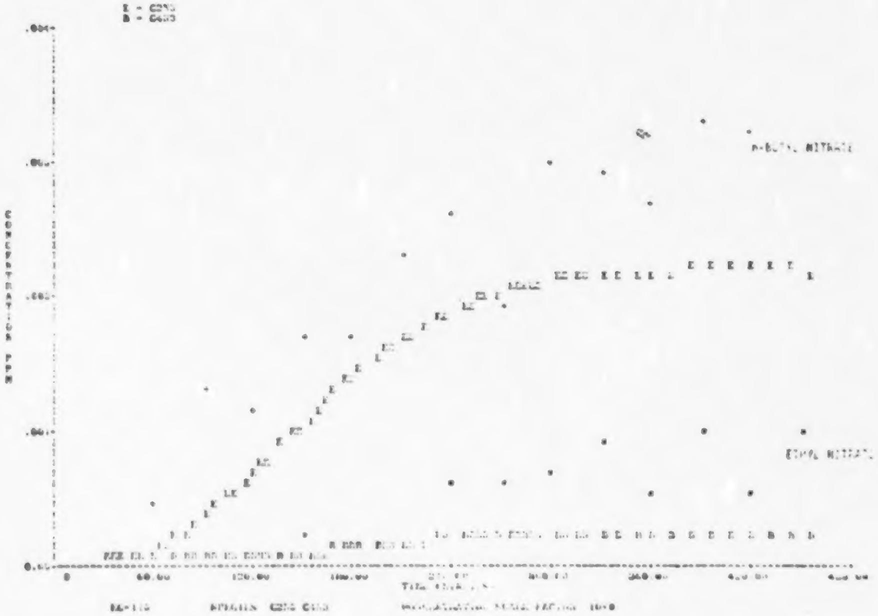

FIGURE III-154

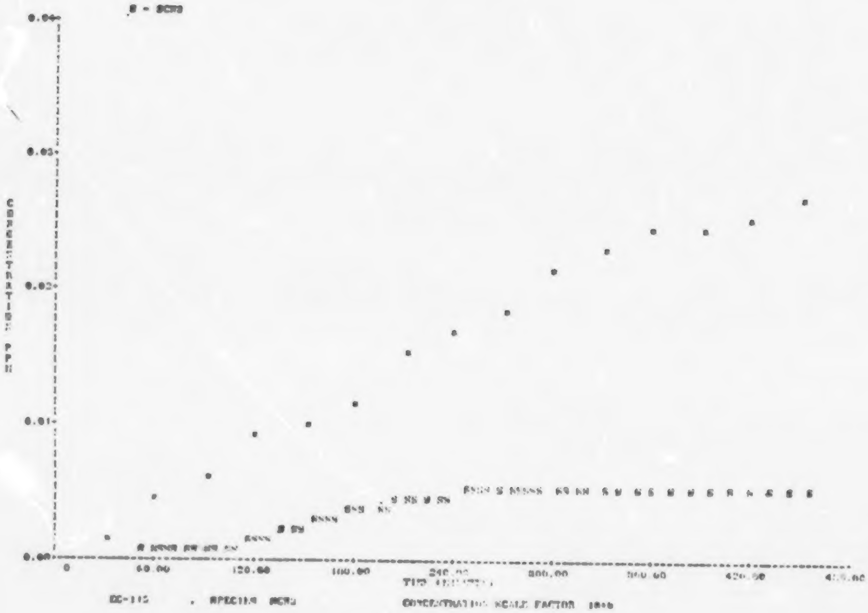

FIGURE III-155

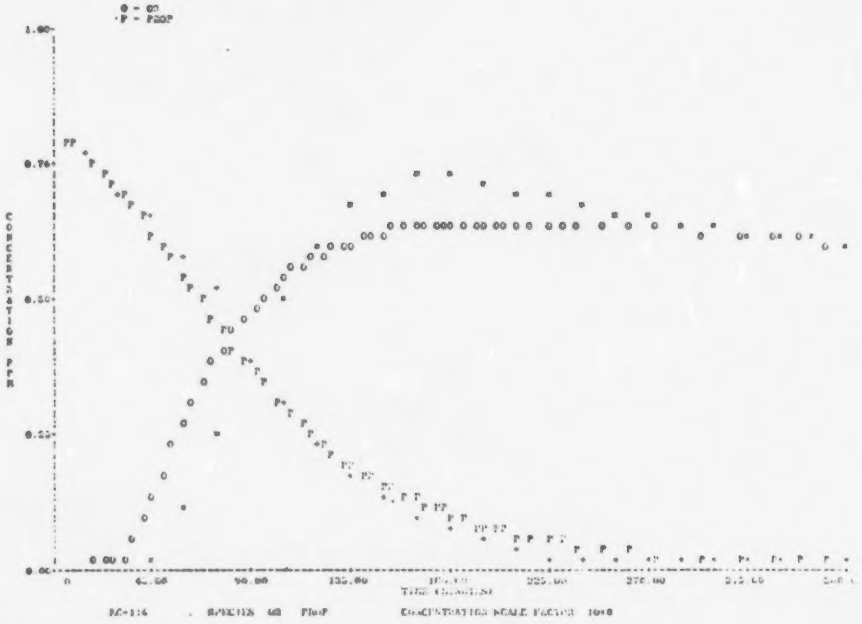

FIGURE III-156

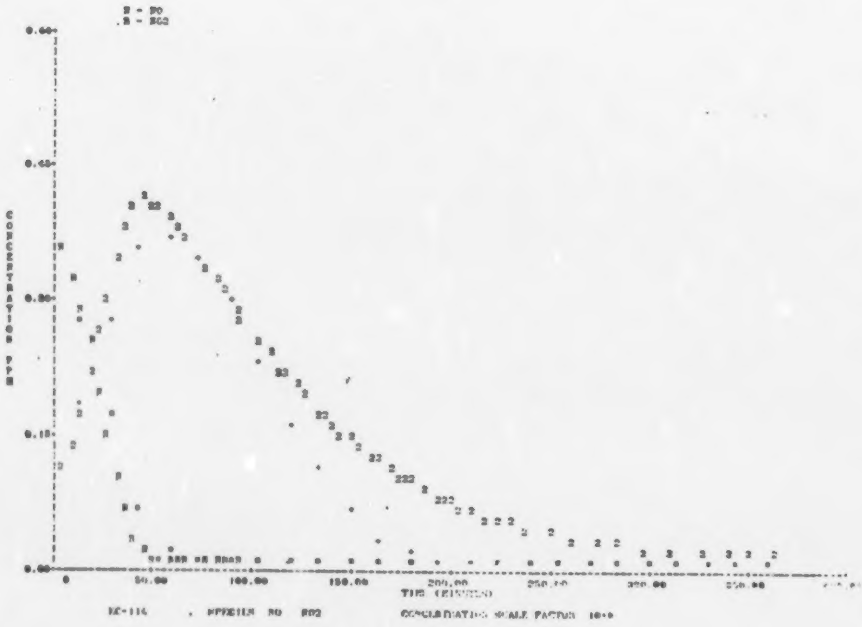

FIGURE III-157

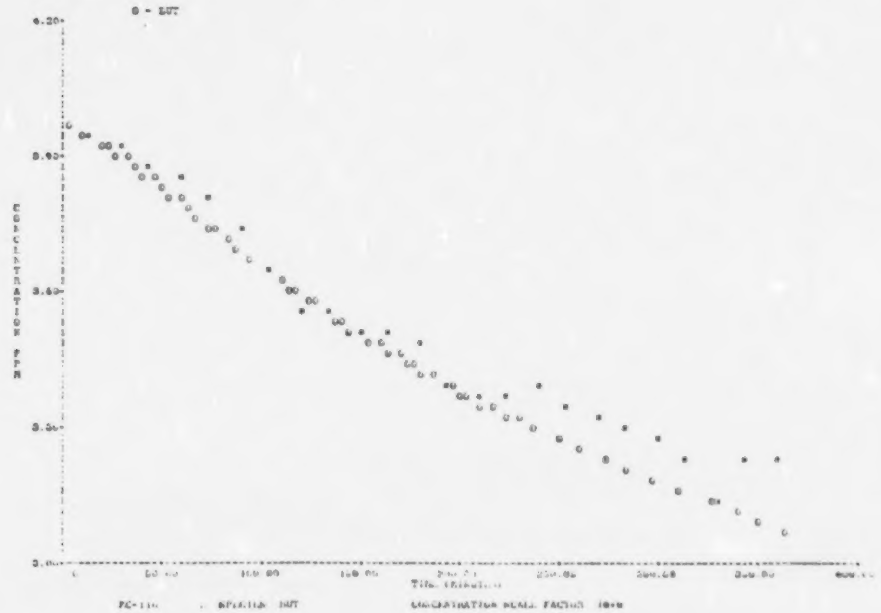

FIGURE III-158

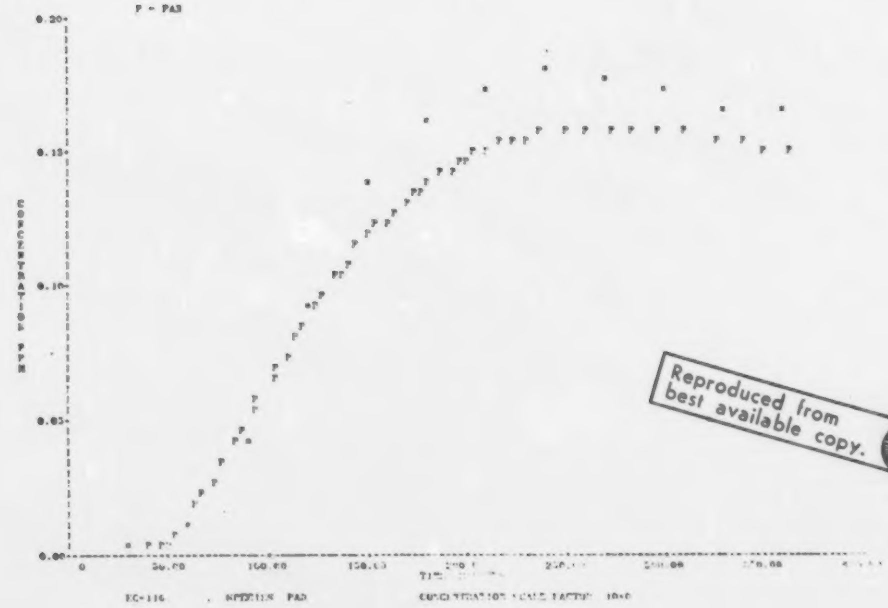

Reproduced from best available copy.

FIGURE III-159

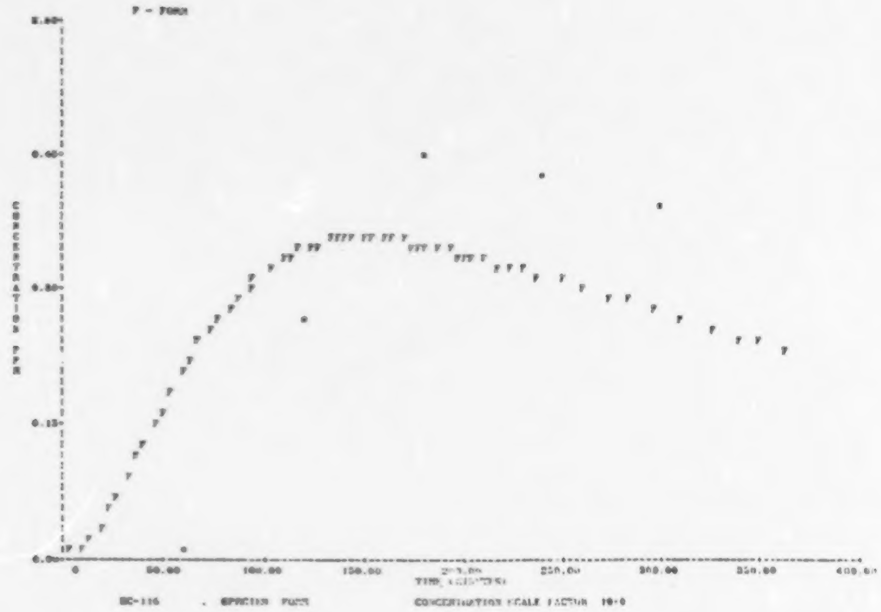

FIGURE III-160

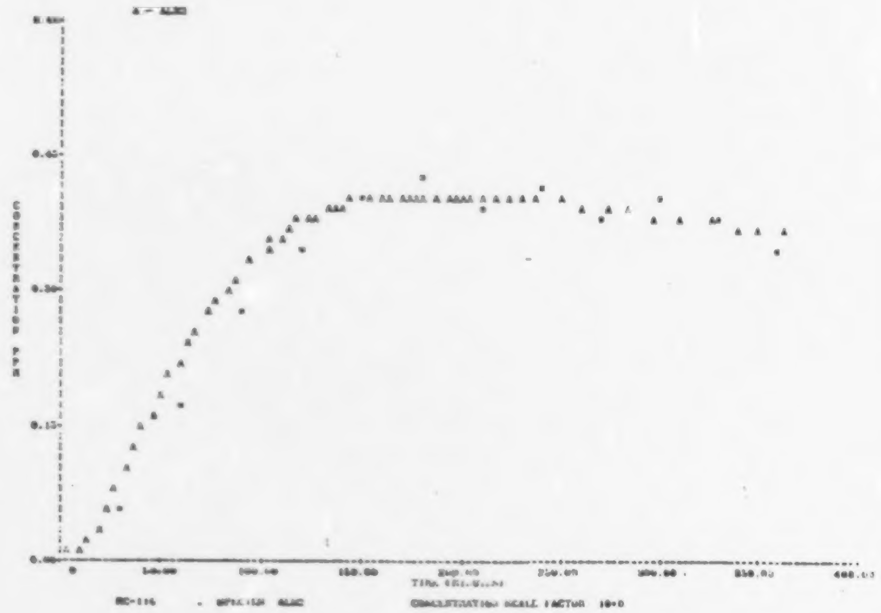

FIGURE III-161

Reproduced from
best available copy.

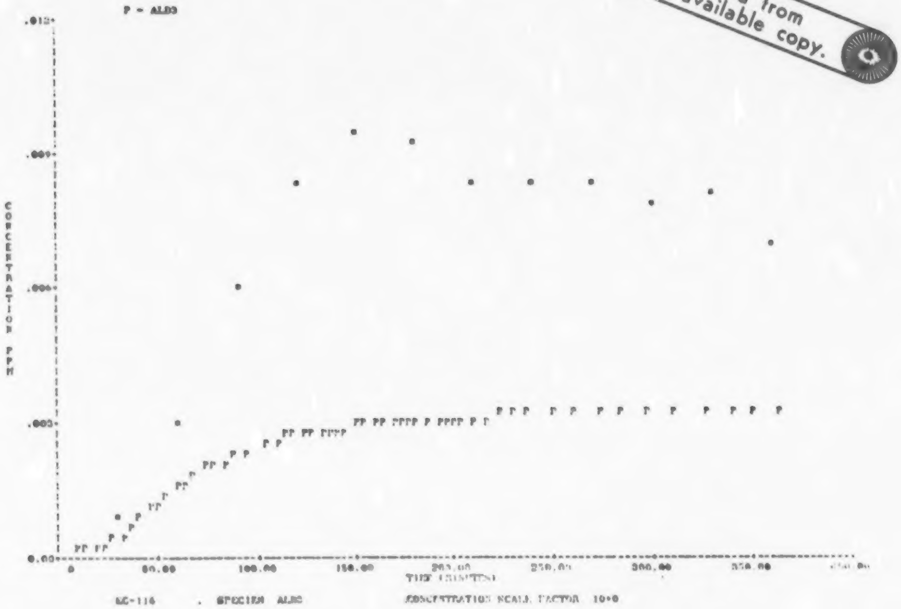

FIGURE III-162

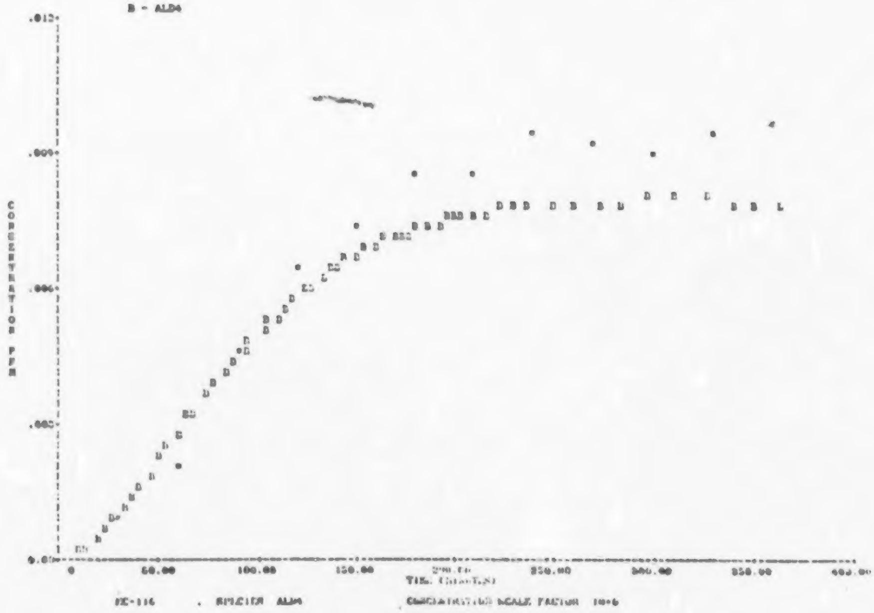

FIGURE III-163

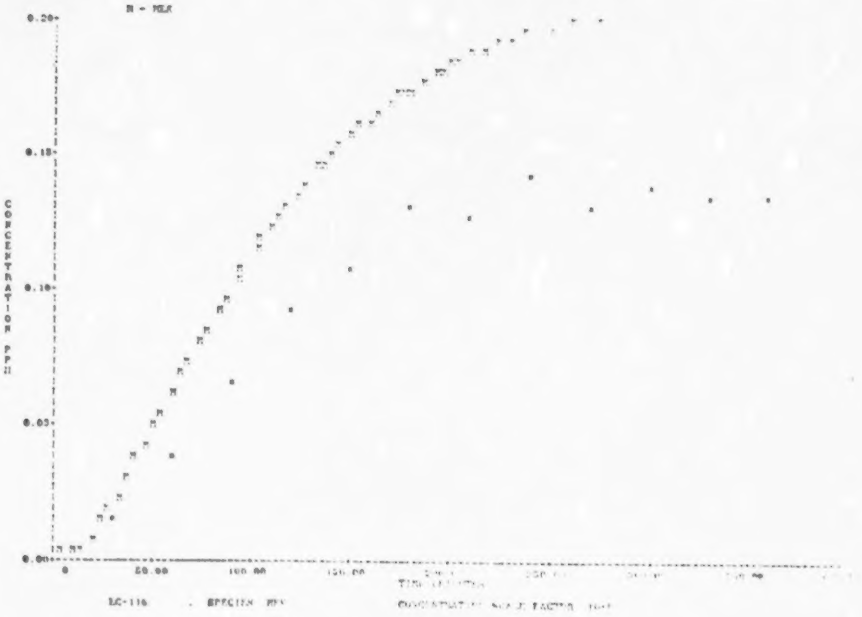

FIGURE III-164

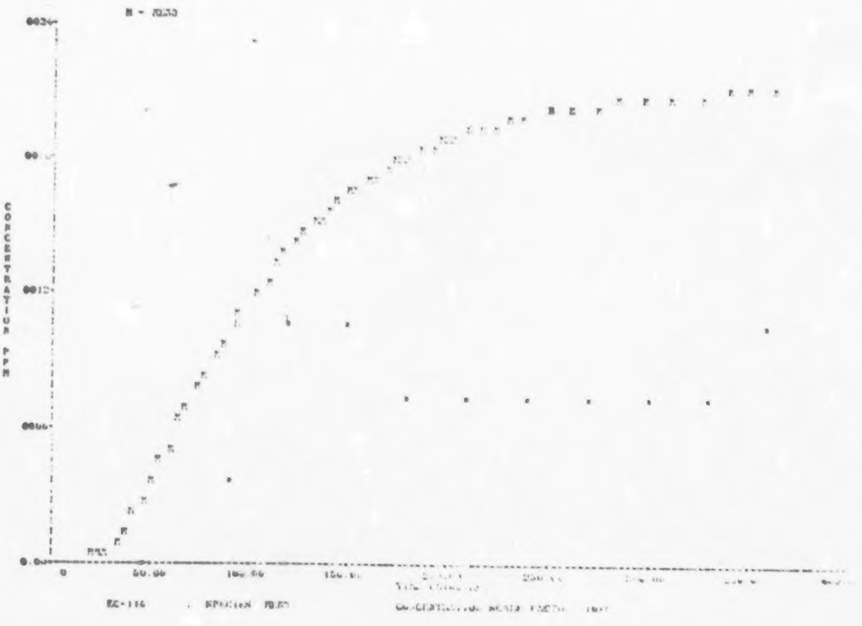

FIGURE III-165

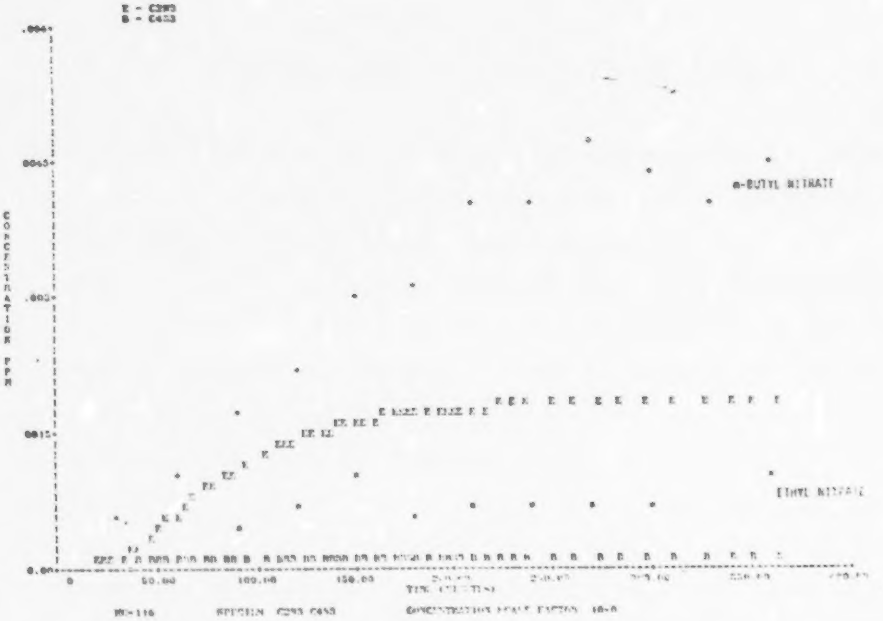

FIGURE III-166

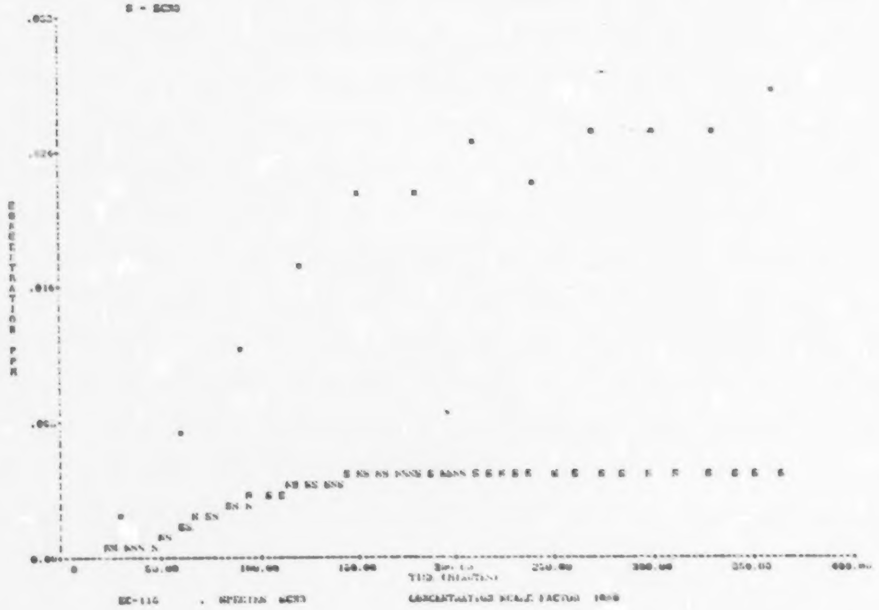

FIGURE III-167

2. Discussion of the Propylene/Butane/NO_x Systems

This set of experiments represents the only test to date of more than one hydrocarbon using the present explicit mechanisms. It also represents the highest levels of ozone formed in all the experiments reported to us by UCR--0.74 ppm ozone was measured in runs EC-114 and EC-116. The combined mechanism for propylene/butane totaled over 120 reactions, and the computer program carried some 54 different species; so this set of simulations was the most severe test of numerical efficiency. A typical simulation required about 11 seconds of computing time on a CDC 7600 using our present version of the CHEMK computer program.

The only reactions added to the sum of the explicit mechanisms for propylene and for butane were the cross peroxy radical/peroxy radical reactions. As expected from the high hydrocarbon concentrations and resulting high ozone concentrations in these experiments, the simulations indicated very high peroxy radical concentrations (e.g., HO_2 was 2.7×10^{-4} ppm at two hours in run EC-116). The peroxy-peroxy radical reactions are more important in this series of experiments than in other series because their rate of reaction depends on the square of their concentration. In the simulation for EC-116, the highest predicted ozone concentration is lower than that observed. Thus, it appears that the rate constant used for these reactions, 4×10^3, is too fast. If a slower rate constant is used or if these reactions are omitted in simulating EC-116, the fits for ozone and NO_2 are improved. EC-113 shows a similar effect. However, we continued to use 4×10^3 $ppm^{-1}min^{-1}$ as the rate constant for all peroxy-peroxy reactions (except peroxyacyl-peroxy) because of the lack of gas-phase data on these reactions. We used a faster rate, 1×10^4 $ppm^{-1}min^{-1}$, for the peroxyacyl/peroxy reaction to improve the fit of PAN data in the propylene system.

Another distinguishing feature of the propylene/butane experiments is the considerable number of additional products measured by UCR. Most of these extra products were nitrates. If one assumes that all nitrate formation rate constants are equal, then the amounts of nitrate products reflect the concentrations of the various alkoxy radicals. UCR found no nitrate for which the explicit mechanism did not contain the corresponding alkoxy radical. In addition, the shapes of the observed and calculated nitrate concentration-time profiles were similar--this provides some validation for the mechanism. At this time it is not clear whether the UCR data or the mechanism or the assumption of equal formation rates causes the differences in absolute concentrations.

Table III-17 presents a comparison between the experimental and simulated maximum one-hour-average ozone concentrations near the observed ozone peak. The combined system shows the most consistent set of percent differences, with an average difference of +5.6 percent and a standard deviation of 7.4 percent.

TABLE III-17. PREDICTED AND MEASURED MAXIMUM ONE-HOUR-AVERAGE OZONE CONCENTRATIONS FOR THE PROPYLENE/BUTANE/NO_x SYSTEMS

	Maximum One-Hour-Average Ozone Concentration (ppm)		
EC Run No.	Measured	Predicted	Percent Difference
97	0.56	0.61	8.9
99	0.55	0.59	7.3
106	0.55	0.62	12.0
113	0.342	0.36	5.3
114	0.73	0.77	5.5
115	0.58	0.64	10.3
116	0.72	0.646	-10.3

The simulations of this set of experiments seem to justify our choice of the ratio of the rate constants for the propylene/OH· and butane/OH· reactions. One apparent exception is run EC-113, where the predicted butane decay rate fits the data but the propylene decay rate does not. Run EC-113 had the lowest initial NO_x concentration of the set of propylene/butane experiments. Perhaps an NO_x species reacting with propylene is giving rise to a fortuitous fit in all runs except EC-113, and the ratio of the rate constants for propylene/OH· and butane/OH· is in error. A confirmation experiment may be necessary at some future time. We also feel that an experiment with minimal hydrocarbon and NO_x, for example, 0.1 ppm NO_x, 0.1 ppm propylene as in EC-17, and 0.2 ppm butane as in EC-43, would be useful and closer to atmospheric concentrations. The most puzzling aspect of these experiments which the mechanism does not follow is the radical concentration of the peroxy-oxyl pool in the later stages of some experiments. This is shown most severely in run EC-115, in which the decay rates of both propylene and butane decrease markedly between two and three hours. It is possible that this decrease was caused by a sudden deterioration of the light source at UCR. (The light source exploded after run EC-116). However, runs EC-99, EC-106, EC-114, and EC-116 show the same effect, yet runs EC-97 and EC-113 do not.

D. TOLUENE/NO_x CHEMISTRY

UCR performed ten experiments on toluene/NO_x chemistry. Our initial analysis for this system is the carbon balance. Table III-18 shows the carbon mass recovery for the toluene/NO_x system. The low mass recovery indicates that many species were not observed by UCR.

The chemistry of the aromatic hydrocarbons in smog is still not known. Finlayson and Pitts (1976) and Calvert and McQuigg (1975) reported that they were not aware of the details of any of the important products of the oxidation of aromatic hydrocarbons, although there have been detailed investigations of the rate constants of the oxidation reactions of certain aromatic hydrocarbons.

TABLE III-18. PERCENT CARBON MASS RECOVERY FOR TOLUENE/NO_x SYSTEMS

Time (minutes)	EC-77	EC-78	EC-79	EC-80	EC-81	EC-82	EC-83	EC-84	EC-85	EC-86
60	3%	11%	8%	4%	1%	2%	4%	*	2%	1%
120	5	19	11	5	5	2	5	0.5%	7	1
180	5	18	8	6	6	3	6	*	7	2
240	5	21	8	7	6	4	6	2	8	3
300	*	18	7	7	5	5	7	2	7	2

---

*Data not available

Davis (1976) recently measured rate constants of reactions involving hydroxyl radicals with aromatic hydrocarbons. Table III-19 presents a list of his results. Hansen et al. (1975) also measured the rate constants for reactions involving hydroxyl radicals with aromatic hydrocarbons. Both Hanson et al. and Davis agreed on a value of the rate constant for the toluene/OH· reaction consistent with measurements by Doyle et al. (1975).

Reaction of toluene with atomic oxygen is slow compared with reactions involving hydroxyl radicals. Recent measurements by Furuyama and Ebara (1975) show good agreement with Atkinson and

Pitts' work (1974) on toluene + $O(^3P)$ reactions. They found that the rate constant for the reaction of toluene with atomic oxygen is approximately 120 $ppm^{-1}min^{-1}$.

TABLE III-19. RATE CONSTANTS FOR REACTIONS INVOLVING HYDROXYL RADICALS AND AROMATIC HYDROCARBONS

Hydrocarbon	Rate Constant ($ppm^{-1}min^{-1}$)	
Benzene	2.9×10^3	
Toluene	1×10^4	
o-Xylene	1.8×10^4	Low Pressure Measurements (200 torr)
m-Xylene	3.04×10^4	
Ethyl benzene	1.2×10^4	
n-Propylbenzene	9.2×10^3	
iso-Propylbenzene	1.1×10^4	

Source: Davis (1976).

There have been several reaction pathways postulated for the reaction of toluene with hydroxyl radicals:

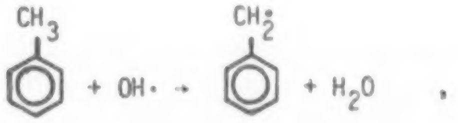

(III-1)

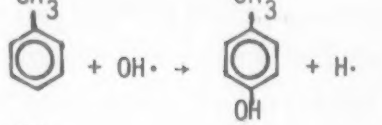

, (III-2)

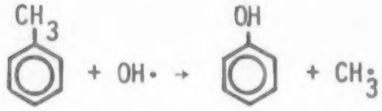

, (III-3)

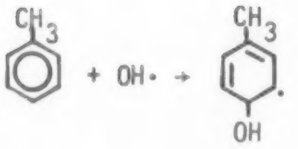

. (III-4)

Reactions (III-2) and (III-4) also have ortho analogs. Finlayson and Pitts (1976) and Davis (1976) believe the main pathway for OH· attack is addition of OH· to the ring rather than abstraction of a hydrogen from the methyl group. This conclusion is based on the similarity of the toluene/OH· rate constant to those of the reactions of hydroxyl radicals and many other alkyl benzenes. We estimated heats of enthalpy for the above four reactions using the techniques of Benson (1968) and data taken from Domalski (1972), with the following results:

$$\Delta H_1^o = -34.4 \text{ kcal mol}^{-1} \quad ,$$

$$\Delta H_2^o = -0.47 \text{ kcal mol}^{-1} \quad ,$$

$$\Delta H_3^o = -10.7 \text{ kcal mol}^{-1} \quad ,$$

$$\Delta H_4^o = -46.6 \text{ kcal mol}^{-1} \quad .$$

The large enthalpy change associated with Reaction (III-4) indicates that formation of a hydroxymethylcyclohexadienyl radical may be the major pathway. The smallest enthalpy change is for formation of cresols. The hydroxymethylcyclohexadienyl radical reacts readily with molecular oxygen. The peroxyhydroxymethylcyclohexacienyl radical may react with NO in three general ways:

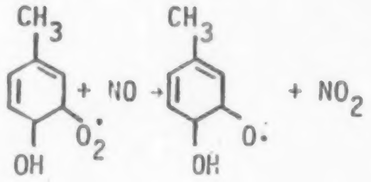

$\Delta H = -37.8$ kcal mol^{-1}, (III-5)

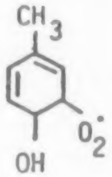

+ NO → Nitrotoluene + Products , (III-6)

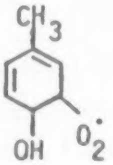

+ NO → Nitrocresol + Products . (III-7)

The products of Reactions (III-6) and (III-7) determine the enthalpy changes for the reactions. Possible products and corresponding enthalpies for Reaction (III-6) are:

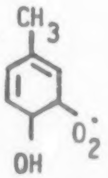

+ NO → Nitrotoluene + 2OH· , $\Delta H^o = 38.9$ kcal mol^{-1} ,

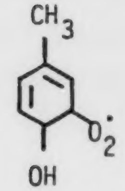

+ NO → Nitrotoluene + H_2O + O , $\Delta H^o = 21.7$ kcal mol^{-1} ,

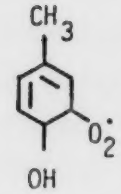

+ NO → Nitrotoluene + HO_2 + H· , $\Delta H^o = 77.1$ kcal mol^{-1} ,

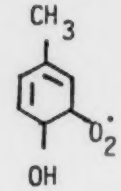

+ NO → Nitrotoluene + H_2O_2 , $\Delta H^o = -12.7$ kcal mol^{-1} .

We see that the formation of H_2O_2 is the most favored reaction thermodynamically. For Reaction (III-7) possible products are:

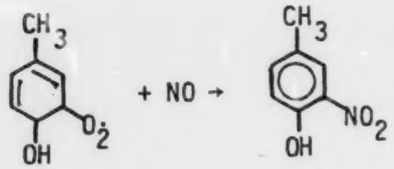

+ NO → + OH· + H· , $\Delta H^o = 38.5$ kcal mol^{-1} ,

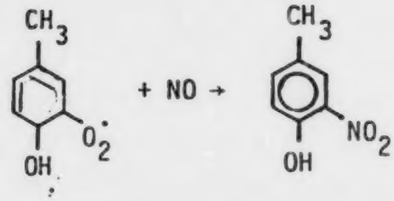

+ NO → + H_2O , $\Delta H^o = -80.9$ kcal mol^{-1} .

The main reaction pathway from this analysis appears to be the formation of nitrocresols. Nitrocresols have been reported by Schwartz (1974), who also reported nitrotoluene and aerosol formation in toluene/NO_x systems.

Akimoto et al. (1976) investigated the products of the toluene-OH· reaction. They found the products in an oxygen-free system were o-cresol, α-nitrotoluene, and m-nitrotoluene. They concluded that the production of α-nitrotoluene, which occurred only in the absence of oxygen, suggests the presence of benzyl radicals and implies hydrogen abstraction from the methyl group of toluene by oxygen atoms. Indeed, in the presence of oxygen benzaldehyde was found instead of α-nitrotoluene. The nitrocresol and nitrotoluene may photolyze as follows:

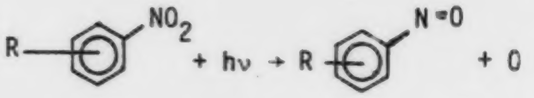

This reaction is discussed by Calvert and Pitts (1966). The aromatic nitroso compound may decompose to form a peroxyphenyl radical. Owing to the lack of detailed product analyses in the UCR data and the lack of supportive experimental evidence, we have not included an explicit toluene kinetic mechanism. We have simulated UCR's toluene runs with the new carbon bond mechanism (see Chapter IV). We hope that in future UCR experiments on aromatic NO_x systems more products will be identified.

E. 1-BUTENE/NO_x CHEMISTRY

Near the end of the work reported in the foregoing sections, we received data on three 1-butene/NO_x experiments done at the UCR evacuable smog chamber. An explicit mechanism for 1-butene systems was constructed by expanding the propylene mechanism. Working on 1-butene experiments has been beneficial to our understanding of the propylene experiments because of their analogous product distributions.

1. Oxidation of 1-Butene

The reaction of 1-butene with atomic oxygen apparently produces the following products:

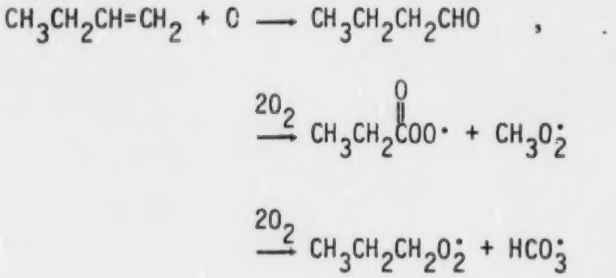

$$CH_3CH_2CH{=}CH_2 + O \longrightarrow CH_3CH_2CH_2CHO \quad ,$$

$$\xrightarrow{2O_2} CH_3CH_2\overset{\overset{O}{\|}}{C}OO\cdot + CH_3O_2^{\cdot} \quad ,$$

$$\xrightarrow{2O_2} CH_3CH_2CH_2O_2^{\cdot} + HCO_3^{\cdot} \quad .$$

The total measured rate constant reported by Japar and Niki (1975) is $5.3 \times 10^3\ ppm^{-1}min^{-1}$. The n-peroxypropyl radical will react with nitric oxide to form n-propyl radicals as in the propylene/NO_x mechanism. The peroxypropionyl radical will react with NO_2 to produce peroxypropionyl nitrate (PPN). The path to butyraldehyde is included in analogy to the propylene system and because in two similar experiments (EC-123 and EC-124), the observed initial rate of butyraldehyde production increased when the initial nitrogen dioxide concentration was increased--the latter, of course, increases the initial oxygen atom concentration. The initial rates of 1-butene disappearance (due primarily to attack by OH·) in the two experiments were similar, so the hydroxyl radical did not seem to play a role in butyraldehyde production.

Reaction of hydroxyl radicals with 1-butene is assumed to lead to the production of propionaldehyde, formaldehyde, and a hydroperoxy radical ($HO_2^{\cdot}$). The mechanism for hydroxyl addition is:

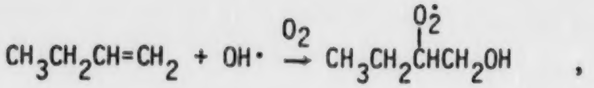

$$CH_3CH_2CH{=}CH_2 + OH\cdot \xrightarrow{O_2} CH_3CH_2\overset{O_2\cdot}{C}HCH_2OH \quad ,$$

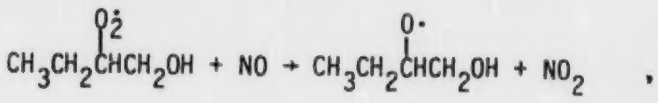

$$CH_3CH_2\overset{O_2\cdot}{C}HCH_2OH + NO \rightarrow CH_3CH_2\overset{O\cdot}{C}HCH_2OH + NO_2 \quad ,$$

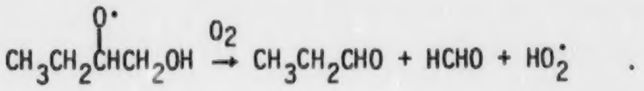

$$CH_3CH_2\overset{O\cdot}{C}HCH_2OH \xrightarrow{O_2} CH_3CH_2CHO + HCHO + HO_2\cdot \quad .$$

1-butene can also react with ozone:

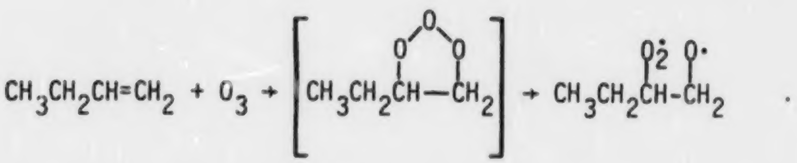

The biradical will presumably decompose to form the peroxypropionyl radical, formaldehyde, and a hydroxyl radical. As discussed earlier, Niki et al. (1976b) found that the alkyl ozonide is also a stable product of the ozone-olefin reaction:

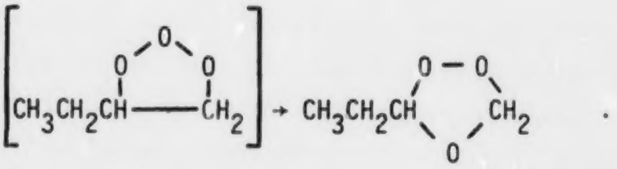

As in the propylene system, we have not fully investigated the reactions of the ozonide or its effects on the kinetic mechanism.

2. Simulation Results

Table III-20 presents the kinetic mechanism for 1-butene/NO_x chemistry. This mechanism is similar to the propylene/NO_x kinetic mechanism except for the chemistry of the four carbon atoms. Figure III-168 shows the factorial block for this system, Table III-21a shows the initial conditions for the computer simulations, and Table III-21b shows the photolysis rate constants. We also performed a carbon mass recovery analysis of the 1-butene/NO_x system, the results of which are presented in Table III-22. Analogous to the propylene/NO_x carbon mass recovery, there is only a 60 to 80 percent carbon recovery for the three 1-butene runs.

Initial computer simulations of the three UCR runs (EC-122, 123, 124) are shown in Figures III-169 through III-180.

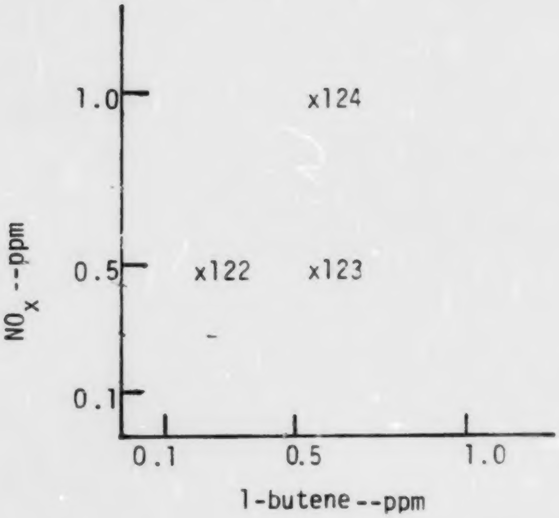

FIGURE III-168. FACTORIAL BLOCK FOR 1-BUTENE/NO_x SYSTEM

TABLE III-20. THE 1-BUTENE/NO_x MECHANISM

Reaction	Rate Constant (ppm^{-1} min^{-1})
$NO_2 + h\nu \rightarrow NO + O(^3P)$	Experimental*
$O(^3P) + O_2 + M \rightarrow O_3 + M$	2.08×10^{-5} †
$O(^3P) + NO_2 \rightarrow NO + O_2$	1.34×10^{4}
$O_3 + NO \rightarrow NO_2 + O_2$	25.2
$O(^1D) + M \rightarrow O + M$	8.6×10^{4}
$O(^1D) + H_2O \rightarrow 2OH\cdot$	5.1×10^{5}
$O_3 + OH\cdot \rightarrow HO_2\cdot + O_2$	87.0
$O_3 + HO_2\cdot \rightarrow OH\cdot + 2O_2$	1.2
$O_3 + NO_2 \rightarrow NO_3 + O_2$	5×10^{-2}
$O_3 + h\nu \rightarrow O(^1D) + O_2$	Experimental*
$O_3 + h\nu \rightarrow O(^3P) + O_2$	Experimental*
$O_3 \rightarrow$ wall	1×10^{-3}
$NO_3 + NO \rightarrow 2NO_2$	1.3×10^{4}
$NO_3 + NO_2 \rightarrow N_2O_5$	5.6×10^{3}
$N_2O_5 + H_2O \rightarrow 2HNO_3$	5×10^{-6}
$N_2O_5(+ M) \rightarrow NO_3 + NO_2(+ M)$	24.0 *
$NO + NO_2 + H_2O \rightarrow 2HNO_2$	2.2×10^{-9}

TABLE III-20 (Continued)

Reaction	Rate Constant (ppm^{-1} min^{-1})
$2HNO_2 \rightarrow NO + NO_2 + H_2O$	1.3×10^{-3}
$HNO_2 + h\nu \rightarrow OH\cdot + NO$	Experimental*
$NO_2 + OH\cdot(+ M) \rightarrow HNO_3(+ M)$	9.2×10^{3}
$NO + OH\cdot \rightarrow HNO_2$	9×10^{3}
$HO_2^{\cdot} + NO \rightarrow OH\cdot + NO_2$	2×10^{3}
$HO_2^{\cdot} + NO_2 \rightarrow HNO_2 + O_2$	20
$H_2O_2 + h\nu \rightarrow 2OH\cdot$	Experimental*
$CH_3CH_2CH{=}CH_2 + O \rightarrow CH_3CH_2CH_2CHO$	1.77×10^{3}
$CH_3CH_2CH{=}CH_2 + O \xrightarrow{2O_2} CH_3O_2^{\cdot} + CH_3CH_2C(O)O_2^{\cdot}$	1.77×10^{3}
$CH_2CH_2CH{=}CH_2 + O \xrightarrow{2O_2} CH_3CH_2CH_2O_2^{\cdot} + HC(O)O_2^{\cdot}$	1.77×10^{3}
$CH_3CH_2CH{=}CH_2 + OH\cdot \xrightarrow{O_2} CH_3CH_2CH(O_2^{\cdot})CH_2OH$	4.8×10^{4}
$CH_3CH_2CH{=}CH_2 + NO_3 \rightarrow NO_2 + \text{Products}$	12.0
$CH_3CH_2CH{=}CH_2 + O_3 \xrightarrow{O_2} H_2CO + CH_3CH_2C(O)O_2^{\cdot} + OH\cdot$	5×10^{-3}
$CH_3CH_2CH{=}CH_2 + O_3 \rightarrow CH_3CH_2CHO + HC(O)O_2^{\cdot} + OH\cdot$	5×10^{-3}
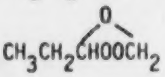 $CH_3CH_2CH{=}CH_2 + O_3 \rightarrow CH_3CH_2\overset{O}{CHOOCH_2}$	5×10^{-3}
$CH_3CH_2CH_2C(O)O_2^{\cdot} + NO \xrightarrow{O_2} NO_2 + CH_3CH_2CH_2O_2^{\cdot} + CO_2$	2×10^{3}
$CH_3CH_2C(O)O_2^{\cdot} + NO \xrightarrow{O_2} NO_2 + CH_3CH_2O_2^{\cdot} + CO_2$	2×10^{3}
$CH_3C(O)O_2^{\cdot} + NO \xrightarrow{O_2} NO_2 + CH_3O_2^{\cdot} + CO_2$	2×10^{3}

TABLE III-20 (Continued)

Reaction	Rate Constant (ppm^{-1} min^{-1})
$HC(O)O_2^{\cdot} + NO \xrightarrow{O_2} NO_2 + HO_2^{\cdot} + CO_2$	2×10^3
$CH_3CH(O_2^{\cdot})CH_2OH + NO \rightarrow NO_2 + CH_3CH(O\cdot)CH_2OH$	2×10^3
$CH_3CH_2CH(O_2^{\cdot})CH_2OH + NO \rightarrow NO_2 + CH_3CH_2CH(O\cdot)CH_2OH$	2×10^3
$CH_3CH_2O_2^{\cdot} + NO \rightarrow NO_2 + CH_3CH_2O\cdot$	2×10^3
$CH_3O_2^{\cdot} + NO \rightarrow NO_2 + CH_3O\cdot$	2×10^3
$CH_3CH_2CH(O\cdot)CH_2OH \xrightarrow{O_2} CH_3CH_2CHO + H_2CO + HO_2^{\cdot}$	3×10^5 *
$CH_3CH_2CH_2O\cdot + O_2 \rightarrow CH_3CH_2CHO + HO_2^{\cdot}$	0.95
$CH_3CH_2O\cdot + O_2 \rightarrow CH_3CHO + HO_2^{\cdot}$	0.95
$CH_3O\cdot + O_2 \rightarrow H_2CO + HO_2^{\cdot}$	0.95
$H_2CO + h\nu \xrightarrow{2O_2} HO_2^{\cdot} + HC(O)O_2^{\cdot}$	Experimental *
$H_2CO + h\nu \rightarrow H_2 + CO$	Experimental *
$CH_3CHO + h\nu \xrightarrow{2O_2} CH_3O_2^{\cdot} + HC(O)O_2$	Experimental *
$CH_3CH_2CHO + h\nu \xrightarrow{2O_2} CH_3CH_2O_2^{\cdot} + HC(O)O_2^{\cdot}$	Experimental *
$CH_3CH_2CH_2CHO + h\nu \xrightarrow{2O_2} CH_3CH_2CH_2O_2^{\cdot} + HC(O)O_2^{\cdot}$	Experimental *
$CH_3CH_2CH_2CHO + h\nu \rightarrow CH_3CHO + C_2H_4$	Experimental *
$H_2CO + OH\cdot \xrightarrow{O_2} HC(O)O_2^{\cdot} + H_2O$	1×10^4
$CH_3CHO + OH\cdot \xrightarrow{O_2} CH_3C(O)O_2^{\cdot} + H_2O$	1×10^4

TABLE III-20 (Continued)

Reaction	Rate Constant (ppm^{-1} min^{-1})
$CH_3CH_2CHO + OH\cdot \xrightarrow{O_2} CH_3CH_2C(O)O_2^{\cdot} + H_2O$	1×10^4
$CH_3CH_2CH_2CHO + OH\cdot \xrightarrow{O_2} CH_3CH_2CH_2C(O)O_2^{\cdot} + H_2^{\cdot}$	1×10^4
$CH_3CH_2CH_2C(O)O_2^{\cdot} + HO_2^{\cdot} \rightarrow CH_3CH_2CH_2C(O)OOH + O_2$	1×10^4
$CH_3CH_2C(O)O_2^{\cdot} + HO_2^{\cdot} \rightarrow CH_3CH_2C(O)OOH + O_2$	1×10^4
$CH_3C(O)O_2^{\cdot} + HO_2^{\cdot} \rightarrow CH_3C(O)OOH + O_2$	1×10^4
$HC(O)O_2^{\cdot} + HO_2^{\cdot} \rightarrow HC(O)OOH + O_2$	1×10^4
$CH_3CH_2CH(O_2^{\cdot})CH_2OH + HO_2^{\cdot} + HO_2^{\cdot} \rightarrow CH_3CH_2CH(OOH)CH_2OH$	4×10^3
$CH_3CH_2CH_2O_2^{\cdot} + HO_2 \rightarrow CH_3CH_2CH_2OOH + O_2$	4×10^3
$CH_3CH_2O_2^{\cdot} + HO_2^{\cdot} \rightarrow CH_3CH_2OOH + O_2$	4×10^3
$CH_3O_2^{\cdot} + HO_2^{\cdot} \rightarrow CH_3OOH + O_2$	4×10^3
$HO_2^{\cdot} + HO_2^{\cdot} \rightarrow H_2O_2 + O_2$	4×10^3
$CH_3CH_2CH_2C(O)O_2^{\cdot} + NO_2 \rightarrow CH_3CH_2CH_2C(O)O_2NO_2$	4×10^2
$CH_3CH_2C(O)O_2^{\cdot} + NO_2 \rightarrow CH_3CH_2C(O)O_2NO_2$	4×10^2
$CH_3C(O)O_2^{\cdot} + NO_2 \rightarrow CH_3C(O)O_2NO_2$	4×10^2
$CH_3C(O)O_2NO_2 \rightarrow NO_2 + CH_3C(O)O_2^{\cdot}$	1.7×10^{-2} *
$CH_3CH_2C(O)O_2NO_2 \rightarrow NO_2 + CH_3CH_2C(O)O_2^{\cdot}$	2×10^{-2} *

TABLE III-20 (Concluded)

Reaction	Rate Constant (ppm^{-1} min^{-1})
$CH_3CH_2CH_2C(O)O_2NO_2 \rightarrow CH_3CH_2CH_2C(O)O_2^{\cdot} + NO_2$	2.5×10^{-2} *
$CH_3O\cdot + NO_2 \rightarrow CH_3ONO_2$	2×10^4
$CH_3O\cdot + NO_2 \rightarrow H_2CO + HNO_2$	2.2×10^3
$CH_3CH_2O\cdot + NO_2 \rightarrow CH_3CH_2ONO_2$	2.0×10^4
$CH_3CH_2O\cdot + NO_2 \rightarrow CH_3CHO + HNO_2$	2.2×10^3
$CH_3CH_2CH_2O\cdot + NO_2 \rightarrow CH_3CH_2CH_2ONO_2$	2×10^4
$CH_3CH_2CH_2O\cdot + NO_2 \rightarrow CH_3CH_2CHO + HNO_2$	2.2×10^3
$CO + OH\cdot \xrightarrow{O_2} HO_2 + CO_2$	2.06×10^2
$CH_3CH_2CH(O_2^{\cdot})CH_2OH + CH_3CH_2CH(O_2^{\cdot})CH_2OH \rightarrow 2CH_3CH_2CH(O\cdot)CH_2OH + O_2$	4×10^3

---

* Units of min^{-1}.

† Units of $ppm^{-2}min^{-1}$

TABLE III-21a. INITIAL CONDITIONS FOR SIMULATIONS OF 1-BUTENE/NO_x SYSTEMS

EC Run Number	NO	NO_2	1-Butene	HNO_2	k_1
122	0.398	0.103	0.217	0.01	0.29
123	0.401	0.106	0.404	0.01	0.28
124	0.608	0.385	0.424	0.01	0.27

TABLE III-21b. PHOTOLYSIS RATE CONSTANTS FOR SIMULATIONS OF 1-BUTENE/NO_x SYSTEMS

(10^4 min^{-1})

EC Run Number	$O_3 \rightarrow O^1D$	$O_3 \rightarrow O^3P$	$HNO_2 \rightarrow$	$H_2O_2 \rightarrow$	$HCHO \rightarrow H\cdot + HCO\cdot$	$HCHO \rightarrow CO + H_2$	$CH_3CHO \rightarrow$	$CH_3CH_2CHO \rightarrow$	$CH_3CH_2CH_2CHO \rightarrow$
122 123	38.0	93.0	540	6.7	7.3	20	5.0	5.5	9.4
124	34.0	82.0	500	6.2	6.5	18	4.5	5.0	7.7

TABLE III-22. PERCENT CARBON MASS RECOVERY FOR 1-BUTENE/NO_x SYSTEMS

Time (minutes)	EC-122	EC-123	EC-124
60	76	80	85
120	70	71	81
180	63	69	82
240	63	64	81
300	61	60	78
360	*	*	78
480	*	*	75
540	*	*	74
600	*	*	73

---

* Data not available.

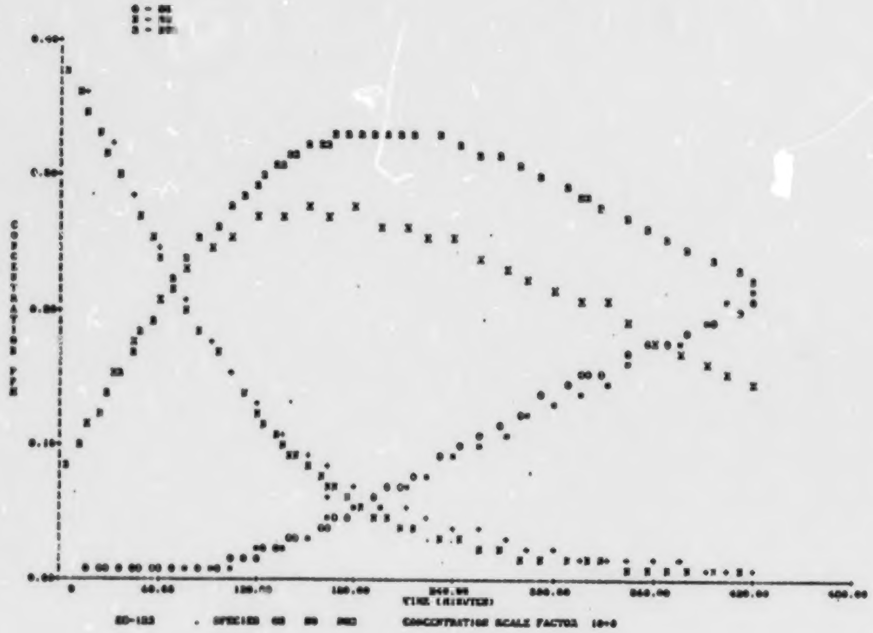

FIGURE III-169

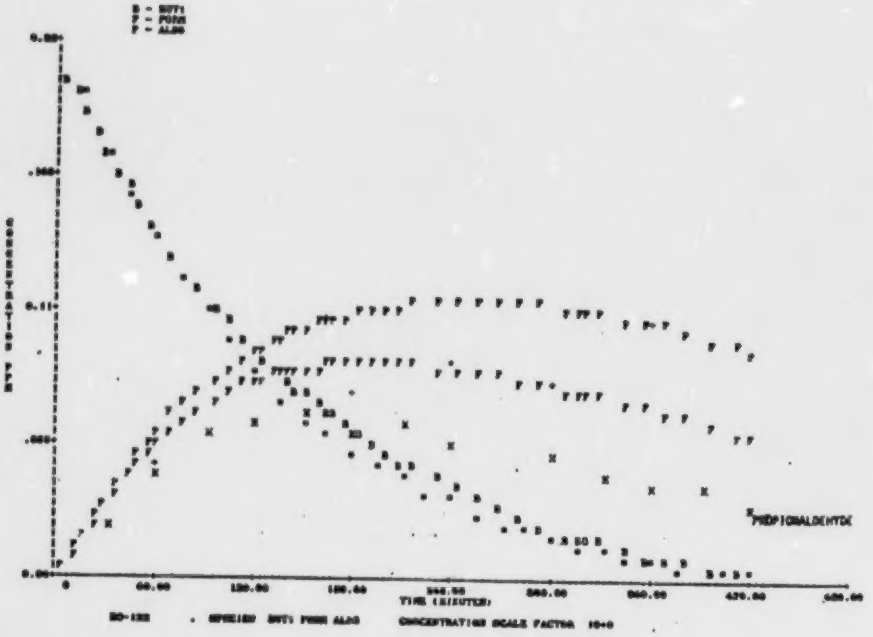

FIGURE III-70

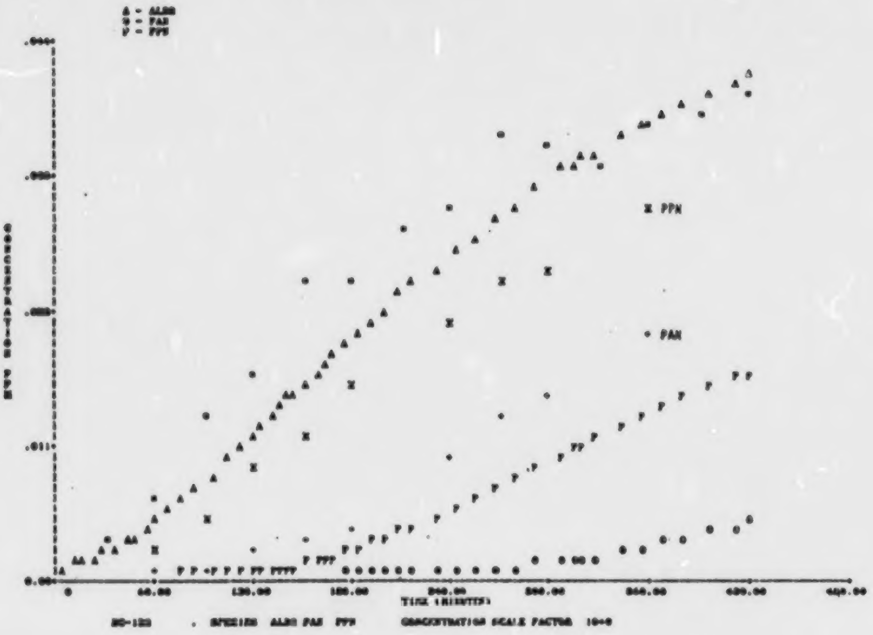

FIGURE III-171

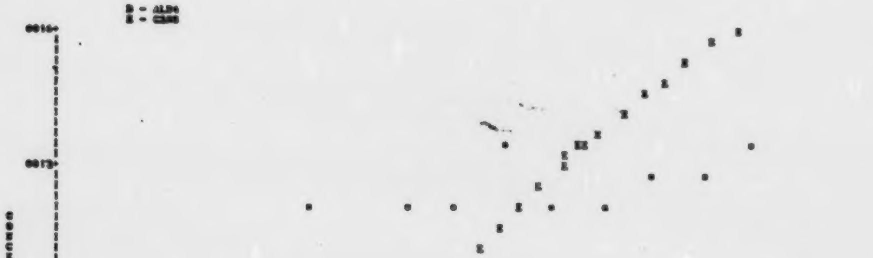

FIGURE III-172

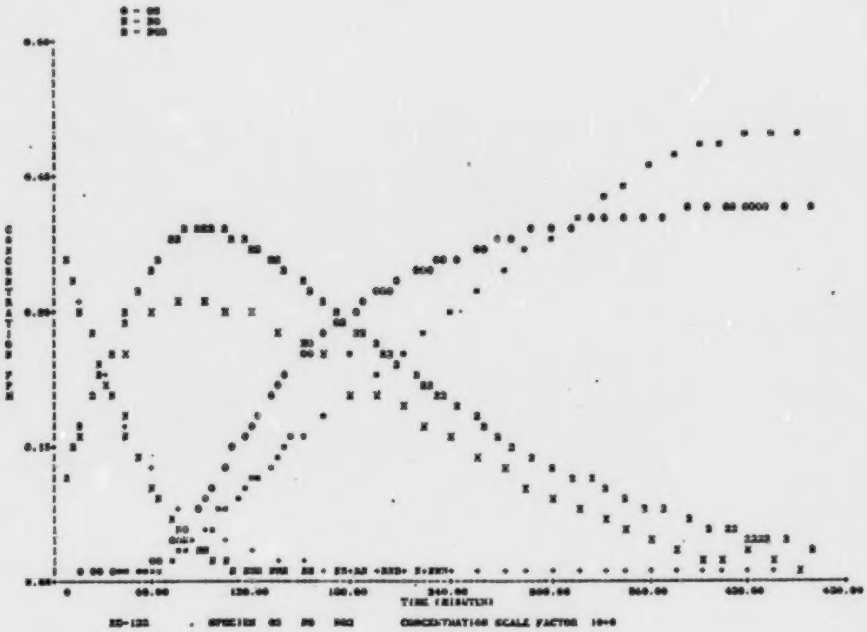

FIGURE III-173

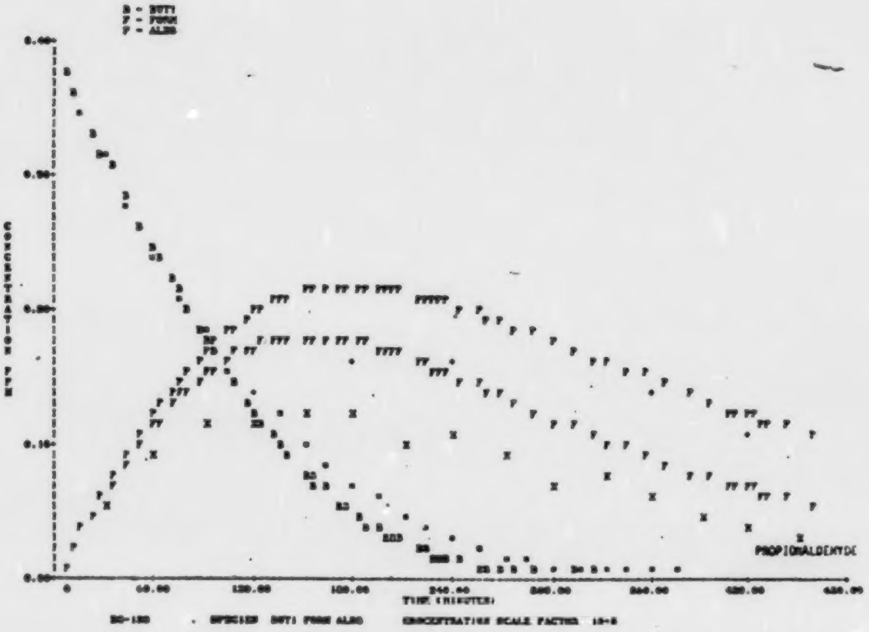

FIGURE III-174

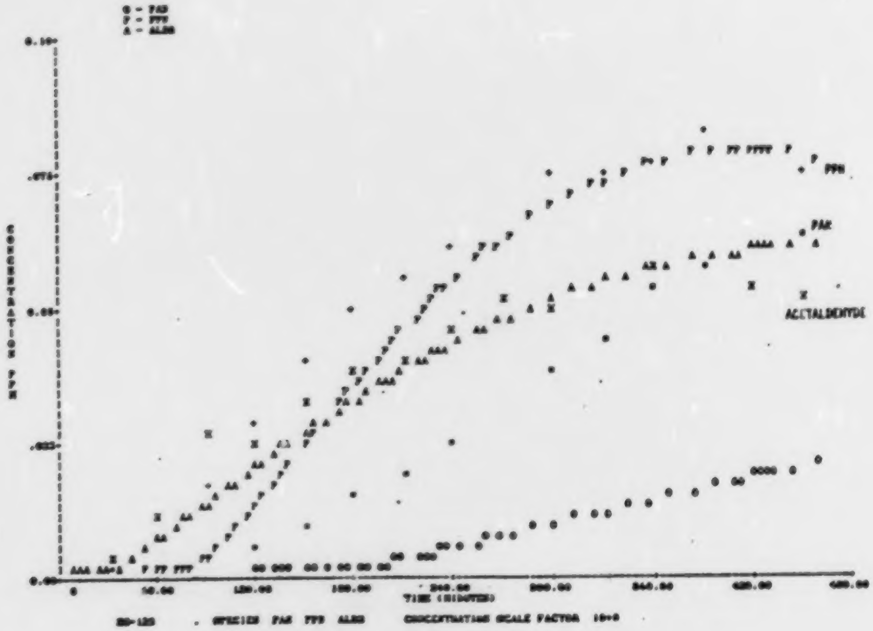

FIGURE III-175

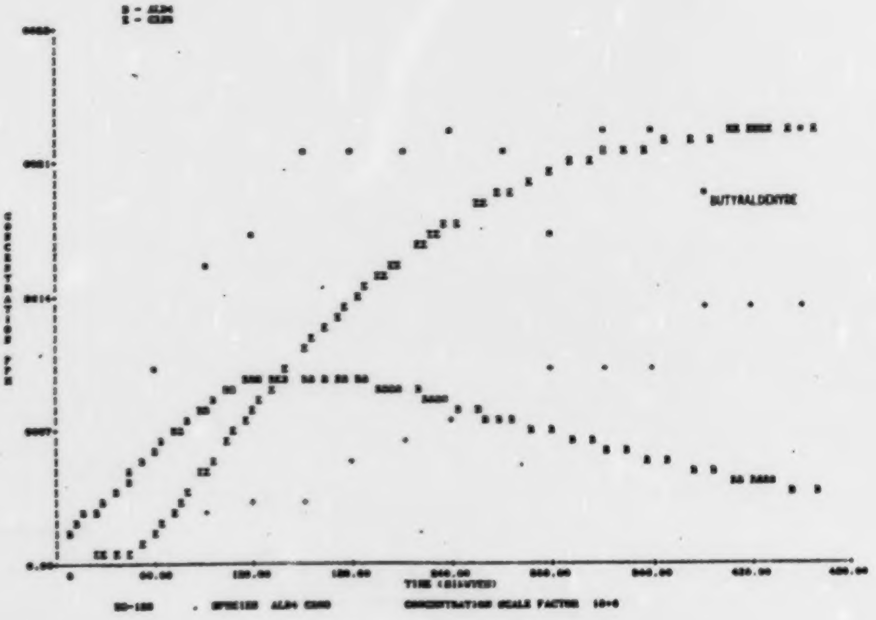

FIGURE III-176

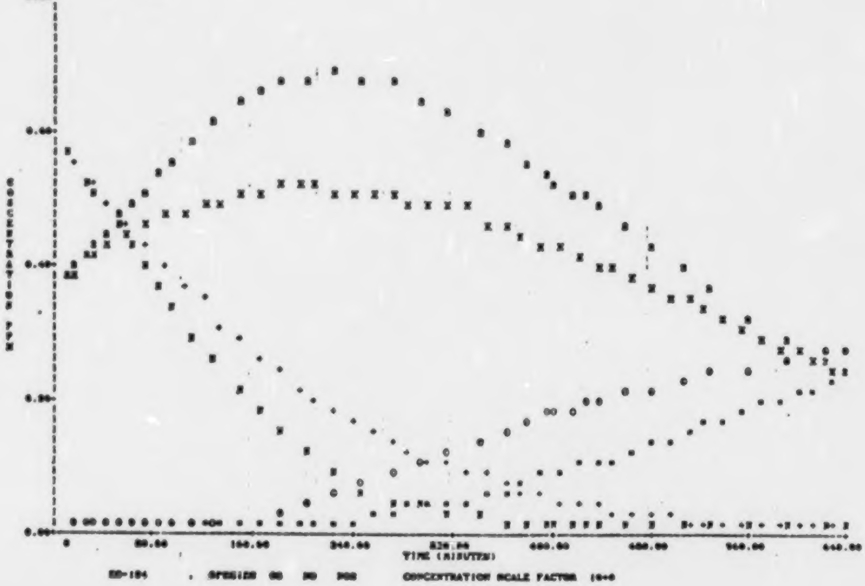

FIGURE III-177

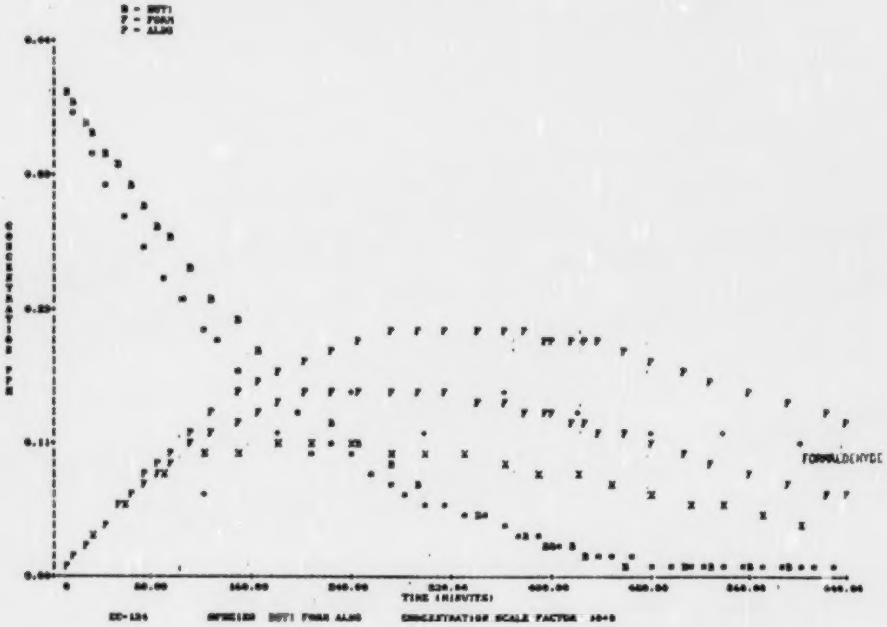

FIGURE III-178

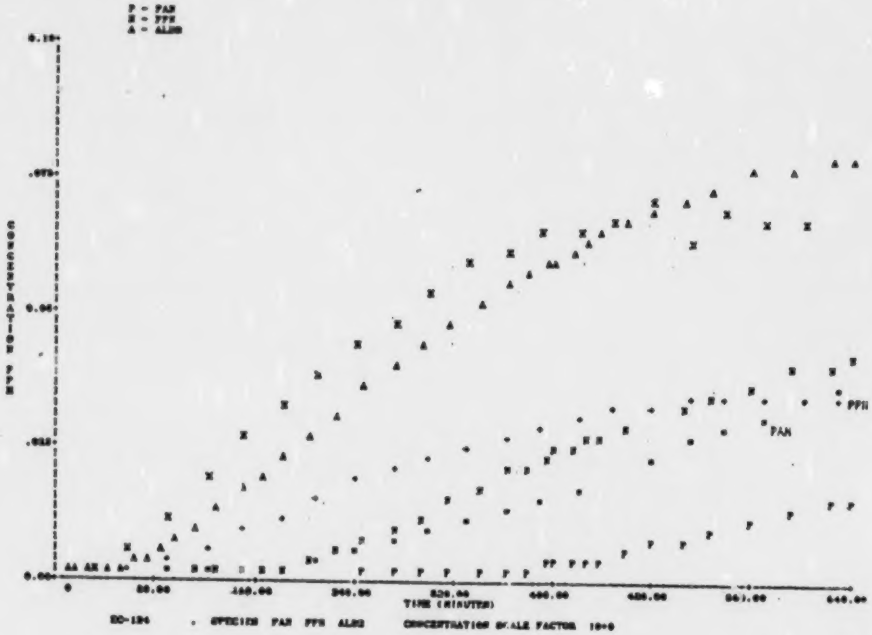

FIGURE III-179

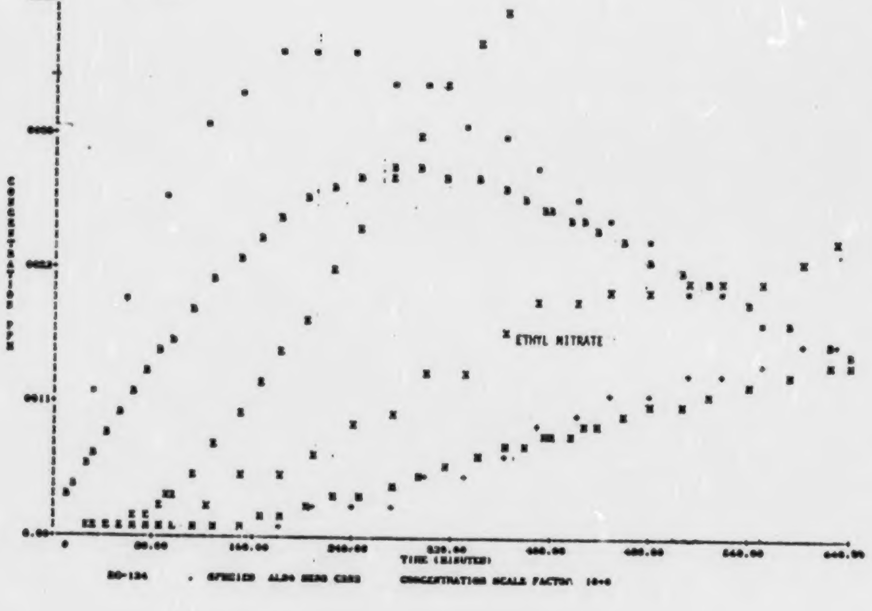

FIGURE III-180

3. Discussion of 1-Butene/NO_x Systems

Only three 1-butene experiments were simulated, yet the results are very helpful to the understanding of olefin behavior in smog formation. Modifying the propylene mechanism seems to give the overall pattern of products. By studying the observation from runs EC-123 and EC-124 for the production of butyraldehyde, we learned that the rate of its formation correlated with the initial NO_2 concentration. The propylene-OH· reaction with a hydride shift postulated by Durbin et al. (1975) leads to propionaldehyde formation. Similarly, one would expect that butyraldehyde would form from hydroxyl attack on 1-butene. But butyraldehyde formation correlates with initial NO_2, implying oxygen atoms from NO_2 photolysis attack 1-butene. Thus, the hydride shift reaction may be incorrect.

A comparison between the predicted and measured maximum one-hour-average ozone concentrations is shown in Table III-23. The average difference is +6.6 percent with a standard deviation of 24.8 percent.

The problems involved in NO_x loss and PAN chemistry (in this case PPN), which occurred in all simulations in this report, appear to be more severe in the 1-butene experiments. We hope to use these experiments to help evaluate some changes in the mechanisms that may resolve these problems.

TABLE III-23. PREDICTED AND MEASURED MAXIMUM ONE-HOUR-AVERAGE OZONE CONCENTRATIONS FOR THE 1-BUTENE/NO_x SYSTEMS

EC Run No.	Maximum One-Hour-Average Ozone Concentration (ppm) Predicted	Measured	Percent Difference
122	0.208	0.216	-3.5
123	0.43	0.48	-11.5
124	0.283	0.21	34.9

IV A NEW GENERALIZED LUMPED MECHANISM

Thus far in this document, we have discussed the development of explicit kinetic mechanisms. In earlier works (Hecht et al., 1974a,b), a generalized kinetic mechanism was developed for use in modeling urban air pollution. That mechanism groups each individual hydrocarbon into a general class; for example, propylene, 1-butene, and ethylene are classified as olefin. The use of that mechanism has highlighted certain difficulties, such as:

- The average carbon number for each class of hydrocarbon must be known; such determinations are sometimes not available.
- If the average carbon numbers for the different general classes are quite different, then the stoichiometric coefficient that relates to the overall average chain length is difficult to determine and remains untested.
- It is difficult to model high concentrations of less reactive species and low concentrations of highly reactive species in one group with one set of reaction rate constants.

The original Hecht, Seinfeld, and Dodge (HSD) mechanism is based on the concept that the concentrations to be used as input data for each general class are converted into units of ppm by volume of some representative compound with an average carbon number. Experimental data for mixtures of hydrocarbons are often reported in units of ppm as carbon (ppmC), and additional measurements that characterize individual hydrocarbons, the number of double bonds, carbonyl bonds, or aromatic rings might be known. In order to utilize the HSD mechanism, one must proceed through a series of conversions and assumptions to obtain the relative amounts of the hydrocarbon classes (olefins, paraffins, aromatics). One must also estimate an average carbon number for each class.

Another difficulty with the original HSD mechanism comes from a noninteger stoichiometric coefficient used to estimate the number of times that $RO_2^{\cdot}$ radicals normally react with NO to produce NO_2 and $RO\cdot$ radicals, which can lead to carbonyl compounds. The carbonyl compounds in reality react to form an $RO_2^{\cdot}$ or $RCO_3^{\cdot}$ with fewer carbon atoms and $HO_2^{\cdot}$. However, in the HSD mechanism some fraction of the original $R\cdot$ reappears at the end of each of these cycles, the fraction depending on the stoichiometric coefficient, β. This coefficient acts like an amplifier in that any number of reaction cycles up to infinity is possible depending on the choice of β.

With the original HSD mechanism, it is difficult to simulate a mixture of olefins of widely different reactivities. In the actual atmosphere, the most abundant olefin measured has been ethylene (Calvert, 1976). Even though ethylene is the least reactive olefin, its high concentration makes it an important factor in smog chemistry. The other olefins are much less abundant, but much more reactive. Mixing all olefins together as one lumped species makes it impossible in principle to model the ethylene/other-olefin chemistry (Hecht et al., 1974b).

In the sections that follow, we first discuss the specific revisions we have made to the original HSD mechanism, we then describe the development of a new generalized mechanism, and finally we present and analyze the results of simulations using this new mechanism.

A. REVISION OF THE HSD MECHANISM

The original HSD mechanism, as shown in Table IV-1, has been updated to include recent findings from our work on explicit kinetic mechanisms. The main changes are as follows:

- Formyl radicals are treated as forming peroxyformyl radicals rather than breaking down to $HO_2\cdot$ and CO.
- The $HO_2\cdot$-$NO_2\cdot$ reaction has been included; this reaction may be important in the late afternoon and evening chemistry.
- An aldehyde photolysis path leading to stable products has been added.
- PAN decomposition has been added.
- A path to form nitroaromatics has been added.
- Decomposition of RO· radicals has been incorporated into the mechanism.

B. THE NEW GENERALIZED MECHANISM

Because of the association of reactions and reactivities with carbon bonds, the range of reactions and the range of rate constants in a kinetic mechanism can be narrowed considerably when each carbon atom is treated according to its bond type. This concept is the basis for the new carbon-bond mechanism, which is listed in Table IV-2. In this mechanism, hydrocarbons are divided into four groups: single-bonded carbon atoms, fast double bonds (i.e., relatively reactive double bonds), slow double bonds, and carbonyl bonds. Single-bonded carbon includes not only paraffin molecules but also the single-bonded carbon atoms of olefins, aromatics, and aldehydes. Double bonds are treated in pairs of carbon atoms. Therefore, the concentrations of ethylene, olefins, and aromatics are taken as the concentrations of the double bonds in those species, which are one-half of the ppmC concentrations after the single-bonded carbons are subtracted. An activated aromatic ring is considered as three double bonds in the present formulation of the mechanism, and because of a

TABLE IV-1. THE ORIGINAL HECHT, SEINFELD, DODGE MECHANISM

$NO_2 + h\nu \xrightarrow{1} NO + O$	The NO_2-NO-O_3 Cycle
$O + O_2 + M \xrightarrow{2} O_3 + M$	
$O_3 + NO \xrightarrow{3} NO_2 + O_2$	
$O + NO + M \xrightarrow{4} NO_2 + M$	Important Reactions of O with Inorganic Species
$O + NO_2 \xrightarrow{5} NO + O_2$	
$O + NO_2 + M \xrightarrow{6} NO_3 + M$	
$O_3 + NO_2 \xrightarrow{7} NO_3 + O_2$	The Chemistry of NO_3, N_2O_5, and HNO_3
$NO_3 + NO \xrightarrow{8} 2NO_2$	
$NO_3 + NO_2 \xrightarrow{9} N_2O_5$	
$N_2O_5 \xrightarrow{10} NO_2 + NO_3$	
$N_2O_5 + H_2O \xrightarrow{11} 2HNO_3$	
$NO + HNO_3 \xrightarrow{12} HNO_2 + NO_2$	Reactions of HNO_3 with Inorganic Species
$HNO_2 + HNO_3 \xrightarrow{13} H_2O + 2NO_2$	
$NO + NO_2 + H_2O \xrightarrow{14} 2HNO_2$	Chemistry of HNO_2
$2HNO_2 \xrightarrow{15} NO + NO_2 + H_2O$	
$HNO_2 + h\nu \xrightarrow{16} OH + NO$	

TABLE IV-1 (Continued)

$$OH + NO_2 \xrightarrow{17} HNO_3$$

$$OH + NO + M \xrightarrow{18} HNO_2 + M$$

$$OH + CO + (O_2) \xrightarrow{19} CO_2 + HO_2$$

Important Reactions of OH with Inorganic Species

$$HO_2 + NO \xrightarrow{20} OH + NO_2$$

Oxidation of NO by HO_2

$$H_2O_2 + h\nu \xrightarrow{21} 2OH$$

Photolysis of H_2O_2

$$HC_1 + O \xrightarrow{22} ROO + \alpha R\underset{\overset{\|}{O}}{C}OO + (1-\alpha)HO_2$$

$$HC_1 + O_3 \xrightarrow{23} R\underset{\overset{\|}{O}}{C}OO + RO + HC_4$$

$$HC_1 + OH \xrightarrow{24} ROO + HC_4$$

$$HC_2 + O \xrightarrow{25} ROO + OH$$

$$HC_2 + OH \xrightarrow{26} ROO + H_2O$$

$$HC_3 + O \xrightarrow{27} ROO + OH$$

$$HC_3 + OH \xrightarrow{28} ROO + H_2O$$

$$HC_4 + h\nu \xrightarrow{29} \beta ROO + (2-\beta)HO_2$$

$$HC_4 + OH \xrightarrow{30} \beta R\underset{\overset{\|}{O}}{C}OO + (1-\beta)HO_2 + H_2O$$

Organic Oxidation Reactions

HC_1 = Olefins

HC_2 = Aromatics

HC_3 = Paraffins

HC_4 = Aldehydes

TABLE VI-1 (Concluded)

$ROO + NO \xrightarrow{31} RO + NO_2$	Reactions of Organic Free Radicals with NO, NO_2, and O_2
$R\underset{\overset{\|}{O}}{C}OO + NO + (O_2) \xrightarrow{32} ROO + NO_2 + CO_2$	
$R\underset{\overset{\|}{O}}{C}OO + NO_2 \xrightarrow{33} R\underset{\overset{\|}{O}}{C}OONO_2$	
$RO + O_2 \xrightarrow{34} HO_2 + HC_4$	
$RO + NO_2 \xrightarrow{35} RONO_2$	
$RO + NO \xrightarrow{36} RONO$	
$HO_2 + HO_2 \xrightarrow{37} H_2O_2 + O_2$	Other Peroxy Radical Reactions
$HO_2 + ROO \xrightarrow{38} RO + OH + O_2$	
$2ROO \xrightarrow{39} 2RO + O_2$	

TABLE IV-2. THE CARBON-BOND MECHANISM

Reaction	Rate Constant (ppm^{-1} min^{-1})
$NO_2 + h\nu \rightarrow NO + O\cdot$	k_1^*
$O\cdot + O_2 (+ M) \rightarrow O_3 (+ M)$	2.08×10^{-5}
$O_3 + NO \rightarrow NO_2 + O_2$	25.2
$O\cdot + NO_2 \rightarrow NO + O_2$	1.34×10^4
$O_3 + NO_2 \rightarrow NO_3 + O_2$	5×10^{-2}
$NO_3 + NO \rightarrow NO_2 + NO_2$	1.3×10^4
$NO_3 + NO_2 + H_2O \rightarrow 2HNO_3$	$1.66 \times 10^{-3\dagger}$
$NO + NO_2 + H_2O \rightarrow 2HNO_2$	$2.2 \times 10^{-9\dagger}$
$HNO_2 + h\nu \rightarrow NO + OH$	$k_{HNO_2}^*$
$NO_2 + OH\cdot \rightarrow HNO_3$	9×10^3
$NO + OH\cdot \rightarrow HNO_2$	9×10^3
$CO + OH\cdot \rightarrow CO_2 + HO_2$	2.06×10^2
$OLE + OH\cdot \xrightarrow{O_2} HCHO + CH_3O_2$	3.8×10^4
$PAR + OH\cdot \xrightarrow{O_2} CH_3O_2 + H_2O$	1.3×10^3
$ARO + OH\cdot \xrightarrow{O_2} HCHO + CH_3O_2$	8×10^3
$OLE + O\cdot \xrightarrow{2O_2} HC(O)O_2\cdot + CH_3O_2$	5.3×10^3
$PAR + O\cdot \xrightarrow{O_2} CH_3O_2^{\cdot} + OH\cdot$	20
$ARO + O\cdot \xrightarrow{2O_2} HC(O)O_2 + CH_3O_2$	37
$OLE + O_3 \xrightarrow{O_2} HC(O)O_2 + HCHO + OH\cdot$	0.01

TABLE IV-2 (Concluded)

Reaction	Rate Constant ($ppm^{-1}min^{-1}$)
$ARO + O_3 \xrightarrow{O_2} HC(O)O_2 + HCHO + OH\cdot$	0.002
$OLE + O_3 \rightarrow$ ozonide	0.005
$HCHO + h\nu \xrightarrow{2O_2} HC(O)O_2 + HO_2$	$k^*_{HCHO \rightarrow radicals}$
$HCHO + h\nu \rightarrow CO + H_2$	$k^*_{HCHO \rightarrow CO}$
$HCHO + OH\cdot \xrightarrow{O_2} HC(O)O_2 + H_2O$	1×10^4
$HO_2 + NO \rightarrow OH\cdot + NO_2$	2×10^3
$CH_3O_2 + NO \rightarrow NO_2 + HCHO + HO_2$	2×10^3
$HC(O)O_2 + NO \rightarrow NO_2 + CO_2 + HO_2$	2×10^3
$H_2O_2 + h\nu \rightarrow OH\cdot + OH\cdot$	$k^*_{H_2O_2}$
$HO_2 + HO_2 \rightarrow H_2O_2 + O_2$	4×10^3
$CH_3O_2 + HO_2 \rightarrow H_3COOH + O_2$	4×10^3
$HC(O)O_2^{\cdot} + HO_2 \rightarrow HC(O)OOH + O_2$	1×10^4
$HC(O)O_2 + NO_2 \rightarrow PAN$	150
$PAN \rightarrow HC(O)O_2^{\cdot} + NO_2$	0.02
$ARO + NO_3 \rightarrow$ PRODUCTS	50
$HO_2 + NO_2 \rightarrow HNO_2$	20.

---

* Photolysis rate constants in units of min^{-1}.

† Units of $ppm^{-2}min^{-1}$.

similarity in reactivities, aromatics are lumped with the slow (ethylene) double bonds rather than with the fast double bonds.

One of the goals in the development of the carbon-bond mechanism has been a mechanism responsive to the range of analytical detail in field measurements. At one end of the range the only hydrocarbon data available might be the total ppmC of hydrocarbons at one time. At the other extreme, the time dependence of many hydrocarbons may be known. The carbon-bond mechanism will accept these data and any others concerning the concentrations of double bonds, carbonyl groups, and aromatic rings. These data might be available through either spectral analysis or gas chromatography. Thus, the carbon-bond mechanism is directly responsive to the most basic measurement (nonmethane hydrocarbon), yet will accept data at any level of sophistication. The HSD mechanism requires a knowledge of the average carbon numbers in addition to overall concentrations. Of course, using the new mechanism with minimum data requires making an assumption as to the percentages of single, double, and carbonyl bonds.

The present formulation and parameterization of the carbon-bond mechanism has not been validated for complex hydrocarbon mixes in either smog chambers or the actual atmosphere. We expect that such an effort will be undertaken in the near future. The actual guidelines for determining the proper rate parameter averages should be part of the validation effort. We hope that validation efforts will confirm the fundamental theoretical foundation of the mechanism and that the averaging procedures for the mechanism will be simple and straightforward.

1. Rate Constants for Hydrocarbon Classes

In order to perform computer simulations with the carbon-bond mechanism, we had to select rate constants for the oxidation of the different hydrocarbon classes. This section describes our choice of a rate constant for each class of hydrocarbons.

a. Single-Bonded Carbon Atoms

Paraffins apparently undergo the following oxidation reactions:

$$PAR + OH\cdot \rightarrow RO_2\cdot + H_2O \quad , \qquad (IV\text{-}1)$$

$$RO_2\cdot + NO \rightarrow HO_2\cdot + ALD + NO_2 \quad , \qquad (IV\text{-}2)$$

$$HO_2\cdot + NO \rightarrow OH\cdot + NO_2 \quad . \qquad (IV\text{-}3)$$

In this set of reactions, one hydroxyl radical reacts and is regenerated while two nitric oxide molecules are converted to nitrogen dioxide and the paraffin is converted into an aldehyde.

From Greiner's (1970) formula for calculating alkane-OH· rate constants, primary carbon atoms at 300°K have a reactivity of 290 $ppm^{-1}min^{-1}$; secondary carbon atoms of normal alkanes have a reactivity of 1600 $ppm^{-1}min^{-1}$; and tertiary carbons have a reactivity of 4200 $ppm^{-1}min^{-1}$. The creation of a side chain converts two secondary carbons into one primary carbon and one tertiary carbon, for an average reactivity of 2240 $ppm^{-1}min^{-1}$. Table IV-3 lists the reactivity per carbon atom for several common alkanes. Many of the alkanes--except propane and those containing the tertiary-butyl group--have reactivities within about 35 percent of 1300 $ppmC^{-1}min^{-1}$. The compounds with tert-butyl groups may be present in low concentrations in typical atmospheric mixes. They were reported by Calvert (1976) to be less than 8 percent of the alkanes in observations made during the Los Angeles Reactive Pollutant Program (LARPP).

b. Fast Double Bonds

Olefin chemistry is represented by the following reactions (for ethylene):

$$OLE + O \rightarrow HCO_3\cdot + CH_3O_2\cdot \quad , \qquad (IV\text{-}4)$$

$$OLE + OH\cdot \rightarrow HCHO + CH_3O_2^{\cdot} \quad , \qquad \text{(IV-5)}$$

$$OLE + O_3 \rightarrow HCHO + HCO_3^{\cdot} + OH\cdot \quad . \qquad \text{(IV-6)}$$

Olefins are treated with greater difficulty than paraffins. The rate constant for OH· oxidation differs greatly between ethylene and the longer chain olefins, especially the internal olefins. The mechanism is further complicated because olefins react with ozone to a significant extent.

TABLE IV-3. REACTIVITIES PER CARBON ATOM FOR SEVERAL ALKANES

Alkane	Reactivity ($ppm^{-1}min^{-1}$)
Propane	730
n-Butane	950
i-Butane	1250
n-Pentane	1080
neo-Pentane	232
i-Pentane	1340
n-Hexane	1170
i-Hexane	1380
2,3-Dimethyl-butane	1590
2,2-Dimethyl-butane	460
n-Heptane	1220
i-Heptane	1410
2,3-Dimethylpentane	1590
n-Octane	1280
i-Octane	1440
2,3,4-Trimethylpentane	1760
n-Nonane	1310
i-Nonane	1460

Per double bond, the reaction rates of olefins with OH· jump from 8000 $ppm^{-1}min^{-1}$ for ethylene to 38,000 $ppm^{-1}min^{-1}$ for propylene (Davis, 1976) and stay constant within a factor of 2 for longer olefins. The reactivity increases for 1-butene (to 4.3×10^4 $ppm^{-1}min^{-1}$) and for internal olefins such as cis-2-butene (6.3×10^4 $ppm^{-1}min^{-1}$). Table IV-4 lists reactivities in $ppm^{-1}min^{-1}$ for five olefins. Because of the low variation in rate constants of olefins (except ethylene), we treat all olefins except ethylene as one lumped species in the carbon-bond mechanism. In the near future efforts will be made to develop methods for estimating "averaged" rate constants for olefin reactions. Currently, we are using rate constants for the specific olefin in the simulation runs (see Section C-2).

TABLE IV-4. RATE CONSTANTS PER DOUBLE BOND FOR THE REACTIONS OF SOME OLEFINS WITH OH· AT 300°K

Olefin	Rate Constant ($ppm^{-1}min^{-1}$)
Ethylene	7.9×10^3
Propylene	3.8×10^4
1-Butene	4.3×10^4
cis-2-Butene	6.3×10^4
Tetramethylethylene	8.4×10^4

The olefin-O_3 reactions are more complicated than the olefin-OH· reactions. Table III-3 shows rate constants for the same olefin-O_3 reactions. The propylene reaction with ozone is roughly seven times faster than the ethylene reaction, and nonterminal olefins such as cis-2-butene react even faster (terminal olefins such as isobutene have reaction rate constants comparable to that of propylene). Substituted internal olefins, such as 2,3-dimethyl-2-butene, react with ozone roughly 10^3 faster than does ethylene.

Thus, we are confronted with the task of devising lumping parameters capable of spanning a 10^3 difference in rate constants. This task has not yet been performed; it seems possible only if the slower O_3-olefin reactions are neglected. In future work, we hope to incorporate the reactions of olefins with $NO_3^{\cdot}$. These reactions are insignificant for smaller olefins (ethylene, propylene, and 1-butene), but are fast for longer chain olefins (Japar et al., 1975). At present, we do not include this reaction in the carbon-bond mechanism because little is known about the products of this reaction.

c. Slow Double Bonds

In the carbon-bond mechanism, the aromatic oxidation reactions produce the same products as the olefin oxidation reactions:

$$ARO + O \rightarrow HCO_3^{\cdot} + CH_3O_2^{\cdot} \quad , \qquad (IV\text{-}7)$$

$$ARO + OH^{\cdot} \rightarrow HCHO + CH_3O_2^{\cdot} \quad , \qquad (IV\text{-}8)$$

$$ARO + O_3 \rightarrow HCHO + HCO_3^{\cdot} + OH^{\cdot} \quad . \qquad (IV\text{-}9)$$

In these equations, ARO represents one slow double bond; thus, the toluene molecule equals three AROs. We have found that an aromatic ring activated by the addition of an alkyl group, such as toluene, can be treated by the carbon-bond mechanism as three ethylenic double bonds (olefins). Thus, we treat ethylene and the aromatics together as one lumped species. This lumping is used primarily because the oxidation rate of ethylene by $OH^{\cdot}$ is closer to that of aromatics than to the other olefins. In addition, ethylene typically makes up 50 percent of the atmospheric olefins, as compared to only 10 to 20 percent of the aromatics (on the basis of total double bonds).

One question we had to resolve was whether ozone-aromatic reactions similar to ozone-olefin reactions should be included in the mechanism for toluene systems. As the aromatic ring decomposes, it surely must lead to some olefin species which, of course, would react with ozone. We have tentatively included ozone-olefin reactions for two reasons:

> The rate constant for the reaction of ethylene with ozone is very slow. It may be similar to the rate constant for the ozone-aromatic reaction, which has not been measured accurately but is known to be slow (Finlayson and Pitts, 1976).

> We wanted to maintain the treatment of aromatic bonds and ethylene together as one lumped species.

We hope that some ethylene/toluene smog chamber experiments can be carried out in the near future to provide a better test for the mechanism.

The choice of rate constant for the reaction of slow double bonds with oxygen atoms is more difficult because the rate constants for aromatics and ethylene reacting with oxygen atoms differ greatly. We did not use the rate constant for the reaction of oxygen atoms with ethylene because that rate constant caused too high a radical concentration early in a simulation of a toluene system. We plan to develop a procedure for estimating a rate constant in accordance with the relative amounts of aromatics and ethylene in the system being simulated. This is not a great difficulty because the reactions of slow double bonds with oxygen atoms are not very important. We did include a reaction between $NO_3^{\cdot}$ and aromatics to account for the internal olefins that are formed as the aromatic rings open. The rate constant of 50 $ppm^{-1}min^{-1}$ is adequate at present for most of the smog chamber runs to date. It is faster than that measured for the reaction of NO_3 with ethylene (1.4 $ppm^{-1}min^{-1}$) by Japar and Niki (1975), but far slower than their value for the reaction with substituted internal olefins (5×10^4 $ppm^{-1}min^{-1}$). The inclusion of the reaction of $NO_3^{\cdot}$ with aromatics is partially justified by the observation that no $NO_3^{\cdot}$ is formed in smog chamber simulations until some toluene has reacted.

As mentioned above, the aromatic ring is represented by three double bonds (ethylene groups) in the carbon-bond mechanism. Therefore, observed aromatic concentrations in ppm are multiplied by three to give input data for the mechanism. Any alkyl groups or carbonyl groups on the aromatics are considered separately. For toluene, we use three times the measured toluene concentration of slow double bonds and the toluene concentration of single-bonded carbon atoms.

d. Carbonyl Bonds

The carbon-bond mechanism treats carbon-oxygen double bonds, whether in ketones or aldehydes, as a single group. We are currently using a value of 1×10^4 $ppm^{-1}min^{-1}$ for the aldehyde-OH· reaction rate. This compares to an estimate of 9.8×10^3 $ppm^{-1}min^{-1}$ as the lower limit of the reaction rate (Herron and Penzhorn, 1969). Our present value falls midway between the value of 2.1×10^4 $ppm^{-1}min^{-1}$ measured by Morris and Niki (1971) and the Volman and Gorse (1972) estimate of 5.6×10^3 $ppm^{-1}min^{-1}$ for the reaction of propionaldehyde-OH·. Data on the rate constants of larger aldehydes are sketchy, but seem to be in accord with our choice of rate constant.

2. Sources of Radicals in the Carbon-Bond Mechanism

In computer simulations of smog chamber experiments, the initial concentration of hydroxyl radicals is produced by photolysis of nitrous acid:

$$HNO_2 + h\nu \rightarrow OH\cdot + NO \quad . \qquad \text{(IV-10)}$$

The amounts of HNO_2 that give the best fits between predictions and measurements are generally about one-third of the equilibrium concentration of HNO_2 from the reaction

$$H_2O + NO + NO_2 \rightleftarrows 2HNO_2 \quad . \qquad \text{(IV-11)}$$

HNO_2 is only an initial radical source because its half-life due to photolysis is about 15 minutes.

Some radicals can also come from oxygen atom attack on hydrocarbons:

$$O + PAR \rightarrow RO_2^{\cdot} + OH\cdot \quad , \qquad \text{(IV-12)}$$

$$O + OLE \rightarrow RO_2^{\cdot} + RCO_3^{\cdot} \quad . \qquad \text{(IV-13)}$$

This reaction is slower for paraffins, particularly for butane, than it is for olefins (Hampson and Garvin, 1975). Both of these radical sources are used in the carbon-bond mechanism.

The third source of radicals in the mechanism is the photolysis of carbonyls:

$$RR'CO + h\nu \rightarrow RO_2^{\cdot} + RCO_3^{\cdot} \quad . \qquad \text{(IV-14)}$$

Maintaining the total concentration of radicals in the mechanism by carbonyl photolysis is necessary because of the numerous temporary and permanent radical sinks. For example, both nitrous acid and hydrogen peroxide are temporary radical sinks because they are formed rapidly via reactions that consume radicals:

$$OH\cdot + NO \rightarrow HNO_2 \quad , \qquad \text{(IV-15)}$$

$$HO_2^{\cdot} + HO_2^{\cdot} \rightarrow H_2O_2 \quad . \qquad \text{(IV-16)}$$

However, both species can reproduce radicals at a later time by photolysis. The most important permanent radical sink in the UCR smog chamber experiments on butane/NO_x systems also appears to be the most important sink for oxides of nitrogen:

$$OH\cdot + NO_2 \rightarrow HONO_2 \quad . \qquad \text{(IV-17)}$$

Carbonyl photolysis is most important in maintaining the radical concentration, but it is also the most complex to treat in the mechanism. The complexity arises from the three reaction pathways of carbonyls--photolysis that produces radicals [Reaction (IV-18)], photolysis that does not produce radicals [Reaction (IV-19)], and reaction with hydroxyl radicals [Reactions (IV-20) and (IV-21)], which leads to oxidation of the carbonyl without net production of radicals:

$$\mathrm{RR'CO + h\nu \rightarrow RO_2^{\cdot} + R'CO_3^{\cdot}} \quad , \qquad \text{(IV-18)}$$

$$\mathrm{RR'CO + h\nu \rightarrow RR' + CO} \quad , \qquad \text{(IV-19)}$$

$$\mathrm{RCHO + OH\cdot \rightarrow H_2O + RCO_3^{\cdot}} \quad , \qquad \text{(IV-20)}$$

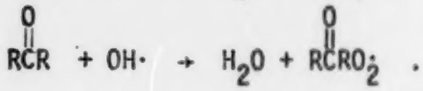

$$\mathrm{R\overset{\overset{O}{\|}}{C}R + OH\cdot \rightarrow H_2O + R\overset{\overset{O}{\|}}{C}RO_2^{\cdot}} \quad . \qquad \text{(IV-21)}$$

The magnitude of radical production from carbonyl photolysis is a function of the carbonyl concentration and the photolysis constant. In the explicit mechanism study we found that the principal carbonyl compound was MEK, but an important source of radicals was the photolysis of biacetyl (which presumably has a large photolysis constant). In the UCR data, the actual light spectrum was uncertain, as was the total carbonyl concentration because of the considerable mass recovery problem. Even if the explicit mechanism and the light spectrum were known completely and the mass recovery were perfect, the photolysis constants would still be uncertain, primarily because of the uncertainties in the quantum yield data.

The relative importance of HNO_2 and carbonyl photolysis as sources of radicals in the atmosphere has yet to be determined. Available data--ambient concentrations of the species, solar spectral data, quantum yields--are insufficient to allow anything but the crudest estimates. The selection of initial conditions and photolysis rates for the initiation of the smog formation process in computer simulations is arbitrary.

C. SIMULATION RESULTS

The use of this lumped mechanism to model data on a single hydrocarbon species presents a paradoxical situation. Optimal performance for a mixture of hydrocarbons may not be the best for certain specific hydrocarbons taken one at a time. However, this mechanism is based on the explicit chemistry of specific hydrocarbons (except aromatics). Thus, the rate parameters used to optimize the present mechanism results may not be optimal for use in the atmosphere.

The carbonyl photolysis constants used in the carbon-bond simulations were derived from the constants used in the corresponding explicit studies using average values weighted according to the explicitly simulated fraction of each carbonyl compound at the time of maximum total carbonyl concentration. The initial values of nitrous acid were in all cases identical to the values used in the corresponding explicit studies.

1. Butane/NO_x Systems

Simulations of the butane/NO_x system with the carbon-bond mechanism are presented in Figures IV-1 through IV-17. As discussed above, paraffins are the simplest species to generalize since the reactions involve only O atoms and OH· radicals. In the factorial design set of butane systems, the simplest NO_x data are in run EC-42; these data are shown in Figure IV-8. Essentially no ozone formed in this experiment; thus, complications from species such as NO_3 and N_2O_5 that form late in the smog reaction were minimized. The NO_x crossover in EC-42 was reached just before the end of the six-hour experiment. The NO_x/carbon ratio in this run was higher than in any other run, thus exaggerating the radical-NO_x sink effect. Although the carbon-bond mechanism does not follow the data for EC-42 closely, it is no worse than the explicit mechanism. If the initial concentration of nitrous acid is raised to or above the equilibrium value of 0.03 ppm, the initial slope of NO disappearance is too steep and then it flattens out. If the maintenance source of radicals from carbonyl photolysis is increased by using

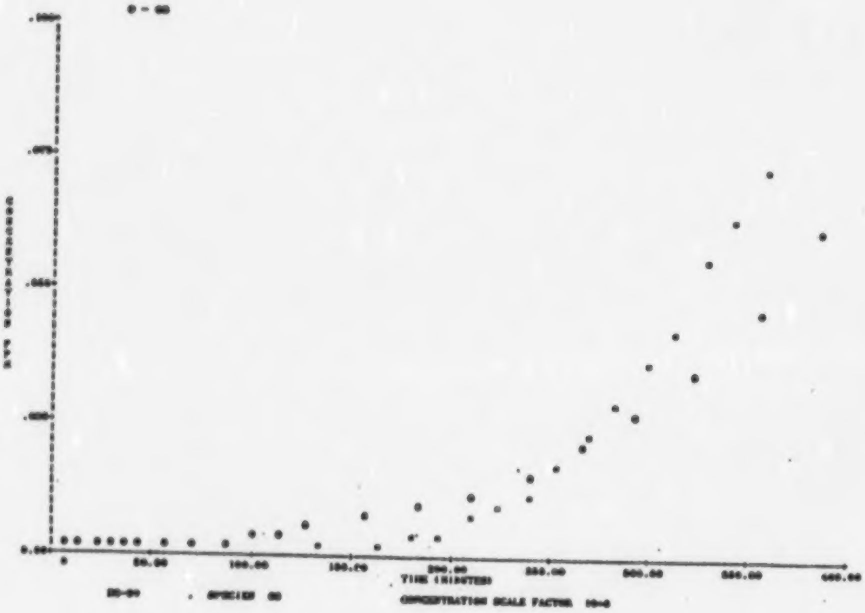

FIGURE IV-1

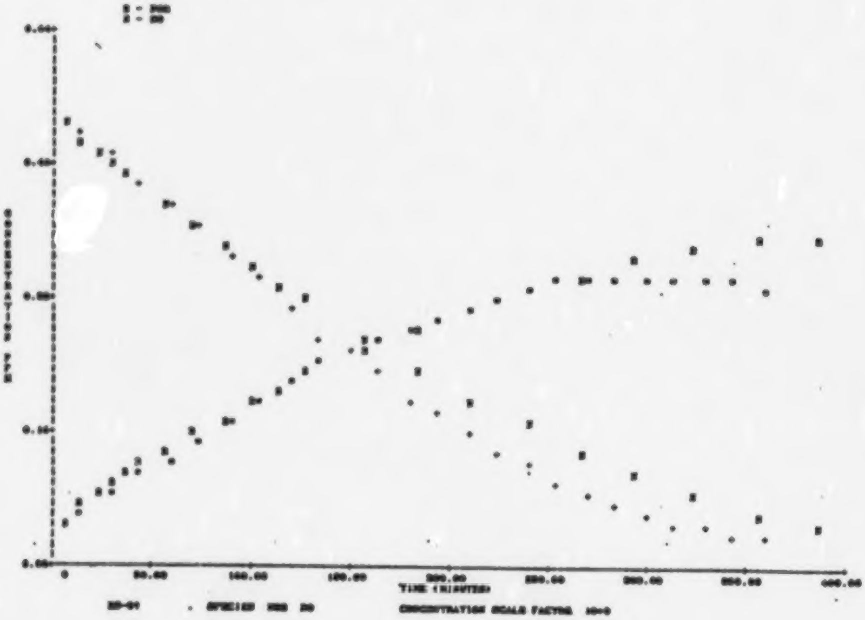

FIGURE IV-2

Reproduced from best available copy.

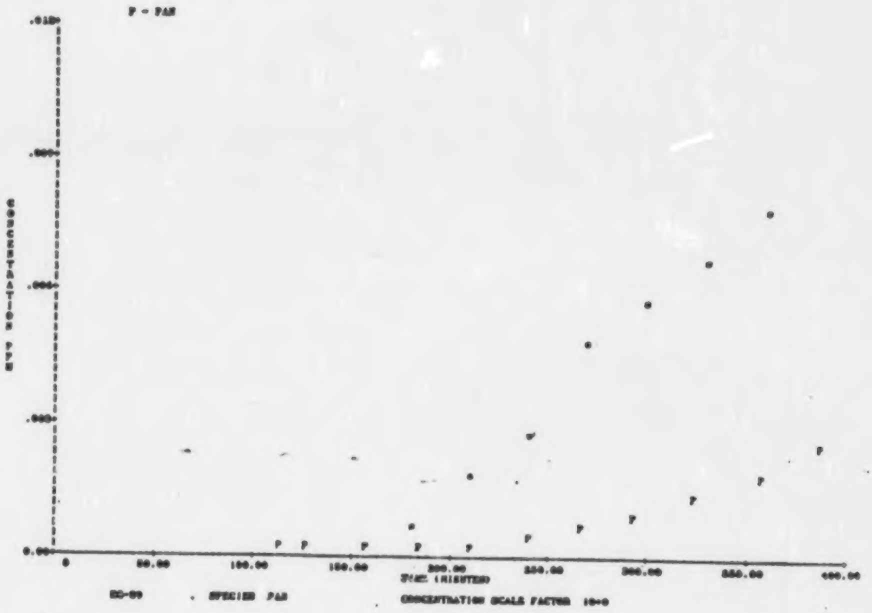

FIGURE IV-3

Reproduced from
best available copy.

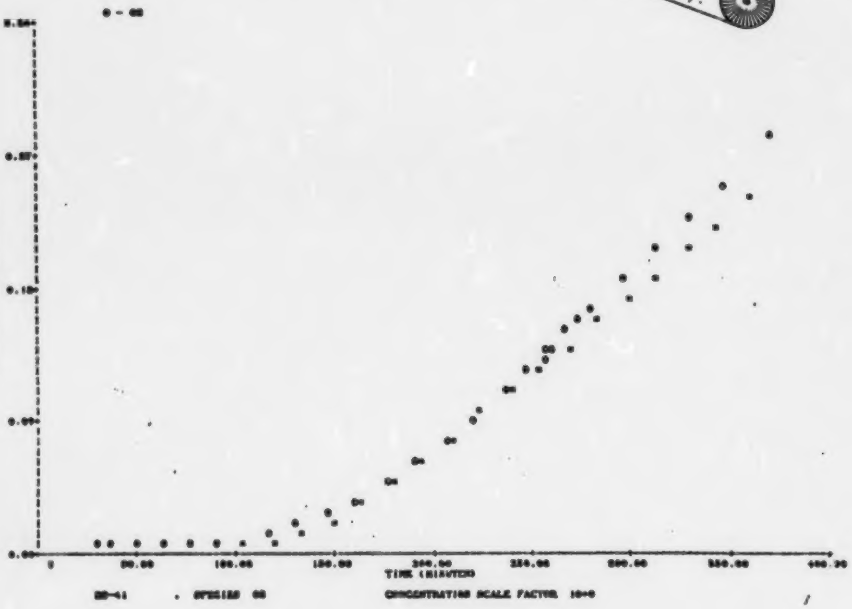

FIGURE IV-4

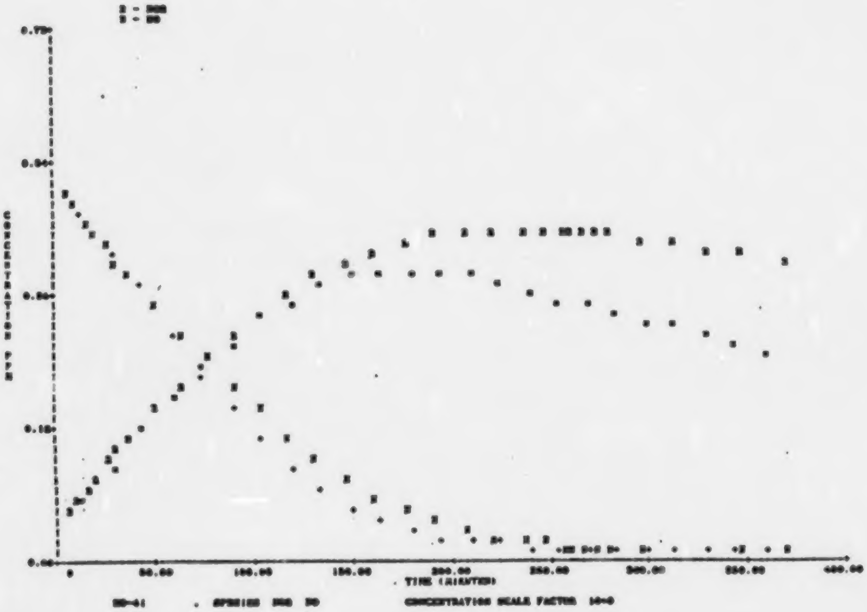

FIGURE IV-5

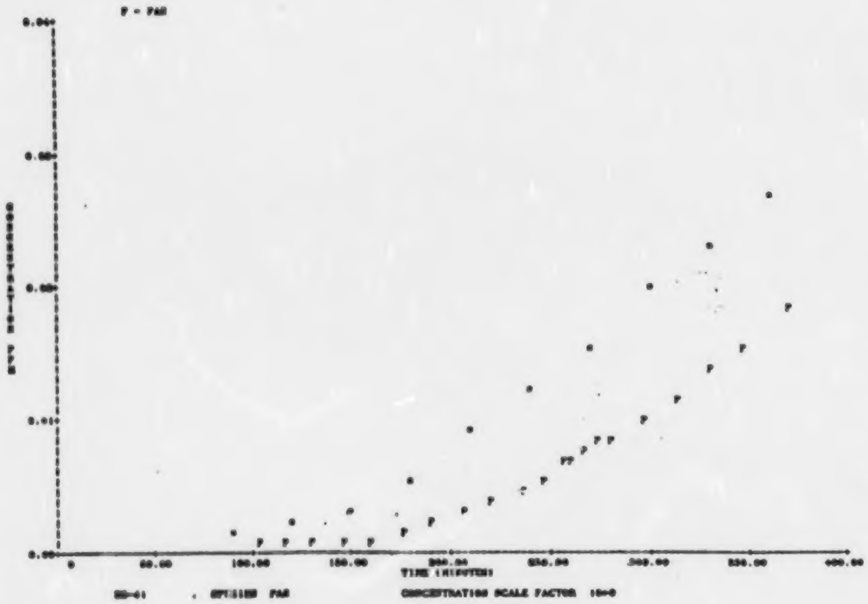
0.04
0.03
0.02
0.01
0.00
0
50.00
100.00
150.00
200.00
250.00
300.00
350.00
400.00
TIME (MINUTES)
CONCENTRATION SCALE FACTOR

FIGURE IV-6

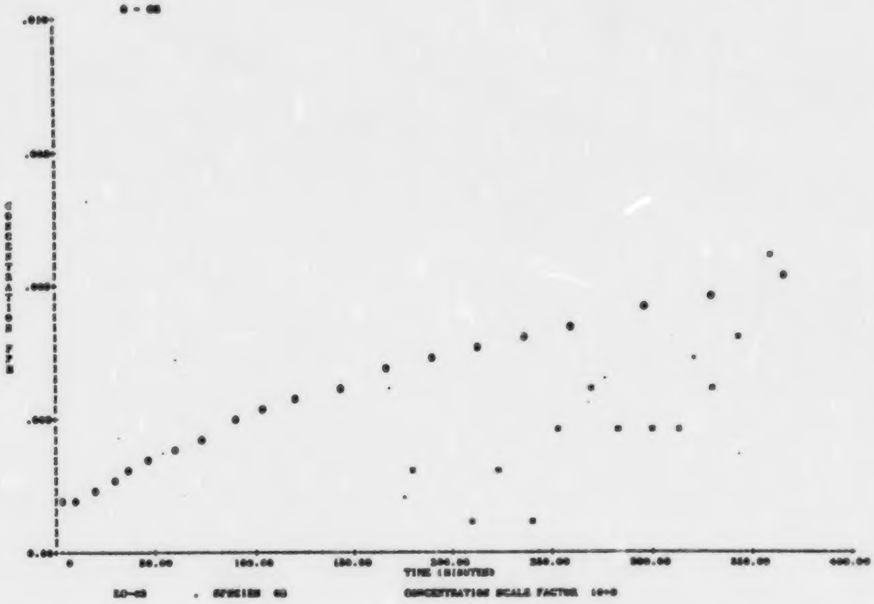

FIGURE IV-7

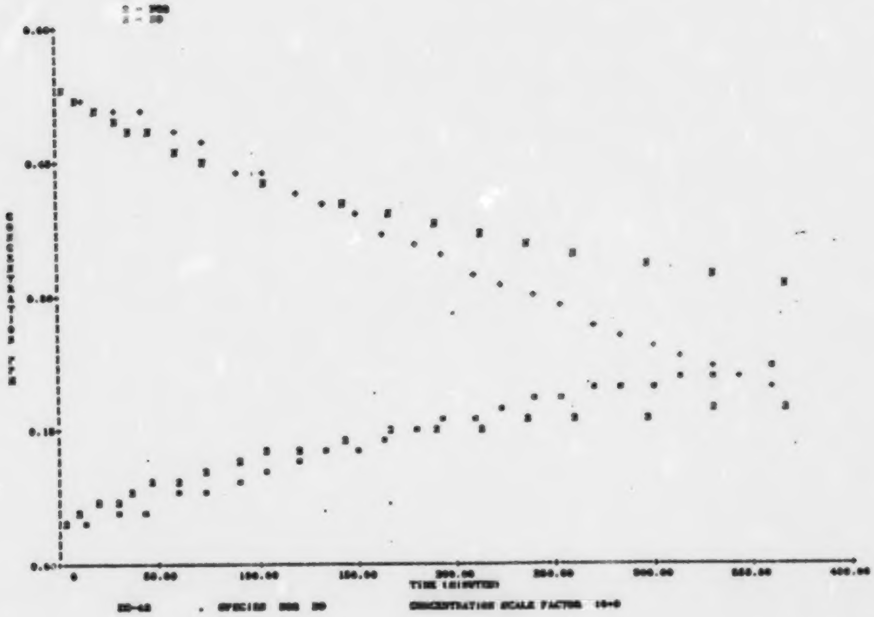

FIGURE IV-8

Reproduced from best available copy.

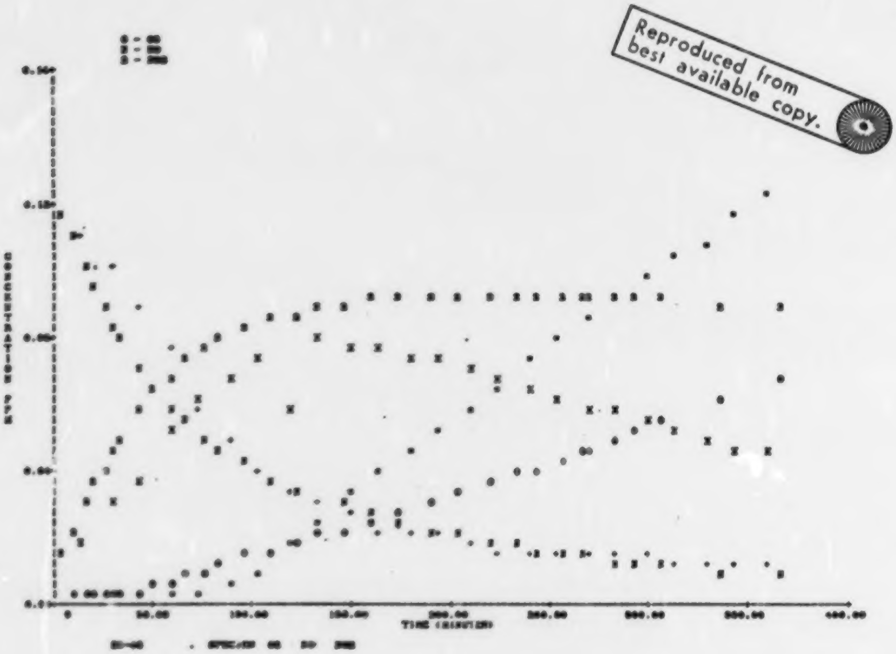

FIGURE IV-9

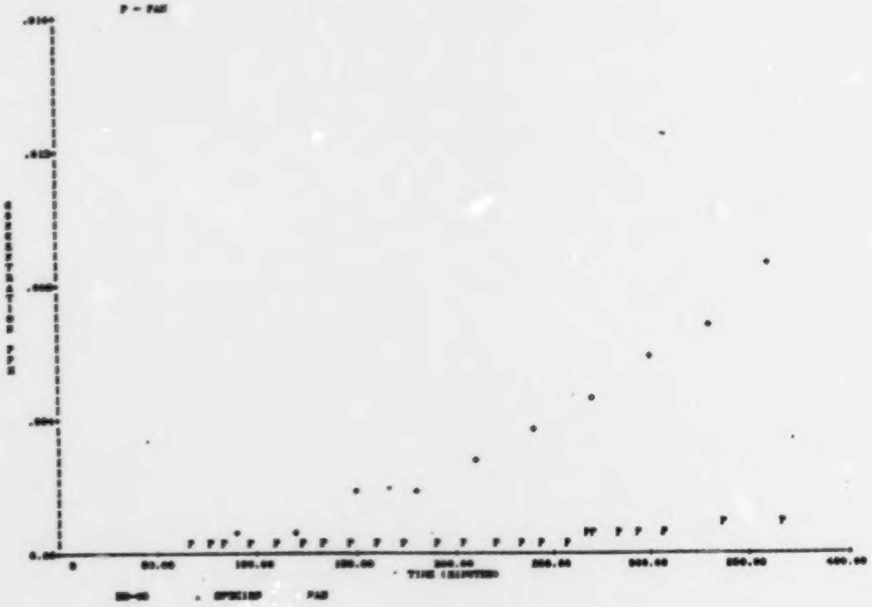

FIGURE IV-10

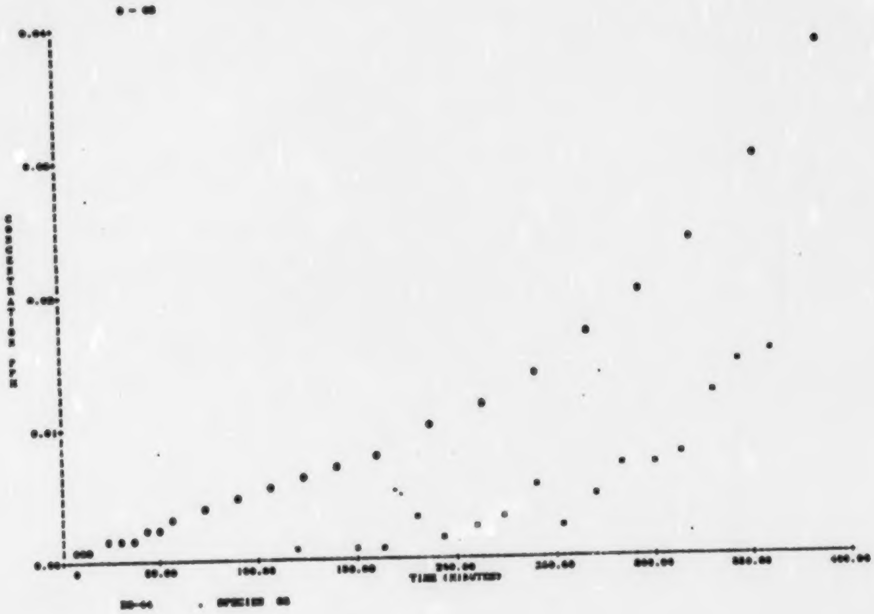

FIGURE IV-11

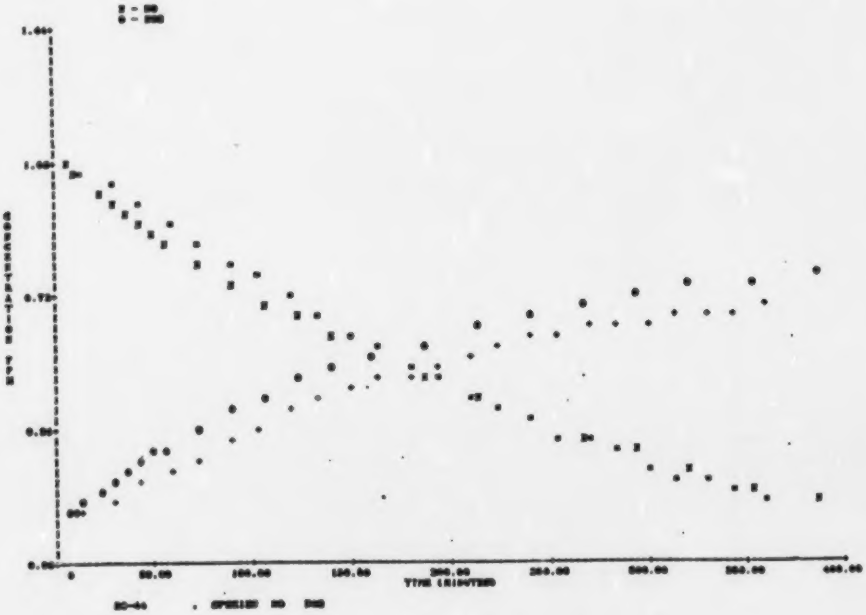

FIGURE IV-12

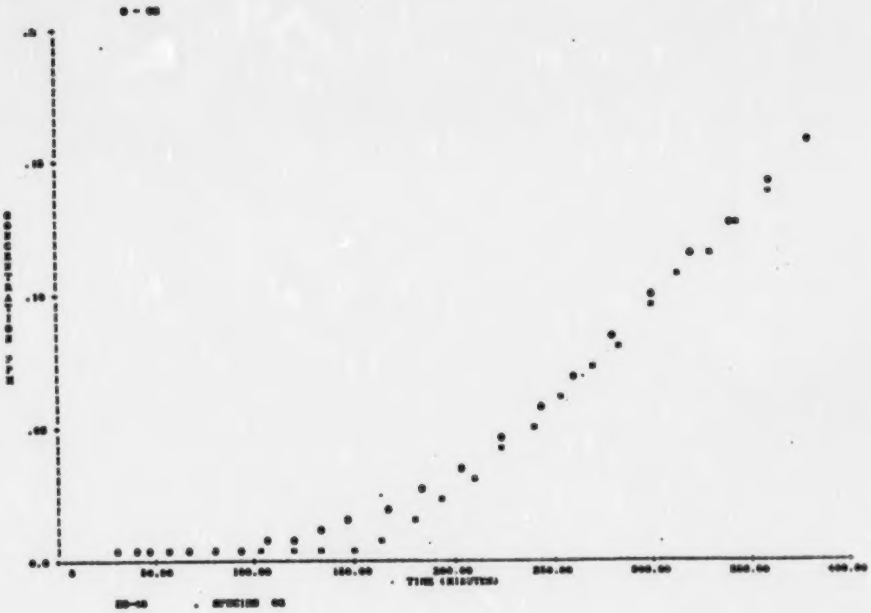

FIGURE IV-13

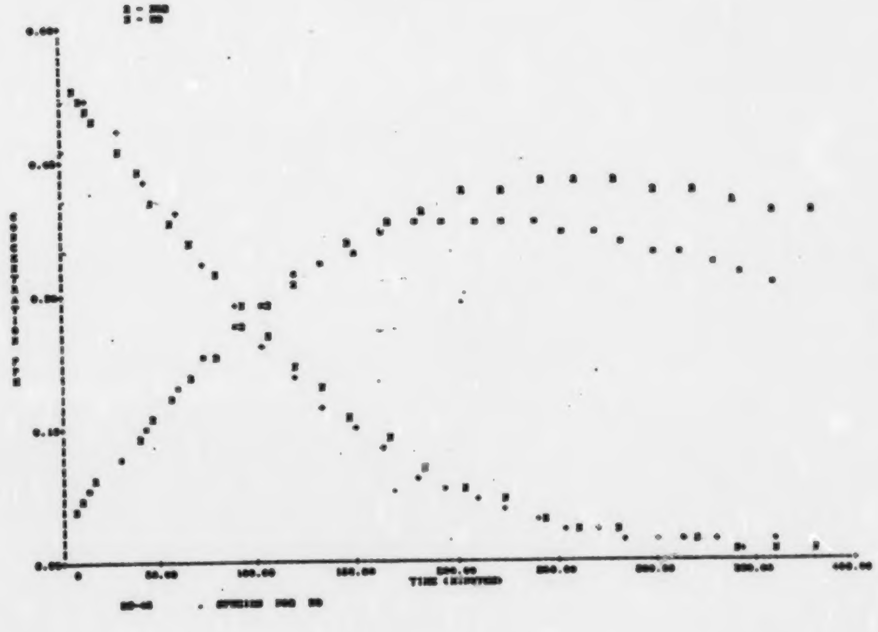

FIGURE IV-14

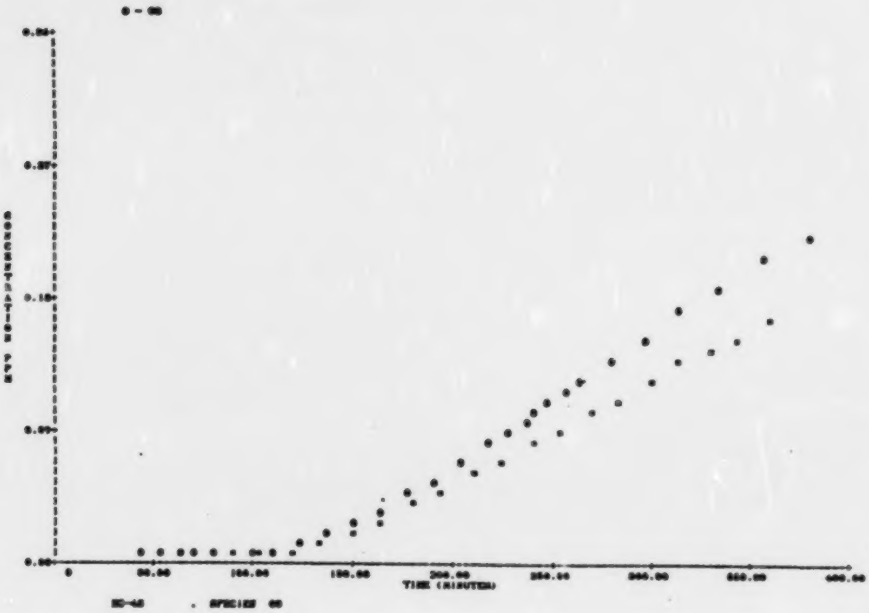

FIGURE IV-15

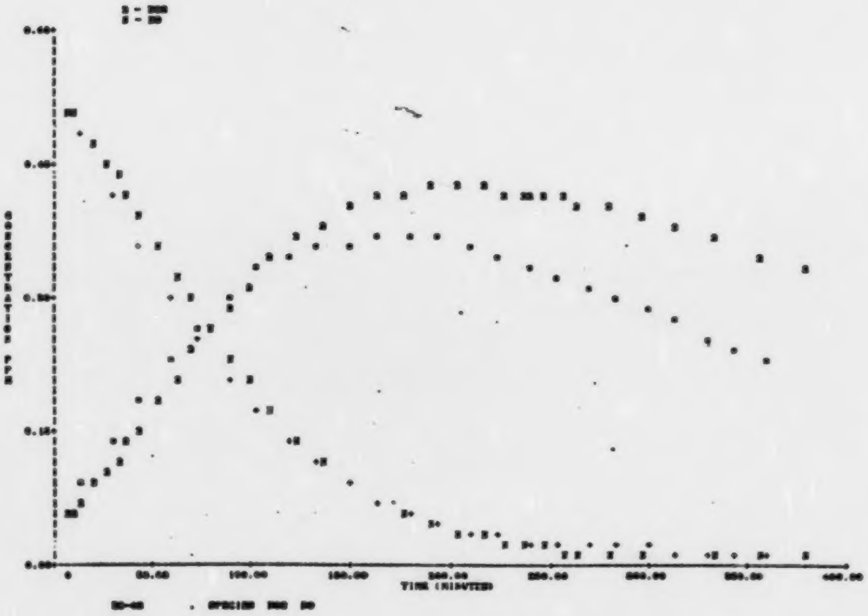

FIGURE IV-16

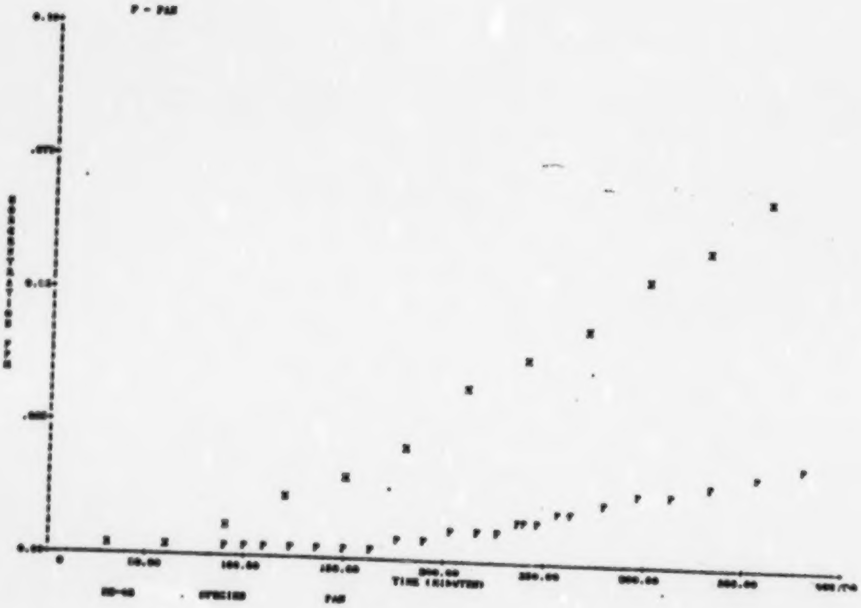
P - PAN
0.10
.075
0.05
.025
0.00
0
50.00
100.00
150.00
200.00
TIME (MINUTES)
250.00
300.00
350.00
SPECIES
PAN

FIGURE IV-17

a photolysis constant larger than about 1.5 x 10^{-3} min^{-1}, a somewhat better fit is obtained for EC-42. However, a poorer fit is then obtained for EC-45 because the aldehydes present initially in this run are predicted to produce radicals at too fast a rate. Finally, if the rate of the main radical and NO_x sink [Reaction (IV-17)] is lowered, the total NO_x data cannot be followed.

Thus, the mechanism for oxidation of butane as presented in Table IV-2 is not complete. For many runs, one can achieve a reasonable fit of predictions to measurements by using initial and maintenance sources of radicals within the bounds of uncertainty of the various reaction rates. However, it is not yet possible to obtain a good fit to measurements of systems in which the hydrocarbon/NO_x ratio and the rate of hydrocarbon oxidation are low.

The simulations of UCR's butane/NO_x data (Figures IV-1 through IV-17) were performed assuming paraffins behave chemically as a methane molecule. Therefore, the input data for paraffins would be four times the total butane concentration. All the symbols R and R' are represented by the symbols $CH_3^{\cdot}$ and H·, respectively. Therefore, $RO_2^{\cdot}$ and $R'CO_3^{\cdot}$ are written as $CH_3O_2^{\cdot}$ and $HCO_3^{\cdot}$. Formaldehyde is the representative carbonyl in the carbon-bond mechanism. The formation of peroxyacyl nitrates is represented as peroxyformyl nitrate in the mechanism with a rate constant estimated to fit UCR's PAN (peroxyacetyl nitrate) data. The single-bonded carbon atom rate constant for the reaction with OH· was lowered to 1100 ppm^{-1} min^{-1} to account for butane having a particularly slow value.

2. Propylene/NO_x Systems

The basic factorial design block of experiments for propylene, runs EC-11 through EC-21, was simulated with the carbon-bond mechanism. Many of the features of the results are the same as those obtained using the explicit mechanism, which is discussed in Chapter III. EC-21 is similar the butane run (EC-42) discussed above. These low hydrocarbon to NO_x ratio runs are also discussed in Chapter III. The carbon-bond mechanism results are presented in Figures IV-18 through IV-39.

3. Propylene/Butane/NO_x Systems

This series of experiments performed at UCR combined high activity and high hydrocarbon concentrations. Therefore, the reaction of OH· with NO_2, which is the main radical sink in the butane system, is not as important in these experiments. Instead, radical-radical reactions are more important as radical sinks:

$$HO_2^{\cdot} + HO_2^{\cdot} \rightarrow H_2O_2 \quad ,$$

$$HO_2^{\cdot} + RO_2^{\cdot} \rightarrow \text{Products} \quad ,$$

$$HO_2^{\cdot} + HCO_3^{\cdot} \rightarrow \text{Products} \quad .$$

We found that removing these reactions from the mechanism produced substantial differences between predictions and measurements. In other series of experiments, the removal of such reactions had little effect. Other radical-radical reactions are:

$$RO_2^{\cdot} + RO_2^{\cdot} \rightarrow ALD + ALD + HO_2^{\cdot} + HO_2^{\cdot} \quad ,$$

$$HCO_3^{\cdot} + HCO_3^{\cdot} \rightarrow CO_2 + CO_2 + HO_2^{\cdot} + HO_2^{\cdot} \quad ,$$

$$HCO_3^{\cdot} + RO_2^{\cdot} \rightarrow CO_2 + ALD + HO_2^{\cdot} + HO_2^{\cdot} \quad .$$

The use of such reactions in a large airshed model would cause considerable computational problems in solving the steady-state equations for radical concentrations (Reynolds, 1976). We felt that the propylene/butane experiments would be most appropriate for testing whether these last three

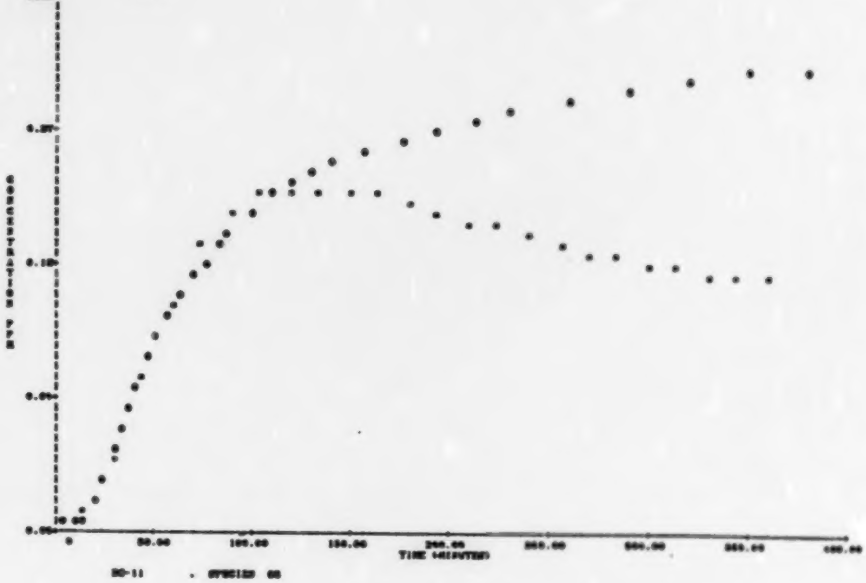

FIGURE IV-18

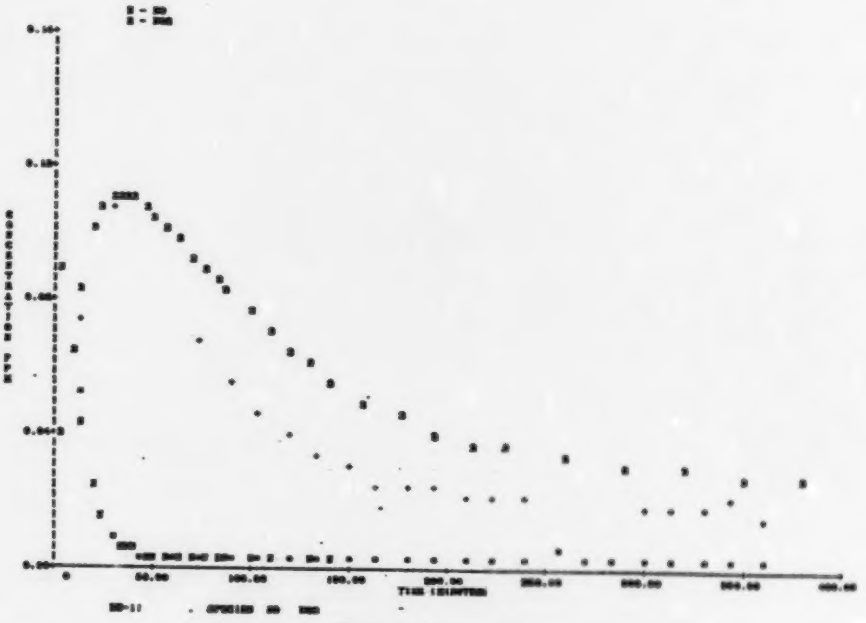

FIGURE IV-19

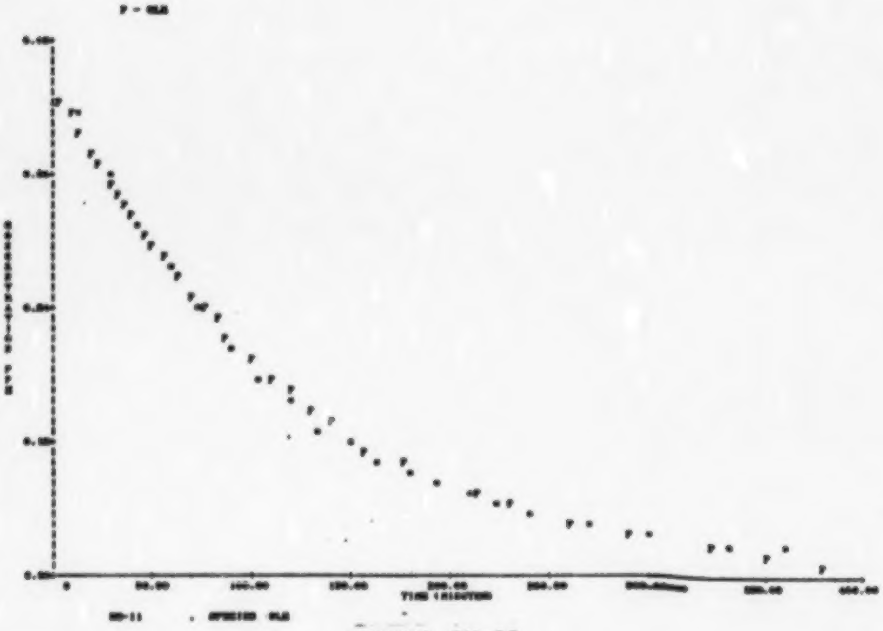

FIGURE IV-20

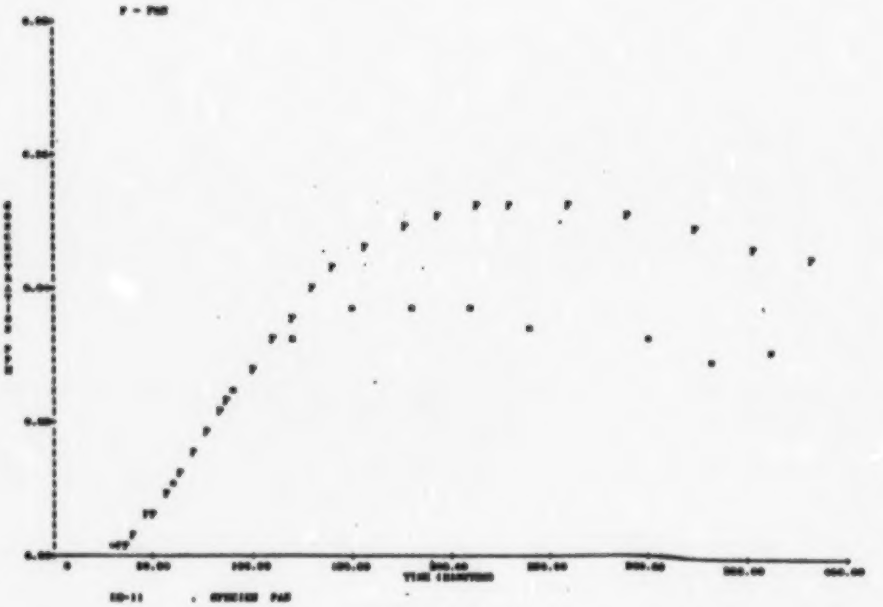

FIGURE IV-21

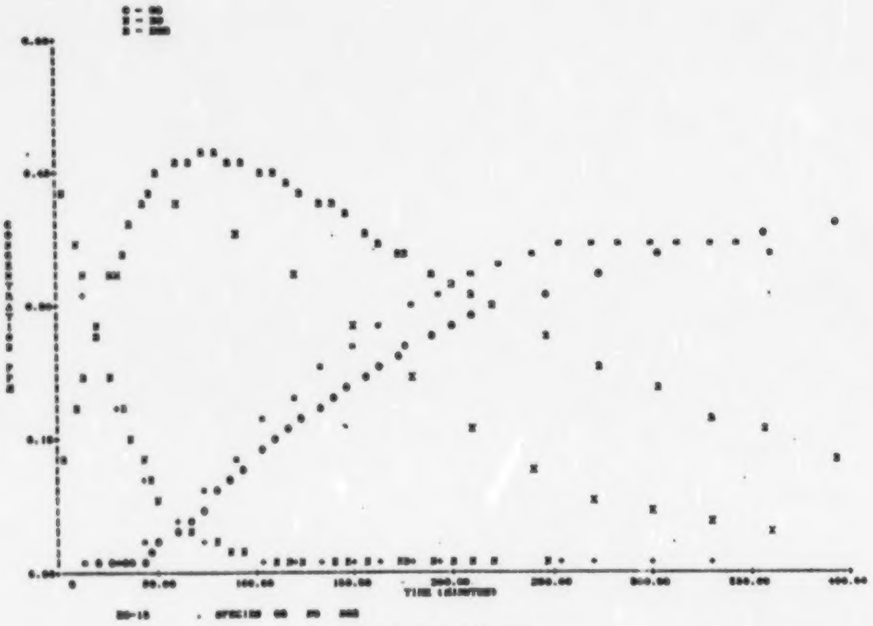

FIGURE IV-22

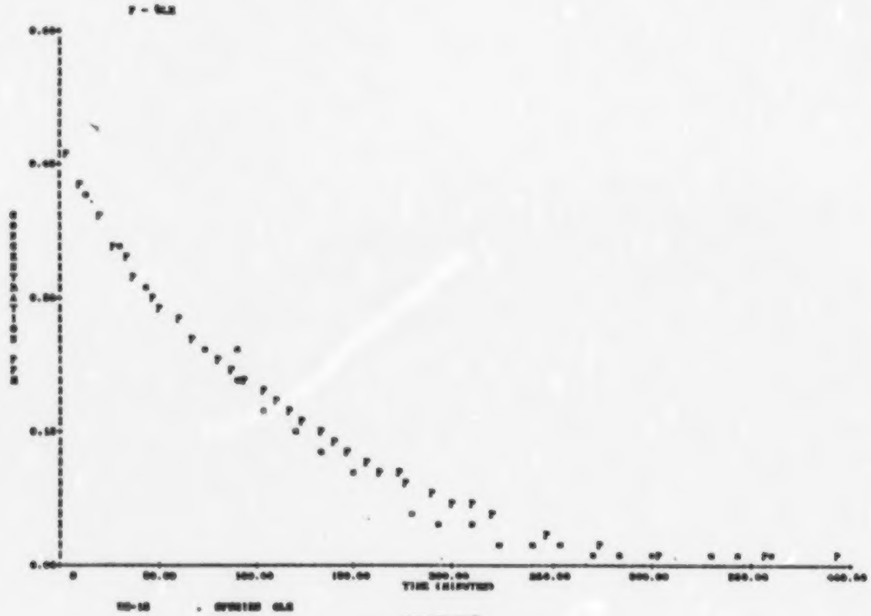

FIGURE IV-23

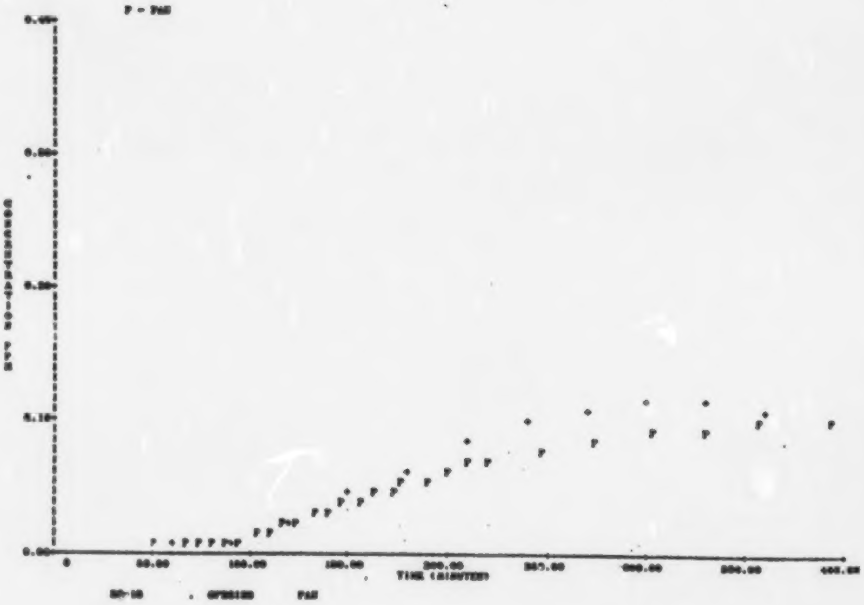
P - PAN
0.40
0.30
0.20
0.10
0.00
0
50.00
100.00
150.00
200.00
250.00
300.00
350.00
400.00
TIME (MINUTES)

FIGURE IV-24

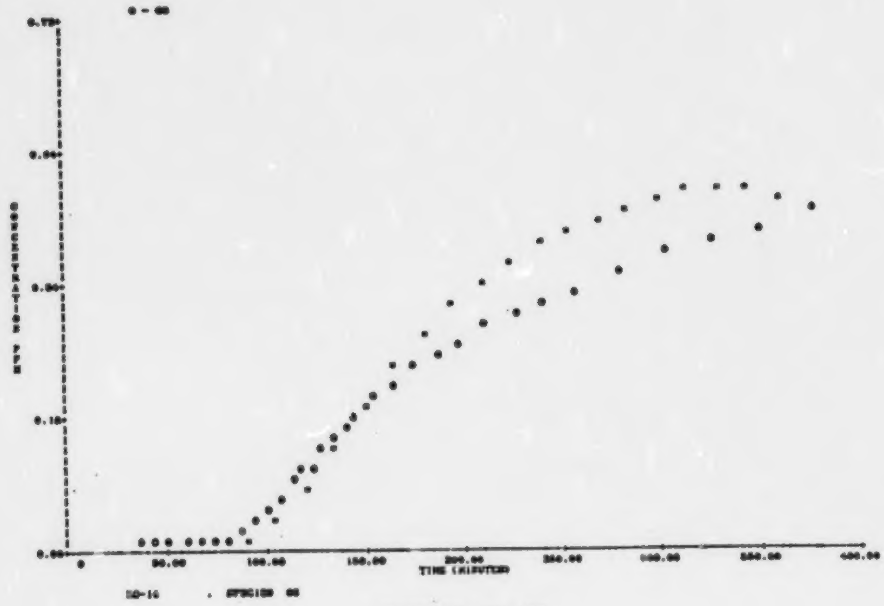

FIGURE IV-25

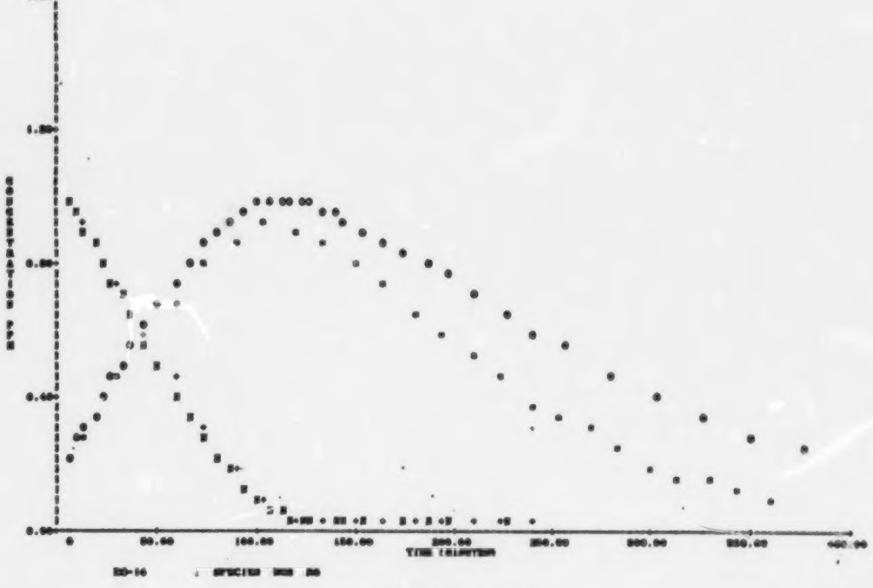

FIGURE IV-26

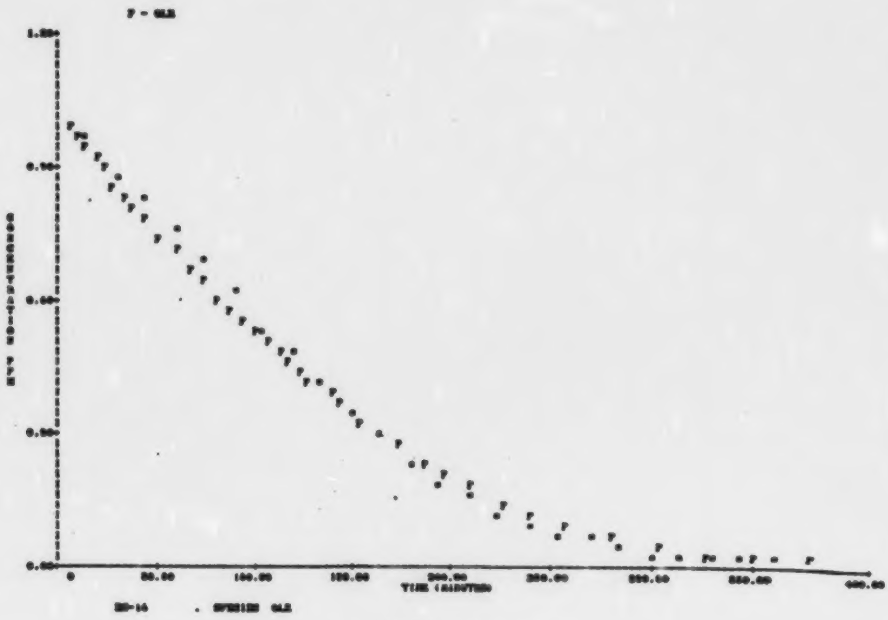

FIGURE IV-27

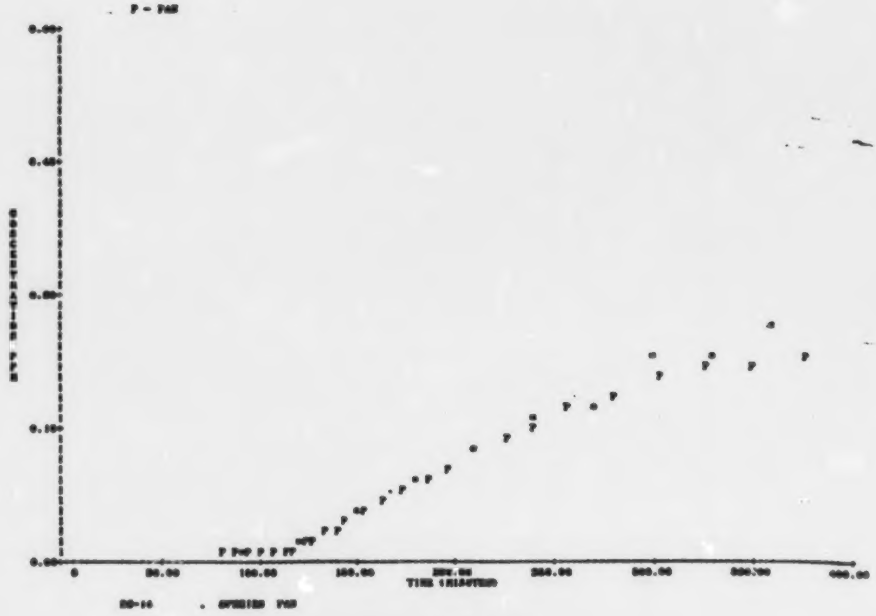

FIGURE IV-28

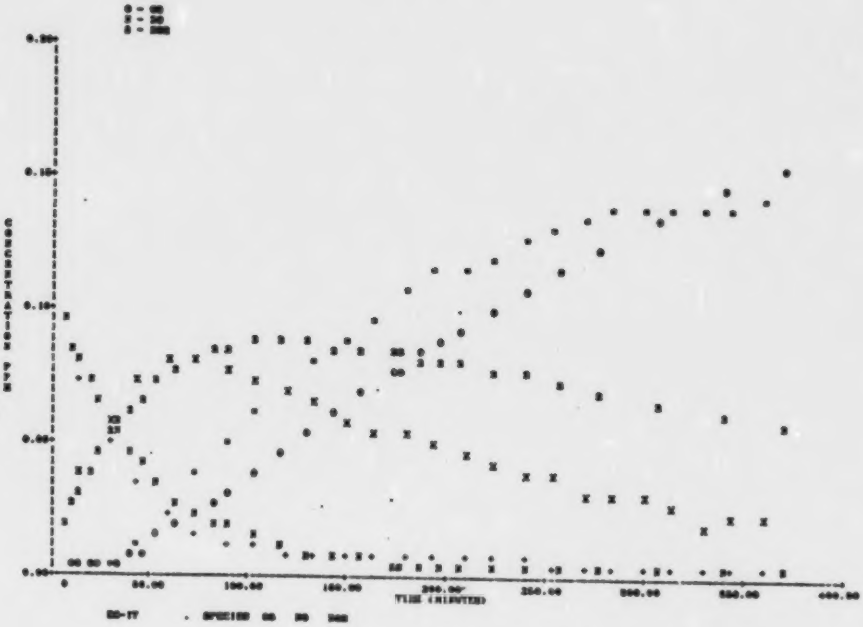

FIGURE IV-29

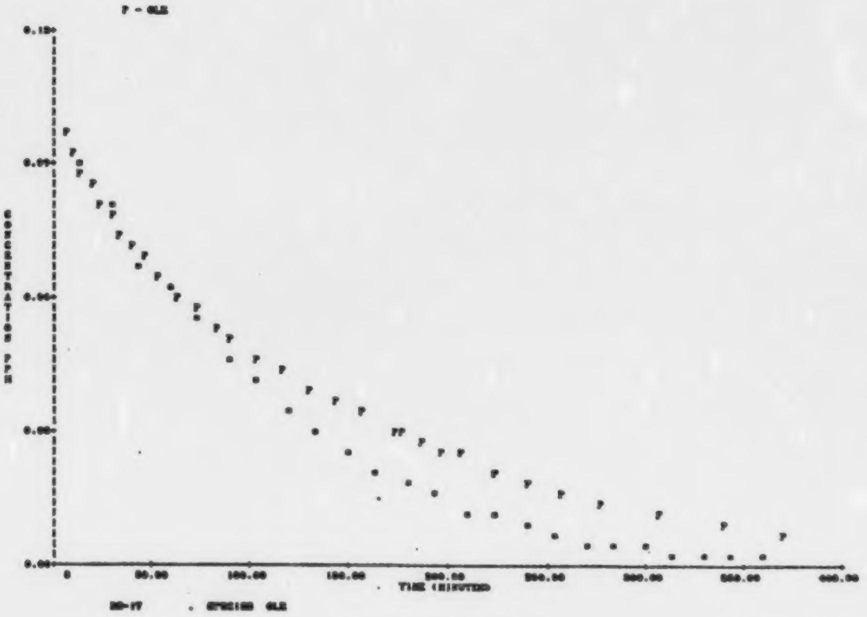

FIGURE IV-30

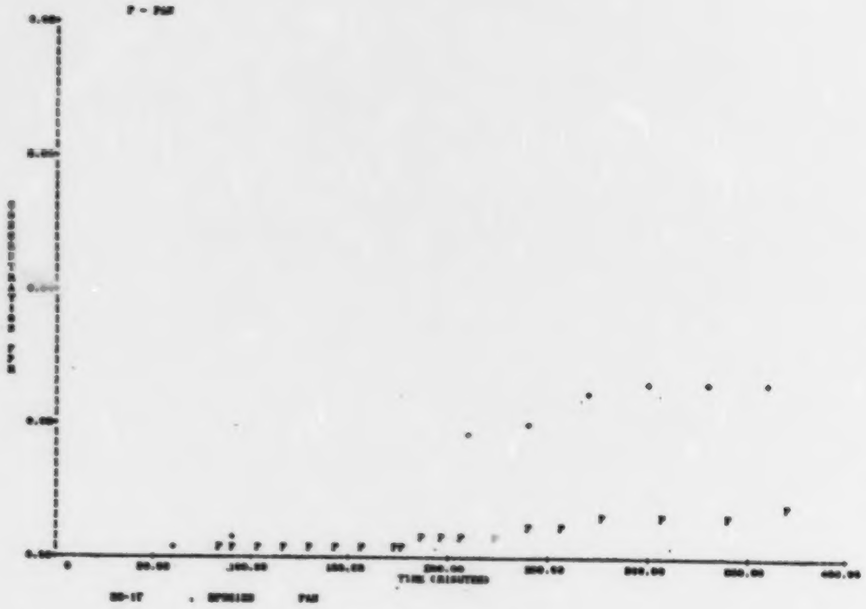
P - PAN
CONCENTRATION PPM
0
50.00
100.00
150.00
200.00
250.00
300.00
350.00
400.00
TIME (MINUTES)

FIGURE IV-31

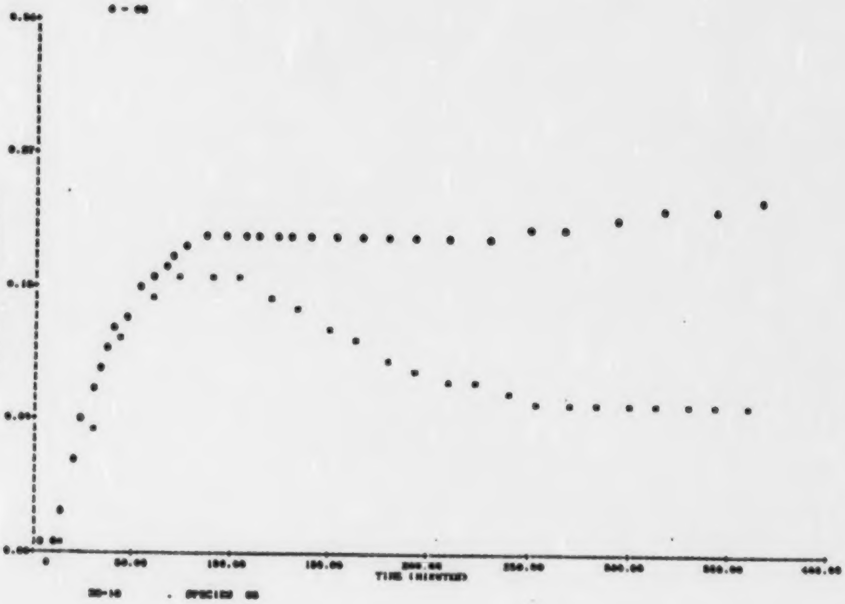

FIGURE IV-32

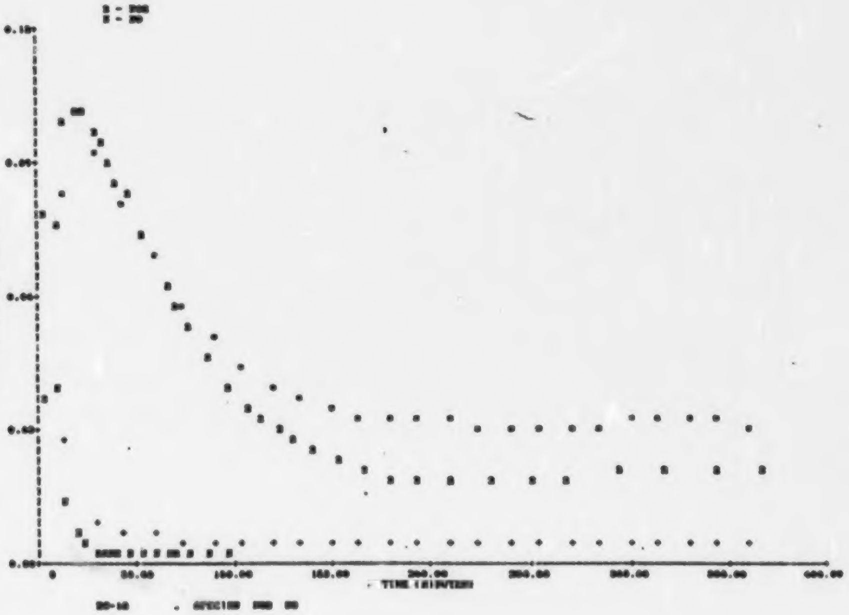

FIGURE IV-33

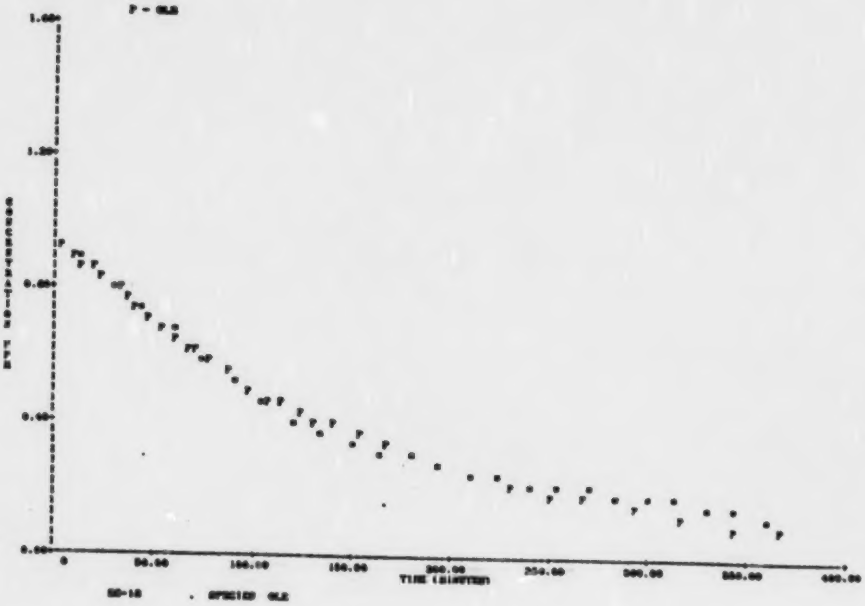

FIGURE IV-34

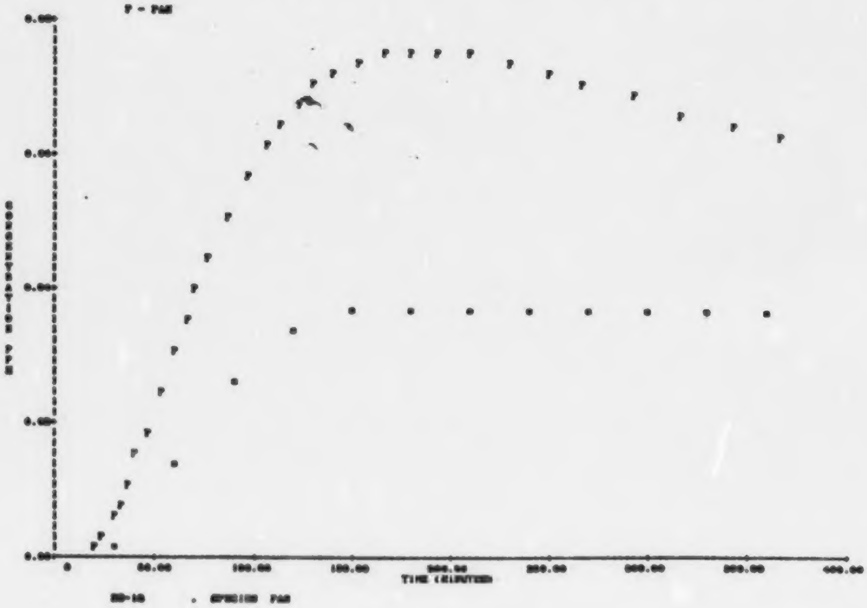

FIGURE IV-35

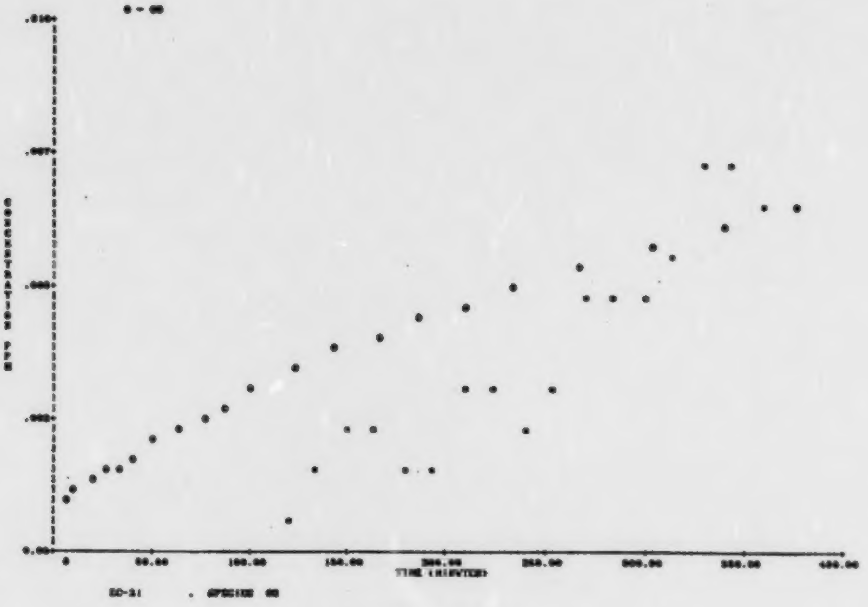

FIGURE IV-36

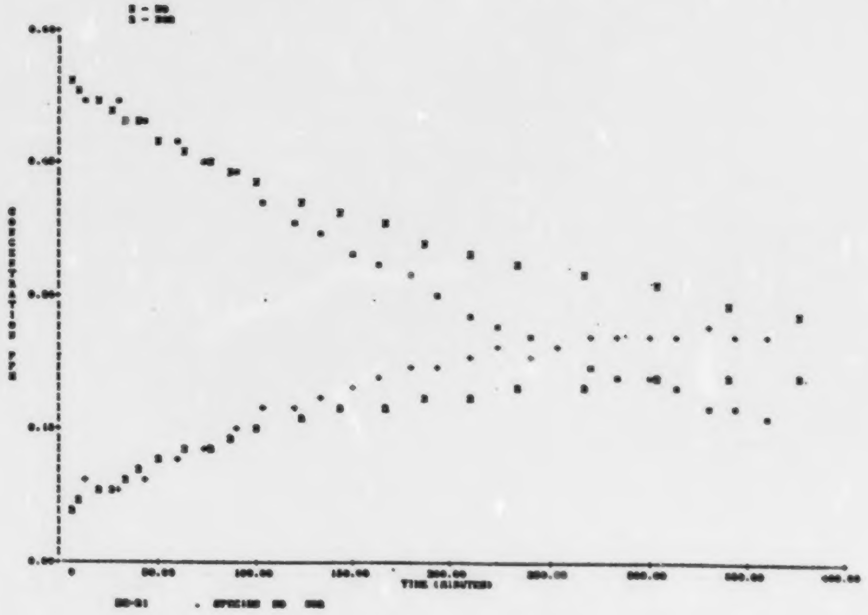

FIGURE IV-37

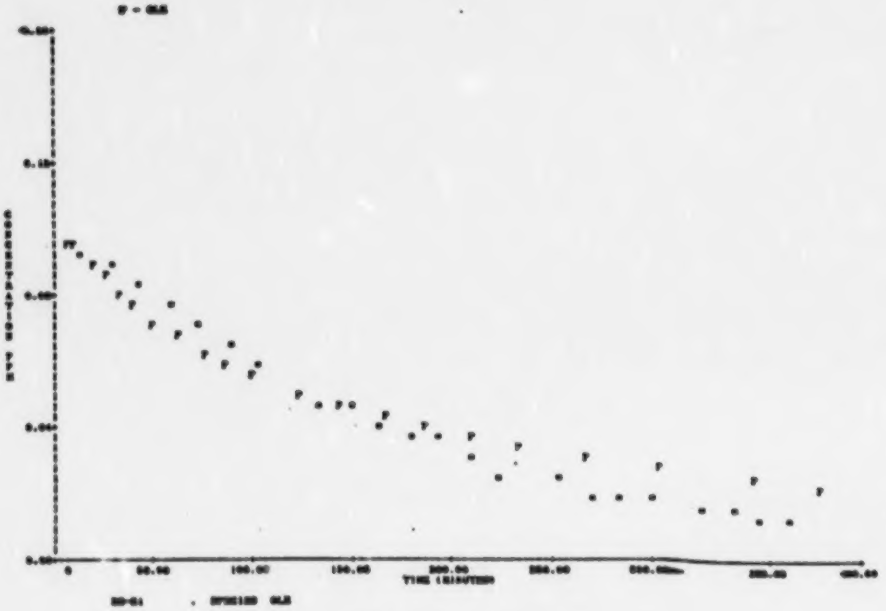

FIGURE IV-38

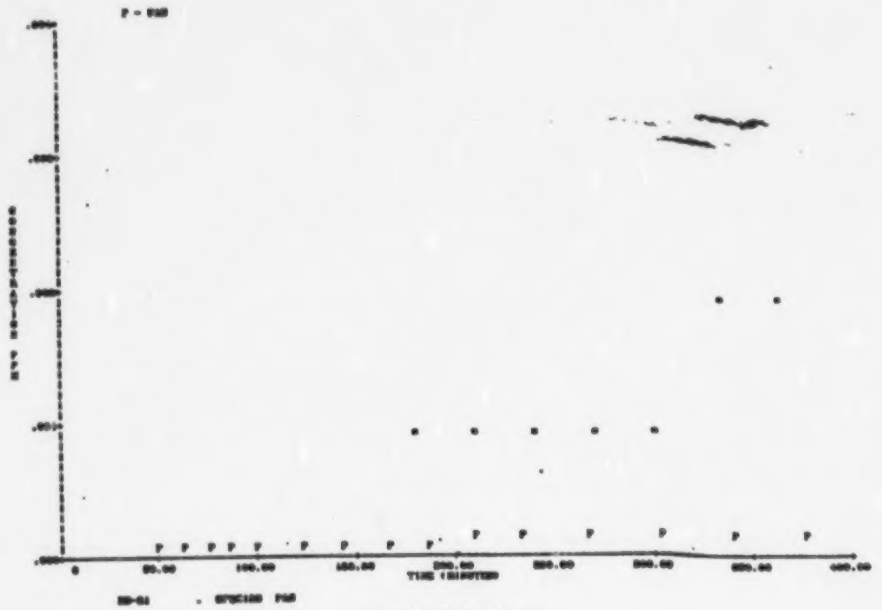

FIGURE IV-39

reactions must be included in the kinetic mechanism. We found that removing them had no noticeable effect on predictions. They are not included in the carbon-bond mechanism. Figures IV-40 through IV-60 show the predictions and measurements for the propylene/butane series of experiments.

One disturbing aspect of the carbon-bond mechanism simulations for this set of experiments was that we had to lower the carbonyl photolysis constant to 3×10^{-4} min^{-1} for radical production to produce the simulations shown. The calculated value from the explicit mechanisms was 7.2×10^{-4} min^{-1}, yet the use of this value produced too many maintenance radicals in the simulations. During the coming year, we hope to elucidate the reasons for this discrepancy.

4. 1-Butene/NO_x Systems

As discussed in Chapter III, three experiments using 1-butene performed at UCR gave us an opportunity to check the olefin chemistry by extending the propylene chemistry to 1-butene. For the results shown in Figures IV-61 through IV-69 using the carbon-bond mechanism, we changed only the OH reaction with double bonds to the value for 1-butene of 4.8×10^4 ppm^{-1} min^{-1}.

5. Toluene/NO_x Systems

Since there is no explicit mechanism to account for the complete oxidation of toluene carbon atoms, we did not have the explicit mechanism as a basis for photolysis rates or initial nitrous acid values. An overall carbonyl photolysis constant of 2×10^{-4} min^{-1} was chosen to be consistent with the low NO_2 photolysis of 0.16 min^{-1} reported by UCR and the deterioration of the solar simulator that we assumed for the EC-50 to EC-60 series. For simplicity we did not include a carbonyl photolysis to stable products. The results are presented in Figures IV-70 through IV-92.

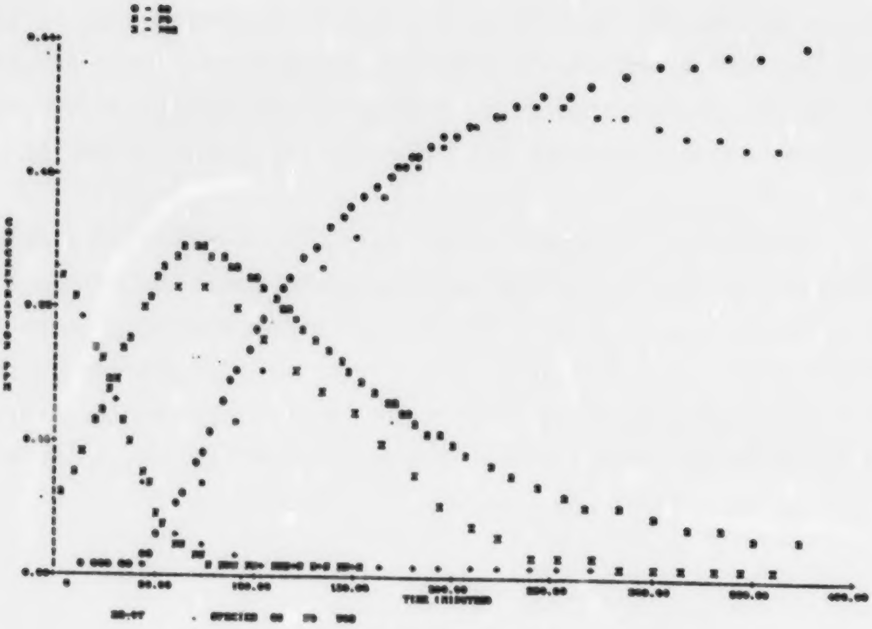

FIGURE IV-40

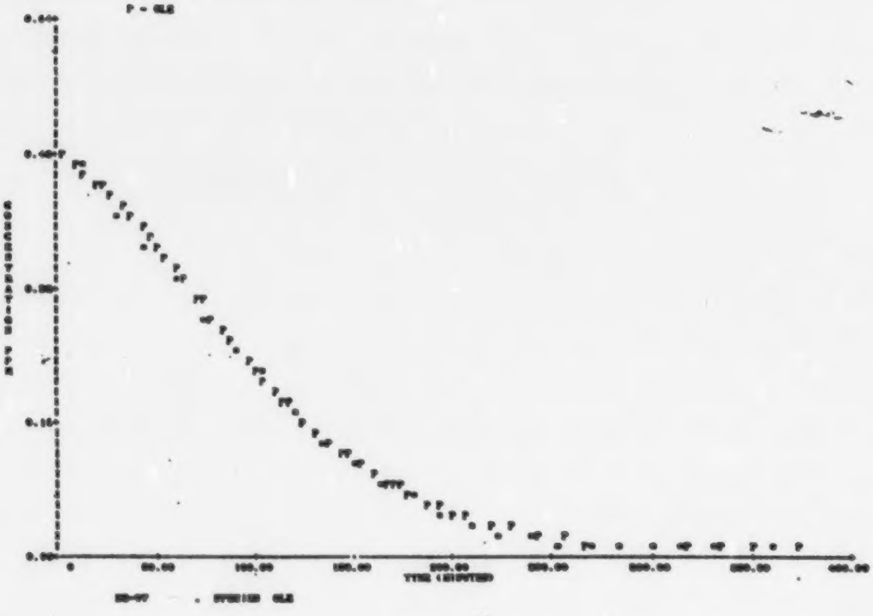

FIGURE IV-41

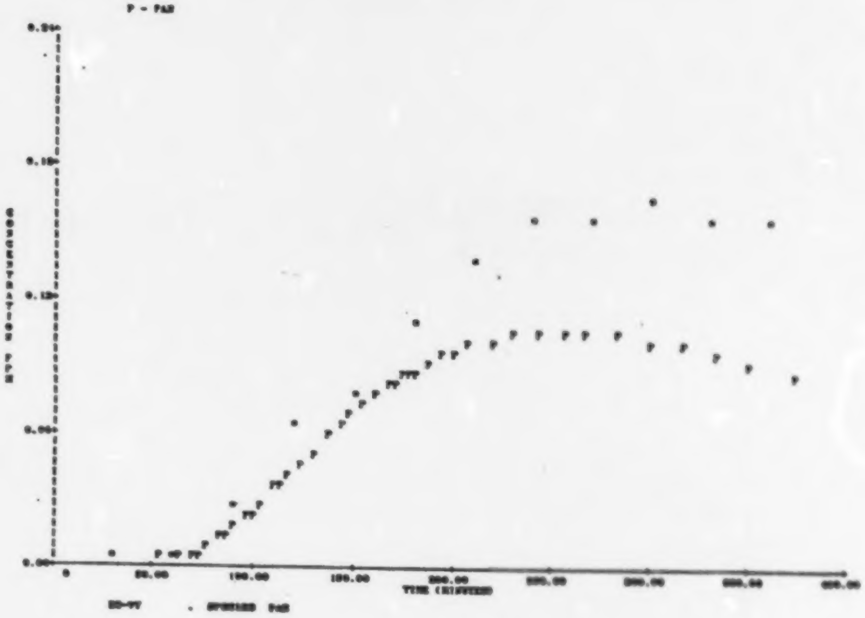
P - PAN
0.24
0.18
0.12
0.06
0.00
0
50.00
100.00
150.00
200.00
250.00
300.00
350.00
400.00
TIME (MINUTES)
* OBSERVED PAN

FIGURE IV-42

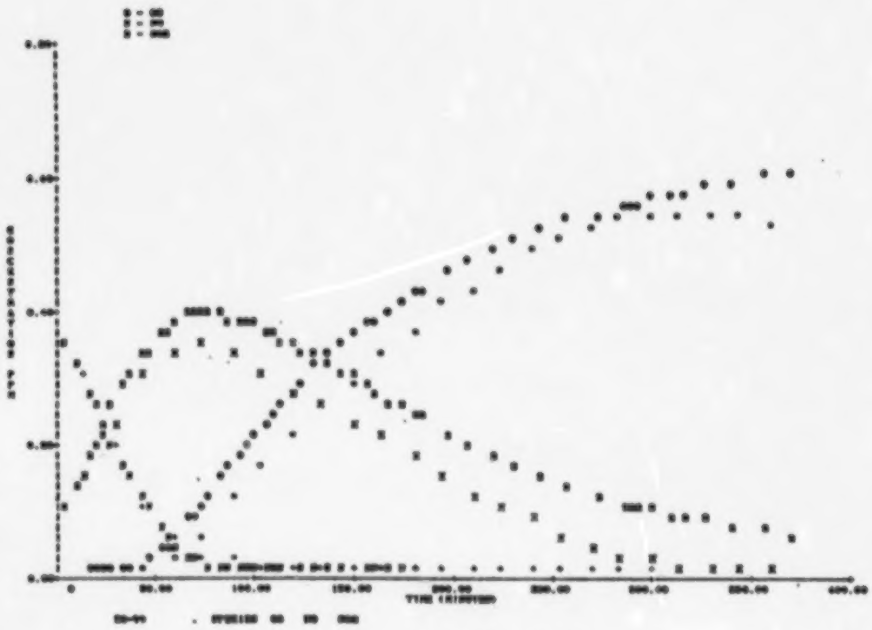

FIGURE IV-43

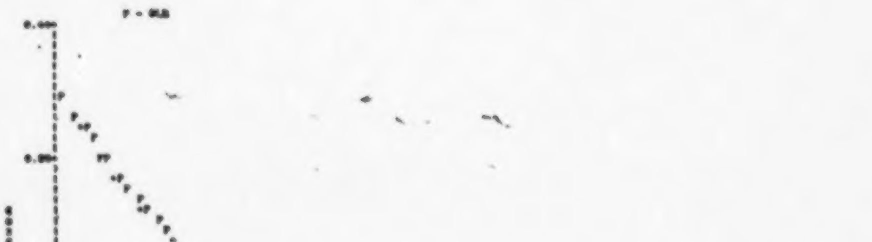

FIGURE IV-44

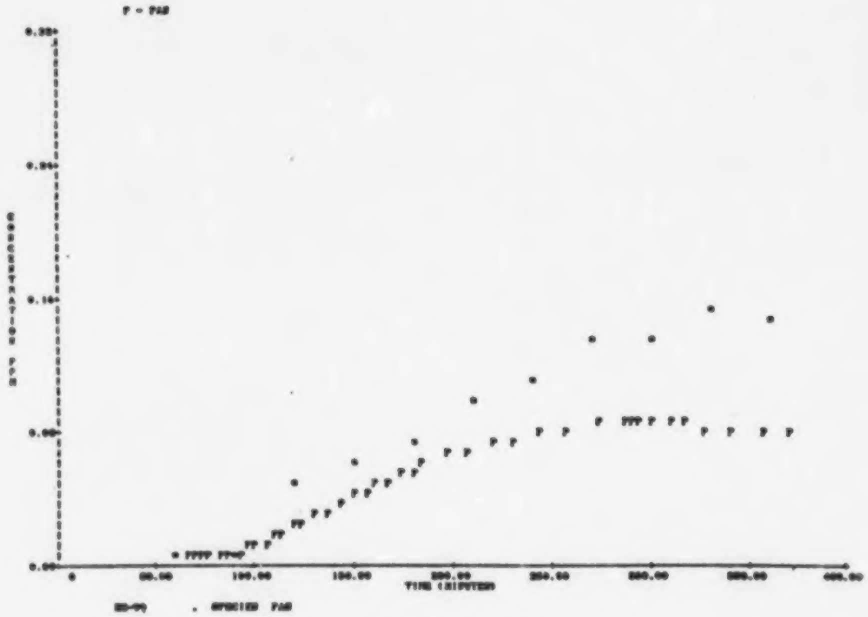
F - PAN
0.20
0.15
0.10
0.05
0.00
CONCENTRATION PPM
0
50.00
100.00
150.00
200.00
250.00
300.00
350.00
400.00
TIME (MINUTES)
. SPECIES PAN

FIGURE IV-45

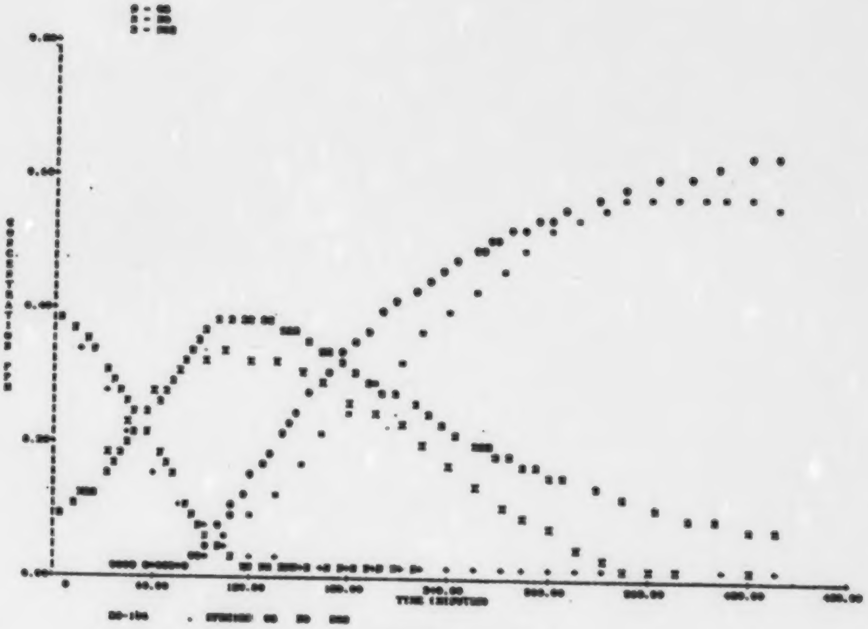

FIGURE IV-46

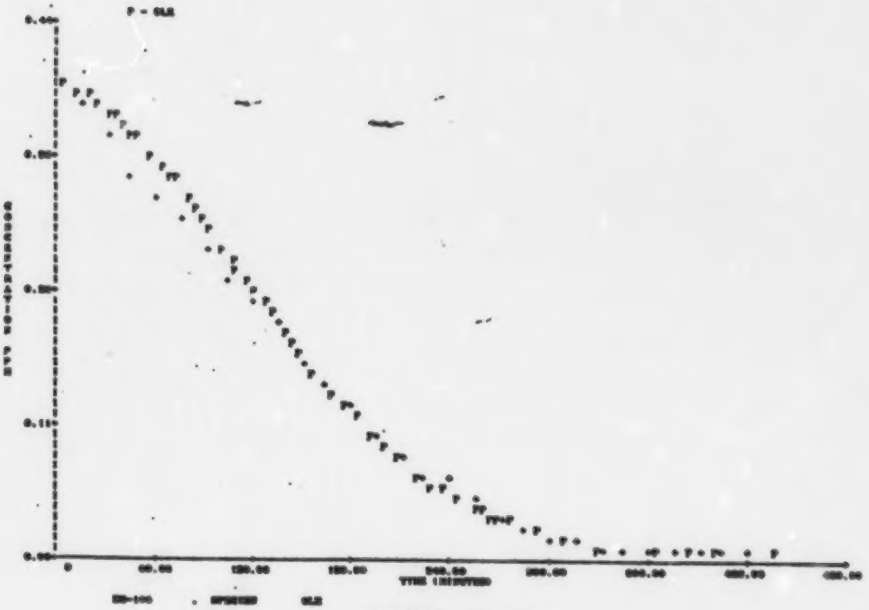

FIGURE IV-47

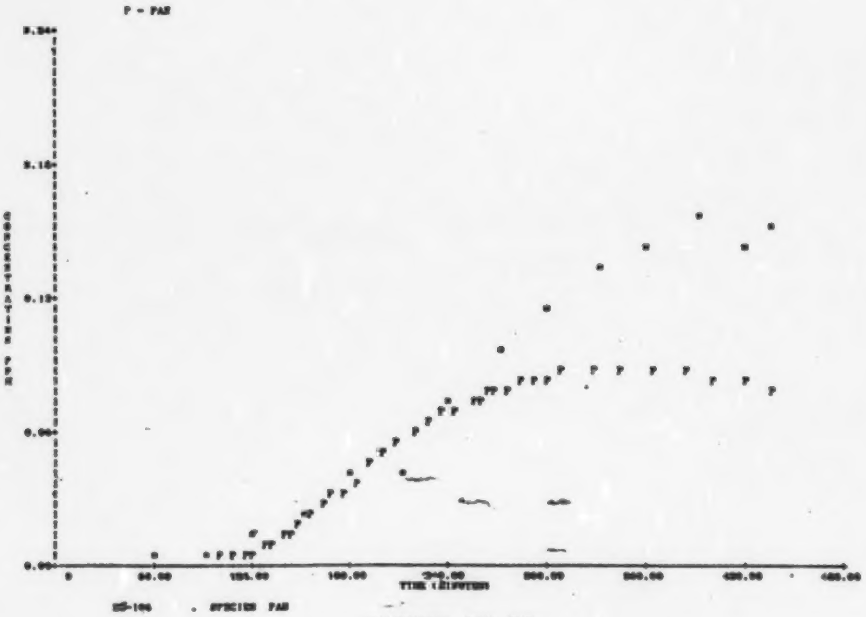
P - PAN
0.24
0.18
0.12
0.06
0.00
CONCENTRATION PPM
0
60.00
120.00
180.00
240.00
300.00
360.00
420.00
480.00
TIME (MINUTES)
EC-106
. SPECIES PAN

FIGURE IV-48

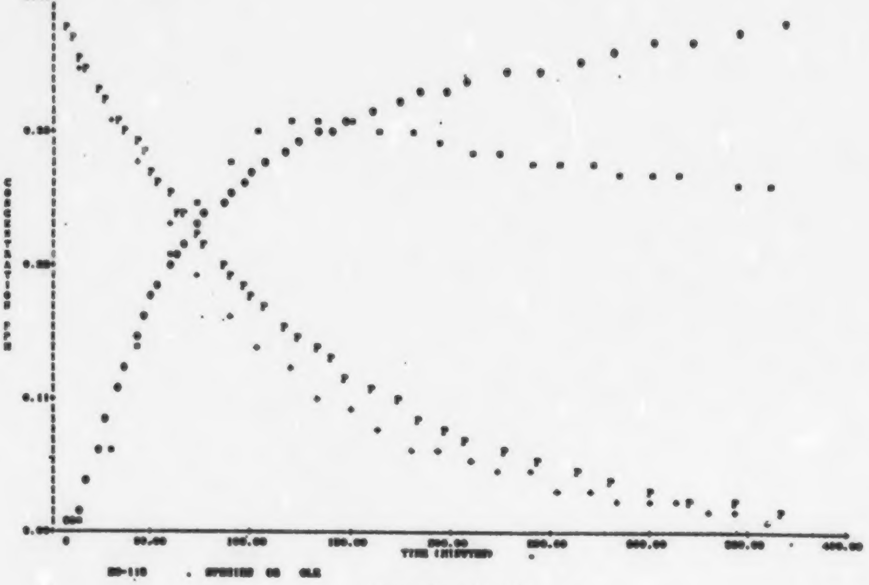

FIGURE IV-49

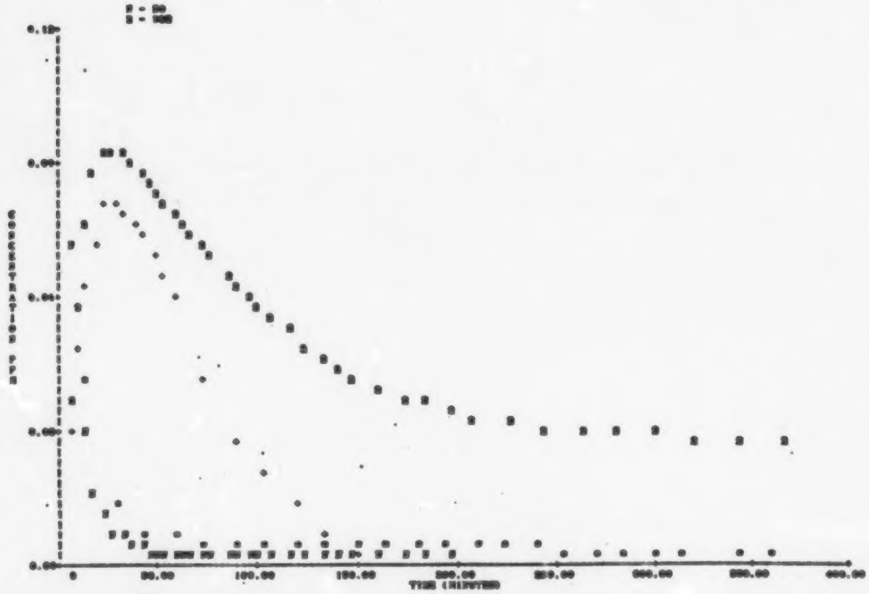

FIGURE IV-50

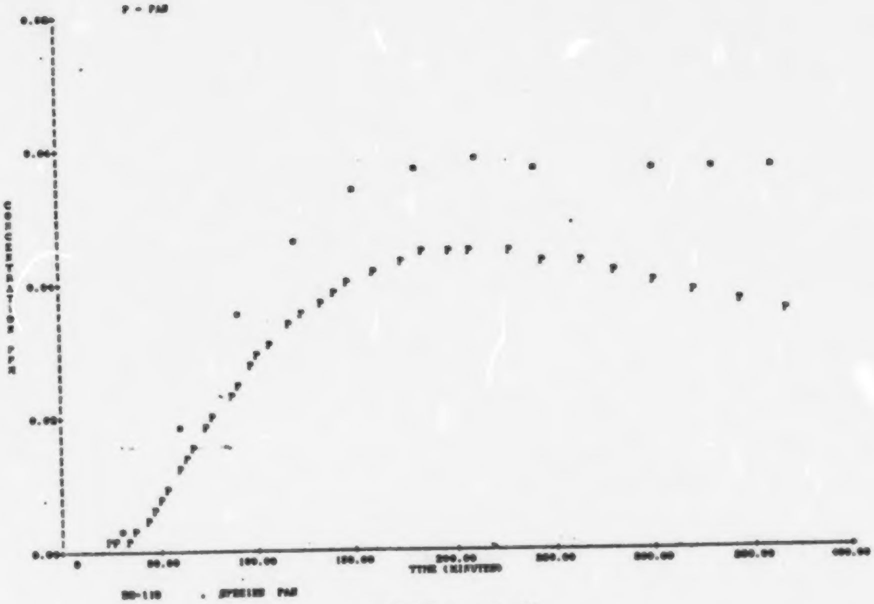
P - PAN
CONCENTRATION PPM
0.00
0
50.00
100.00
150.00
200.00
TIME (MINUTES)
250.00
300.00
350.00
400.00
. SPECIES PAN

FIGURE IV-51

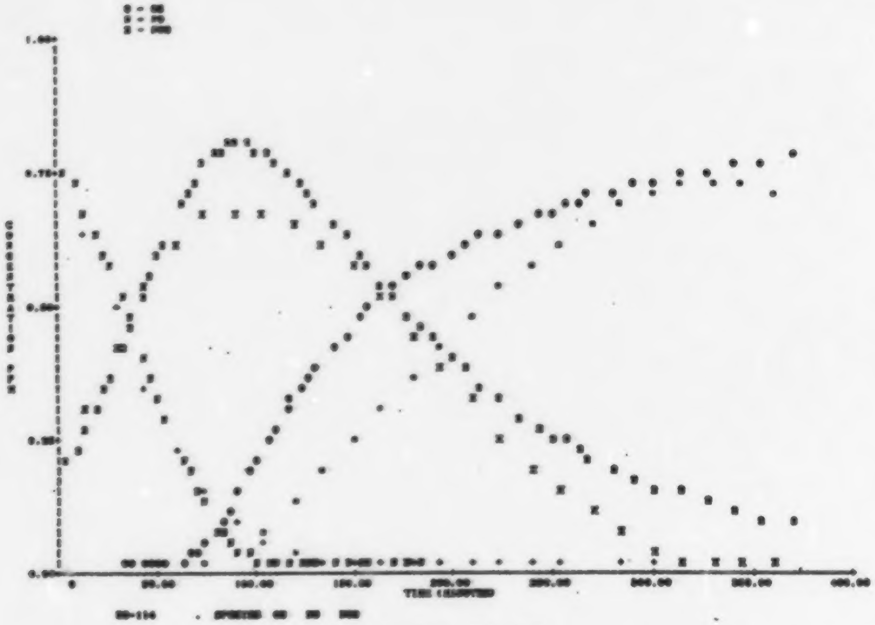

FIGURE IV-52

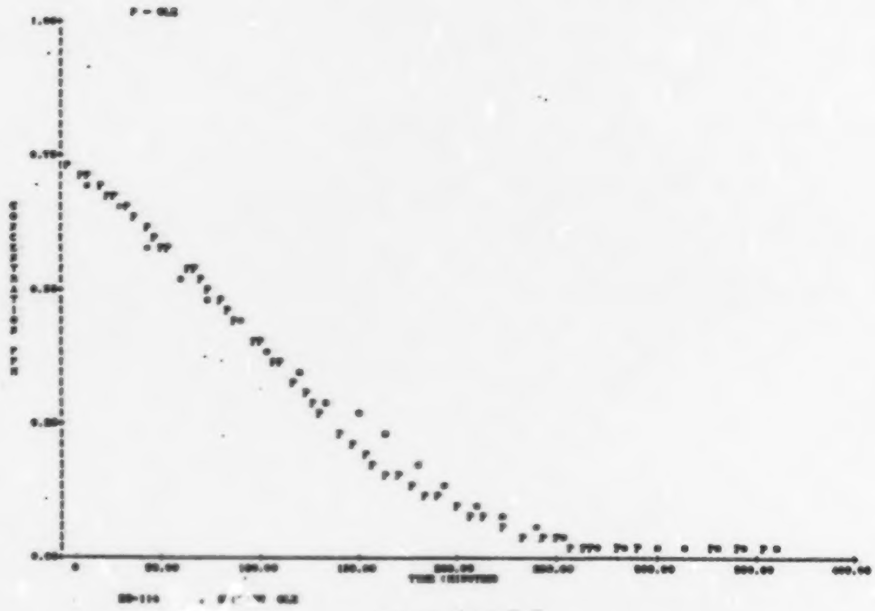

FIGURE IV-53

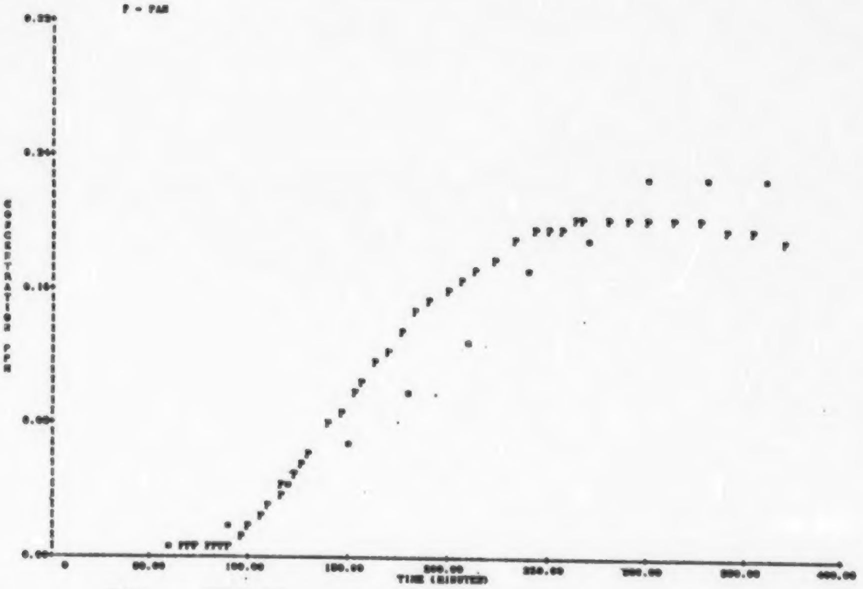
P - PAN
CONCENTRATION PPM
0.00
0
50.00
100.00
150.00
200.00
250.00
300.00
350.00
400.00
TIME (MINUTES)
SPECIES PAN

FIGURE IV-54

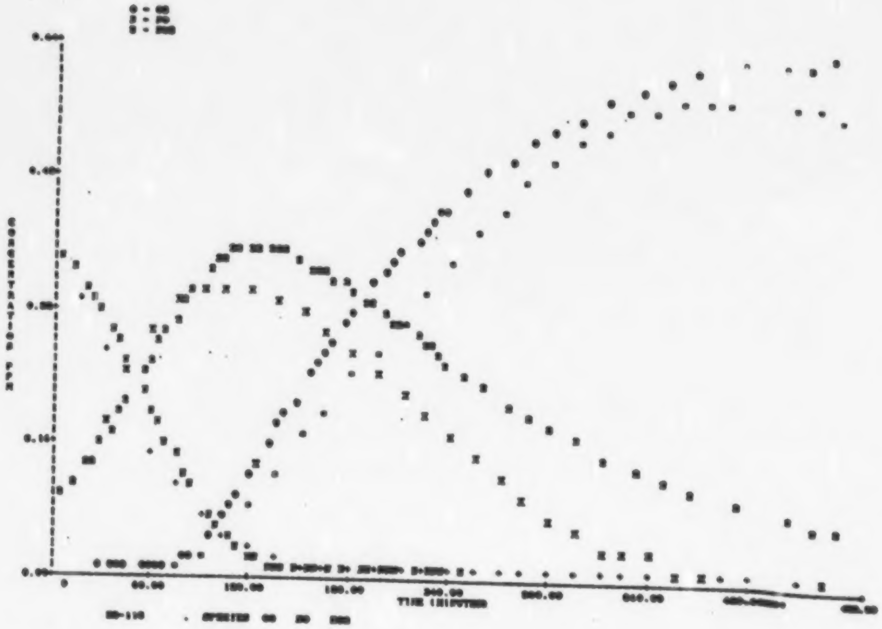

FIGURE IV-55

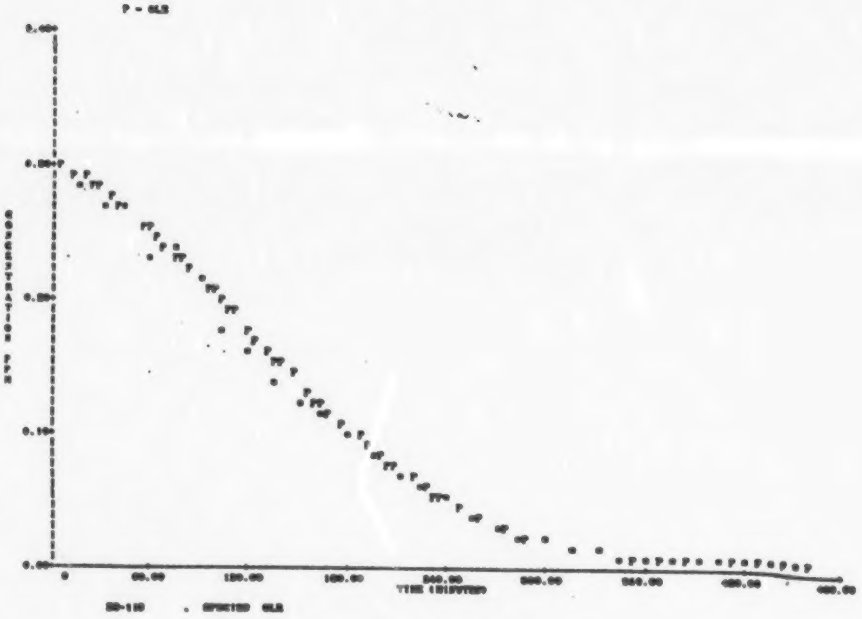

FIGURE IV-56

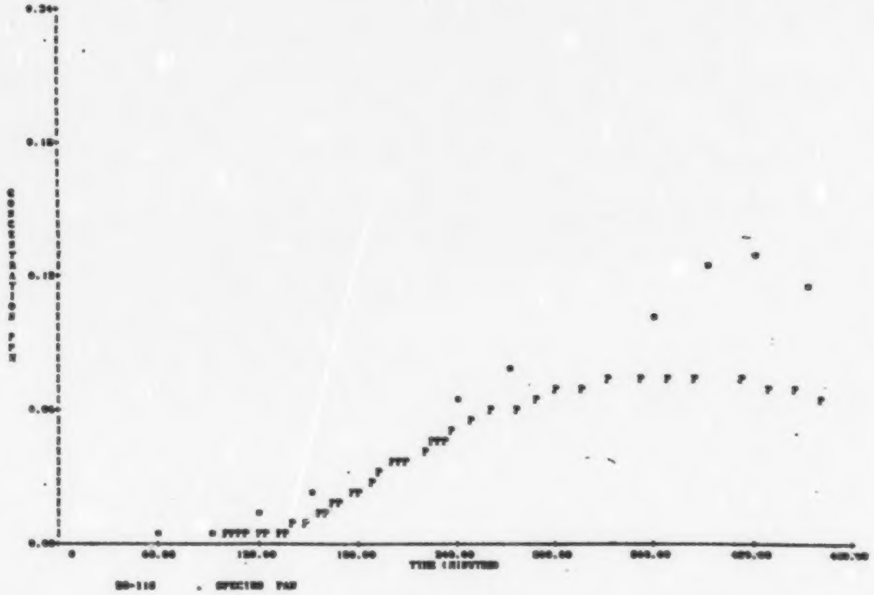
P - PAN
0.24
0.18
0.12
0.06
0.00
CONCENTRATION PPM
0
60.00
120.00
180.00
240.00
300.00
360.00
420.00
480.00
TIME (MINUTES)
EC-115 . SPECIES PAN

FIGURE IV-57

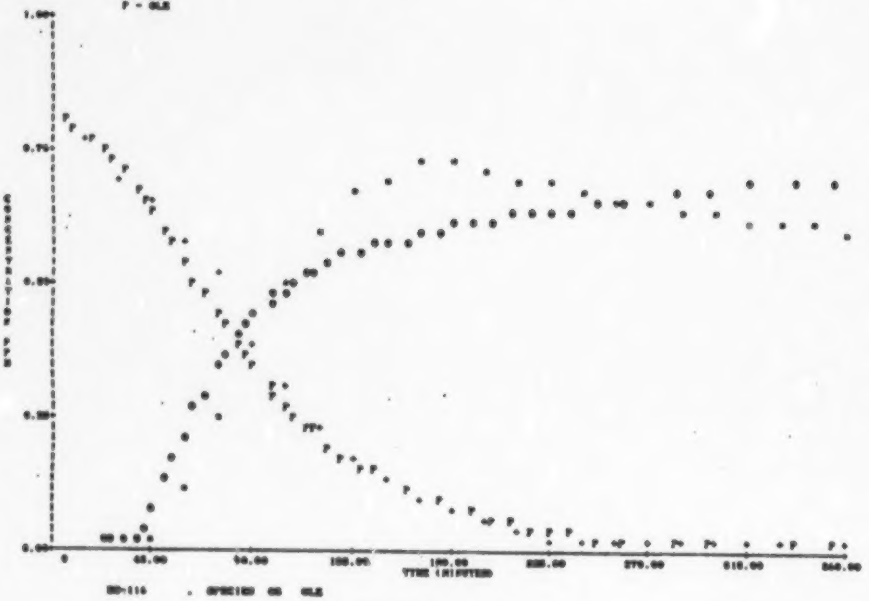

FIGURE IV-58

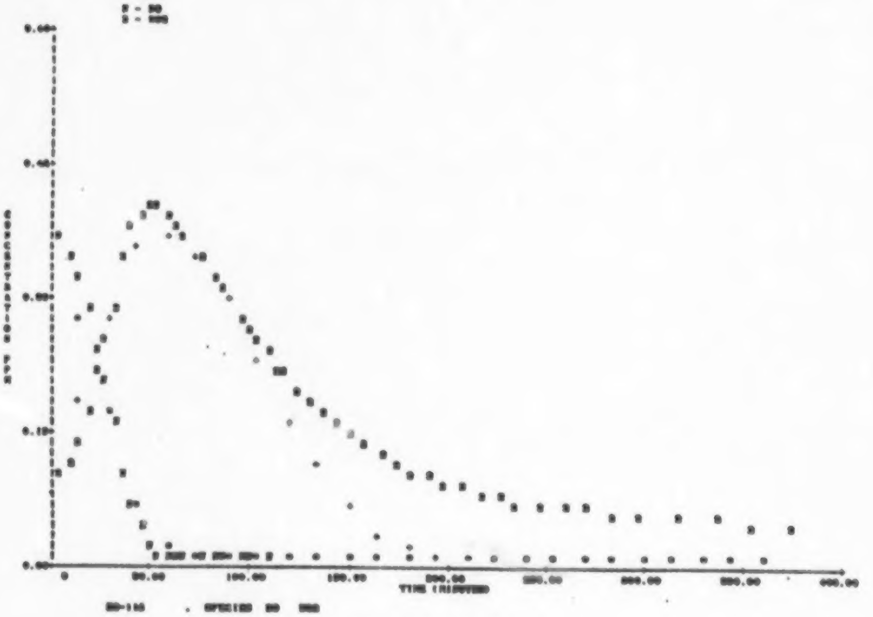

FIGURE IV-59

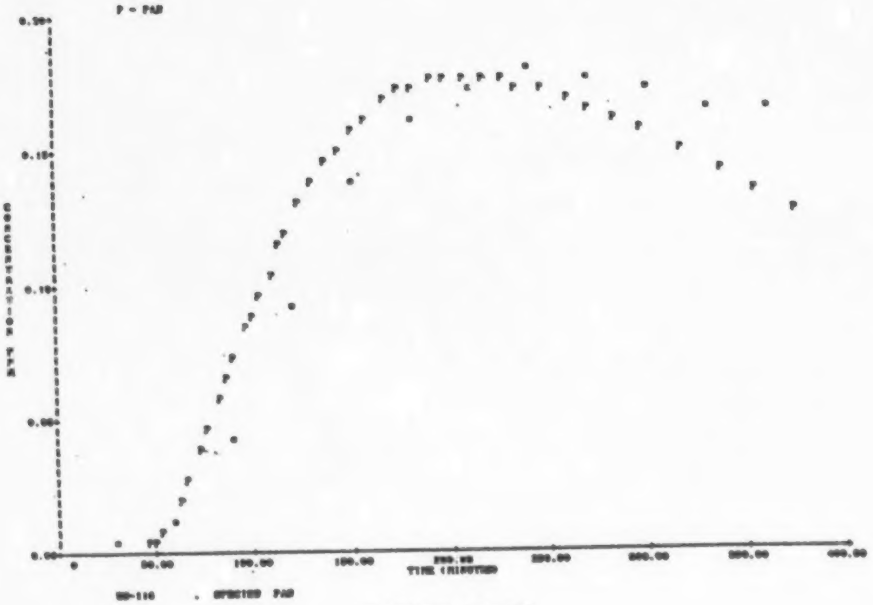
P = PAN
0.20
0.15
0.10
0.05
0.00
CONCENTRATION PPM
0
50.00
100.00
150.00
200.00
250.00
300.00
350.00
400.00
TIME (MINUTES)
. SPECIES PAN

FIGURE IV-60

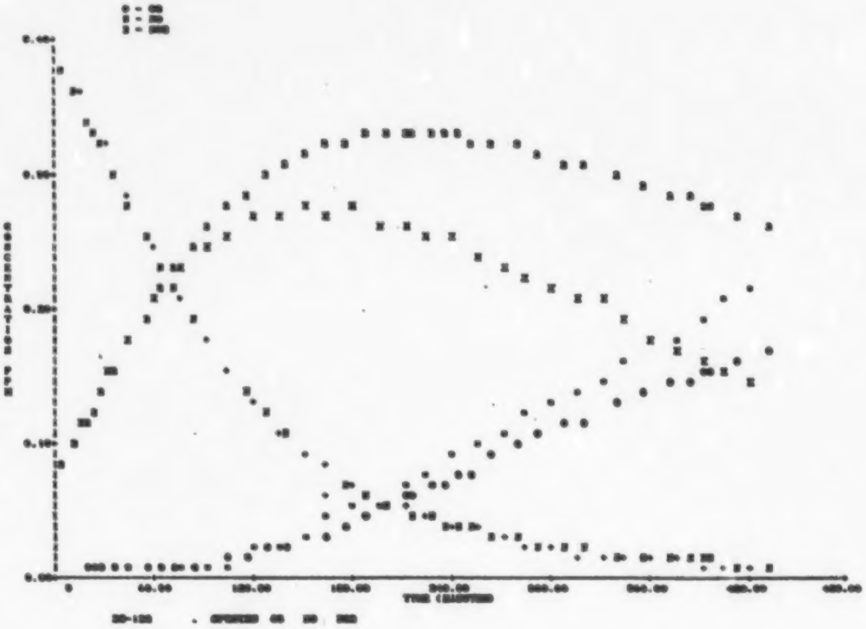

FIGURE IV-61

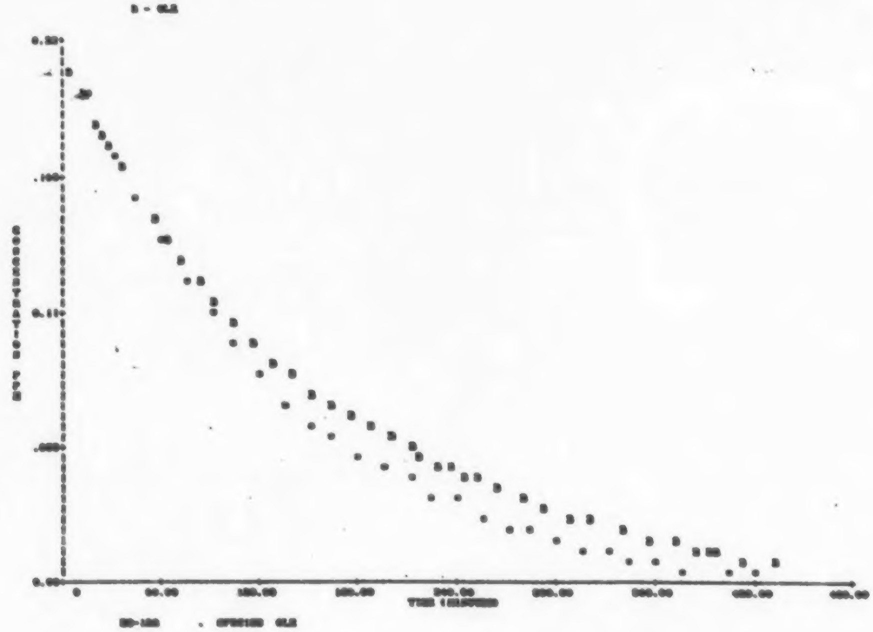

FIGURE IV-62

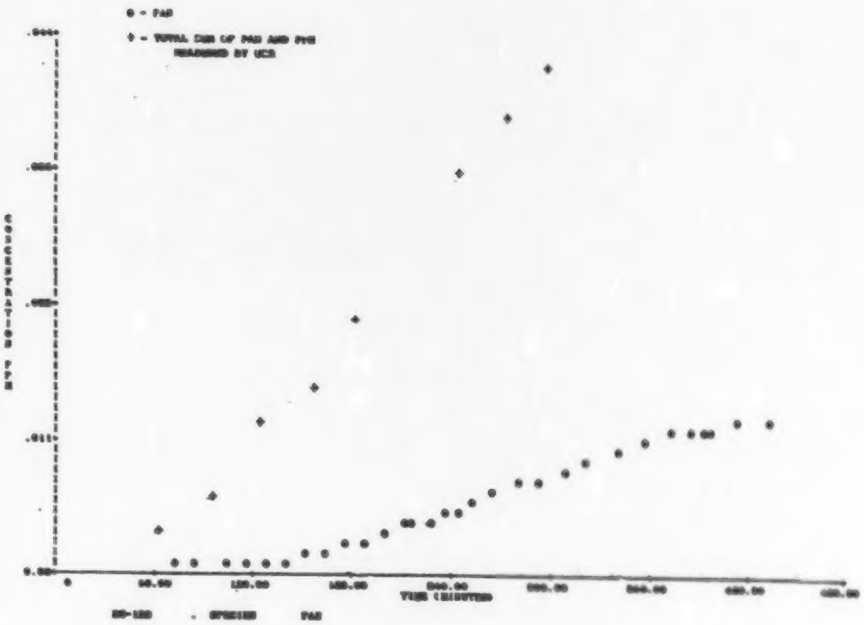
● - PAN
◆ - TOTAL SUM OF PAN AND PPN
MEASURED BY UCR
.044
.033
.022
.011
0.00
CONCENTRATION PPM
0
50.00
100.00
150.00
200.00
250.00
300.00
350.00
400.00
TIME (MINUTES)
EC-128 . SPECIES PAN

FIGURE IV-63

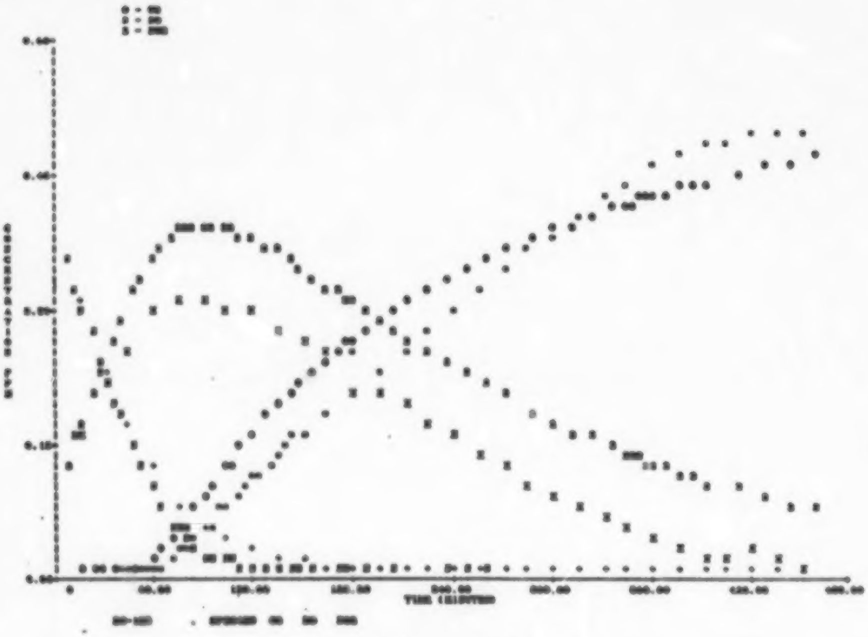

FIGURE IV-64

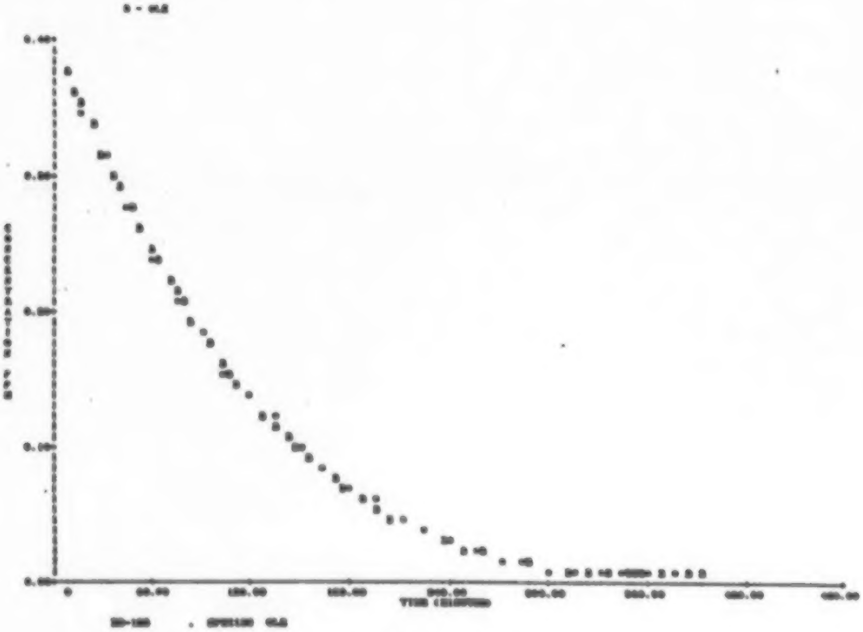

FIGURE IV-65

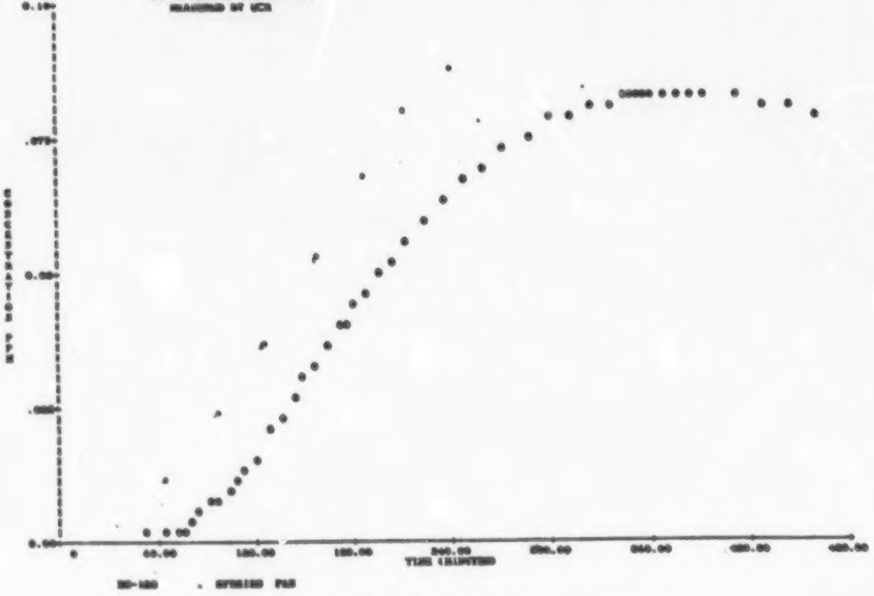
* - TOTAL SUM OF PAN AND PPN
0.10
.075
0.05
.025
0.00
0
60.00
120.00
180.00
240.00
300.00
360.00
420.00
480.00
TIME (MINUTES)

FIGURE IV-66

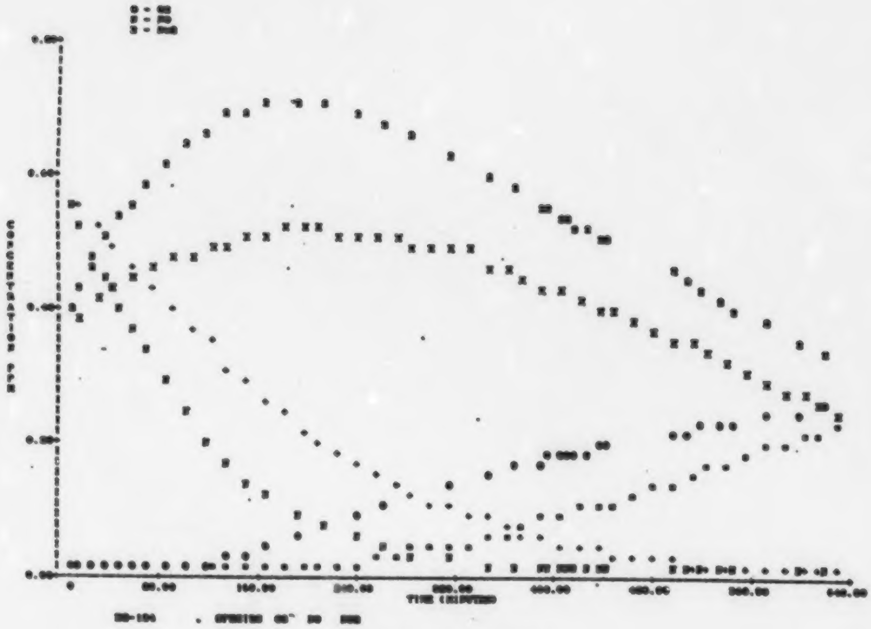

FIGURE IV-67

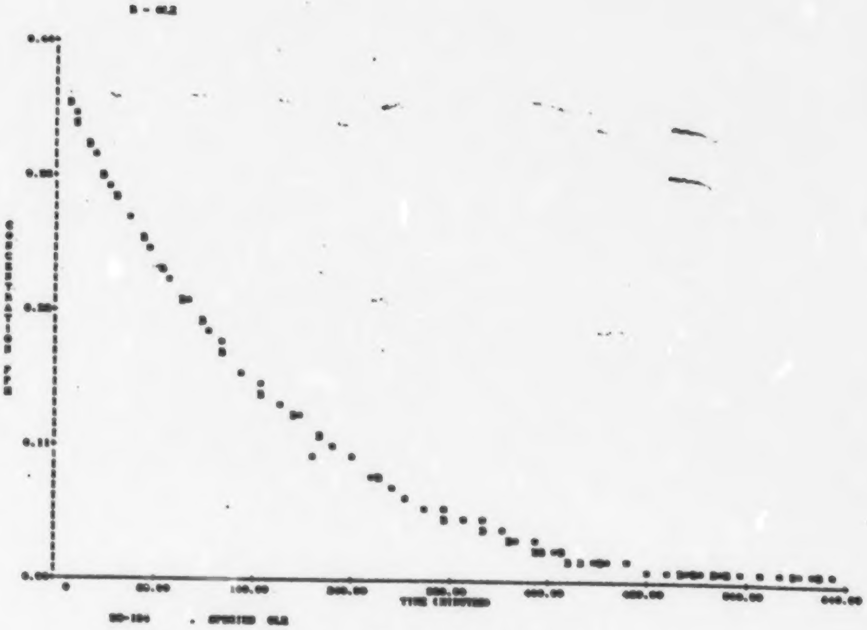

FIGURE IV-68

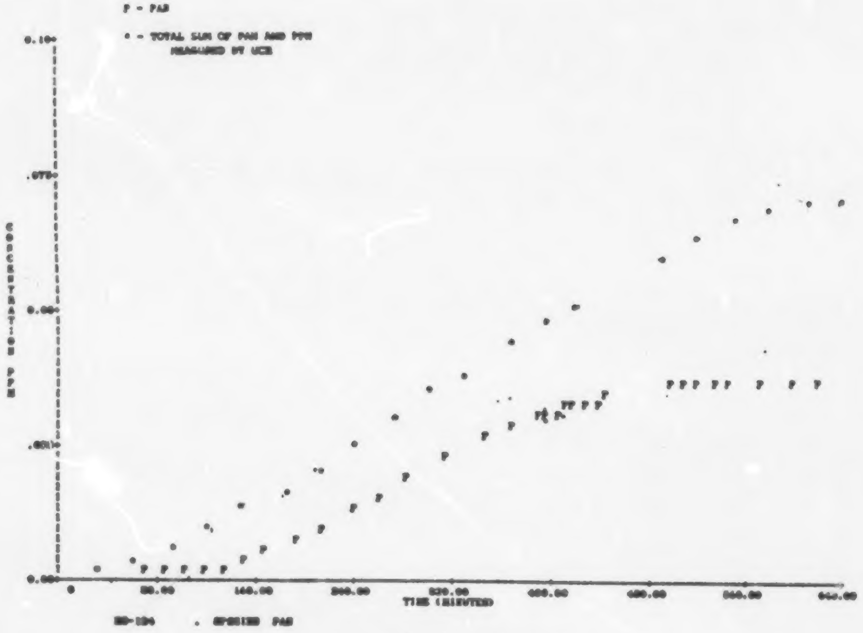
P - PAN
* - TOTAL SUM OF PAN AND PPN MEASURED BY UCR
0.10
.075
0.05
.025
0.00
CONCENTRATION PPM
0
80.00
160.00
240.00
320.00
400.00
480.00
560.00
640.00
TIME (MINUTES)
EC-134
. SPIKED PAN

FIGURE IV-69

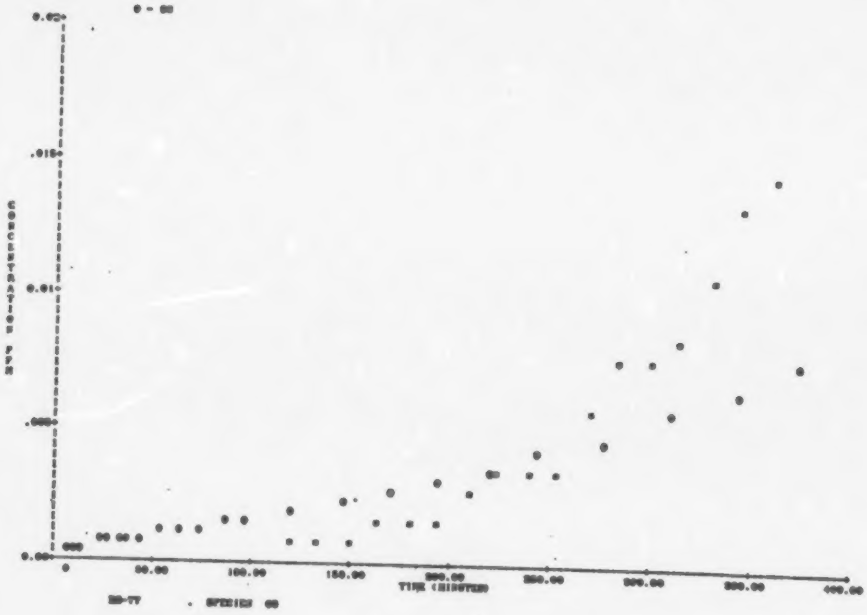

FIGURE IV-70

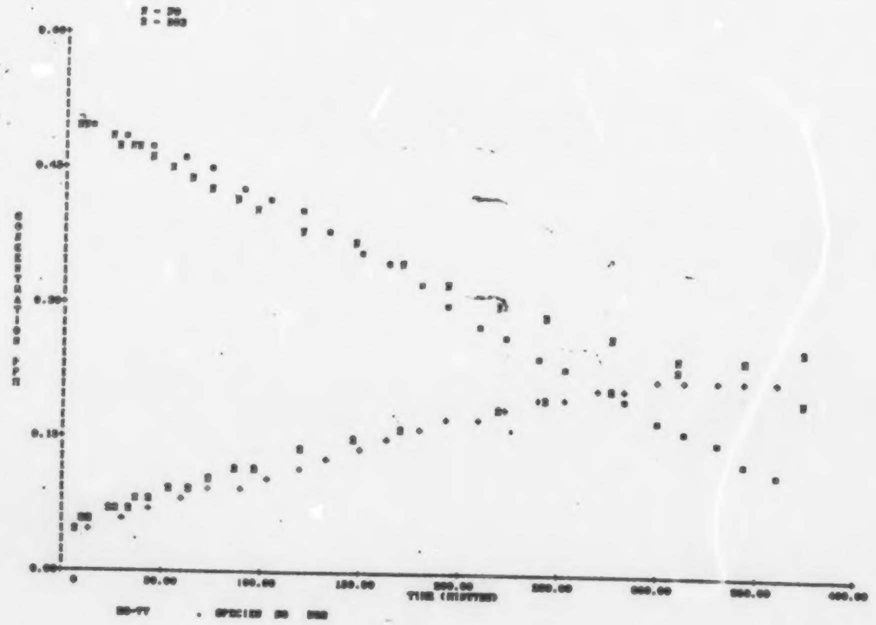

FIGURE IV-71

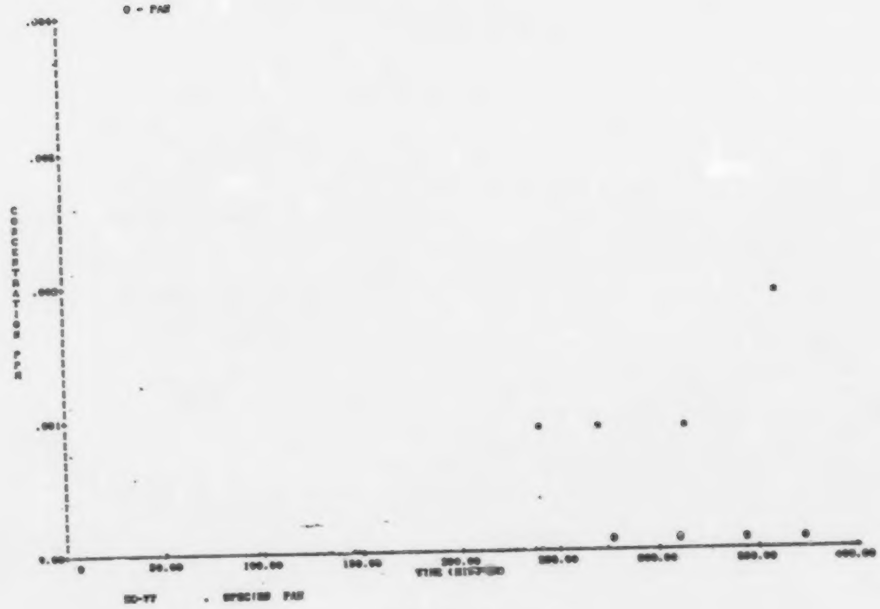

FIGURE IV-72

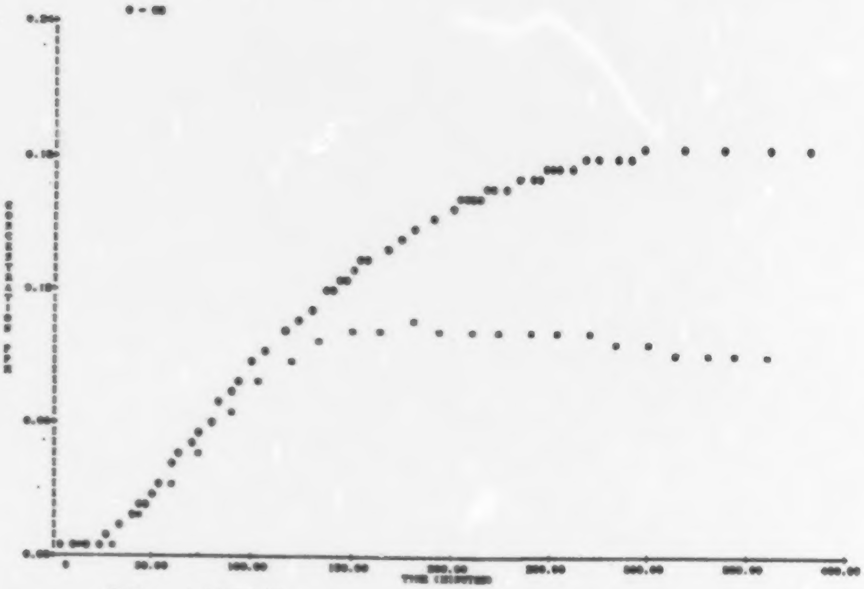

FIGURE IV-73

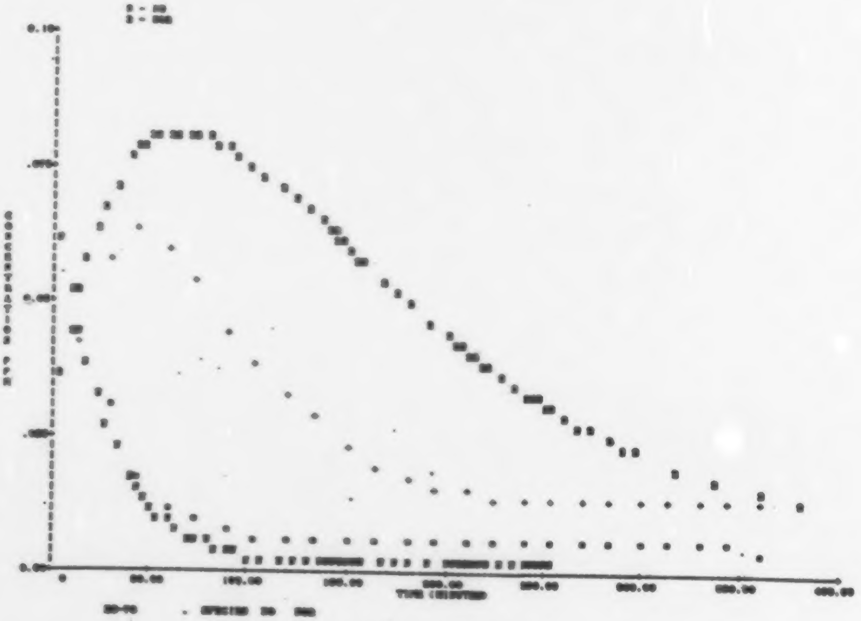

FIGURE IV-74

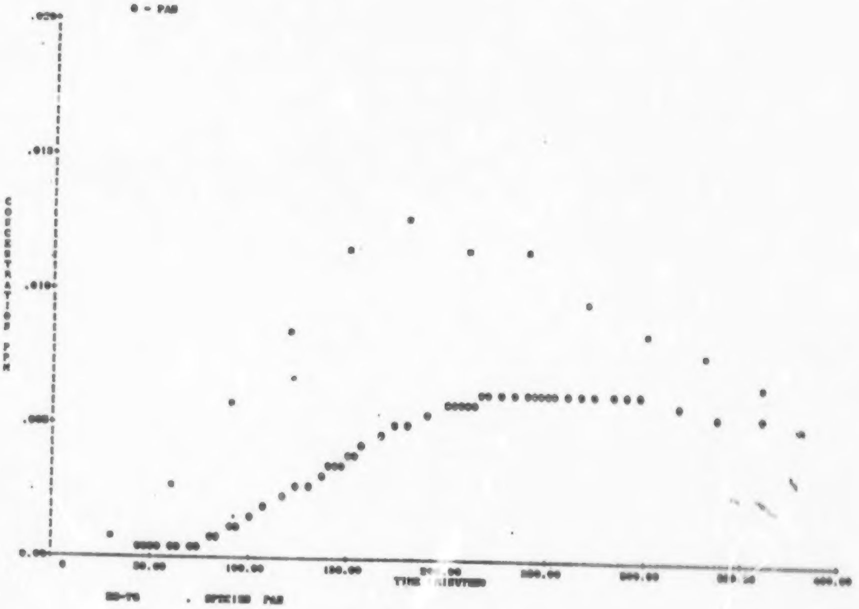
● - PAH
.020
.015
.010
.005
0.00
CONCENTRATION PPM
0
50.00
100.00
150.00
200.00
250.00
300.00
350.00
400.00
TIME (MINUTES)
RD-75
. SPIKED PAH

FIGURE IV-75

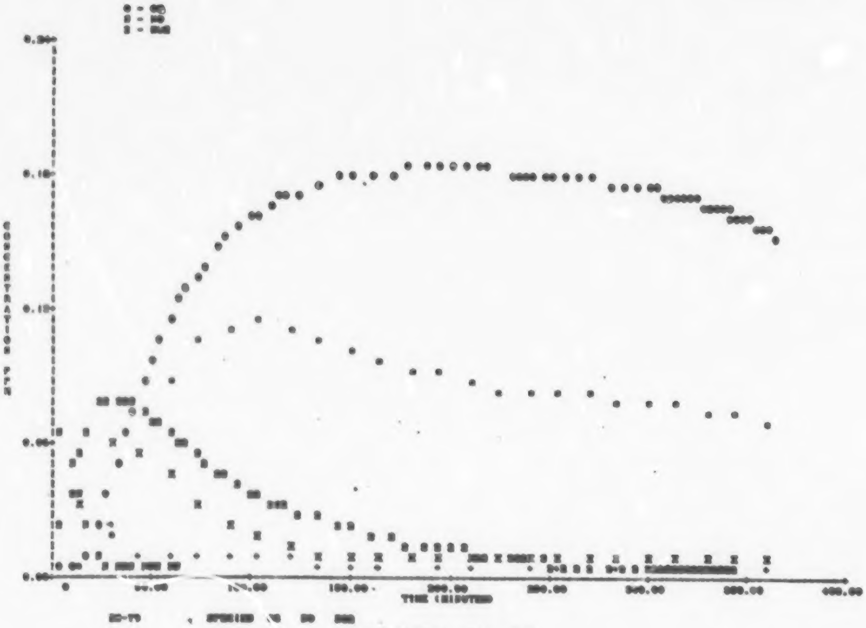

FIGURE IV-76

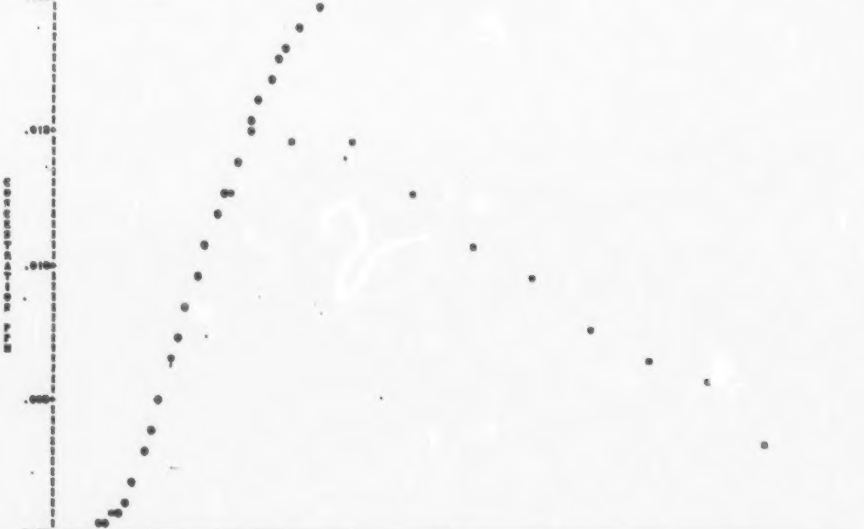

FIGURE IV-77

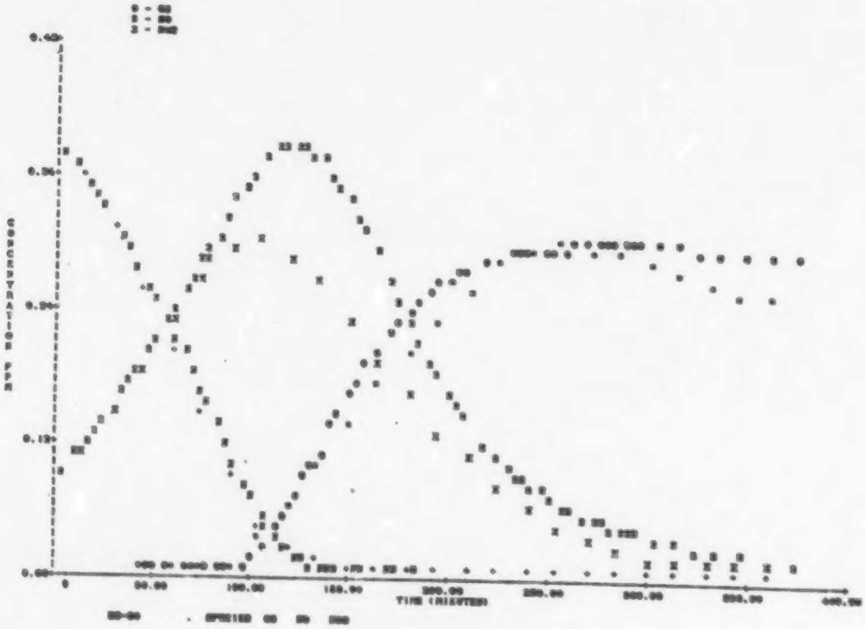

FIGURE IV-78

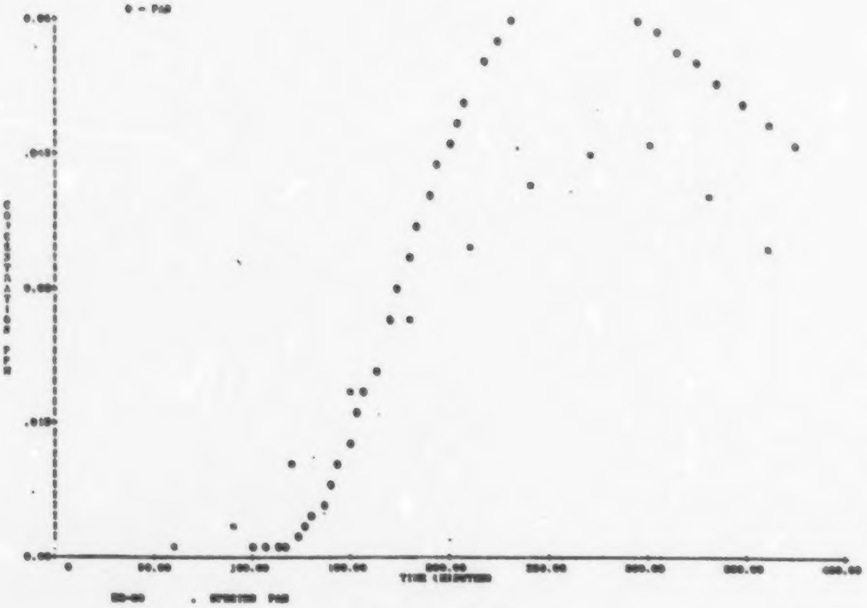

FIGURE IV-79

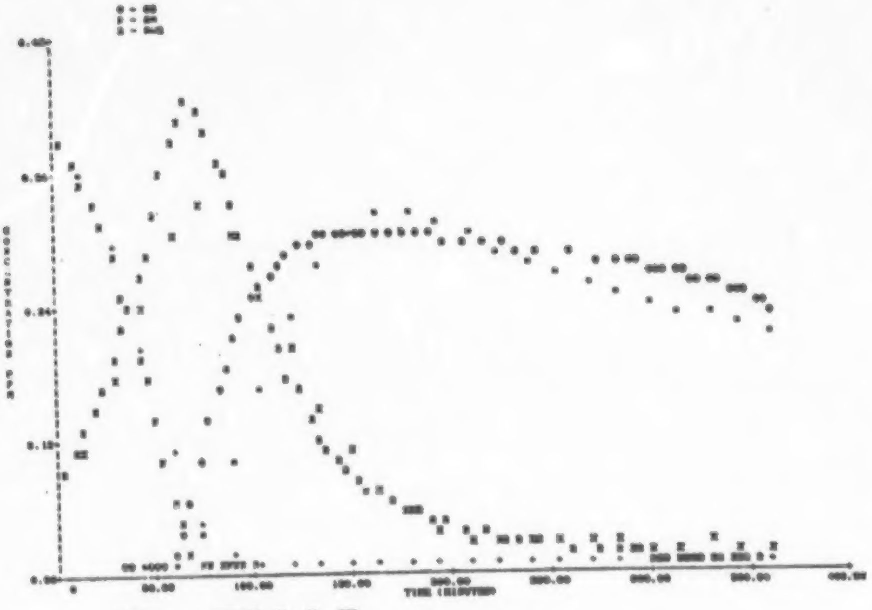

FIGURE IV-80

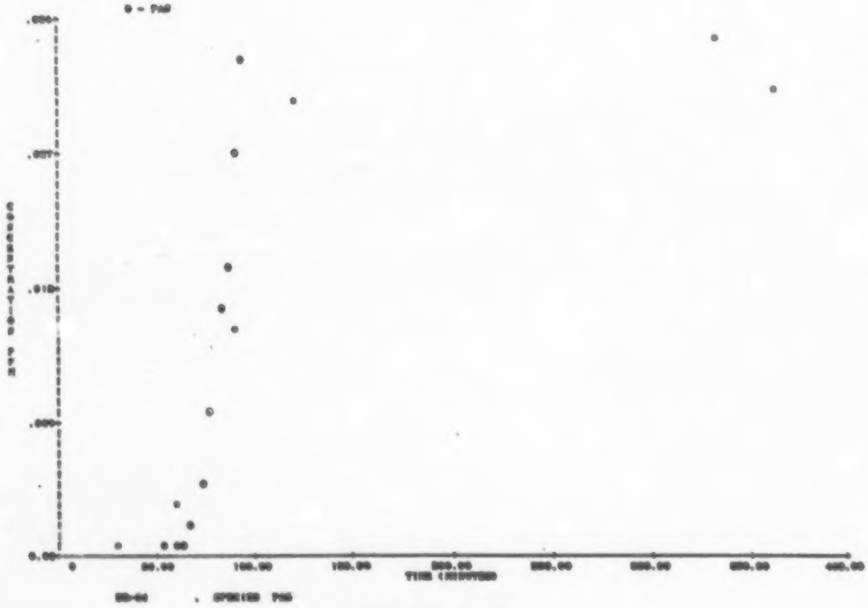

FIGURE IV-81

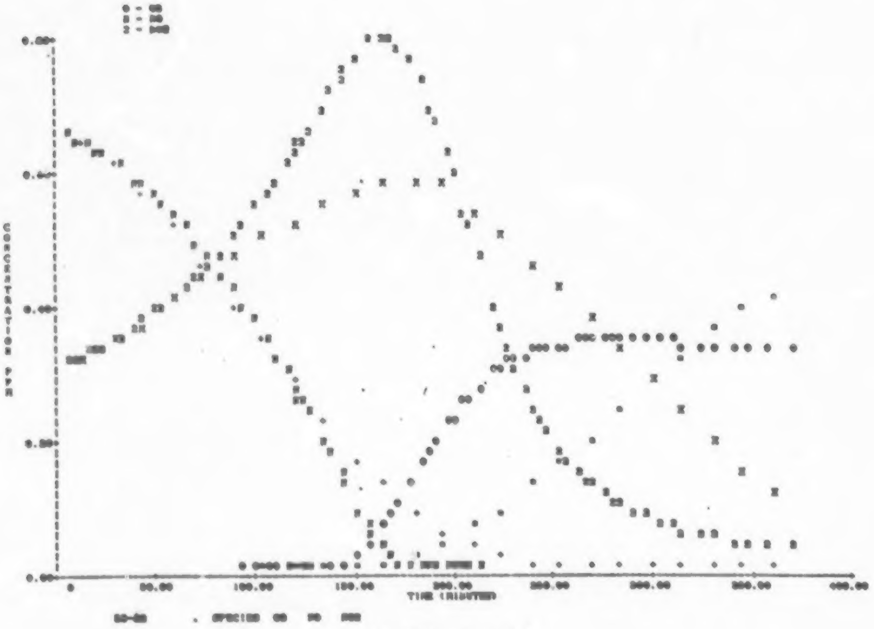

FIGURE IV-82

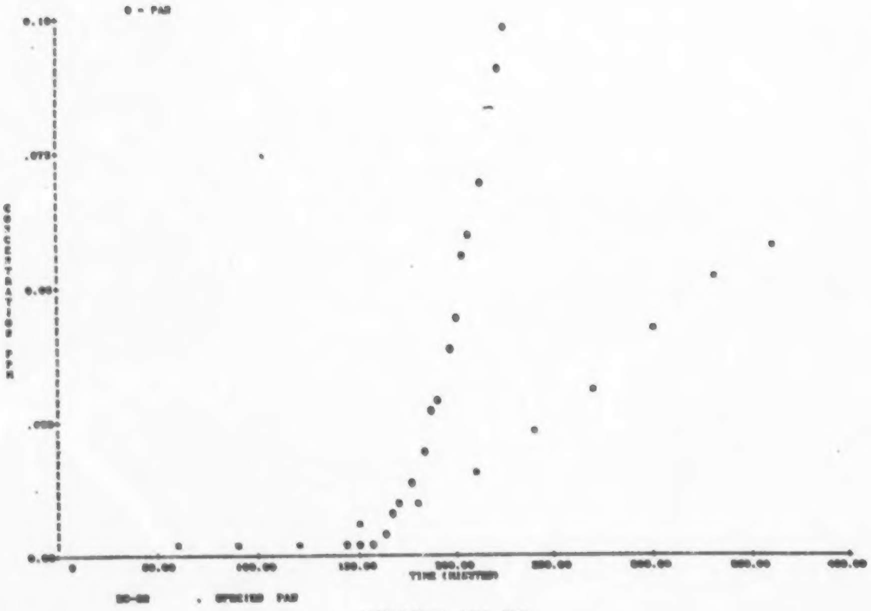

FIGURE IV-83

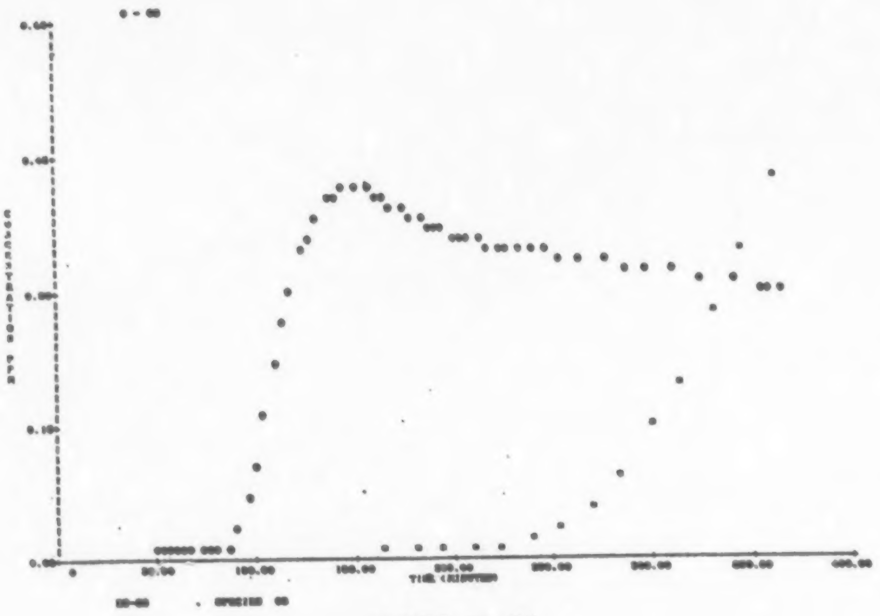

FIGURE IV-84

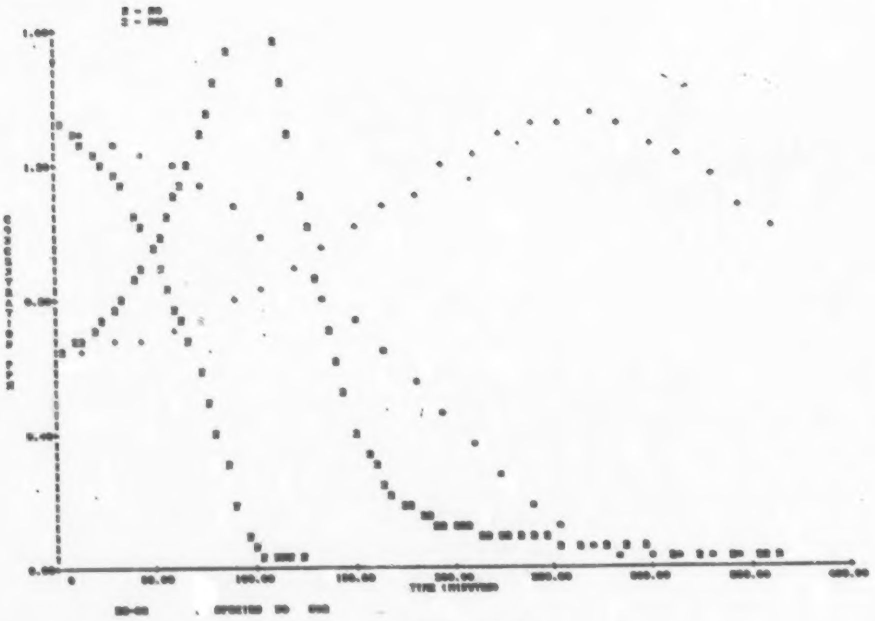

FIGURE IV-85

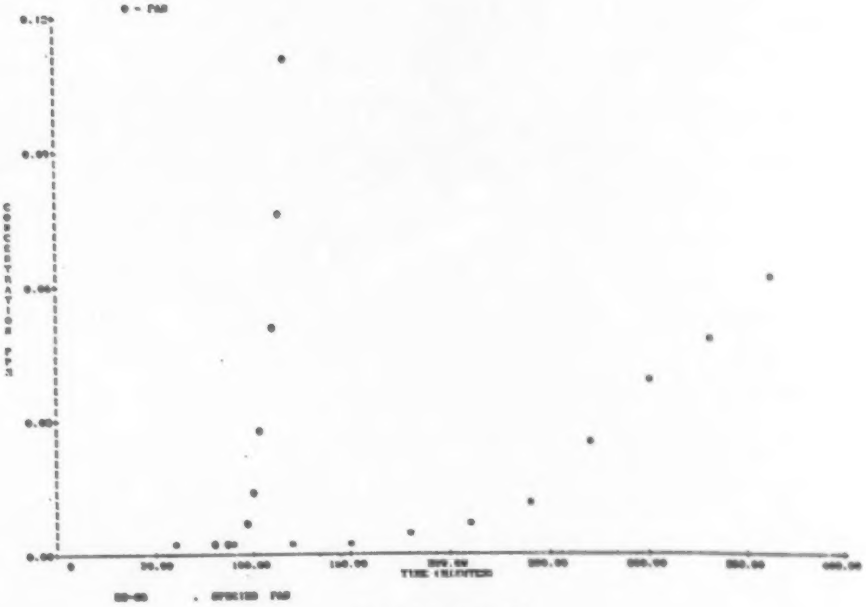
● - PAD
0.12
0.09
0.06
0.03
0.00
CONCENTRATION PPM
0
50.00
100.00
150.00
200.00
TIME (MINUTES)
250.00
300.00
350.00
400.00
. SPIKED PAD

FIGURE IV-86

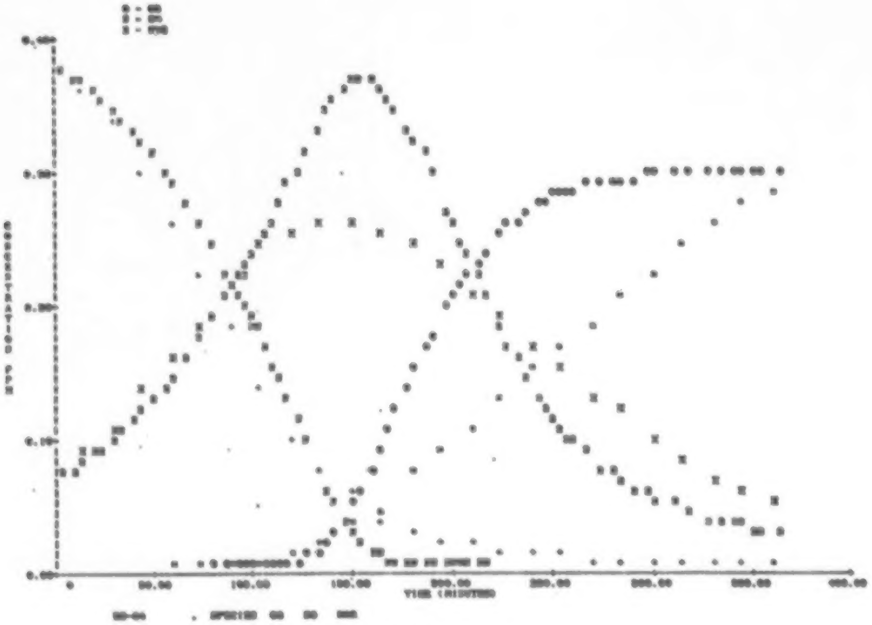

FIGURE IV-87

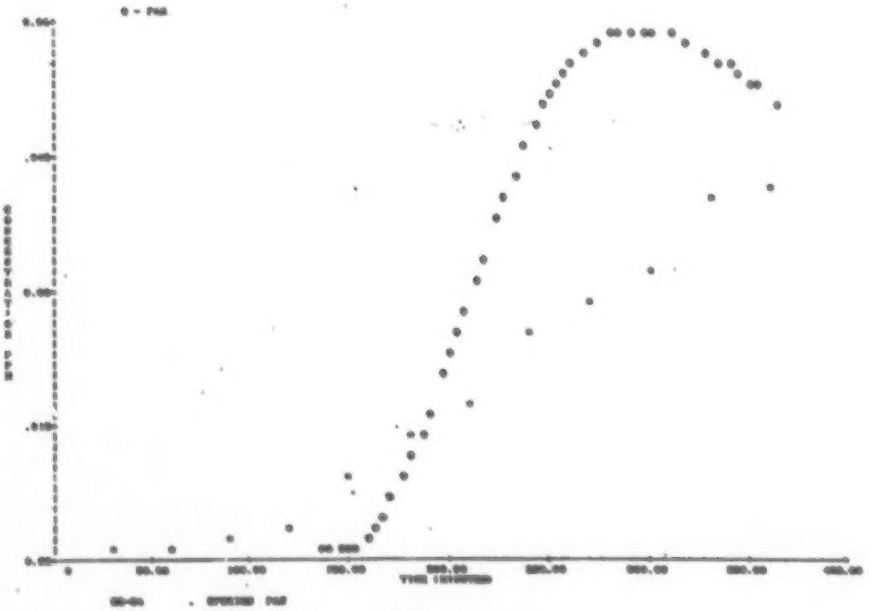

FIGURE IV-88

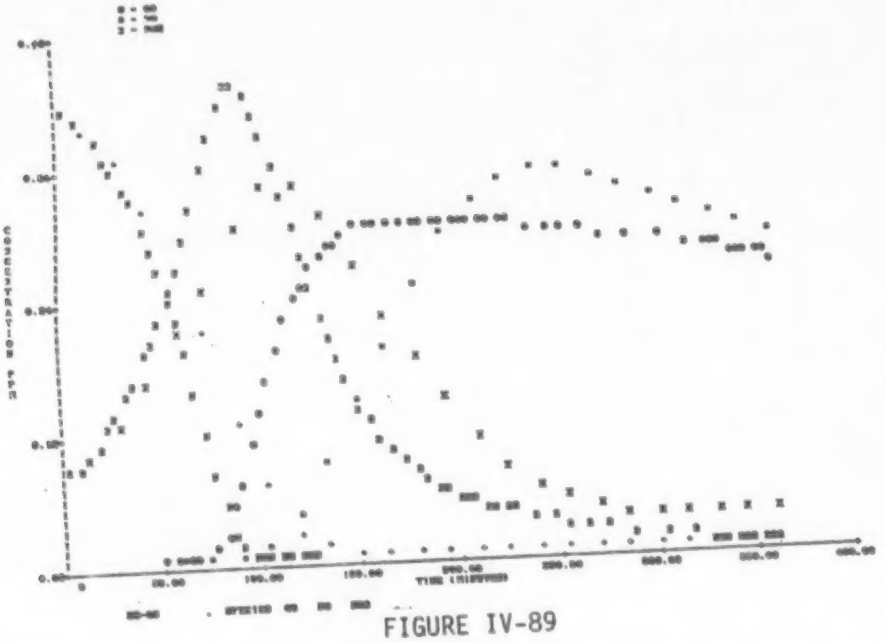

FIGURE IV-89

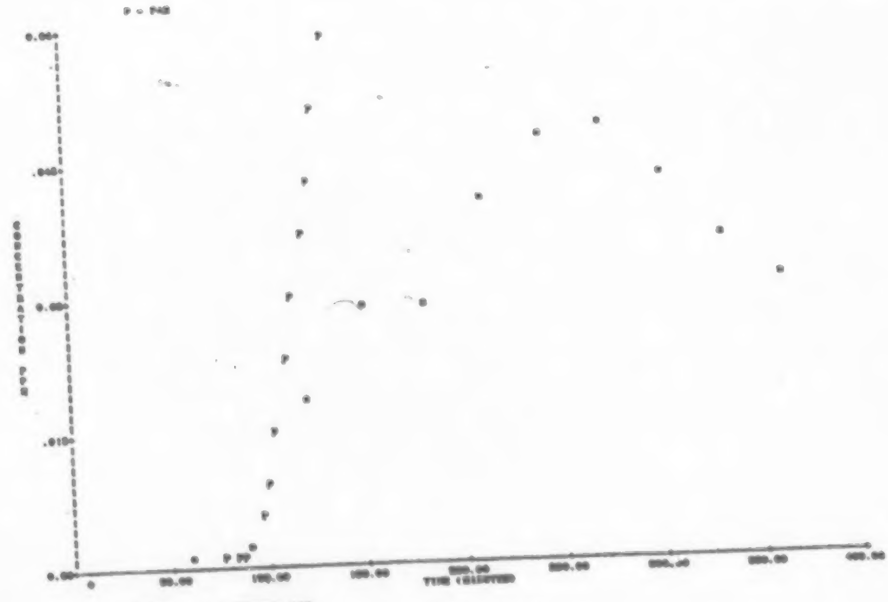

FIGURE IV-90

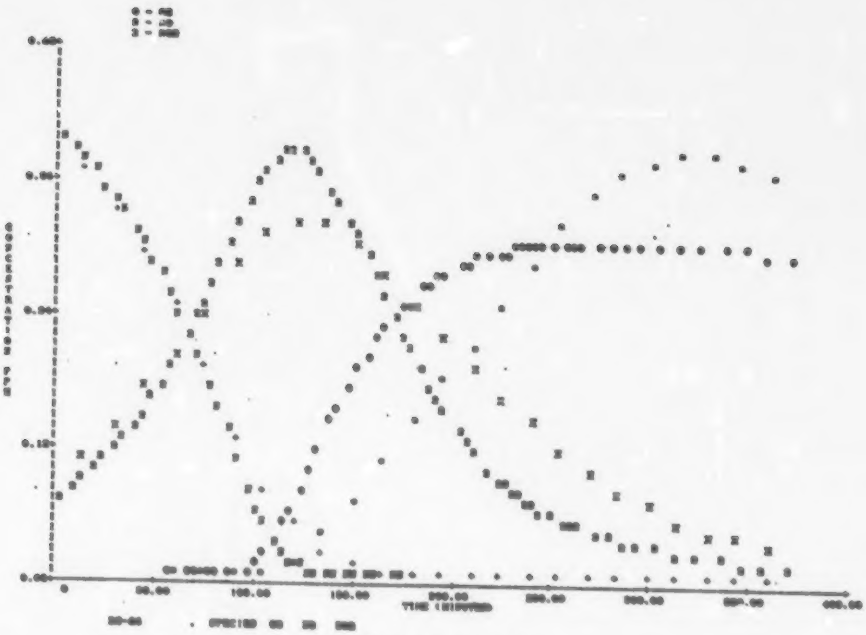

FIGURE IV-91

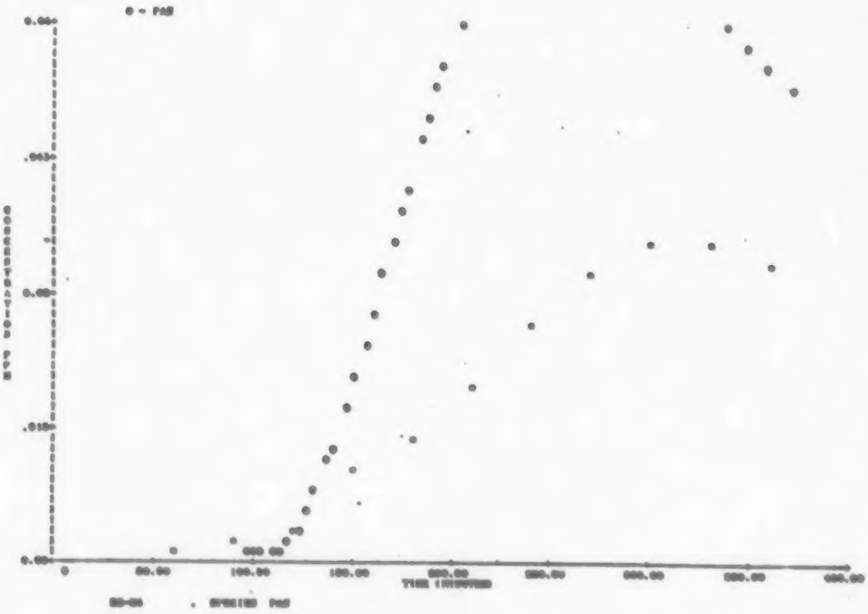

FIGURE IV-92

The run EC-77, shown in Figures IV-70 and IV-71, had the lowest hydrocarbon to NO_x ratio, and the inadequate maintenance radical problem shown in the NO_x curves is consistent with the discussion in Chapter III on Runs EC-21 and EC-42. However, the maintenance radicals in many other runs were numerous and tended to accelerate in production. The runs with high toluene concentrations, EC-82 and EC-83, showed this effect most severely. For Run EC-83 the mechanism was grossly inadequate, but the initial hydrocarbon concentration for this run was nearly 40 ppmC and the humidity was near zero. Such extreme hydrocarbon concentrations at low humidity will require further study to elucidate these effects of hydrocarbon and water.

Comparison of the simulations of EC Runs 80 and 81 with 84 and 85 reveals a curious finding. These two pairs of runs have similar toluene/NO_x concentrations, but the latter pair has somewhat higher NO to NO_2 initial values. The mechanism can follow the maintenance radicals required in the former pair, but too many radicals are simulated in the latter. Perhaps the light source deteriorated between these two and the carbonyl photolysis should be lower for the latter pair. In the other hydrocarbon systems, we could check the lumped mechanism against the corresponding explicit mechanism. Unfortunately, we do not yet have an explicit toluene mechanism to help develop and validate the carbon-bond mechanism for aromatics. Table IV-5 lists the initial conditions for the toluene set of experiments.

TABLE IV-5. INITIAL CONDITIONS FOR SIMULATIONS OF THE TOLUENE/NO_x SYSTEMS

(ppm)

EC Run Number	NO	NO_2	Toluene	HNO_2
77	0.518	0.059	0.276	0.01
78	0.069	0.032	0.228	0.005
79	0.08	0.02	0.976	0.001
80	0.401	0.095	1.02	0.006
81	0.408	0.094	1.96	0.003
82	0.679	0.337	1.88	0.001
83	1.334	0.674	5.63	0
84	0.388	0.081	0.968	0.001
85	0.431	0.093	1.92	0.001
86	0.407	0.080	1.092	0

D. DISCUSSION OF THE CARBON-BOND MECHANISM

Summarizing the results of this chapter, a generalized kinetic mechanism based on the explicit mechanisms discussed in Chapter III has been proposed for future use in airshed models. This generalized kinetic mechanism separates carbon atoms into groups depending on their bonding. The mechanism is validated for the simulation of smog chamber data by explicit mechanisms. Intermediate and overall species behavior are consistent with predictions made by the explicit mechanisms. Table IV-6 presents a comparison of the observed and simulated one-hour-average ozone concentrations for the different sets of UCR data. Even though the sets of experiments are not identical, the individual results and the calculated standard deviations are similar for the explicit and generalized mechanisms.

The carbon-bond mechanism is still in the developmental stage and certain areas of the mechanism must be investigated further. One of these areas is the handling of peroxyacyl radicals with more than one carbon. These radicals generate shorter chain alkylperoxy radicals rather than $HO_2^{\cdot}$ radicals. The carbon-bond mechanism as presented in Table IV-2 only accounts for alkyl radical production from single-bonded carbon atoms. Another important requirement is a set of guidelines for determining the best rate constants to use for a mixture of hydrocarbons with substantially different reactivities. The UCR data available in the contract period included only one set of experiments with a mixture of initial hydrocarbons, the propylene/butane set. In the near future smog chamber data sets using mixtures of olefins and mixtures of paraffins will be used to establish the needed averaging guidelines.

TABLE IV-6. ONE-HOUR-AVERAGE OZONE CONCENTRATIONS MEASURED AND SIMULATED WITH THE CARBON-BOND MECHANISM

EC Run No.	Maximum One-Hour-Average Ozone Concentration (ppm)		Percent Difference	Comments
	Measured	Simulated		
(a) Propylene/NO$_x$ Systems				
11	0.23	0.26	13	
13	0.37	0.38	2.7	
16	0.50	0.43	-14	Average = 2.32% Standard deviation = 11.2%
17	0.14	0.14	1.2	
18	0.18	0.21	16	
21	0.006	0.006	-5	
(b) Butane/NO$_x$ Systems				
39	0.056	0.041	-26.8	
41	0.21	0.24	14.3	
42	0.0042	0.005	19.1	
43	0.113	0.063	-44	Average = -0.28% Standard deviation = 2%
44	0.011	0.027	145	
45	0.12	0.12	0	
48	0.14	0.19	35.7	
(c) Propylene/Butane/NO$_x$ Systems				
97	0.56	0.57	1.8	
99	0.55	0.58	5.5	
106	0.55	0.61	10.9	
113	0.342	0.326	-4.7	Average = 0.834% Standard deviation = 10.1%
114	0.73	0.75	2.74	
115	0.58	0.63	8.6	
116	0.72	0.58	-19	

TABLE IV-6. (Concluded)

EC Run No.	Maximum One-Hour-Average Ozone Concentration (ppm) Measured	Simulated	Percent Difference	Comments
		(d) 1-Butene/NO_x Systems		
122	0.216	0.16	-25.9	Average = 0.2% Standard deviation = 27.3%
123	0.48	0.47	-2.1	
124	0.21	0.27	28.6	

V GENERAL DISCUSSION

In the previous chapters we described the details of the explicit and condensed kinetic mechanisms and presented simulations of some smog chamber experiments at the University of California at Riverside. In this chapter we present a general discussion of the following items:

> The perception of smog chemistry on which the mechanisms are based.
> Some important assumptions about experimental conditions common to all simulations.
> How well the simulations with the explicit and condensed mechanisms reproduce the measurements.
> A summary of recommendations for future experimental studies.

The overall perception of smog formation that is the basis of our present mechanisms can be described in terms of two cyclic series of reactions. One series is the oxygen atom series; it is associated with the photolysis of NO_2 and the production of ozone. The other is the peroxy-oxyl series. In this series of reactions hydrocarbons are oxygenated and NO is converted to NO_2.

In the oxygen atom series NO_2 photolyzes to give NO and an oxygen atom, which immediately combines with an oxygen molecule to form O_3. O_3 completes the cyclic series by reacting with NO to regenerate NO_2:

$$NO_2 + h\nu \rightarrow NO + O \quad , \qquad (V\text{-}1)$$

$$O + O_2 \overset{M}{\rightarrow} O_3 \quad , \qquad (V\text{-}2)$$

$$O_3 + NO \rightarrow NO_2 + O_2 \quad . \qquad (V\text{-}3)$$

The cycle time is inversely proportional to the light flux and the NO_x concentration ([NO] + [NO_2]). This cycle time is typically short enough that the ozone concentration is approximated by a steady-state relationship:

$$[O_3]_{ss} = \frac{k_1[NO_2]}{k_3[NO]} \quad . \qquad (V\text{-}4)$$

Since the ozone concentration is nearly proportional to the ratio of [NO_2] to [NO], an increase in the ozone concentration can be related to the conversion of NO to NO_2. An important feature of the oxygen atom series of reactions is that by itself it does not change the ratio [NO_2] to [NO]. Thus an independent mechanism that changes the ratio of [NO_2] to [NO] will indirectly control the ozone concentration.

The second cyclic series, the peroxy-oxyl series, is associated with a pool of chemical species having unpaired electrons. In this series NO is converted to NO_2 and hydrocarbons are oxidized. The unpaired electrons are passed from peroxy radicals to oxyl radicals and vice versa. Normally the start of this series is the rate-controlling reaction of hydroxyl radicals and hydrocarbons:

$$OH\cdot + HC \rightarrow R\cdot \quad . \qquad (V\text{-}5)$$

The unpaired electron appears on the resulting R•, which rapidly picks up an oxygen molecule to form a peroxy radical, $RO_2^{\cdot}$:

$$R\cdot + O_2 \overset{M}{\rightarrow} RO_2^{\cdot} \quad . \qquad (V\text{-}6)$$

Typically, the next reaction in the series converts NO to NO_2 and transfers the electron to an oxyl radical, RO•:

$$RO_2^{\cdot} + NO \rightarrow RO\cdot + NO_2 \quad . \qquad (V\text{-}7)$$

Then a hydrogen abstraction by molecular oxygen passes the unpaired electron to a hydroperoxyl radical, $HO_2\cdot$. The rest of the RO· radical typically forms a carbonyl compound, OHC.

$$RO\cdot + O_2 \rightarrow OHC + HO_2\cdot \quad , \qquad (V\text{-}8)$$

Finally, the unpaired electron is returned to a hydroxyl radical by a second NO to NO_2 conversion:

$$HO_2\cdot + NO \rightarrow OH\cdot + NO_2 \quad . \qquad (V\text{-}9)$$

Although this description is very simplified, these two cyclic series contain the essential features of ozone formation. The two series are partially connected by the reactions of oxygen atoms with hydrocarbons, the reactions of ozone with olefins, and a few others. This smog mechanism depends on the formation and maintenance of a pool of unpaired electrons. A portion of this pool is formed and maintained by the reactions of oxygen atoms and ozone that link the two cyclic series:

$$O + HC \rightarrow R\cdot + OH\cdot \quad , \qquad (V\text{-}10)$$

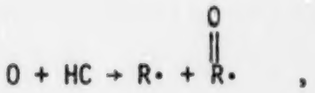

$$O + HC \rightarrow R\cdot + \overset{\displaystyle O}{\overset{\|}{R}}\cdot \quad , \qquad (V\text{-}11)$$

$$O_3 + OLE \rightarrow R\cdot + OH\cdot \quad . \qquad (V\text{-}12)$$

In computer simulations, however, these reactions alone do not form enough radicals to reproduce the measurements. The initial rates of hydrocarbon disappearance and conversion of NO to NO_2 observed in smog chambers indicate that the pool of unpaired electrons involved in the peroxy-oxyl series is formed very rapidly.

We resolved this difficulty by making an assumption that is common to all simulations discussed in this report--that some nitrous acid is present at the start of each smog chamber experiment. In the simulations, the nitrous acid is rapidly depleted by photolysis, which produces NO and hydroxyl radicals. The concentration of nitrous acid required to simulate UCR experiments is generally about one-third of the equilibrium concentration that would form eventually from the initial concentrations of NO, NO_2, and H_2O. Nitrous acid is known to form during the loading of large vessels (Chan et al., 1976), but whether it is present in the amounts we have assumed is unknown. The amounts of nitrous acid required to simulate the propylene/NO_x, butane/NO_x, 1-butene/NO_x, and toluene/NO_x systems are consistent.

Another important assumption in all simulations involves the spectral distribution of the light source. The primary maintenance source of radicals for the peroxy-oxyl series, the photolysis of carbonyls, is very sensitive to the intensity of short wavelength UV. The nitrogen dioxide photolysis rate reported by UCR depends on the intensity of long wavelength UV. This rate was formerly used to adjust the rates of all photolysis reactions to account for variations in light intensity. However, the light source in the UCR chamber is known to deteriorate, and the deterioration is most rapid at short wavelengths. Thus, we chose a spectral distribution for each simulation that was consistent with the age of the light source used in the corresponding experiment. The range of spectral distributions used for all simulations was chosen to give the best overall fit for all the simulations and still be consistent with the range of spectral distribution measurements.

The objective of these assumptions, and of the entire contract, is to produce simulations based on scientific knowledge that also fit the measurements. How well this objective was achieved can best be seen by examining the many figures in this report that show UCR measurements and our simulations. The overall fit for most species is good. A notable exception is NO_x. In most simulations the fit between predicted and measured NO_x concentrations is poor, even though the conversion of NO to NO_2 is correctly simulated. The poor fit is usually seen as an overprediction of the NO_2 concentration. It could be caused by NO_x losses in the UCR smog chamber, the absence or incorrect treatment of some important aspect of the chemistry in the mechanisms, or both. Nitrogen compounds measured at UCR include NO_2, NO, PAN, and alkyl nitrates. In every UCR experiment the sum of the concentrations of these compounds, after correction for dilution, decreased during the experiment. A similar but smaller decrease occurs in the corresponding simulation, primarily because of the formation of nitric acid. Nitric acid is not routinely measured at UCR, but has been reported in smog chambers in amounts consistent with our simulations by Spicer and Miller (1976). Modifications to the mechanisms designed to improve the fit to the UCR nitrogen data by forming more nitric acid have been unsatisfactory; they quantitatively remove radicals from the peroxy-oxyl pool and thus degrade the overall fit.

Some indication of the validity of the mechanisms presented in this report for ozone prediction is provided by Figures V-1, V-2, and V-3. Figures V-1 and V-2 show the absolute and percentage differences between predicted and measured maximum one-hour-average ozone concentrations for the explicit and carbon-bond mechanisms, respectively. All UCR systems except toluene/NO_x are included. These figures show that the average absolute difference and the average percentage difference are small and positive. The indicated positive bias is not statistically significant for two reasons: the number of experiments is small, and the standard deviation is much larger than average difference.

As discussed in Chapter IV, the carbon-bond mechanism was designed as a condensation of the explicit mechanisms. Thus its validity is determined not by how well it reproduces smog chamber data but by how well it reproduces the simulations with the explicit mechanisms. Figure V-3 shows the absolute and percentage differences between the maximum one-hour-average ozone concentrations predicted by the carbon-bond mechanism and those predicted by the explicit mechanisms. Again, toluene/NO_x systems are not included. The small differences and standard deviations in Figure V-3 demonstrate that the carbon-bond mechanism does retain

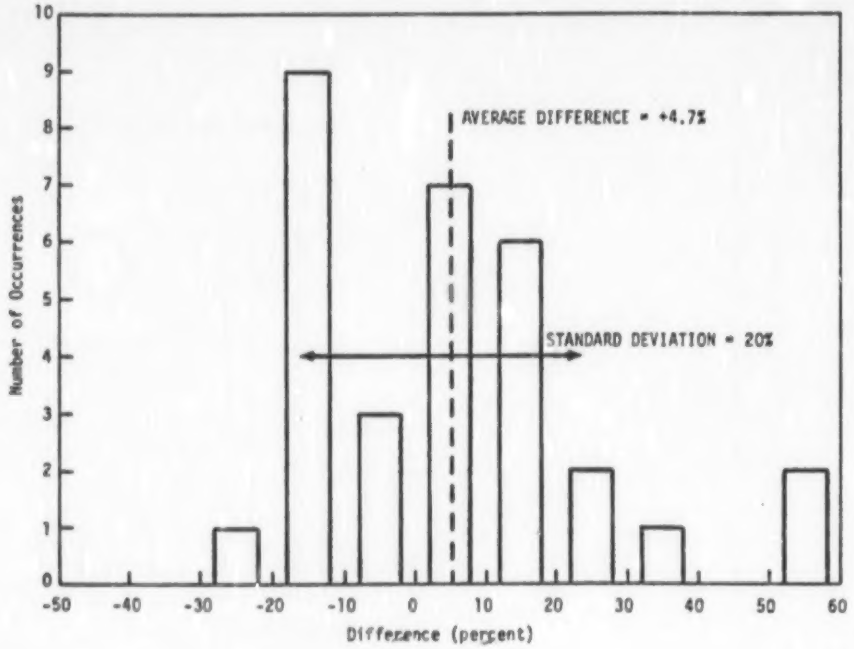

FIGURE V-1a. PERCENTAGE DIFFERENCES BETWEEN PREDICTIONS OF EXPLICIT MECHANISMS AND MEASUREMENTS OF MAXIMUM ONE-HOUR-AVERAGE OZONE CONCENTRATIONS

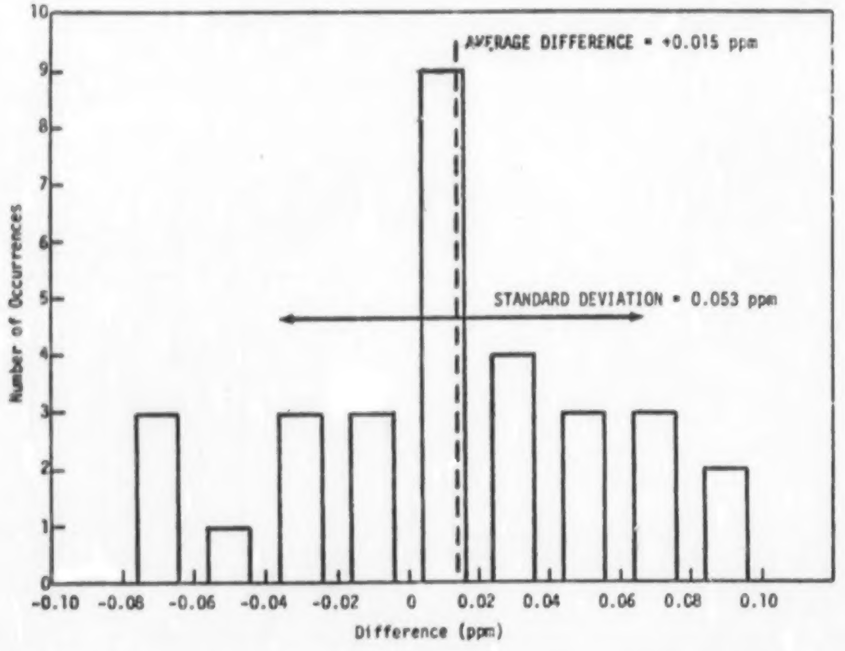

FIGURE V-1b. DIFFERENCES BETWEEN PREDICTIONS OF EXPLICIT MECHANISMS AND MEASUREMENTS OF MAXIMUM ONE-HOUR-AVERAGE OZONE CONCENTRATIONS

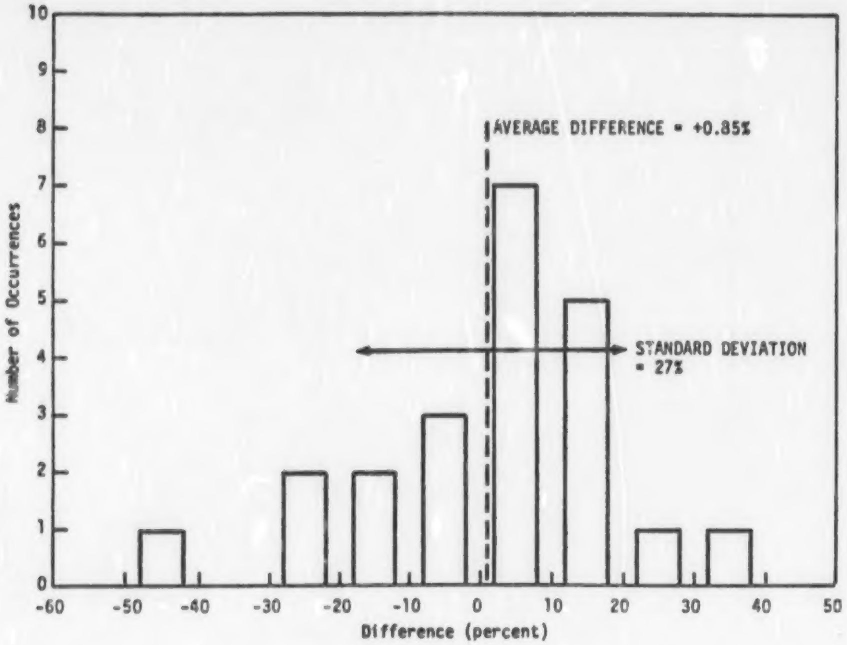

FIGURE V-2a. PERCENTAGE DIFFERENCES BETWEEN CARBON-BOND MECHANISM PREDICTIONS AND MEASUREMENTS OF MAXIMUM ONE-HOUR-AVERAGE OZONE CONCENTRATIONS

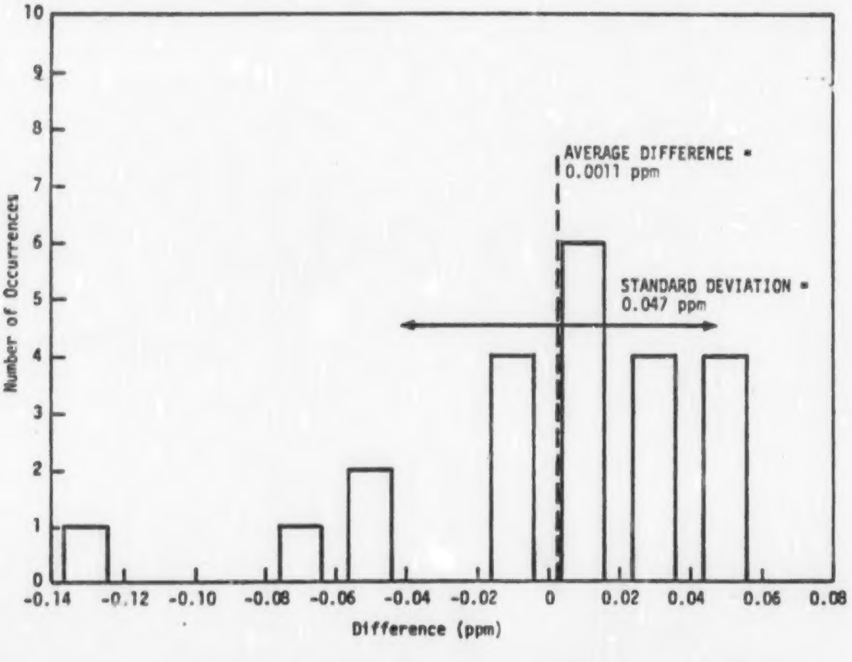

FIGURE V-2b. DIFFERENCES BETWEEN PREDICTIONS OF CARBON-BOND MECHANISM AND MEASUREMENTS OF MAXIMUM ONE-HOUR AVERAGE OZONE CONCENTRATIONS

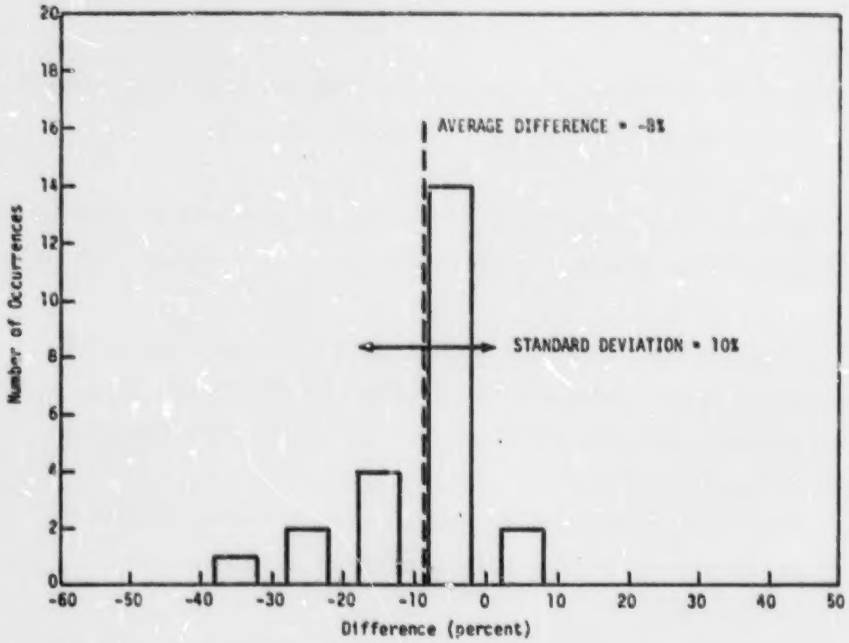

FIGURE V-3a. PERCENT DIFFERENCES BETWEEN THE MAXIMUM ONE-HOUR-AVERAGE OZONE CONCENTRATIONS PREDICTED BY THE CARBON-BOND MECHANISM AND BY THE EXPLICIT MECHANISMS

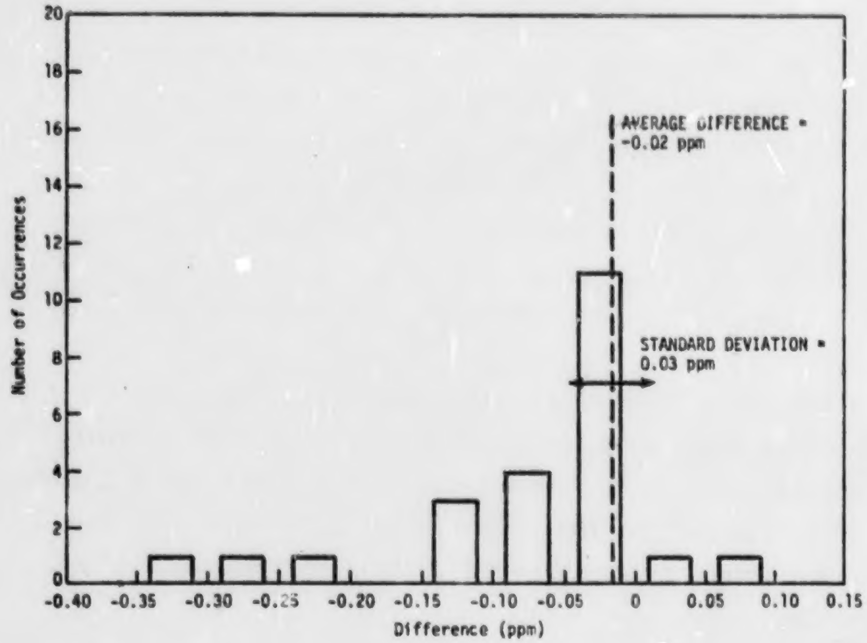

FIGURE V-3b. DIFFERENCES BETWEEN THE MAXIMUM ONE-HOUR-AVERAGE OZONE CONCENTRATIONS PREDICTED BY THE CARBON-BOND MECHANISM AND BY THE EXPLICIT MECHANISMS

the significant features of the explicit mechanisms even though it requires only 10-20 percent as much computing time.

Throughout this report we have made suggestions regarding future smog chamber experiments. These suggestions are summarized below:

- > Light intensity measurements should be more detailed.
- > Experiments with slowly reacting hydrocarbons (e.g. butane) should be carried out for more than the usual six-hour period.
- > More experiments using hydrocarbon mixtures should be performed to aid in the validation of generalized mechanisms.
- > More detailed product measurements are needed for the paraffin/NO_x and aromatic/NO_x systems so that a mass balance for carbon can be approached.
- > More consistent carbonyl data are needed in the propylene/NO_x experiments. UCR runs EC-13, 51, 52, 57, 95, 96, and 121 are propylene/NO_x experiments with the same initial conditions, but the formaldehyde and acetaldehyde concentrations and their ratios in these runs varied widely.
- > More detailed measurements of nitrogen compounds are needed in all experiments.
- > Experiments on aldehyde/NO_x systems are needed.

As discussed in Chapter III and above, the light source in the UCR chamber is known to deteriorate, resulting in lower photolysis rate constants. The light intensity changes mainly between 300 and 340 nm, which is the part of the spectrum that photolyzes aldehydes. Therefore detailed intensity measurements in this part of the spectrum are very important.

As discussed in Chapter III, the ozone concentration did not reach a peak in any of the butane runs. There is also a large carbon atom loss in these runs. Longer experiments with such hydrocarbons are required to elucidate the chemistry. As longer chain hydrocarbons (with more than four carbon atoms in the skeleton) are investigated, more detailed observations of products are desirable. Product measurements in aromatic/NO_x systems at UCR are extremely sparse; in addition, the percent carbon recovery is too low to validate an explicit mechanism. More of the carbon atoms in the initial hydrocarbons must be accounted for in order to improve explicit kinetic mechanisms for aromatics. Also, a consistent set of data is required for validation of kinetic mechanisms. In the propylene/NO_x system, the early runs (EC-5 to EC-21) show equal maximum concentrations of formaldehyde and acetaldehyde, but later runs (EC-95, 96, and 121) show much more formaldehyde than acetaldehyde. Inconsistencies of this nature must be resolved if correct reaction pathways are to be established. Experiments should be performed with simple mixtures of similar hydrocarbons. Such experiments, even without detailed product analyses, will assist in the development of the condensed mechanism because average rate constants must be derived to account for mixtures of similar hydrocarbons.

The chemistry of inorganics, aldehydes, and PAN is common to all smog mechanisms. It is difficult to evaluate this chemistry in current mechanisms because all recent smog chamber experiments are complicated by the numerous chemical species resulting from the oxidation of hydrocarbons. The uncertainties in simulating this chemistry may be reduced most easily by modeling smog chamber experiments on very simple systems. Experiments with formaldehyde/NO_x systems would be useful in verifying the basic inorganic and formaldehyde chemistry. Such experiments would not involve hydrocarbon or PAN chemistry. Experiments with acetaldehyde/NO_x would add only PAN chemistry to this basic set. The round of mechanism development just completed proceeded from parameterized mechanisms to explicit mechanisms. The next round of mechanism development will involve reducing uncertainties in individual chemical reactions. We recommend that experiments be performed on very simple systems in the most advanced chambers so that some of the basic chemical reactions in smog may be studied with as few complications as possible.

REFERENCES

Akimoto, H., et al. (1976), "Photo-Oxidation of Toluene-NO_2-O_2-N_2 System in Gas Phase," 12th Informal Conference on Photochemistry, National Bureau of Standards, Extended Abstracts, pp. K8-1 to K8-4.

Anastasi, C., P. P. Bemand, and I.W.M. Smith (1976a), "Rate Constant for: $OH + NO_2 (+ N_2) \rightarrow HNO_3 (+ N_2)$ Between 220 and 358K," Chem. Phys. Letters, Vol. 37, p. 370.

Anastasi, C., I.W.M. Smith, and R. Zellner (1976b), "Kinetics of the Reaction $OH + NO_2 (+ M) \rightarrow HNO_3 (+ M)$ over a Wide Range of Temperature and Pressure," 12th Informal Conference on Photochemistry, National Bureau of Standards, Extended Abstracts, pp. P7-1 to P7-4.

Atkinson, R., D. A. Hansen, and J. N. Pitts, Jr. (1975), "Rate Constants for the Reaction of the OH Radical with H_2 and NO ($M = Ar$ and N_2)," J. Chem. Phys., Vol. 62, pp. 3284-3288.

Atkinson, R., and J. N. Pitts, Jr. (1975), "Rate Constants for the Reaction of OH Radical with Propylene and the Butanes over the Temperature Range 297-425K," J. Chem. Phys., Vol. 63, p. 3591.

__________ (1974), J. Phys. Chem., Vol. 78, p. 1780.

Baker, G., and R. Shaw (1965), "Reactions of Methoxyl, Ethoxyl, and t-Butoxyl Radicals with Nitric Oxide and with Nitrogen Dioxide," J. Chem. Soc., Vol. 61, pp. 6965-6970.

Barker, J. R., S. W. Benson, and D. M. Golden (1976), "The Decomposition of Dimethyl Peroxide and the Rate Constant for $CH_3O + O_2 \rightarrow CH_2O + HO_2$," SRI Project No. 2554, Stanford Research Institute, Menlo Park, California.

Batt, L., R. D. McCulloch, and R. T. Milne (1975), "Thermochemical and Kinetic Studies of Alkyl Nitrites (RONO) - D(RONO), the Reactions Between RO· and NO, and the Decomposition of RO·," Int. J. Chem. Kinet. Symposium No. 1, pp. 441-461.

Baulch, D. L., D. D. Drysdale, and D. G. Horne (1973), unpublished data sheets prepared for NBS Technical Note 866, University of Leeds.

Bell, E. R., et al. (1951), Disc. Faraday Soc., Vol. 10, p. 242.

Bennett, J. E., D. M. Brown, and B. Mile (1970), "Studies by Electron Spin Resonance of the Reactions of Alkylperoxy Radicals," Trans. Faraday Soc., Vol. 66, pp. 386-396.

Benson, S. W. (1975), "Current Status of Methods for the Estimation of Rate Parameters," Int. J. Chem. Kinetics Symposium No. 1, pp. 359-378.

________ (1968), Thermochemical Kinetics (John Wiley & Sons, New York, New York).

Benson, S. W., and H. E. O'Neal (1970), Kinetic Data on Gas Phase Unimolecular Reactions, NSRDS-NB521 (U.S. Government Printing Office, Washington, D.C.).

Bufalini, J. J., S. L. Kopczynski, and M. C. Dodge (1972), "Contaminated Smog Chambers in Air Pollution Research," Environ. Letters, Vol. 3, pp. 101-109.

Calvert, J. G. (1976), "Hydrocarbon Involvement in Photochemical Smog Formation in Los Angeles Atmosphere," Environ. Sci. Technol., Vol. 10, p. 256.

Calvert, J. G., and R. D. McQuigg (1975), "The Computer Simulation of the Rates and Mechanisms of Photochemical Smog Formation," Int. J. Chem. Kinet. Symposium No. 1, pp. 113-154.

Calvert, J. G., and J. N. Pitts, Jr. (1966), Photochemistry (John Wiley & Sons, New York, New York).

Carter, W.P.L., et al. (1976), "Evidence for Alkoxy Radical Isomerization in C_4-C_6 Alkanes in NO_x-Air Systems," 12th Informal Conference on Photochemistry, National Bureau of Standards, Extended Abstracts, pp. N4-1 to N4-5.

Chan, W. H., et al. (1976), "Kinetic Study of HONO Formation and Decay Reactions in Gaseous Mixtures of HONO, NO, NO_2, H_2O, and N_2," Environ. Sci. Technol., Vol. 10, pp. 674-682.

Cox, R. A. (1975), "The Photolysis of Nitrous Acid in the Presence of Carbon Monoxide and Sulfur Dioxide," J. Photochem., Vol. 4, pp. 291-304.

________ (1974), "The Photolysis of Gaseous Nitrous Acid," J. Photochem., Vol. 3, pp. 175-188.

Cox, R. A., and R. G. Derwent (1975), "Kinetics of the Reaction of $HO_2^{\cdot}$ with Nitric Oxide and Nitrogen Dioxide," J. Photochem., Vol. 4, pp. 139-153.

Davis, D. D. (1976), private communication with Dr. M. Dodge of EPA.

Davis, D. D., W. Heaps, and T. McGee (1976), "Direct Measurements of Natural Tropospheric Levels of OH via an Aircraft Borne Tunable Dye Laser," Geophys. Res. Lett., Vol. 3, pp. 331-333.

Demerjian, K. L., J. A. Kerr, and J. G. Calvert (1974), "The Mechanism of Photochemical Smog Formation," in Advances in Environmental Science Technology, J. N. Pitts and R. L. Metcalf, eds. (John Wiley & Sons, New York, New York).

Domalski, E. S. (1972), "Selected Values of Heats of Combustion and Heats of Formation of Organic Compounds Containing the Elements C, H, N, O, P, and S," J. Phys. and Chem. Ref. Data, Vol. 1, pp. 221-277.

Doyle, G. J., et al. (1975), "Gas Phase Kinetic Study of Relative Rates of Reaction of Selected Aromatic Compounds with Hydroxyl Radicals in an Environmental Chamber," Environ. Sci. Technol., Vol. 9, No. 3, pp. 237-241.

Durbin, P. A., T. A. Hecht, and G. Z. Whitten (1975), "Mathematical Modeling of Simulated Photochemical Smog," EPA-650/4-75-026, Systems Applications, Incorporated, San Rafael, California.

Farrow, L. A., T. E. Graedel, and T. H. Weber (1975), "Heterogeneous Removal of Free Radicals by Aerosols in the Urban Troposphere," American Chemical Society Symposium Series, in press.

Finlayson, B. J., and J. N. Pitts, Jr. (1976), "Photochemistry of the Polluted Troposphere," Science, Vol. 192, pp. 111-119.

Furuyama, S., and N. Ebara (1975), "A Kinetic Study of the Reaction of $O(^3P)$ with Toluene," Int. J. Chem. Kinet., Vol. 7, pp. 689-698.

Graedel, T. E., L. A. Farrow, and T. H. Weber (1975), "The Influence of Aerosols on the Chemistry of the Troposphere," Int. J. Chem. Kinet. Symposium No. 1, pp. 581-594.

Graham, R. (1975), private communication.

Gray, P., R. Shaw, and J.C.J. Thynne (1967), "The Rate Constants of Alkoxyl Radical Reactions," Prog. in React. Kinet., Vol. 4, pp. 63-117.

Greiner, N. R. (1970), "Hydroxyl Radical Kinetics by Kinetic Spectroscopy: VI--Reactions with Alkanes in the Range 300 to 500K," J. Chem. Phys., Vol. 53, pp. 1070-1076.

Hampson, R. F., and D. Garvin (1975), "Chemical Kinetic and Photochemical Data for Modelling Atmospheric Chemistry," NBS Technical Note 866, National Bureau of Standards, Washington, D.C.

Hansen, D. A., R. Atkinson, and J. N. Pitts, Jr. (1975), "Rate Constants for the Reaction of OH Radicals with a Series of Aromatic Hydrocarbons," J. Phys. Chem., Vol. 79, No. 17, pp. 1763-1766.

Hecht, T. A., J. H. Seinfeld, and M. C. Dodge (1974a), "Further Development of a Generalized Kinetic Mechanism for Photochemical Smog," Environ. Sci. Technol., Vol. 8, pp. 327-339.

Hecht, T. A., M. K. Liu, and D. C. Whitney (1974b), "Mathematical Simulations of Smog Chamber Photochemical Experiments," EPA-650/4-74-040, Systems Applications, Incorporated, San Rafael, California.

Heicklen, J. (1968), "Oxidation of Organic Compounds--II," Adv. Chem., No. 76, p. 23.

Hendry, D. G. (1976), private communication.

Herron, J. T., and R. D. Penzhorn (1969), "Mass Spectrometric Study of the Reactions of Atomic Oxygen with Ethylene and Formaldehyde," J. Phys. Chem., Vol. 73, pp. 191-196.

Japar, S. M., and H. Niki (1975), "Gas-Phase Reactions of the Nitrate Radical with Olefins," J. Phys. Chem., Vol. 79, No. 16, pp. 1629-1632.

Japar, S. M., C. H. Wu, and H. Niki (1974), "Rate Constants for the Reaction of Ozone with Olefins in the Gas Phase," J. Phys. Chem., Vol. 78, No. 23, pp. 2318-2320.

Johnston, H. S., and R. Graham (1973), "Gas Phase Ultraviolet Absorption Spectrum of Nitric Acid Vapor," J. Phys. Chem., Vol. 77, pp. 62-63.

Lloyd, A. C. (1974), "Evaluated and Estimated Kinetic Data for Gas Phase Reactions of the Hydroperoxyl Radical," Int. J. Chem. Kinetics, Vol. 6, pp. 169-228.

Lloyd, A. C., et al. (1976), "Relative Rate Constants for Reactions of the Hydroxyl Radical with a Series of Alkanes, Alkenes, and Aromatic Hydrocarbons," J. Phys. Chem., Vol. 80, No. 8, pp. 789-794.

Mabey, W. R., and A. G. Hendry (1974), "Reactions of Hydroperoxy Radicals," Stanford Research Institute, Menlo Park, California.

Mendenhall, G., D. M. Golden, and S. W. Benson (1975), "The Very-Low-Pressure Pyrolysis (VLPP) of n-Propyl Nitrate, tert-Butyl Nitrite, and Methyl Nitrite. Rate Constants for Some Alkoxy Radical Reactions," Int. J. Chem. Kinet., Vol. 7, pp. 725-737.

Mill, T., and G. Montorsi (1973), "The Liquid-Phase Oxidation of 2,4-Dimethylpentane," Int. J. Chem. Kinetics, Vol. 5, pp. 119-136.

Morris, E. D., Jr., and H. Niki (1971), "Mass Spectrometric Study of the Reaction of Hydroxyl Radical with Formaldehyde," J. Chem. Phys., Vol. 55, pp. 1991-1992.

__________ (1973), "Reaction of Dinitrogen Pentoxide with Water," J. Phys. Chem., Vol. 77, pp. 1929-1932.

Niki, H., et al. (1976a), "IR Fourier-Transform Spectroscopic Studies of Atmospheric Reactions," 12th Informal Conference on Photochemistry, National Bureau of Standards, Extended Abstracts, pp. N1-N4 (peroxynitrate data given at meeting).

__________ (1976b), "Fourier Transform Spectroscopic Studies of Gas Phase Ozone-Olefin Reactions," 171st American Chemical Society National Meeting.

Niki, H., E. E. Daby, and B. Weinstock (1972), Photochemical Smog and Ozone Reactions, Advances in Chemistry Series 113 (American Chemical Society, Washington, D. C.).

O'Neal, H. E., and C. Blumstein (1973), "A New Mechanism for Gas Phase Ozone-Olefin Reactions," Int. J. Chem. Kinet., Vol. 5, pp. 397-413.

Osif, T. L., and J. I. Heicklen (1976), "Oxidation of HCO Radicals," J. Phys. Chem., Vol. 80, pp. 1526-1531.

Parkes, D. A., et al. (1973), "The Ultraviolet Absorption by Alkylperoxy Radicals and Their Mutual Reactions," Chem. Phys. Letters, Vol. 23, pp. 425-429.

Pate, C. T., R. Atkinson, and J. N. Pitts, Jr. (1976), "Rate Constants for the Gas Phase Reaction of Peroxyacetyl Nitrate with Selected Atmospheric Constituents," J. Environ. Sci. Health, Vol. A-11, p. 19-33.

Reynolds, S. D. (1976), private communication.

Schwartz, N. (1974), "Chemical Characterization of Model Aerosols," EPA-650/3-74-011, Environmental Protection Agency, Research Triangle Park, North Carolina.

Simonaitis, R., and J. I. Heicklen (1974), "Reactions of CH_3O_2 with NO and NO_2," J. Phys. Chem., Vol. 78, pp. 2417-2421.

Spicer, C. W., et al. (1973), "The Reactions of Methylperoxy Radicals with NO and NO_2," J. Amer. Chem. Soc., Vol. 95, p. 13.

Stuhl, F., and H. Niki (1971), J. Chem. Phys., Vol. 55, p. 3904.

Tsang, W. (1973), "Comparison between Experimental and Calculated Rate Constants for Dissociation and Combination Reactions Involving Small Polyatomic Molecules," Int. J. Chem. Kinet., Vol. 5, pp. 947-963.

Volman, D. H., and R. A. Gorse (1972), "Photochemistry of the Gaseous Hydrogen Peroxide-Carbon Monoxide Systems: Rate Constants for Hydroxyl Radical Reactions by Competitive Kinetics," Final Report, Project 5-143-2, University of California, Davis, California.

Wang, C. C., et al. (1975), "Hydroxyl Radical Concentrations Measured in Ambient Air," Science, Vol. 189, pp. 797-800.

Weaver, J., et al. (1975), "The Photooxidation of $CD_3N_2CD_3$," J. Photochem., Vol. 4, pp. 109-120.

Weinstock, B. (1976), private communication.

Whitbeck, M. R., et al. (1976), "A Kinetic Study of CH_3O_2 and $(CH_3)_3CO_2$ Radical Reactions by Kinetic Flash Spectroscopy," 12th Informal Conference on Photochemistry, National Bureau of Standards, Extended Abstracts, pp. K1-1 to K1-5.

Wiebe, H. A., et al. (1973), "Photolysis of Methyl Nitrite in the Presence of Nitric Oxide, Nitrogen Dioxide, and Oxygen," J. Amer. Chem. Soc., Vol. 95, pp. 7-12.

Wijnen, M.H.J. (1958), J. Amer. Chem. Soc., Vol. 80, p. 2394.